VIBRATIONAL POWER TRANSMISSION BETWEEN SOURCES AND SUBSTRUCTURES

by

ROGER JAMES PINNINGTON

of the

INSTITUTE OF SOUND AND VIBRATION RESEARCH
FACULTY OF ENGINEERING AND APPLIED SCIENCE
UNIVERSITY OF SOUTHAMPTON
ENGLAND

A Thesis submitted for the Degree of

DOCTOR OF PHILOSOPHY

MARCH 1982

UNIVERSITY OF SOUTHAMPTON

ABSTRACT

FACULTY OF ENGINEERING AND APPLIED SCIENCE
INSTITUTE OF SOUND AND VIBRATION RESEARCH

Doctor of Philosophy

VIBRATIONAL POWER TRANSMISSION BETWEEN SOURCES AND SUBSTRUCTURES

by Roger James Pinnington

The thesis is in three sections. The first is a theoretical study, to gain an understanding of the parameters which control the power transmission between machine sources and seatings. For this study a simplified structure, namely an end-excited beam, was selected with which to model a resonant seating structure. Three types of simplified machine source were considered, a pure force, a rigid body and a short resonant beam. These sources were connected to the seating via a single isolator. The outcome of this first study was to be able to express the frequency averaged power transmission or the peak power transmission to the seating structure in terms of approximate source and seating mobility formulae. Theoretical predictions were compared with experimental measurements.

Although it is useful to be able to predict power transmission from machines, a more profound understanding and a greater confidence in the approach will not be gained unless measurements can be made. Therefore, the second part of the thesis proposes three practical methods for measuring power transmission. The methods use measured frequency domain acceleration data and structural frequency response information, and are: power input to a structure at a single point; power transmitted through an isolator using accelerations above and below each isolator; and power absorbed by a finite resonant structure, using accelerations at one, two or four points. Such measurements require confidence in measured frequency response data in complex form, and therefore the accuracy with which this quantity may be measured is discussed.

Finally, some practical experiments were conducted on a d.c. motor coupled by four isolators to a beam stiffened plate. Power transmission measurements were made and the results compared with simple predictions.

ACKNOWLEDGEMENTS

The author wishes to thank Dr. R.G. White for his guidance and encouragement. He also gratefully acknowledges the support by the Ministry of Defence (Admiralty Marine Technology Establishment) of the unclassified contract under which his research was carried out.

He gives power to the faint,
and to him who has no might he
increases strength.

Isaiah Ch. 40 v. 28,29.

CONTENTS

LIST OF SYMBOLS

A_o	area
A	apparent mass
$\bar{A}_I^{(1)}$	transfer apparent mass of the isolator at position 1, motor test
$\bar{A}_{12}$	transfer apparent mass of the isolator
$\bar{A}_3$	apparent mass at position 3
$\bar{A}_S$	apparent mass of the mass + spring + beam
$\bar{A}_R$	receiver apparent mass
B	travelling wave amplitude
C	mobility sum (equation (3.11))
E	modulus of elasticity
$E(\ )$	estimate
$\bar{F}$	force
$\bar{F}_1$, $\bar{F}_2$, $\bar{F}_R$, $\bar{F}_N$, $\bar{F}_r$, $\bar{F}_s$	forces at points 1, 2, R, N, r and s
G_{FF}	force spectral density
$\bar{G}_{FV}$	force velocity cross spectral density
G_{VV}	velocity spectral density
G_{ss}	acceleration power spectrum at point s
$\bar{G}_{rs}$	acceleration cross spectrum between points r and s
I	second moment of area
$\bar{I}_1$, $\bar{I}_2$, $\bar{I}_s$	point inertances at positions 1, 2 and s
I_o	impulse magnitude
$\bar{I}_{12}$, $\bar{I}_{13}$, $\bar{I}_{rs}$	transfer inertance between points 1 and 2, 1 and 3, r and s
$\bar{I}_s^{(1)}$, $\bar{I}_s^{(13)}$	seating point and transfer inertances
$\hat{I}_s$, $\hat{I}_{rs}$	envelope functions taken from $\bar{I}_s$ and $\bar{I}_{rs}$
$\bar{I}_{1c}$	inertance at point 1 of the coupled source beam
J	sum of squared mobility
K	spring stiffness
K_L	stiffness of local structure

K_2, K_R	are the local stiffnesses at the source and receiver, respectively
K_c	stiffness of end-loaded cantilever
$\bar{M}$	mobility
$\bar{M}_1$, $\bar{M}_2$, $\bar{M}_3$, $\bar{M}_s$, $\bar{M}_r$	point mobilities at points 1, 2, 3, s and r
$\hat{M}_s$	envelope function taken from $\bar{M}_s$
$\bar{M}_b$	mobility on a beam
$\bar{M}_R$	the receiver or seating point mobility
$\bar{M}_{rs}$, $\bar{M}_{12}$	transfer mobility between points r and s, 1 and 2
$\hat{M}_{rs}$	envelope function taken from $\bar{M}_{rs}$
$\bar{M}^{(p)}$, $\bar{M}^{(q)}$	modal mobilities for p'th and q'th modes
$\hat{M}_{rs}$	peak transfer mobility for p'th mode between points r and s
$M_s^{(p)}$	peak mobility for p'th mode at point s
$\hat{M}^{(p)}$	resonance peak value of $\bar{M}^{(p)}$
N	integer
P	time averaged power
$<P>$	power averaged over θ interval
$<\hat{P}>$	peak value of, θ averaged, power
$<\check{P}>$	trough value of, θ averaged, power
$<<P>>$	power averaged over ϕ interval
P_{in}	power input
$\hat{P}_{in}$	peak power input
$\hat{P}_{in}^{(p)}$	peak power input for the p'th mode
P_{tr}	power transmitted
$P_{tr}^{(p)}$	power transmitted by p'th mode of the source structure
$\hat{P}$	envelope of peaks in power
$\check{P}$	trough value of power
P_p, P_q	power absorbed by p'th and q'th modes
Q	real component of mobility of an infinite receiver
$\hat{Q}$	resonance peak value of real component of mobility
Q_i	frequency dependent part of imaginary component of receiver mobility
Q_r	frequency dependent part of real component of receiver mobility

a	distance from centre of gravity to excitation point on motor
$\bar{a}_m^{(n)}(f)$, $\bar{a}_s^{(n)}(f)$	Fourier transforms of accelerations above and below the n'th isolator, respectively
a_1, a_2, a_3	accelerations at points 1, 2 and 3
b	amplitude of decaying wave
c	amplitude of decaying wave
e	exponential factor
f	frequency
f_o	resonance frequency of fundamental
f_p	generalised force to the p'th mode
$f(t)$	force in time domain
g	peak to mean ratio of power (equation (2.23))
k	wavenumber
k_x, k_y	wavenumbers in x and y directions
ℓ	length
m	mass
m_w, m_F	mass of web and flange of a beam
m_p	modal mass of p'th mode
n,p,q	integers
r	reflection coefficient magnitude
t	transmission coefficient from source beam
t	time
t_d	transmission coefficient with isolator damping
$\hat{t}$	peak transmission coefficient
u, u_1, u_2	sum of square of mobility moduli, equations (3.13), (A4.11), (5.6)
x	distance
x_s	x coordinate of point s
y	displacement
y_s	y coordinate at point s
$\sin(\epsilon_s^{(p)})$	the attenuation in the mean square velocity of the p'th mode, from the excitation point to the measurement point s

S	frequency averaged value of real component of source mobility
S_i	frequency dependent part of imaginary component of source mobility
S_r	frequency dependent part of real component of source mobility
T	torque
T_o	time for decay of free vibration
T_n	time for response to reach noise level
T_f	time over which forcing function is applied
$\bar{V}$	velocity
$\bar{V}_1$, $\bar{V}_2$, $\bar{V}_r$, $\bar{V}_s$, $\bar{V}_R$, $\bar{V}_j$	velocities at points 1, 2, r, s, R and j
$\bar{V}_f$	free velocity
$\bar{V}_f^{(p)}$	free velocity contribution from the p'th mode of vibration
$X(f)$	envelope function
$\bar{Z}$	impedance
α	attenuation due to damping
β	receiver beam damping term
γ	phase change
δ	phase of reflection coefficient
ϵ	source beam damping parameter
η	loss factor
η_b	beam material loss factor
θ	receiver beam frequency parameter
ν	Poisson's ratio
ζ	viscous damping ratio
π	3.1415....
ρ	density
λ	wavelength
ϕ	source beam frequency parameter
$\psi_R^{(p)}$	eigenvector of p'th mode at point R
μ	mass/unit length, or area
ω	angular frequency
ω_o	natural frequency of mass upon a spring
ω_1	mass-spring-infinite beam resonance
ω_p	p'th natural frequency
Ω	spring mobility ratio
$\Delta\omega$	angular frequency bandwidth
Δf	frequency bandwidth
$\Delta N/\Delta\omega$	modal density, number of modes in an interval $\Delta\omega$

CHAPTER 1

INTRODUCTION

In many engineering installations, machines are, by necessity, mounted on large flexible structures, such as ship hulls or building floors. The machine, when in operation, transmits vibrations to the structure, thereby causing unwanted sound radiation at stations close to and remote from the excitation region.

The most usual step taken to reduce such sound radiation is to attempt to decouple the machine from the structure by mounting it upon vibration isolators. Naturally, such measures never achieve complete isolation and a certain amount of vibration transmission still occurs, which must either be tolerated, or quantified with a view to imposing further vibration control.

Two questions then arise: what physical parameter should be used to quantify either the vibration transmitted to a structure or the effectiveness of isolation, and can this parameter be measured?

Traditionally the force or acceleration level at the mounting points on the seating structure have been used to define the vibration transmission; in the case of acceleration this may be because it is an easily measurable quantity [1-6]. However, the answers provided only have meaning in relation to the particular installation, as no account is taken of the 'impedance' or frequency response of the vibrating structure.

An alternative approach, which is adopted here, is to define the vibration transmission in terms of the vibrational power flowing into the seating. Power is a single quantity giving an absolute measure of the vibration transmission as it embodies both the force and acceleration at the input points on the structure. This means that not only is the level of vibration monitored but also the 'impedance' or frequency response of the structure is also taken into account.

The power transmitted to a seating is a function of the characteristics of the machine, the isolator and the seating. Therefore if these characteristics are known it is possible to predict the power transmission. Little work has been done on the prediction of power transmission

between structures, nevertheless the already available methods for vibration analysis of coupled structures would be still appropriate. These methods may be split into two broad groups, namely, exact methods and approximate methods, both of which are briefly reviewed in the following paragraphs.

For the exact approach, for example [3, 7] matrix equations of machine, isolator and seating characteristics at all the connection points are set up, and solved using a digital computer. However, this approach requires a considerable amount of basic data which must be either measured or predicted.

The measurement of the point and transfer characteristics of structures with a view to making predictions of coupled behaviour has been carefully studied [8-11]. This involves great care, as for accurate prediction of resonance frequencies all the degrees of freedom at each of the connecting points must be considered [10]. This does not necessarily imply direct measurement of each of the degrees of freedom as, a 'modal' model of the structure can be made with the use of measured data at selected points [11,12], although such models are likely to break down when heavily damped structures are dealt with.

Alternatively it could be possible to predict the necessary characteristics using the 'Finite Element technique', a type of computer modelling [13,14]. However, such a method would only be useful at low frequencies as at high frequencies a prohibitively large number of points would be necessary to model the machine and seating. Also, the damping which would still have to be determined experimentally, can be so large in practice as to prevent clear modal behaviour.

Since these 'exact' approaches require much time and effort for their application and the final result cannot be always relied upon to be sufficiently accurate, some approximate methods for predicting power transmission between structures have been proposed. To make these estimates, much less data is needed than for the exact methods, and although the answers are only correct in an average sense, this is often all that is required.

The most well known, existing, approximate method for this type of structural study is Statistical Energy Analysis [15,16]. The method predicts the space and time averaged energy content of each component of a

coupled system. The transmission of power is calculated on the basis that the power flow between two arbitrarily coupled single degree of freedom oscillators is directly proportional to the energy difference between the oscillators. This principle is extended, with less rigour, to predict the power transmitted between multimodal systems, each mode being modelled as a single degree of freedom oscillator. Prediction is only straightforward if it is possible to assume 'weak coupling' between components. If the coupling is 'strong', rather complicated formulations become necessary [e.g., 17], which offer little advantage over any other 'exact' approach.

However, there appears to be little evidence that Statistical Energy Analysis has been applied to the machine isolator situation. This could be because extensive seating structures such as ships are damped to the extent that at higher frequencies they behave as systems of infinite extent rather than multimodal systems. Also the method is only suitable for random excitation, giving answers in terms of energy in a certain frequency bandwidth, whereas some machines mainly generate pure tones.

An alternative approach was hinted at by Skudrzyk [18] on observing that on a damped finite structure there was a frequency above which the point characteristic was the same as that of a structure of infinite extent. This phenomenon is explained thus: waves generated at the excitation point which then return via the reflecting boundaries are too heavily attenuated by losses to significantly interfere with the outgoing waves from the excitation point. References [19,20,21] give tables of the point characteristics of various infinite beam and plate components of the type which are incorporated in finite form in typical built up structures such as ships and buildings.

Therefore, by making these high frequency approximations to the seating characteristics it is relatively straightforward to predict approximate power transmission from simple machine sources [22,23]. Goyder [23] considers power transmission from machines which apply a 'velocity source' or 'force source' (see Section 1.2iv) at the top of an isolator, single and two-stage isolation systems are considered.

The first objective of this thesis is therefore to extend this work and to consider:

(i) the low frequency vibration when the seating, being finite, has resonant behaviour;

(ii) the effect of damping of the isolator;

(iii) not only rigid body motion of the machine (source) but also the resonant high frequency behaviour;

(iv) both broad band and pure tone excitation.

However, the same approach is adopted, that is, to derive algebraic formulae for power transmission in terms of frequency average or high frequency approximations of machine and seating characteristics. The advantage of this method is that the data are easily obtainable, and the significance of the various parameters can be readily understood, unlike those in a numerical solution generated by a computer.

Unless practical measurements of power flow can be made any theoretical predictions will have little credibility; therefore the second objective of this thesis was to propose various methods with which to measure the power transmitted to a structure from a machine. These methods require only acceleration data and a limited amount of structural frequency response data.

The thesis is presented in three parts. First the theoretical basis, second the power transmission measurement methods and, lastly, an experiment on a semi-practical machine-seating system which demonstrates application of the proposed techniques.

The most important step in the theory was the choice of model with which to represent a finite seating structure, having the resonant behaviour of many modes excited to different extents depending upon the distribution of the excitation. As only approximate formulae were being considered, the simplest possible type of seating that supports flexural wave motion was chosen, i.e., an end excited beam. The simplicity of this model is such that all the resonance modes are equally excited and evenly spaced in frequency. The advantage of this model is that the algebraic formula describing its point characteristic can be readily manipulated to give closed form solutions to various problems.

After the point characteristics of the structure are described, power transmission from a rigid mass in an isolator to a finite beam are calculated. The rigid mass could represent a machine in the low frequency region. At high frequencies, a machine can move in its natural modes of

vibration and behaves as a resonant source of vibration at the top of the isolator. Again a short finite beam was chosen to represent a machine in this region. Power transmission from this resonant source to a long finite beam or infinite beam was calculated. The results are presented in terms of frequency averaged power, appropriate for broad band excitation, and the peak possible power transmitted for the case of pure tone excitation.

The relevance of theoretical formulae have been checked using appropriate experiments.

1.1 Conventions and Definitions

(i) The convention chosen with which to describe a wave propagating in the positive x direction is

$$e^{i(\omega t - kx)} \tag{1.1}$$

where ω is the angular frequency or rate of change of phase with time, and k is the wavenumber, the rate of change of phase with distance.

(ii) Damping in solid structures is commonly modelled as being proportional to strain, thus it is conveniently incorporated in a complex Young's modulus [1].

$$\frac{\text{stress}}{\text{strain}} = E(1 + i\eta) \quad \text{assuming an } e^{i\omega t} \text{ frequency dependence} \tag{1.2}$$

where E is the Young's modulus and η is the hysteretic loss factor of the material.

This representation leads to a complex wave number, $\bar{k}$, which for flexural wave motion of a beam is approximately

$$k(1 - \frac{i\eta}{4}) \tag{1.3}$$

where

$$k = \omega^{\frac{1}{2}} \sqrt[4]{\frac{\rho A_o}{EI}} , \tag{1.4}$$

and I is the second moment of area of the cross section and A_o the cross sectional area.

(iii) All the analyses presented here assume the structural components to be passive linear mechanical systems. If such a system is excited with force of harmonic time dependence represented by $Fe^{i\omega t}$, then the response $\bar{X}e^{i\omega t}$ is simply related by the frequency response function $\bar{H}(\omega)$, i.e.,

$$\frac{\bar{X}}{F} = \bar{H}(\omega). \quad ^{\dagger}$$

Likewise, if the system is excited by a transient force $F(t)$, the force and response are simply related in the frequency domain by the frequency response function,

$$\frac{\bar{X}(\omega)}{\bar{F}(\omega)} = \bar{H}(\omega), \tag{1.5}$$

where $\bar{X}(\omega)$ and $\bar{F}(\omega)$ are the Fourier transforms of the response $x(t)$ and force $F(t)$, i.e.,

$$F(\omega) = \frac{1}{2\pi}\int_{0}^{\infty} F(t)e^{i\omega t}dt \tag{1.6a}$$

$$X(\omega) = \frac{1}{2\pi}\int_{0}^{\infty} X(t)e^{i\omega t}dt. \tag{1.6b}$$

There are several types of frequency response function referred to in the text, which are defined as follows.

$$\frac{\text{velocity}}{\text{force}} = \frac{\bar{V}(\omega)}{\bar{F}(\omega)} = \bar{M} \quad \text{mobility} \tag{1.7}$$

$$\frac{\text{force}}{\text{velocity}} = \frac{\bar{F}(\omega)}{\bar{V}(\omega)} = \bar{Z} \quad \text{impedance} \tag{1.8}$$

---

† Complex functions or parameters are denoted with a bar, thus: $\bar{X}$, $\bar{H}$, etc. Therefore complex frequency response functions which often take the form $H(i\omega)$ are equivalent to $\bar{H}(\omega)$ in this text.

$$\frac{\text{acceleration}}{\text{force}} = \frac{a(\omega)}{F(\omega)} = \bar{I} \quad \text{inertance} \quad (i\omega\bar{M}) \qquad (1.9)$$

$$\frac{\text{force}}{\text{acceleration}} = \frac{F(\omega)}{a(\omega)} = \bar{A} \quad \text{apparent mass} \quad \left(\frac{\bar{Z}}{i\omega}\right) \qquad (1.10)$$

(iv) There are two idealised types of excitation which may be applied to a structure; a 'force source' and a 'velocity source'.

A force source applies a constant force irrespective of the motion of the structure.

A velocity source moves the structure, at its point of application, inexorably with a constant velocity, irrespective of the loading.

(v) A force with harmonic time dependence $\bar{F}e^{i\omega t}$ acting at a point on a structure of mobility $\bar{M} = |M|e^{i\gamma}$ causes a velocity $\bar{V}e^{i\omega t}$ at that point. The time averaged power input P is given by

$$P = \frac{\omega}{2\pi}\int_{o}^{\frac{2\pi}{\omega}} \text{Re}\{\bar{F}e^{i\omega t}\}.\text{Re}\{\bar{V}e^{i\omega t}\}dt \qquad (1.11)$$

which on integration leads to the following alternative forms.

$$P = \tfrac{1}{2}.\text{Re}\{\bar{F}.\bar{V}^*\} = \tfrac{1}{2}|F|^2.\text{Re}\{\bar{M}\} = \tfrac{1}{2}|V|^2.\text{Re}\{Z\}. \qquad (1.12a\text{-}c)$$

In practice, acceleration rather than velocity would be monitored, and forces of random rather than harmonic time dependence often occur. In this case the expectation of time averaged $\omega \times$ power/Hz is given as

$$\omega \times P/Hz = \text{Im}\{\bar{G}_{Fa}\} = G_{FF}.\text{Im}\{\bar{I}\} = G_{aa}.\text{Im}\{\bar{A}\}. \qquad (1.13a\text{-}c)$$

where $\bar{G}_{Fa}$ is the force acceleration cross spectral density, G_{FF}, G_{aa} are the 'force and acceleration spectral densities', respectively. Re{ }, Im{ } denote real and imaginary parts. $\bar{M}$, $\bar{Z}$, $\bar{I}$, $\bar{A}$ are mobility, impedance, inertance and apparent mass, respectively. Only time averaged power P will be referred to in this text, as opposed to instantaneous power (the integrand of equation (1.11)).

(vi) G_{FF}, G_{aa}, equations (1.13a-c), would normally be referred to as power spectral densities to indicate that they have units (quantity)^2/Hz. However, this title is misleading when there is the possibility of true "power spectral densities" having units of Power/Hz. To avoid confusion therefore, G_{FF}, G_{aa} will be referred to as "force spectral density" or "acceleration spectral density" as appropriate.

(vii) Predictions for power transmission will be expressed in terms of power P, averaged over various frequency bands. These are: $\langle P \rangle$ is P averaged between two adjacent resonance frequencies of the seating structure; $\langle\langle P \rangle\rangle$ is $\langle P \rangle$ averaged between two adjacent resonance frequencies of the machine source structure. The average frequency interval between two source structure resonances will be much larger than that for the seating structure on account of the fact that the source structure is usually much smaller than the seating.

(viii) The envelopes of the peaks in power transmission will be predicted and denoted as: $\hat{P}$ as the peak value of P, $\langle \hat{P} \rangle$ as the peak value of $\langle P \rangle$.

PART 1

POWER TRANSMISSION TO RESONANT AND NON RESONANT BEAMS FROM RIGID AND RESONANT SOURCES

The power transmitted to a seating structure by a vibrating machine, supported upon vibration isolators, is dependent upon the frequency response characteristics of the individual components, namely: the machine or source structure, the isolators and the seating structure. In practice these components are complex structures and a thorough analysis would only be possible, for specific cases, using a digital computer.

However, in this first section, these complex structures are represented by simple elements, which, although very different in detailed behaviour, will have similar overall frequency characteristics. Using these simple elements, algebraic expressions for power transmission are obtained in terms of easily understood, controlling parameters. Furthermore, the results are presented in a form convenient for making approximate power transmission calculations for more complex configurations, which are less easily modelled.

The seating structure, which will be referred to as the receiver, is modelled by a beam with one end free and the other with an arbitrary termination. The excitation or coupling is always applied to the free end. The beam is studied in Chapter 2, and is then used in combination with various source structures in the subsequent chapters.

The isolator is always modelled by a simple stiffness with hysteretic damping. Only a single isolator is considered in this section for simplicity.

In Chapter 3, low frequency vibration is considered, that is when a machine moves as a rigid body, and may therefore be modelled as a simple mass element. At higher frequencies a machine can be a resonant source of vibration, deflecting in its natural modes of vibration. In Chapters 4 to 6 a free-free beam was chosen to represent such a source of vibration, being the simplest continuous structure with resonant behaviour.

The power transmission is expressed in two ways. Firstly, frequency averaged power, which is applicable for broad band excitation and, secondly, peak possible power, which can occur for single frequency excitation. In order to obtain these two quantities it is shown that it is only necessary to know the frequency averaged values at the real and imaginary components of mobility and the peak mobility, of the source and receiver, at the connection points.

CHAPTER 2

INPUT CHARACTERISTICS OF A FINITE BEAM AND POWER TRANSMISSION FROM A FINITE BEAM

2.1 Introduction

The power input to a structure is a function of the excitation and the input point characteristics of the structure. Equation (1.12) shows that if a 'force source' is applied to the structure, the power input is determined by the real component of mobility at that point. Likewise, when a velocity source is applied to the structure the power input is controlled by the real component of impedance at that point.

The purpose of this chapter is therefore to investigate the form of the real component of mobility and impedance of a finite continuous structure such as a beam or plate, which has internal damping and boundaries which allow for power transmission.

The structure chosen for this analysis is a damped finite beam terminated at an arbitrary boundary, which is excited at the free end. It was chosen because it was the simplest structure which satisfied the requirements, and the algebraic properties of the point mobility make it a useful 'approximate' representation for modelling the point mobility of general structures.

The real component of mobility of this structure is compared with two models.

(i) A beam of infinite extent, the simplified model with which to represent the point mobility of structures at high frequencies [21].

(ii) A single degree of freedom oscillator, which is commonly used to represent each mode of a structure at low frequencies, see for example [21].

The theoretical work was supplemented by experimental measurements comparing the point mobility of an infinite and finite beam.

2.2 Point Mobility and Impedance for an End Excited Beam

Figure 2.1 shows the beam chosen for the analysis. The force is applied at the free end at $x = 0$. The beam at $x = \ell$ is attached to an arbitrary structure.

The discontinuity at this boundary causes flexural waves incident upon it to be reflected with a fractional decrease in amplitude 'r' and a phase change δ radians, so $\frac{\text{reflected wave}}{\text{incident wave}} = re^{i\delta}$. The beam also has a frequency independent loss factor η_b. For harmonic excitation by a force at $x = 0$, the displacement along the beam 'y', with reference to figure 2.1, can be written as

$$\bar{y} = Be^{-ikx(1-i\eta_b/4)} + be^{-kx} + \alpha\hat{r}Be^{ikx(1-i\eta_b/4)} \qquad (2.1)$$

provided that $k\ell > 2.3$, which allows the near field term at $x = \ell$ to be omitted. k is the flexural wavenumber, $\alpha = e^{-\eta_b k\ell/2}$ is the attenuation due to damping of a wave travelling a distance 2ℓ, $\hat{r} = re^{i\theta}$. $\theta = \delta - 2k\ell$ is the phase change in a wave travelling distance 2ℓ.

Inserting the boundary conditions at $x = 0$,

$$F = EI \left.\frac{\partial^3 y}{\partial x^3}\right|_{x=0} \qquad 0 = \left.\frac{\partial^2 y}{\partial x^2}\right|_{x=0}$$

into (2.1), yields

$$b = B(1 + \alpha\hat{r}), \qquad B = -\frac{F}{EIk^3} \cdot \frac{1}{(1 + \alpha\hat{r} - i(1 - \alpha\hat{r})} . \qquad (2.2)$$

For harmonic excitation the velocity V is given as

$$\bar{V} = i\omega\bar{y}.$$

The mobility at $x = 0$, is found from equations (2.1) and (2.2) to be

$$\bar{M} = \frac{\bar{V}}{\bar{F}}\Big|_{x=0} = \frac{\omega}{EIk^3} \cdot \{\frac{1 - \alpha^2r^2 - i2\alpha r \cos\theta}{1 + \alpha^2r^2 - 2\alpha r \sin\theta} - i\}. \qquad (2.3)$$

Likewise, the impedance at $x = 0$ is

$$\bar{Z} = \frac{\bar{F}}{\bar{V}}\Big|_{x=0} = \frac{EIk^3}{2\omega} \cdot \{\frac{1 - \alpha^2r^2 - i2\alpha r \sin\theta}{1 + \alpha^2r^2 + 2\alpha r \cos\theta} + i\}. \qquad (2.4)$$

It is interesting to note that the point impedance and mobility are of similar form, hinting at the versatility of these functions in algebraic manipulation. On account of this similarity, only mobility will be considered in detail.

First, it can be seen that α and r are interchangeable. This permits equation (2.3) to be written in a more convenient form, i.e.,

$$\bar{M} = Q\{\frac{\cos\beta - i \sin\beta \cos\theta}{1 - \sin\beta \sin\theta} - i\}, \qquad (2.5)$$

where $\cos\beta = \frac{1 - \alpha^2r^2}{1 + \alpha^2r^2}$, $\sin\beta = \frac{2\alpha r}{1 + \alpha^2r^2}$, $Q = \frac{\omega}{EIk^3}$.

Note: $Q = \frac{\omega}{2EIk^3}$ for a beam constrained to have zero slope at the excited end;

$Q = \frac{\omega}{4EIk^3}$ for a beam with identical supports, excited at the centre.

A few observations may now be made.

(i) When αr becomes small, $\cos\beta$ tends towards unity and the mobility tends to that of a semi-infinite beam, i.e.,

$$\bar{M} = Q(1 - i) \qquad \alpha r \to 0$$

(ii) The real component of mobility is shown in figure 2.2 for various values of αr. Only values for $0 < \theta < 2\pi$ are plotted as the function is periodic. The beam resonance frequencies occur when $\theta = 2\pi n + \frac{\pi}{2}$ where n is an integer. At these frequencies the real component of mobility attains its maximum value of $\hat{Q}$ of magnitude

$$\hat{Q} = Q(1 + \alpha r)/(1 - \alpha r)$$

$$\simeq 2Q/\cos\beta \quad \text{for moderate damping } \alpha r > \tfrac{1}{2} \qquad (2.6)$$

Therefore from equation (1.12) it may be deduced that for 'force source' excitation, maximum power is input at these frequencies. Minimum power is input for this type of excitation when $\theta = 2\pi n - \frac{\pi}{2}$; at this frequency the real component of mobility takes a minimum value of $\check{Q}$

$$\check{Q} = Q(1 - \alpha r)/(1 + \alpha r)$$

$$\simeq (Q/2)\cos\beta \qquad (2.7)$$

(iii) However, if a velocity source is applied to the beam, maximum power is input when the real component of impedance is a maximum, which from equation (2.4) is when $\theta = (2n + 1)\pi$.

(iv) If a force source of constant spectral density, $\omega_1 < \omega < \omega_2$, equivalent to $0 < \theta < 2\pi$ in the θ plane, is applied to the beam, the frequency averaged power $\langle P \rangle$ may be derived from equation (2.3), $\langle P \rangle/Hz = G_{FF}.\langle Re\{\bar{M}\} \rangle$. In Appendix 1 it is shown that provided that θ does not change at a rate comparable with αr then

$$\langle Re\{\bar{M}\} \rangle = Q \qquad (2.8)$$

i.e., the average value of the real component of mobility of a finite beam is equal to that of a semi-infinite beam. ($\alpha r = 0$ in figure 2.2.) Therefore the average power to a beam can be written as $\langle P \rangle/Hz = G_{FF}.Q$. The restriction that θ does not change at a rate comparable with αr means that the result does not hold rigorously for periodically supported structures, or structures with built in boundaries for frequencies below the first resonance. In reference [24] the result in equation (2.8) has been demonstrated for a finite plate using a modal approach.

Note that the frequency averaged value of mobility (eqn. (2.8) is the geometric mean of the peak and trough values (eqns. (2.6), (2.7)).

2.3 The Ratio Between Power Input to and Transmitted from an End Excited Beam

The ratio between the power input to the beam at $x = 0$, and that transmitted through the boundary at $x = \ell$, can be determined from the power flow along the beam at these two points.

The power flow at any point along the beam is proportional to

$$|B_i(x)|^2 - |B_r(x)|^2. \tag{2.9}$$

$|B_i(x)|$ and $|B_r(x)|$ are the moduli of the incident travelling wave and reflected travelling wave at any position x on the beam. From equation (2.1), $|B_i(x)| = Be^{-k\eta_b x/4}$, $|B_r(x)| = \alpha r Be^{k\eta_b x/4}$. The power input and power transmitted are found by substituting in equation (2.9) with $x = 0$ and $x = \ell$, respectively. Thus the ratio of power transmitted P_{tr}, to power input, P_{in}, is given as

$$P_{tr}/P_{in} = \alpha(1 - r^2)/(1 - \alpha^2 r^2). \tag{2.10}$$

This ratio, which is necessarily less than unity, is constant for all values of θ. Therefore, maximum power is transmitted from $x = \ell$ when maximum power is input at $x = 0$, and minimum power is transmitted when minimum power is input at $x = 0$. Therefore the frequency averaged power transmitted is simply

$$\langle P_{tr} \rangle = \langle P_{in} \rangle \ .\alpha(1 - r^2)/(1 - \alpha^2 r^2). \tag{2.11}$$

For force source excitation, $\langle P_{in} \rangle$ is given from equation (2.8) as

$$\tfrac{1}{2}|F|^2.Q.$$

The importance of the relative magnitude of α and r is discussed in Chapter 4.

2.4 The Vector Plot Form of the End Excited Beam Mobility

Finite continuous structures, composed of beam and plate-like elements, theoretically have an infinite number of natural frequencies. In the region of each natural frequency the behaviour can be modelled by that of a single degree of freedom oscillator, and the overall behaviour is therefore given by the sum from an infinite number of oscillators. It is therefore of interest to compare the behaviour of the finite beam model, equation (2.5), with that of a single degree of freedom system. This is best done by comparing the vector diagrams of the two system responses.

Equation (2.5) can be written as:

$$\bar{M} = X + iY$$

where

$$X = \frac{Q \cos \beta}{1 - \sin \beta \sin \theta} ; \qquad Y = - \frac{Q \sin \beta \cos \theta}{1 - \sin \beta \sin\theta} - Q.$$

By eliminating θ from the above two equations, the vector diagram form of the point mobility is defined by the function:

$$(Y + Q)^2 + (X - Q/\cos \beta)^2 = Q^2 \tan^2\beta. \qquad (2.12)$$

This function is plotted in figure 2.3. The following observations may be made.

(i) The plot is circular like that of a single degree of freedom system. The radius is $Q \tan \beta$, which for very heavy damping ($\cos \beta = 1$) tends to zero.

(ii) The centre of the circle is offset from the real axis by a distance Q. This effect is characteristic of beam point mobilities, and is caused by the wave which decays exponentially away from the driving point (see equation (2.1)). This decaying wave term does not occur for point driven plates or for longitudinal vibration of rods, and so the comparable form of mobility vector plot would have no offset in this direction.

(iii) The base of the circle is displaced from the imaginary axis by a distance $Q(1 - \alpha r)/(1 + \alpha r)$, which is approximately $(Q \cos \beta)/2$ for light damping. Thus it is seen that the real component of mobility is always greater than zero, unlike that of a single degree of freedom system, which tends to zero away from resonance.

2.5 Modal Loss Factor in Terms of the Material Loss Factor and the Boundary Reflection Coefficients

The loss factor of a piece of material vibrating in a certain mode, is described as the 'modal loss factor' η_m, defined as

$$\eta_m = \frac{\text{Energy dissipated/cycle of harmonic motion}}{2\pi . \text{ maximum energy stored in the cycle}} .$$

For a linear material the maximum energy stored is proportional to σ^2, where σ is the stress at a point, while the energy dissipated is proportional to σ^n. n for low stress levels, lies between 2 and 3 (see, for example, [25]). This being the case, it can be seen that the loss factor for a piece of material is a function of the stress, and therefore a function of amplitude of vibration and mode shape. However, if $n = 2$, the loss factor η_m becomes independent of stress, and therefore mode shape, and has the value of what is described as 'the material loss factor' η. In the following analysis it is assumed that $n = 2$, so that η, the material loss factor, is independent of wavelength and stress level.

Practical structures usually have modal loss factors which are a function of both the internal damping, and the energy transmission across the boundaries. Such a structure is modelled by the beam in figure 2.1. The modal loss factors of structures are often measured from the vector plot of the point mobility. This is done on the assumption that the behaviour in the frequency range close to resonance may be compared to that of a single degree of freedom system with a loss factor equal to the modal loss factor η_m. The objective of this analysis is therefore to express the modal loss factors of the beam (figure 2.1), measured in this manner, in terms of the material loss factor η and reflection coefficient r.

The vector diagram of the cantilever mobility for $0 < \theta < 2\pi$ is an offset circle (see figure 2.3). If the offset is ignored the vector diagram

becomes equivalent to that of a single degree of freedom system. Therefore, a comparison of the two circular vector diagrams will yield the equivalent modal loss factor η_m for the cantilever. The two diameters are

$$\frac{1}{\omega m \eta_m} = \frac{k}{2\omega\mu} \left(\frac{4\alpha r}{1 - \alpha^2 r^2}\right)$$

where m is the mass of the equivalent single degree of freedom system, μ is the mass/unit length of the beam. For higher modes of the beam $m = \frac{\mu \ell}{2}$. On substituting for m in the equation above the modal loss factor becomes

$$\eta_m = \frac{1 - \alpha^2 r^2}{\alpha r} \cdot \frac{1}{k\ell} \quad . \tag{2.13}$$

Above the first resonance, $k\ell \simeq p\pi$, where p is the mode number. Therefore the modal loss factor becomes

$$\eta_m \simeq \frac{1 - \alpha^2 r^2}{\alpha r} \cdot \frac{1}{p\pi} \quad . \tag{2.14}$$

Considering now the two limiting cases:

(i) no damping, i.e., $\alpha = 1$

$$\eta_m = \frac{1}{p\pi} \cdot \frac{1 - r^2}{r} \quad . \tag{2.15}$$

The modal loss factor is therefore only a function of the reflection coefficient 'r' and the mode number. The apparent loss factor decreases as the mode number increases.

(ii) no power transmitted through the boundary, i.e., $r = 1$.

By substituting for α (equation (2.1)), equation (2.14) becomes

$$\eta_m = \frac{2}{p\pi} \sinh \frac{p\pi\eta}{2} \quad . \tag{2.16}$$

When $\eta \frac{p\pi}{2}$ is small, the modal loss factor η_m is approximately equal to the material loss factor. However, as the mode number increases so the modal loss factor increases. The modal loss factor for a beam excited at the centre may also be found to be

$$\eta_m = \frac{4}{p\pi} \sinh \frac{p\pi\eta}{4} \ . \qquad (2.17)$$

The behaviour of the modal loss factor of a finite structure with internal damping, and boundaries allowing for power transmission, may be summarised as follows. At low frequencies, the modal loss factor will be controlled by transmission through the boundaries (equation (2.15)). The modal loss factor will decrease with increasing frequency until the damping becomes dominated by the internal damping (equation (2.16)). This value will then increase with increasing frequency. The material loss factor is therefore the lowest value of the modal loss factor.

2.6 Experimental Measurement of the Real Component of Mobility of an Infinite and Finite Beam

In the previous section, the theoretical relationship between the real components of mobilities of finite and infinite structures was established. This section describes experimental mobility measurements on a finite and 'infinite' beam* to verify these theoretical expressions.

The first mobility measurement was made on the 'infinite' beam. The experimental layout is shown in figure 2.4. A steel beam, of 6 mm by 5 cm cross section, and 6.21 m length, was suspended by four piano wires; 80 cm at each end of the beam were embedded in sand boxes designed to be anechoic terminations. The beam was excited in the centre of the 5 cm face by a coil and magnet arrangement. The rapid sweep method was used to measure the mobility [26].

Figure 2.5 shows the measured mobility of the 'infinite' beam in the usual form of presentation, i.e., modulus and phase. The measured and theoretical values agree well at frequencies above about 100 Hz. The theoretical value of mobility for an infinite beam is [21]

$$\bar{M} = \frac{\omega}{4EIk^3} (1 - i).$$

---

*The experimental model of an infinite beam will be referred to as the 'infinite' beam.

The real and imaginary components are equal in magnitude, giving rise to a constant phase of $-\frac{\pi}{4}$. The low frequency data was corrupted by noise.

The second set of mobility measurements were made on the beam after the sand boxes had been removed, as in figure 2.6. Both sides of this finite beam were covered with AQUAPLAS damping tape. The loss factor, as calculated from the decay time at free vibration, was found to have a frequency independent value of 0.008 between 0 and 1 kHz, the frequency range considered.

The same measurement conditions applied as for the 'infinite' beam.

The measured real component of mobility is shown in figure 2.7. The form compares reasonably well with that expected from figure 2.2, with the exception that all modes were not excited for the beam, as is the case for an end excited cantilever. The value of the real component of mobility of the infinite beam lies logarithmically between the peak and trough values.

It is worth noting from figure 2.8 that the small steps in the integral correspond to the contributions from each mode. The contribution by each mode is equal to that of an equivalent single degree of freedom system of mass m_p, i.e., $\pi/2m_p$ [21], where $m_p = \mu\ell/2$ for a centre-excited beam.

The peak heights are less than predicted as the beam was excited slightly off centre, thus causing the asymmetric modes to be excited more with increasing frequency, and the symmetrical modes to be excited less with increasing frequency.

In order to find the average value of the real component of mobility a running integral of figure 2.7 was made, which is shown in figure 2.8. It can be seen that this integral is close to that calculated for an infinite beam over the same frequency range. This therefore verifies the theoretical statement of equation (2.9).

2.7 Summary

A useful formula for point mobility of a finite structure has been derived having the following properties: (i) it has a similar form to the point impedance; (ii) the frequency averaged value is equivalent to that

of a structure of infinite extent; (iii) the formula models both high frequency 'infinite' beam behaviour and low frequency modal behaviour.

The ratio between power input to and transmitted from a finite structure is only a function of transmission coefficient at the boundary and the structure internal damping. Therefore, for force source excitation, maximum power is transmitted at resonance, when maximum power is input.

CHAPTER 3

POWER TRANSMISSION TO A FINITE AND INFINITE BEAM FROM A MASS, SUPPORTED UPON A SPRING, EXCITED BY A FORCE SOURCE

3.1 Introduction

In the previous chapter, the power input to a seating structure as a result of force or velocity source excitation was considered. However, in general the vibration of a machine at its support point cannot be represented so simply as it may have a mobility comparable with that of the seating structure. Therefore this chapter presents a general expression for power transmission between two structures coupled at a single point. The structure that generates the vibration will subsequently be referred to as the 'source', which transmits the power to the 'seating' structure or 'receiver'.

The general expression is applied to the specific example of power transmission, from a mass upon a damped spring, to a finite beam. This model was designed to represent the behaviour of an isolated machine upon a finite structure in the lower frequency range, through which the structure moves as a rigid body. The finite beam used in the theoretical analysis was that considered in the previous chapter.

Experimental measurements are made on a physical model of the above configuration to confirm the results.

3.2 Power Transmission Between Two Coupled Structures

Two structures, shown in figure 3.1 are coupled at points 2 and 3 by a hinge, which transfers normal force but no moments.

When the two structures are uncoupled, the velocity at point 2 is $\bar{V}_f$. On coupling, the velocity at point 2 becomes $\bar{V}_2$

$$\bar{V}_2 = \bar{V}_f + \bar{F}_2\bar{M}_2 \qquad (3.1)$$

which is equal to the velocity at point 3 on the receiving structure,

i.e.,

$$\bar{V}_2 = -\bar{F}_2\bar{M}_3 \tag{3.2}$$

where $\bar{M}_2$ and $\bar{M}_3$ are the point mobilities at points 2 and 3, respectively. Using equations (3.1) and (3.2) the force acting on the receiver $\bar{F}_2$ is given as

$$\bar{F}_2 = \frac{\dot{\bar{V}}_f}{\bar{M}_2 + \bar{M}_3} . \tag{3.3}$$

The time averaged power transmission to the receiver, P_{tr}, is

$$P_{tr} = \tfrac{1}{2}|\bar{F}_2|^2.\mathrm{Re}\{\bar{M}_3\} \tag{3.4}$$

or

$$P_{tr} = \tfrac{1}{2}\frac{|V_f|^2}{|\bar{M}_2 + \bar{M}_3|^2}.\mathrm{Re}\{\bar{M}_3\}.$$

If only a single force $\bar{F}_1$, acts on the source structure

$$P_{tr} = \tfrac{1}{2}|\bar{F}_1|^2.\ \frac{|\bar{M}_{12}|^2}{|\bar{M}_2 + \bar{M}_3|^2}.\mathrm{Re}\{\bar{M}_3\} \tag{3.5}$$

where $\bar{M}_{12}$ is the transfer mobility between points 1 and 2.

3.3 Power Transmission Between Two Structures Coupled by a Damped Spring

Figure 3.2 shows the systems under consideration. The source and receiving structures are coupled by a spring of mobility $(i + \eta)\omega/K$.[1] With reference to the previous sections, the mobility at point 3 is given as

$$\bar{M}_3 = (i + \eta)\omega/K + \bar{M}_R \tag{3.6}$$

where $\bar{M}_R$ is the point mobility of the receiving structure. On making this substitution into equation (3.3), $\bar{F}_2$ becomes

$$\bar{F}_2 = \bar{V}_f \ / \ (\bar{M}_2 + (i + \eta)\omega/K + \bar{M}_R) \tag{3.7}$$

---

(1) The mobility of a hysteretically damped spring is $(i + \eta)/(K(1 + \eta^2))$, but the η^2 term in the denominator is generally small enough to be neglected.

Because the force, $\bar{F}_2$, is the same at both ends of the massless spring, the power transmitted to the receiving structure becomes

$$P_{tr} = \tfrac{1}{2}|\bar{F}_2|^2 . \mathrm{Re}\{\bar{M}_R\}$$

or

$$P_{tr} = \tfrac{1}{2}|F_1|^2 . \frac{|\bar{M}_{12}|^2}{|\bar{M}_2 + \bar{M}_R + (i + \eta)\omega/K|^2} . \mathrm{Re}\{\bar{M}_R\} \qquad (3.8)$$

3.4 Power Transmission From a Mass to a Finite Beam via A Damped Spring

Equation (3.3) can be applied to the specific example shown in Figure 3.3, to calculate the frequency averaged and peak power transmission to a finite beam from a mass, m, excited by a force, $F_1 \sin \omega t$. This model is intended to represent a machine, vibrating at low frequencies, which is supported by isolators upon a finite structure.

The mobility $\bar{M}_R$ at the end of the beam is given from equation (2.5) as

$$\bar{M}_R = Q_r - iQ_i - iQ$$

where

$$Q_r = \frac{Q \cos \beta}{1 - \sin \beta \sin \theta} \quad ; \quad Q_i = \frac{Q \sin \beta \cos \theta}{1 - \sin \beta \sin \theta} \qquad (3.9)$$

Q is the frequency averaged value of the real component of mobility, i.e.,

$$Q = \frac{\omega}{EIk^3}$$

for a beam with an unconstrained end.

The source structure is the mass, so its point and transfer mobilities are

$$\bar{M}_2 = \frac{1}{i\omega m}$$

$$\bar{M}_{12} = \frac{1}{i\omega m} . \qquad (3.10)$$

By substituting equation (3.9) into equation (3.8), the power transmitted to the beam, P_{tr}, can be written as

$$P_{tr} = \tfrac{1}{2}.|\bar{F}_1|^2.\frac{1}{(\omega m)^2}.\frac{Q_r}{(Q_r + \frac{\eta\omega}{K})^2 + (Q_i + C)^2}, \qquad (3.11)$$

where

$$C = (Q + \frac{1}{\omega m} - \frac{\omega}{K}).$$

Substituting for Q_r and Q_i, from equation (3.9) and using the identity

$$Q_i^2 + Q_r^2 = Q^2.\frac{1 + \sin\beta \sin\theta}{1 - \sin\beta \sin\theta} \qquad (3.12)$$

in the algebraic manipulation, the power transmission becomes

$$P_{tr} = \tfrac{1}{2}|\bar{F}_1|^2.\frac{1}{(\omega m)^2}.\frac{Q\cos\beta}{u^2 + \frac{2\eta\omega}{K}.Q\cos\beta - \sin\beta\{u^4 - (\frac{2\eta\omega}{K}.Q)^2\}^{\frac{1}{2}}\sin(\theta - \gamma)} \qquad (3.13)$$

where $u^2 = Q^2 + C^2 + (\frac{\eta\omega}{K})^2$,

$$\tan\gamma = \frac{2QC}{C^2 + (\frac{\eta\omega}{K})^2 - Q^2}.$$

It can be observed that equation (3.13) is of the same form as the real component of the beam mobility, equation (3.9), but is a function of $\theta - \gamma$, rather than θ. The peaks in power transmission occur when $\theta - \gamma = 2n\pi + \frac{\pi}{2}$ at the resonances of the coupled system, rather than when $\theta = 2n\pi + \frac{\pi}{2}$ at the beam resonance frequencies.

3.4.1 Frequency average power transmission <P>

If the mass is excited by a random force of constant spectral density, G_{FF}, over a frequency range $\omega_1 < \omega < \omega_2$, equivalent to a θ interval $2n\pi < \theta < 2(n + 1)\pi$, the frequency averaged power transmission <P> is

the solution to the integral

$$\langle P \rangle = \frac{G_{FF}}{2\pi} \cdot \frac{1}{(\omega m)^2} \int_0^{2\pi} \frac{Q \cos \beta}{u^2 + \frac{2\eta\omega}{K} \cdot Q \cos \beta - \sin \beta \{u^4 - (\frac{2\eta\omega}{K} Q)^2\} \sin(\theta - \gamma)} \cdot d\theta \tag{3.14}$$

as it is assumed that θ changes rapidly compared to ω.

Using a standard result, see, for example, reference |27|

$$\frac{1}{2\pi} \int_0^{2\pi} \frac{d}{b - c \sin x} dx = \frac{d}{(b^2 - c^2)^{\frac{1}{2}}} \qquad b > c \tag{3.15}$$

where b, c and d are constants, the integral in equation (3.14) can be solved, giving the frequency averaged power as

$$\langle P \rangle = G_{FF} \cdot \frac{1}{(\omega m)^2} \cdot \frac{Q}{u^2 + \frac{\eta\omega}{K} \hat{Q}} , \tag{3.16}$$

where $\hat{Q}$, the peak receiver mobility is

$$\hat{Q} = \frac{2Q}{\cos \beta} .$$

Therefore $\langle P \rangle$ to a general structure can be estimated if the frequency averaged, Q, and peak values, $\hat{Q}$, of the real component of receiver mobilities are known.

Equation (3.16) is plotted in figure 3.4, from which it can be seen that there are three regions of interest:

(i) At the coupled mass-spring-infinite beam resonance frequency*, ω_1, u^2 takes its minimum value, causing $\langle P \rangle$ to reach a maximum value of $\langle \hat{P} \rangle$, where

$$\langle \hat{P} \rangle = G_{FF} \cdot \frac{1}{(\omega m)^2} \cdot \frac{Q}{Q^2 + \frac{\eta\omega}{K} \hat{Q} + (\frac{\eta\omega}{K})^2} . \tag{3.17}$$

---

*The coupled mass-spring-infinite beam resonance frequency, ω_1, occurs when $C = 0$, and is slightly higher than the resonance frequency of a mass upon a blocked spring ω_o.

The maximum possible value of this expression occurs when the receiver beam is so heavily damped that it behaves as an infinite beam, and the isolator damping is light, i.e., if

$$Q^2 > \frac{\eta\omega}{K} \cdot \hat{Q},$$

$$\langle P \rangle = G_{FF} \cdot \frac{1}{(\omega m)^2} \cdot \frac{1}{Q}, \qquad \omega = \omega_1 .$$

However, by decreasing the receiver beam damping and increasing the isolator damping until

$$Q^2 < \frac{\eta\omega}{K} \hat{Q},$$

the frequency averaged power transmission is reduced to

$$\langle P \rangle = G_{FF} \cdot \frac{1}{(\omega m)^2} \cdot \frac{Q}{\frac{\eta\omega}{K} \hat{Q}}, \qquad \omega = \omega_1 .$$

Therefore it may be said that the isolator damping is important in controlling power transmission at the mass-spring-infinite beam resonance frequency, ω_1.

(ii), (iii) At frequencies above and below ω_1, the force applied to the beam is independent of the beam motion, i.e, it behaves as a 'force source'. This is because the mobility at the foot of the spring and mass is greater than the mobility of the beam. In these regions the frequency averaged power transmission is given by the 'force source approximations'. These are

$$\langle P \rangle = G_{FF} \cdot Q \qquad \omega < \omega_1 \qquad (3.18)$$

$$\langle P \rangle = G_{FF} \cdot \left(\frac{\omega_o}{\omega}\right)^4 \cdot Q \qquad \omega > \omega_1 \qquad (3.19)$$

where $\omega_o^2 = \frac{K}{m}$.

These values are independent of receiver beam and isolator damping and hence are the same for a finite or infinite beam receiver.

3.4.2 Peak and trough values of transmitted power, $\hat{P}$, $\check{P}$

In the previous section the frequency averaged power transmission was calculated. However, if the receiver beam is finite there is a peak and a trough in power transmission associated with each beam mode of vibration, as indicated by equation (3.13). The frequency averaged value is in fact the geometric mean of these peak and trough values. In this section the envelope of the peak $\hat{P}$, and trough P values of power are calculated.

The envelope of peak values of transmitted power $\hat{P}$ can be found from equation (3.13) by letting $\sin(\theta - \gamma) = 1$, and $\sin\beta = 1 - \frac{\cos^2\beta}{2}$, giving

$$\hat{P} = \langle P \rangle . g \tag{3.20}$$

where

$$g = \frac{u^2}{u^2 + \frac{\eta\omega}{K}\hat{Q}} \cdot \frac{\hat{Q}}{Q} . \tag{3.21}$$

Likewise, by substituting $\sin(\theta - \gamma) = -1$ into equation (3.13) the envelope of the trough power is given as

$$\check{P} = \langle P \rangle . \frac{1}{g} .$$

$\hat{P}$ is plotted on figure 3.4; its behaviour may be divided into three regions.

$$\text{(i)} \quad \hat{P} = \langle P \rangle . \frac{\hat{Q}}{Q} \qquad u^2 > \frac{\eta\omega}{K}\hat{Q} \tag{3.22}$$

at high and low frequencies when the 'force source' approximations are valid.

$$\text{(ii)} \quad \hat{P} = G_{FF} . \frac{1}{(\omega m)^2} \cdot \frac{K}{4\eta\omega} \qquad u^2 = \frac{\eta\omega}{K}\hat{Q}. \tag{3.23}$$

This is the maximum possible value of power transmission and is only a function of the mass and real component of the spring mobility. The spring damping is therefore important in limiting the peak possible power transmission. It should be noted that this value does not always occur, but depends upon the correct matching conditions.

Now it is likely that $u^2 = \eta\omega/K.\hat{Q}$ at frequencies close to ω_o, in which case equation (3.23) becomes

$$\hat{P} = G_{FF} \cdot \frac{\omega}{4\eta K}, \quad \omega = \omega_o. \tag{3.24}$$

(iii) $\hat{P}$ has a minimum at the mass-spring-infinite beam resonance when $u^2 < \frac{\eta\omega}{K}\hat{Q}$ and $\langle P \rangle$ is a maximum.

3.5 Experimental Measurements of Power Transmission

Experiments were made on the type of system considered in the previous section. There were two main objectives. First, to measure the power input at the top of the isolator, and the power transmitted to the 'infinite' and finite seatings, and to make comparisons with the theoretical predictions. Secondly to compare two alternative means of measuring the power transmitted to the seating.

3.5.1 Experimental layout

Figure 3.5 shows the arrangement for the power flow experiment. The force excitation, provided by the coil and magnet, acted on a 4 cm x 4 cm x 0.9 cm steel block, weighting 0.142 kg, at position 1. This mass was supported at the corners by four columns of natural rubber, each measuring 1.2 cm x 1.2 cm x 2 cm, arranged to accommodate an accelerometer at the centre of the underside of the mass.

The feet of the four rubber columns were attached to an aluminium block, position 2, which could be regarded as rigid and of negligible mass for the frequency range considered. The aluminium block was connected via a washer, to ensure point loading, to the centre of the beam considered in section 2.5. The beam was made 'infinite' or finite as before using the sand boxes.

3.5.2 Experimental procedure

Three experiments were performed with the following conditions:

(i) Experiment 1: broadband random excitation between 0-1 kHz, for which frequency range the isolator behaves as a simple spring, 'infinite beam' seating.

(ii) Experiment 2: as experiment 1, but with a finite beam seating.

(iii) Experiment 3: broadband random excitation between 0-4 kHz, 'infinite beam' seating.

As a preliminary requirement to each of the power transmission experiments, it was necessary to measure, using the rapid sweep method, the apparent masses of the system elements (apparent mass is defined as the force per unit acceleration). The measurements were:

(a) the point apparent mass of the seating, $\bar{A}_R$ (while the mass and isolator were not attached).

(b) The point apparent mass of the assembled mass, isolator and beam at position (1), $\bar{A}_S$.

(c) The transfer apparent mass of the disconnected isolator $\bar{A}_{12}$. This involved blocking the base of the isolator while imposing an acceleration at the top. The acceleration at the top, and the resulting blocked force at the base were monitored. Figure 3.6 shows the real and imaginary parts of the isolator transfer apparent mass in the 0-1 kHz frequency range. For this range the isolator behaved as a simple spring with hysteretic damping. The transfer apparent mass therefore took the form

$$\bar{A}_{12} = \frac{K}{\omega^2}(1 + i\eta). \qquad (3.25)$$

The stiffness, K, calculated from figure 3.6, agreed well with the statically measured value of 7.6×10^4 N/m. The loss factor can be seen to be 0.1. Figure 3.7 shows the modulus and phase of $\bar{A}_{12}$ in the frequency range 0-4 kHz. The first standing wave in the isolator occurred between 1 and 2 kHz.

For the power transmission experiments a band limited random force acted on the mass. The acceleration signals a_1 and a_2, at points (1) and (2) were monitored, the two signals were conditioned using matched

amplifiers and cut-off filters. The acceleration spectral densities of the two signals G_{a_1}, G_{a_2} and the cross spectral density $\bar{G}_{a_1 a_2}$ were calculated.

Using equation (1.13c), the power input at position (1), P_{in}, is given as:

$$P_{in}/Hz = \frac{1}{\omega} \mathrm{Im}\{\bar{A}_S\}.G_{a_1} . \tag{3.26}$$

Likewise, the power transmitted to the beam P_{tr}, was calculated using the imaginary part of the beam point apparent mass, $\mathrm{Im}\{\bar{A}_R\}$,

$$P_{tr}/Hz = \frac{1}{\omega} \mathrm{Im}\{\bar{A}_R\}.G_{a_2} . \tag{3.27}$$

The power transmitted to the beam was also calculated using the isolator transfer apparent mass $\bar{A}_{12}$ in the expression

$$P_{tr}/Hz = \frac{1}{\omega} \mathrm{Im}\{\bar{A}_{12}.\bar{G}_{a_1 a_2}\} . \tag{3.28}$$

The use of this expression is justified in Section 7.4. Each of the above expressions involves the multiplication of two data files. This is only possible if both files have the same frequency increment, which is ensured by using an identical sampling rate for both measurements.

All power flow spectra were normalised with respect to the force spectral density, to permit comparison of results. In addition, the power flow spectra are all multiplied by a factor of ω, to provide a compact presentation.

3.5.3 Discussion of results

(i) Figure 3.8 shows the power input to the isolator and that transmitted to the 'infinite' beam, for experiment 1.

The curve for force source approximations, equations (3.18) and (3.19), agreed reasonably well with the experimental results for frequencies above and below the power flow peak at about 120 Hz. This power flow peak

occurred at the mass-spring-infinite beam resonance frequency. Its magnitude was accurately predicted from equation (3.17).

The ratio between power input to the isolator, P_{in}, and that transmitted, P_{tr}, is given by the relationship

$$P_{tr}/P_{in} = Re\{\bar{M}_R\}/(Re\{\bar{M}_R\} + \eta\omega/K), \qquad (3.29)$$

where $\bar{M}_R$ is the point mobility of the beam.

Now $Re\{\bar{M}_R\} = \eta\omega/K$ at $\simeq$ 150 Hz. Therefore, at frequencies below about 150 Hz the power transmitted was only slightly less than that input to the isolator because $Re\{\bar{M}_R\} > \eta\omega/K$, but for frequencies above 150 Hz most power was dissipated in the isolator as $\eta\omega/K > Re\{\bar{M}_R\}$. However, although these trends are seen in figure 3.8, the measured level of P_{in} above 150 Hz is suspected to be an over-estimation, caused by noise in the measured value of $Im\{\bar{A}_S\}$, which is likely when the $\{\bar{A}_S\} >> Im\{\bar{A}_S\}$.

(ii) Figure 3.9 compares the power transmitted to the finite beam, from experiment 2, with that transmitted to the 'infinite' beam. It can be seen that the frequency averaged power input to the finite beam was equal to that transmitted to the 'infinite' beam for frequencies above and below the mass-spring-infinite beam resonance. In the region of this resonance the frequency averaged input power to the finite beam was less than that to the 'infinite' beam as was seen in figure 3.4. The prediction of peak frequency averaged power from equation (3.17) is seen to be of the correct order of magnitude. In fact it is worth noting that the 'force source' approximations (equations (3.18) and (3.19)) give reasonable estimations of frequency averaged power through the whole frequency range.

The size of the fluctuations in power from the frequency averaged level are seen to behave as predicted in figure 3.4, the minimum fluctuation occurring when the frequency averaged power is a maximum. It can be observed that the maximum possible value of peak power transmission did not occur, as it is dependent upon the existence of ideal conditions.

Figure 3.10 compares the power input to the isolator with that transmitted to the finite beam. It is seen that, around the region of peak frequency averaged power transmission, only a fraction of the power

input to the isolator is transmitted to the beam. This is because in this region when $\omega \simeq \omega_o$, the point mobility of the spring and mass in series at the free end of the spring is a minimum. This low value is less than the beam point mobility and so the spring and mass act as a velocity source on the beam, thereby transmitting most power when the beam impedance is a maximum, i.e., near the beam antiresonances when $Re\{\bar{M}_R\}$ is small. Therefore, as the power being transmitted when $Re\{\bar{M}_R\}$ is small, from equation (3.29) it can be seen that the isolator damping becomes very effective as

$$\eta\omega/K >> Re\{M_R\}.$$

(iii) Figure 3.11 shows the power input to the isolator and transmitted to the 'infinite' beam between 0-4 kHz. It can be seen that there was a peak in power transmission at the isolator resonances. Again the level of the power input to the isolator is thought to be an overestimation, as for experiment 1.

Figure 3.12 compares the power transmitted as measured using the two methods given in equations (3.27), (3.28). There is good agreement at frequencies up to about 3 kHz when the isolator transfer apparent mass method failed, due to either the cumulative inaccuracies inherent in multiplying two complex data files, or phase errors due to digitizing analogue data. Despite this high frequency limitation, the isolator transfer apparent mass method is probably the most useful for frequencies below the first isolator resonance, as estimations of power can be made using only the isolator dynamic stiffness and the measured accelerations at the ends of the isolator.

3.6 Conclusions

Simple formulae for peak and frequency averaged power transmission from a mass to a finite seating in a spring-like isolator have been developed, describing the following behaviour.

(i) At high and low frequencies when the mass behaves as a force source or velocity source at the top of the isolator, the frequency averaged power transmission to a finite or infinite receiving beam is the same.

(ii) Maximum power transmission occurs between the force and velocity source regions, at the resonance frequency of the coupled mass-spring and infinite beam. At this frequency the power transmission decreases with increasing isolator damping or decreasing receiver beam damping. Therefore in this frequency region the frequency averaged power transmission to a finite beam is less than to an equivalent infinite beam.

Two practical methods of measuring power were successfully used to experimentally verify the above formulae. These were:-

(i) Power input at a point in the structure can be measured by multiplying the imaginary component of the point apparent mass by the acceleration spectral density at that point.

(ii) Power transmission through an isolator can be measured using the isolator transfer apparent mass and the cross spectrum of the accelerations above and below the mount.

CHAPTER 4

POWER INPUT TO AND TRANSMITTED FROM A FINITE SOURCE BEAM TO A SEMI-INFINITE BEAM, VIA A DAMPED SPRING

4.1 Introduction

Low frequency power transmission from a machine to a seating structure was considered in the previous chapter. It is followed here with an investigation of power transmission in the mid-frequency range, when a machine behaves as a resonant source of vibration, moving in its natural modes of vibration.

It is obviously impossible to accurately model a machine with a simple element. Nevertheless, in this chapter a free-free beam has been chosen to represent a machine, this representation being simple enough to permit analysis, but containing the essential features of a resonant structure. Such a representation is not entirely fanciful, as it has been observed in [13] that an automotive diesel engine behaves as a beam in the mid frequency range, i.e., below the first resonance of the individual panels.

The vibration isolator is again represented by a damped spring, and the seating structure in this chapter is a semi-infinite beam.

The analysis is merely an application of section 2.3, predicting power input to the source beam and power transmitted by the isolator in terms of the source beam internal damping and the transmission coefficient at the beam-isolator junction.

An experimental investigation of this arrangement is reported in Chapter 6.

4.2 Power Input to and Transmitted from a Finite Beam Coupled to an Arbitrary Structure

A short finite beam, which will be referred to as the 'source beam', is connected to an arbitrary structure at end 2, as shown in figure 4.1. End 1 of the beam is excited by a force of sinusoidal time dependence $F_1 \sin \omega t$.

When the source beam is disconnected from the arbitrary structure the point mobility at each end of the beam is identical, and is given as

$$\bar{M}_1 = \bar{M}_2 = S_r - iS_i - S,$$

where $$S_r = \frac{S \cos \varepsilon}{1 - \sin \varepsilon \sin \phi}, \qquad S_i = \frac{S \sin \varepsilon \cos \phi}{1 - \sin \varepsilon \sin \phi}, \tag{4.1}$$

where S is the frequency averaged value of the real component of mobility (that of a semi-infinite beam). ε is the damping parameter defined, setting $r = 1$ in equation (2.5), by

$$\cos \varepsilon = \frac{1 - \alpha^2}{1 + \alpha^2} = \tanh \eta_b k\ell/2 \tag{4.2}$$

where $\alpha = e^{-\eta_b k\ell/2}$, is the attenuation due to damping of a wave travelling twice the length of the beam, 2ℓ. For a moderately damped end excited beam $\cos \varepsilon \simeq \eta_b k\ell/2$.

ϕ, the source beam frequency parameter, is the phase change in a wave travelling twice the length of the beam, and for a free-free beam is given as $-(2k\ell + \frac{\pi}{2})$. When $\phi = 2n\pi + \frac{\pi}{2}$, where n is an integer, resonance occurs and the real component of mobility takes its peak value $\hat{S}$ of

$$\hat{S} = 2S/\cos \varepsilon, \tag{4.3}$$

for light damping.

When the source beam is connected to a structure at point 2, the reflection coefficient r at that boundary becomes less than unity and the power input at point 1 can be written, using equations (1.12b) and (2.3) as

$$<P_{in}>^{*} = \tfrac{1}{2}|F_1|^2 \cdot S \cdot \frac{1 - \alpha^2 r^2}{1 + \alpha^2 r^2 - 2\alpha r \sin(\phi + \frac{\pi}{2} + \delta)} \qquad (4.4)$$

where $re^{i\delta}$ is the reflection coefficient at the boundary.

The form of this expression, shown in figure 5.2, can be seen to be similar to that of the real component of mobility of the disconnected source beam, equation (4.1). However, the maximum power, $<\hat{P}>$, is input when $\sin(\phi + \frac{\pi}{2} + \delta) = 1$, at the coupled resonance frequencies, rather than at the resonance of the uncoupled beam, where $\sin \phi = 1$.

The power transmitted to the arbitrary structure is given from equation (2.10) as

$$<P_{tr}> = <P_{in}> \cdot \alpha(1 - r^2)/(1 - \alpha^2 r^2) \qquad (4.5)$$

from which it can be seen that the ratio between input and transmitted power is independent of ϕ_1, (i.e., it is the same at the resonance frequency or remote from the resonance frequency) and is only dependent upon the relative magnitudes of r and α.

The frequency averaged power input, $<<P_{in}>>$, is obtained by averaging equation (4.4) over the frequency range between two source beam resonances, i.e., $0 < \phi < 2\pi$, giving

$$<<P_{in}>> = \tfrac{1}{2}|F_1|^2 \cdot S \qquad (4.6)$$

and can be seen to be independent of α and r.

Likewise, the frequency averaged power transmission $<<P_{tr}>>$ can be calculated from equations (4.5) and (4.6) as

---

Power as a function of the source beam parameter ϕ alone is denoted by $< >$. In this chapter it is assumed that the receiving structure is of infinite extent, having no resonances. Therefore the power is not a function of θ, the receiver frequency parameter.

$$\langle\langle P_{tr}\rangle\rangle = \tfrac{1}{2}|F_1|^2 . S . \frac{\alpha(1 - r^2)}{(1 - \alpha^2 r^2)} . \tag{4.7}$$

The peak power input and transmitted occurs when the term $\sin(\phi + \frac{\pi}{2} + \delta)$ in equation (4.4) is equal to unity. Then the envelope of the peaks is given as

$$\langle \hat{P}_{in} \rangle = \langle\langle P_{in}\rangle\rangle . \frac{1 + \alpha r}{1 - \alpha r} \tag{4.8}$$

and

$$\langle \hat{P}_{tr} \rangle = \langle\langle P_{tr}\rangle\rangle . \frac{1 + \alpha r}{1 - \alpha r} . \tag{4.9}$$

The trough power input and transmitted power occur when $\sin(\phi + \frac{\pi}{2} + \delta) = -1$, then

$$\langle \check{P}_{in} \rangle = \langle\langle P_{in}\rangle\rangle . \frac{1 - \alpha r}{1 + \alpha r} \tag{4.10}$$

$$\langle \check{P}_{tr} \rangle = \langle\langle P_{tr}\rangle\rangle . \frac{1 - \alpha r}{1 + \alpha r} . \tag{4.11}$$

From equations (4.8)-(4.11) it can be observed that the frequency averaged values of input and transmitted power lie geometrically between the peak and trough values. Also the peak to trough ratio is identical in both cases. From equations (4.6)-(4.11) it can be seen that the frequency averaged peak and trough values of power are controlled by the relative magnitudes of α and r. The behaviour may be summarised into three regions, which are given in Table 1.

(i) At low frequencies $r < \alpha$

or $t^2 > 2 \cos \varepsilon$

where t, the modulus of the transmission coefficient is related to the reflection coefficient r by

$$t^2 = 1 - r^2 . \tag{4.12}$$

In this regime all the power input to the source beam is transmitted to the arbitrary structure. The ratio between the peak and trough power is governed by the transmission coefficient. The lower the transmission

coefficient the greater the peak possible power input and transmitted at resonance.

(ii) When $r = \alpha$ or $t^2 = 2 \cos \varepsilon$,

half of the power input to the source beam is dissipated in the source beam, and half of the power is transmitted from the source beam. This is the condition for peak possible power, i.e., $\langle \hat{P}_{tr} \rangle$ takes its maximum value of

$$\langle \hat{P}_{tr} \rangle_{max} = \tfrac{1}{2} |F|^2 . \frac{\hat{S}}{4} . \qquad (4.13)$$

Hence the maximum possible power transmitted from a resonant structure is one quarter of the maximum possible power input to the uncoupled resonant structure $(\tfrac{1}{2}|F|^2.\hat{S})$.

(iii) When $r > \alpha$ or $t^2 < 2 \cos \varepsilon$,

the frequency averaged transmitted power becomes less than that input, as most of the power is dissipated in the source beam. The size of the peak to trough power ratio is controlled by the damping in the source beam, hence end 2 of the source beam behaves as a velocity source to the attached arbitrary structure.

It is worth noting that $\langle P_{tr} \rangle$ is independent of the damping in the first beam and is controlled by t^2.

4.3 Power Input to and Transmitted from a Finite Beam Coupled to a Semi-infinite Beam by a Damped Spring

The configuration for this analysis is shown in figure 4.2. The source beam is excited at end 1 by a force, while end 2 of the beam is coupled to a semi-infinite beam by a damped spring. If the damping of the source beam and the transmission coefficient at the boundary are known, then the frequency averaged $\langle\langle P \rangle\rangle$, peak $\langle \hat{P} \rangle$, and trough $\langle \check{P} \rangle$ values of power can easily be found from equations (4.6)-(4.11). For the sake of clarity the effects of transmission coefficient and source beam damping are considered separately, as follows:-

4.3.1 The effect of transmission coefficient on $\langle\hat{P}\rangle$, $\langle\check{P}\rangle$ and $\langle\langle P\rangle\rangle$

The general expression for the transmission coefficient, t, is derived in Appendix II, equation (A.II.3). For the specific case of two coupled beams, $\bar{M}_2$ and $\bar{M}_R$ in this equation are given by the respective semi-infinite beam mobilities, of the source and receiver

$$\bar{M}_2 = S - iS$$

$$\bar{M}_R = Q - iQ$$

giving

$$t^2 = \frac{4S(Q + \eta\omega/K)}{(Q + S + \eta\omega/K)^2 + (Q + S - \omega/K)^2}. \qquad (4.14)$$

If it is assumed that there is no isolator damping, equation (4.14) can be rearranged in terms of the peak transmission coefficient $\hat{t}^2$ and the spring mobility ratio Ω, i.e.,

$$t^2 = \frac{\hat{t}^2}{1 + (1 - \Omega)^2}, \qquad (4.15)$$

where

$$\hat{t}^2 = \frac{4QS}{(Q + S)^2} \qquad (4.16)$$

$$\Omega = \frac{\omega/K}{Q + S},$$

$\langle\hat{P}\rangle$, $\langle\check{P}\rangle$ and $\langle\langle P\rangle\rangle$ for the power input to, and transmitted from the undamped source beam can now be formed from equations (4.6)-(4.11), by setting $\alpha = 1$, and by making use of the approximation

$$\frac{1 + r}{1 - r} \approx \frac{4}{t^2} - 2, \qquad t^2 < \tfrac{1}{2}. \qquad (4.17)$$

The frequency averaged power input and transmitted become

$$\langle\langle P_{in}\rangle\rangle = \langle\langle P_{tr}\rangle\rangle = \tfrac{1}{2}|F_1|^2.S.$$

The peak and trough power input and transmitted are

$$\langle \hat{P}_{in} \rangle = \langle \hat{P}_{tr} \rangle \simeq \tfrac{1}{2} |F_1|^2 . S . \left| \frac{4}{t^2} - 2 \right| , \tag{4.18}$$

$$\langle \check{P}_{in} \rangle = \langle \check{P}_{tr} \rangle \simeq \tfrac{1}{2} |F_1|^2 . S \left| \frac{t^2}{4 - 2t^2} \right| , \tag{4.19}$$

$\langle\langle P \rangle\rangle$, $\langle \hat{P} \rangle$ and $\langle \check{P} \rangle$ are plotted in figure 4.3 as functions of Ω and $\hat{t}^2$. In general it can be seen that decreasing the transmission coefficient by varying $\hat{t}$ or Ω has no effect on $\langle\langle P \rangle\rangle$ but increases the ratio between the peak $\langle \hat{P} \rangle$ and trough power $\langle \check{P} \rangle$. The effect of varying $\hat{t}$ and Ω individually is now examined.

(a) The effect of varying $\hat{t}^2$

At very low frequencies ($\Omega = 0.1$) the spring mobility is so small that the beams behave as if coupled by a simple hinge. The transmission coefficient is governed only by the relative magnitudes of the two beam mobilities, given by equation (4.15) as

$$t^2 \simeq \frac{\hat{t}^2}{2} ,$$

which is a frequency independent function.

Under this condition the maximum coupling occurs if the two beams are identical, i.e., $Q = S$, giving $\hat{t}^2 = 1$, and

$$t^2 \simeq \tfrac{1}{2} .$$

Looking at values of power at $\Omega = 0.1$ in figure 4.3, it can be seen that as $\hat{t}^2$ decreases, on account of the beam mobility mismatch, so the ratio between peak $\langle \hat{P} \rangle$ and trough power $\langle \check{P} \rangle$ increases.

(b) The effect of varying Ω

If now a constant value of $\hat{t}^2$ is maintained, the envelopes of peak and trough power in figure 4.3 may be divided into two regions:-

(i) First, at low frequencies when $\Omega < 2$ (i.e., $\frac{\omega}{K} < 2(S + Q)$ the ratio between the peak and trough values of power is less than the $\Omega = 0.1$ value, on account of the spring improving the coupling between the two beams. When $\Omega = 1$, the maximum value of transmission coefficient occurs, namely,

$$t^2 = \hat{t}^2.$$

(ii) At higher frequencies, when $\Omega > 2$, the spring causes a decrease in the coupling between the two beams and the transmission coefficient tends towards

$$t^2 \simeq \frac{4QS}{(\omega/K)^2} . \qquad (4.20)$$

As a result of the decrease in t^2 the envelopes of peak and trough power are seen to diverge.

It is interesting to note that, when there is light source damping, the maximum possible power input and transmission at the resonances is very high. At these frequencies the power input is large because the source beam response is large and is therefore able to absorb power very easily from the force source excitation, which has been assumed in this model.

4.3.2 The effect of source beam damping on $\langle\hat{P}\rangle$, $\langle\check{P}\rangle$ and $\langle\langle P\rangle\rangle$ of input and transmitted power

The effect of source beam damping upon $\langle\hat{P}\rangle$, $\langle\check{P}\rangle$ and $\langle\langle P\rangle\rangle$ was covered generally in section 4.2, parts (i), (ii) and (iii), and the results are summarised in Table 1. These equations, as applied to the specific example of a source beam coupled to an infinite beam by a spring, are plotted in figures 4.4-4.7.

Figure 4.4 shows $\langle\hat{P}\rangle$, $\langle\check{P}\rangle$ and $\langle\langle P\rangle\rangle$ of the transmitted power for $\hat{t}^2 = 0.5$ and $2/\cos\varepsilon = 30$.

Figures 4.6 and 4.7 show the effect of varying the source beam damping, while maintaining $\hat{t}^2$ constant.

From figures 4.6 and 4.7 it can be seen that there are two regions of different behaviour:-

(i) First, from figures 4.3 and 4.4 it can be seen that when

$$t^2 > 2 \cos \varepsilon$$

the source beam damping is ineffective, and all power input to the source beam is transmitted to the infinite receiver beam. The values of $\langle \hat{P} \rangle$, $\langle \check{P} \rangle$ and $\langle\langle P \rangle\rangle$ are therefore those given for the undamped source beam in figure 4.3.

However, when the frequency is increased until $t^2 = 2 \cos \varepsilon$ then only half of the power input to the source beam is transmitted to the infinite beam, as seen in figure 4.7. Figure 4.6 shows that under this condition the peak possible value of power transmission can occur, namely,

$$\langle \hat{P} \rangle_{max} = \tfrac{1}{2} |F_1|^2 . \frac{\hat{S}}{4} ,$$

which is controlled by the source beam damping.

(ii) In the second zone, defined by $t^2 < 2 \cos \varepsilon$, most of the power input to the source beam is dissipated by the internal damping. The source beam behaves as a velocity source connected to the spring, therefore the ratio of peak to frequency averaged power is the same as the peak to frequency averaged real component of mobility of the source beam, i.e.,

$$\frac{\langle \hat{P} \rangle}{\langle\langle P \rangle\rangle} = \frac{\hat{S}}{S} = \frac{2}{\cos \varepsilon} .$$

Figure 4.6 shows that $\langle \hat{P} \rangle$ decreases with increasing source beam damping, but $\langle \check{P} \rangle$ is independent of the source beam damping, and is given by

$$\langle \check{P} \rangle \simeq \tfrac{1}{2} |F_1|^2 . S . \frac{t^2}{4} .$$

The frequency averaged power transmission $\langle\langle P \rangle\rangle$, given in figure 4.7 is the geometric mean of $\langle \hat{P} \rangle$ and $\langle \check{P} \rangle$ and is given as

$$\langle\langle P_{tr} \rangle\rangle \simeq \tfrac{1}{2} |F_1|^2 . \hat{S} . \frac{t^2}{4}, \qquad (4.21)$$

which by substituting from equation (4.20), is at high frequencies equal to

$$\langle\langle P_{tr} \rangle\rangle \simeq \tfrac{1}{2} |F_1|^2 . \hat{S} . \frac{QS}{(\omega/K)^2} . \tag{4.22}$$

In summary it can be said that an isolator is only effective in reducing power transmission to a seating of infinite extent when

$$\left(\frac{\omega}{K}\right)^2 > \hat{S}.Q. \tag{4.23}$$

4.3.3 The effect of isolator damping upon $\langle \hat{P} \rangle$, $\langle \check{P} \rangle$ and $\langle\langle P \rangle\rangle$

The transmission coefficient for the system under consideration, when the isolator is damped, is given in equation (4.14), as

$$t^2 = \frac{4S(Q + \frac{\eta\omega}{K})}{(Q + \frac{\eta\omega}{K} + S)^2 + (Q + S - \frac{\omega}{K})^2} .$$

As the isolator is massless, the forces at the opposite ends of the isolator are identical. Hence the ratio of power input at the top of the isolator to that transmitted to the infinite beam is given by the ratio of the real components of mobility, namely,

$$\frac{\text{Power input at top of isolator}}{\text{Power transmitted to infinite beam}} = \frac{Q}{Q + \frac{\eta\omega}{K}} . \tag{4.24}$$

The power transmitted to the receiver beam is given from equations (4.24) and (4.5) as

$$\langle P_{tr} \rangle = \langle P_{in} \rangle . \frac{\alpha(1 - r^2)}{1 - \alpha^2 r^2} . \frac{Q}{Q + \frac{\eta\omega}{K}} . \tag{4.25}$$

Therefore it can be observed that the isolator damping only has any significance when $Q < \frac{\eta\omega}{K}$. This term is therefore not very important at low frequencies when ω/K is comparable with $S + Q$, neither is the damping term important at high frequencies when the source beam behaves as a velocity source. However, the damping term can be most significant when $t^2 = 2 \cos \epsilon$, in the region where comparable quantities of power are dissipated in the source and receiver beams.

In this case the peak possible power transmission becomes

$$\hat{P} = \tfrac{1}{2}|F_1|^2 \cdot \frac{\hat{S}}{4} \cdot \frac{Q}{Q + \frac{\eta\omega}{K}} . \qquad (4.26)$$

If $Q < \frac{\eta\omega}{K}$, by making use of equation (4.23) in equation (4.25) the peak possible power transmission becomes

$$\hat{P} \simeq \tfrac{1}{2}|F_1|^2 . \frac{\omega}{4\eta K}, \qquad \omega^2 = \hat{S}.Q.K^2. \qquad (4.27)$$

Equation (4.27) has the same form as equation (3.24) (the peak power transmission from a mass upon an isolator). Thus it is seen that the isolator damping can limit the maximum possible power transmission between two coupled systems.

4.4 Chapter Summary

The power input at one end of a short source beam, and the power transmitted via an isolator from the source beam to a semi-infinite receiver beam has been investigated. Formulae for peak power and frequency averaged power have been derived.

(i) Power is input and transmitted at the resonances of the coupled beam system.

(ii) At low frequencies all the power input to the source beam is transmitted to the receiver beam, until a frequency is reached when $(\omega/K)^2 = Q\hat{S}$, where (ω/K) is the isolator

mobility, $\hat{S}$ is the peak source beam mobility, and Q is the real component of source beam mobility.

(iii) Above this frequency the source beam behaves as a velocity source of magnitude V_f at the top of the isolator; the power transmitted is then simply given by $\frac{1}{2}|V_f|^2.Q/(\omega/K)^2$.

CHAPTER 5

POWER TRANSMISSION BETWEEN A SHORT FINITE SOURCE BEAM AND A LONG FINITE RECEIVER BEAM COUPLED BY A DAMPED SPRING

5.1 Introduction

The previous chapter dealt with power transmission between a short source beam and a semi-infinite receiver beam. Power transmission was calculated in terms of ϕ the source beam frequency parameter, and the ω dependent mobilities, Q, S and ω/K. It was seen that peaks in power transmission are associated with each source beam mode of vibration, there being one peak in each $2n\pi < \phi < 2(n + 1)\pi$ interval. The envelopes of the peak $\langle\hat{P}\rangle$, and trough power $\langle\check{P}\rangle$ and the frequency averaged power $\langle\langle P\rangle\rangle$ were calculated.

However, when the receiver beam is long, but finite as in figure 5.1, it exhibits resonant behaviour, and each mode of vibration is associated with a peak in power transmission. In this analysis it is assumed that the receiver dimensions are large compared to those of the source thereby having a much higher modal density at a given frequency, i.e., the receiver beam frequency parameter, θ, is much greater than ϕ the source beam frequency parameter. The power transmission plots will therefore take the form shown in figure 5.3, in which the rapid fluctuation in power due to receiver resonances are superimposed upon overall trend governed by the source beam characteristics.

Figure 5.3 indicates the quantities that are calculated in this chapter.

First, $\langle P\rangle$, a function of ϕ, is the frequency averaged power transmitted to the receiver beam obtained by averaging over a frequency interval equal to that of the difference between two receiver resonance frequencies, i.e., $(2n\pi < \theta < 2(n + 1)\pi)$.

Secondly, $\langle\hat{P}\rangle$ and $\langle\check{P}\rangle$ are the envelopes of the peak and trough values of $\langle P\rangle$, respectively.

Thirdly, $\langle\langle P\rangle\rangle$ is the frequency averaged value of $\langle P\rangle$, obtained by averaging over a frequency interval equal to the frequency spacing between two source beam resonances, i.e., $(2m\pi < \phi < 2(m + 1)\pi)$.

Lastly, $\hat{P}$ and $\check{P}$, functions of ϕ, are the envelopes of the peak and trough values of power transmitted to the receiver beam.

These analyses are given in detail in Appendix 4 but the procedure is summarised below.

5.2 General Expressions for Power Transmission to the Finite Receiver Beam

The general expression for power transmission is given in equation (3.8) as

$$P_{tr} = \tfrac{1}{2}|F_1|^2 . \frac{|\bar{M}_{12}|^2 . \mathrm{Re}\{M_R\}}{|\bar{M}_2 + \bar{M}_R + \frac{\omega}{K}(i + \eta)|^2} \qquad (5.1)$$

For the source beam, $\bar{M}_2$ and $|\bar{M}_{12}|^2$ are functions of ϕ. $\bar{M}_2$ is given in equation (4.1) as

$$\bar{M}_2 = \frac{S.\cos\varepsilon - i \sin\varepsilon . \cos\phi}{1 - \sin\varepsilon . \sin\phi} - iS, \qquad (5.2)$$

and it is shown in Appendix 3 that

$$|\bar{M}_{12}|^2 = S_r \hat{S} \sin\varepsilon. \qquad (5.3)$$

Likewise, for the receiver beam, the mobility $\bar{M}_R$ is a function of θ,

$$\bar{M}_R = Q. \frac{\cos\beta - i \sin\beta \cos\theta}{1 - \sin\beta \sin\theta} - iQ \qquad (5.4)$$

where it is assumed that θ changes rapidly compared to ϕ.

By substituting in equation (5.1) with equations (5.2)-(5.4) and averaging P_{tr} over an interval $0 < \theta < 2\pi$, the θ averaged power transmission $\langle P \rangle$ can be written as

$$\langle P \rangle = \tfrac{1}{2}|F_1|^2 \cdot \frac{S \sin\varepsilon \cdot 2SQ}{u_2^2 + S\cos\varepsilon\left[\hat{Q} + 2\frac{\eta\omega}{K}\right] - \sin\varepsilon\left[u_2^4 - 4S^2Q_d^2\right]^{\frac{1}{2}} \cdot \sin(\phi - \gamma)} \tag{5.5}$$

where

$$u_2^2 = (S + Q - \omega/K)^2 + S^2 + Q_d^2 \tag{5.6}$$

$$Q_d^2 = Q^2 + \hat{Q}\eta\omega/K + (\eta\omega/K)^2 \tag{5.7}$$

$$\tan\gamma = 2\,\frac{S.(S + Q - \omega/K)}{u_2^2 - 2S^2}. \tag{5.8}$$

Equation (5.5) now has the form of the real component of the source mobility, except that it is a function of $(\phi - \gamma)$ rather than ϕ. This means that the maximum value of $\langle P \rangle$ does not occur at the source beam resonances when $\sin\phi = 1$, but at the resonances of the coupled system, when $\sin(\phi - \gamma) = 1$. Equation (5.8) shows that γ is slightly less for a finite beam compared with that for an infinite beam on account of the presence of the $\hat{Q}\eta\omega/K$ terms. Thus, theoretically, the peak value of $\langle P \rangle$ occurs at a slightly different frequency for a finite than for an infinite beam.

The envelope of the peak values of $\langle P \rangle$, namely $\langle \hat{P} \rangle$, is formed by setting $\sin(\phi - \gamma) = 1$, in equation (5.5), giving

$$\langle \hat{P} \rangle = \tfrac{1}{2}|F_1|^2 \cdot \frac{(\hat{S})^2.Q \sin\varepsilon \cdot u_2^2}{u_2^4 + u_2^2.\hat{S}\left[\hat{Q} + 2\eta\omega/K\right] + \left|\hat{S}^2 - 2S^2\right|Q_d^2}. \tag{5.9}$$

Likewise, the envelope of the trough values of $\langle P \rangle$, namely $\langle \check{P} \rangle$ is found by setting $\sin(\phi - \gamma) = -1$ in equation (5.5), giving

$$\langle \check{P} \rangle = \tfrac{1}{2}|F_1|^2 \cdot \frac{S^2.Q \sin\varepsilon \cdot u_2^2}{u_2^4 + u_2^2.\check{S}\left[\hat{Q} + \frac{2\eta\omega}{K}\right] - S^2Q_d^2}, \tag{5.10}$$

in which $\check{S} = \dfrac{S\cos\varepsilon}{2}$.

The frequency averaged value of $\langle P \rangle$, namely $\langle\langle P \rangle\rangle$, is found by averaging equation (5.5) over an interval $0 < \phi < 2\pi$, giving

$$\langle\langle P \rangle\rangle = \tfrac{1}{2}|F_1|^2 \cdot \frac{S.\hat{S} \sin \varepsilon . Q}{(u_2^4 + u_2^2 \hat{S}[\hat{Q} + \frac{2\eta\omega}{K}] + [S^2\hat{Q}^2 - 4S^2Q^2 + \hat{S}^2 Q_d^2])^{\frac{1}{2}}} \tag{5.12}$$

It could be shown that $\langle\langle P \rangle\rangle$ lies geometrically between $\langle \hat{P} \rangle$ and $\langle \check{P} \rangle$.

Equations (5.9)-(5.12) can be written in a more convenient form by defining a transmission coefficient t_d,

$$t_d^2 = \frac{4QS}{u_2^2} = \frac{4QS}{S^2 + Q_d^2 + (S + Q - \frac{\omega}{K})^2} \cdot \tag{5.13}$$

This term is very similar to the transmission coefficient to an infinite beam receiver, defined in equation (4.12). Dividing equations (5.9)-(5.10) by u_2^4, gives

$$\langle \hat{P} \rangle = \tfrac{1}{2}|F_1|^2 \cdot \frac{S \sin \varepsilon}{(\frac{\cos \varepsilon}{t_d})^2 + (\frac{\cos \varepsilon}{\cos \beta}) + \frac{t_d^2}{4} \cdot (\frac{Q_d}{Q})^2}, \tag{5.14}$$

$$\langle \check{P} \rangle = \tfrac{1}{2}|F_1|^2 \cdot \frac{S \sin \varepsilon}{\frac{4}{t_d^2} + (\frac{\cos \varepsilon}{\cos \beta})} \cdot \tag{5.15}$$

Likewise, by dividing equation (5.12) by u_2^2 gives

$$\langle\langle P \rangle\rangle = \tfrac{1}{2}|F_1|^2 \cdot \frac{S \sin \varepsilon}{|(\frac{2 \cos \varepsilon}{t_d^2})^2 + (\frac{\cos \varepsilon}{\cos \beta}) \cdot \frac{4}{t_d^2} + (\frac{\cos \varepsilon}{\cos \beta})^2 + (\frac{Q_d}{Q})^2|^{\frac{1}{2}}} \tag{5.16}$$

The parameters controlling the power transmission will now be discussed more fully by comparing the power transmission to infinite and finite receiver beams.

5.3 Power Transmission to a Semi-infinite Receiver Beam

The power transmission to a semi-infinite beam receiver can be found from equations (5.9)-(5.12), by substituting $\hat{Q} = 2Q$ (as $\cos\beta = 1$). Also Q_d from equation (5.7) becomes

$$Q_d = Q + \frac{\eta\omega}{K} ,$$

and t_d, by comparison with equation (4.12), becomes

$$t_d^2 = t^2 . \frac{Q}{Q + \frac{\eta\omega}{K}} .$$

$\langle\hat{P}\rangle$, $\langle\check{P}\rangle$ and $\langle\langle P\rangle\rangle$ can now be written as

$$\langle\hat{P}\rangle \simeq \tfrac{1}{2}|F_1|^2 . \frac{S \sin}{\left|\frac{\cos}{t_d} + \frac{t_d}{2} . \frac{Q_d}{Q}\right|^2} \qquad (5.17)$$

$$\langle\check{P}\rangle \simeq \tfrac{1}{2}|F_1|^2 . \frac{S \sin\varepsilon . t_d^2}{4} \qquad (5.18)$$

$$\langle\langle P\rangle\rangle \simeq \tfrac{1}{2}|F_1|^2 . \frac{S \sin\varepsilon}{\frac{2\cos\varepsilon}{t_d^2} + \frac{Q_d}{Q}} \qquad (5.19)$$

These equations are good approximations to those derived in section (4.3), the only assumption inherent in these above being $Q \neq S$. Although dealt with in the previous section, the effect of the parameters controlling the power transmission to a semi-infinite beam receiver are summarised again here for convenience.

From equations (5.17)-(5.19) it can be seen that there are three main parameters controlling the power transmission:- the transmission coefficient t_d^2, the source beam damping parameter $\cos\varepsilon$, and the ratio $Q/(Q + \frac{\eta\omega}{K})$. Equation (5.19) shows the two regimes of behaviour.

(i) At low frequencies when $t_d^2 > 2 \cos \varepsilon$, the power transmission is controlled by the transmission coefficient and isolator damping.

(ii) At higher frequencies when $t_d^2 < 2 \cos \varepsilon$, the power transmission is controlled by the source beam damping.

5.4 Power Transmission to a Finite Beam Receiver

The power transmission as expressed in equations (5.14)-(5.16) are summarised in Table 2, for convenience, but the main points are covered as follows:

When the receiver beam is finite rather than infinite, $\cos \beta$, in equations (5.14)-(5.16) becomes much smaller than unity. This affects the controlling parameters in a manner now described. First, Q_d, defined in equation (5.7) becomes larger than for the semi-infinite receiver case, indicating that isolator damping is more effective when the receiver is finite. Second, t_d^2, defined in equation (5.13), decreases on account of the increase in Q_d. Finally, a new parameter is introduced, namely $\cos \varepsilon / \cos \beta$, defined by

$$\frac{\cos \varepsilon}{\cos \beta} = \frac{\hat{Q}}{Q} \cdot \frac{\mathbf{S}}{\hat{\mathbf{S}}},$$

which will be referred to as the 'damping ratio' between the two beams. When the receiver beam is semi-infinite this ratio has its minimum value of $\cos \varepsilon$, but the ratio increases as the receiver beam becomes more lightly damped. For practical structures, with the source much smaller than the receiver, one would expect

$$\frac{\cos \varepsilon}{\cos \beta} < 1.$$

(i) The effect of $\frac{\cos \varepsilon}{\cos \beta}$ on $\langle \hat{P} \rangle$, $\langle \check{P} \rangle$ and $\langle\langle P \rangle\rangle$

The effect of this damping ratio $\frac{\cos \varepsilon}{\cos \beta}$ on $\langle \hat{P} \rangle$, $\langle \check{P} \rangle$ and $\langle\langle P \rangle\rangle$ is shown in figures 5.4 and 5.5, respectively, where it is assumed that there is no isolator damping, i.e., $Q_d = Q$.

First, looking at figure 5.4, it is seen that the $\langle \hat{P} \rangle$ for the finite beam receiver has a break point, on account of the $\cos \varepsilon / \cos \beta$ term, when

$$t_d^2 = \cos \beta \cos \varepsilon,$$

or

$$(\frac{\omega}{K})^2 \simeq \hat{S}.\hat{Q}. \tag{5.20}$$

At high frequencies when $t^2 < \cos \beta \cos \varepsilon$, $\langle \hat{P} \rangle$, $\langle \check{P} \rangle$ and $\langle\langle P \rangle\rangle$ are the same as for a semi-infinite beam receiver, as in this frequency regime the source beam behaves as a velocity source connected to the isolator.

However at low frequencies when $t^2 > \cos \beta \cos \varepsilon$, $\langle \hat{P} \rangle$ decreases with decreasing receiver damping, taking the value

$$\langle \hat{P} \rangle = \tfrac{1}{2} |F_1|^2 . \frac{\cos \beta}{\cos \varepsilon} S \sin \varepsilon. \tag{5.21}$$

$\langle \check{P} \rangle$ remains the same as for a semi-infinite beam receiver, namely,

$$\langle \check{P} \rangle = \tfrac{1}{2} |F_1|^2 . S \sin \varepsilon . \frac{t_d^2}{4} \tag{5.22}$$

$\langle\langle P \rangle\rangle$, shown in figure 5.5, is simply the geometric mean of $\langle \hat{P} \rangle$ and $\langle \check{P} \rangle$ namely,

$$\langle\langle P \rangle\rangle = \tfrac{1}{2} |F_1|^2 . \frac{t_d}{2} . (\frac{\cos \beta}{\cos \varepsilon})^{\frac{1}{2}} . S \sin \varepsilon \tag{5.23}$$

Figures 5.4 and 5.5 express the main difference in power transmission to finite and semi-infinite beam receivers. The situation may be summed up in practical terms as follows. A source structure such as a machine is less well coupled to a finite receiver than to an infinite receiver if there is no effective isolator. Therefore adding an isolator does not cause as much further decoupling for the finite receiver case as for the

infinite receiver case. With regard to the frequency averaged power transmission it is obviously advantageous to make the ratio $\cos \varepsilon / \cos \beta$ as large as possible.

In the event of the source beam being so highly damped that

$$\frac{\cos \varepsilon}{\cos \beta} > \frac{4}{t_d^2}$$

equations (5.14)-(5.16) and figure 5.4 show that $\langle \hat{P} \rangle$ becomes so small that it is equal to $\langle \check{P} \rangle$, then

$$\langle \hat{P} \rangle = \langle \check{P} \rangle = \langle\langle P \rangle\rangle = \tfrac{1}{2} |F_1|^2 . S \sin \varepsilon . \frac{\cos \beta}{\cos \varepsilon} \qquad (5.24)$$

which is independent of transmission coefficient.

(ii) The effect of the isolator damping on $\langle\langle P \rangle\rangle$, $\langle \hat{P} \rangle$ and $\langle \check{P} \rangle$

The isolator damping can reduce the power transmission under two sets of circumstances. The first is under the conditions given in the previous section, when the power transmission is partly governed by t_d^2, as seen in equations (5.21)-(5.23). Now if $Q > S$, including isolator damping causes $Q \rightarrow Q_d$ thereby decreasing t_d^2 further. The effect of this is shown in figure 5.6. $\langle \hat{P} \rangle$ remains unaffected but $\langle \check{P} \rangle$ drops with increasing isolator damping. The isolator damping effectively causes a greater mismatch between the two beams.

The second set of circumstances for the isolator damping to have a significant effect is when

$$\left(\frac{Q_d}{Q}\right)^2 > \frac{\cos \varepsilon}{\cos \beta} \cdot \frac{4}{t_d^2} \qquad (5.25)$$

i.e., when the source damping is light compared to that of the receiver and when the source and receiver are well coupled. Under this condition, equations (5.14)-(5.16) become

$$\langle\hat{P}\rangle = \tfrac{1}{2}|F_1|^2.S \sin\varepsilon \cdot \frac{4}{t_d^2} \cdot \left(\frac{Q}{Q_d}\right)^2, \tag{5.26}$$

$$\langle\check{P}\rangle = \tfrac{1}{2}|F_1|^2.S \sin\varepsilon \ \frac{t_d^2}{4}, \tag{5.27}$$

$$\langle\langle P\rangle\rangle = \tfrac{1}{2}|F_1|^2.S \sin\varepsilon. \frac{Q}{Q_d}, \tag{5.28}$$

which are the same expressions as given for the semi-infinite receiver case, only in that instance $Q_d = Q + \frac{\eta\omega}{K}$. $\langle\hat{P}\rangle$ and $\langle\check{P}\rangle$ are plotted in figure 5.7, for the example when $S > Q$. It is seen that the isolator damping reduces $\langle\hat{P}\rangle$ but leaves $\langle\check{P}\rangle$ unaffected. As $\langle\langle P\rangle\rangle$ lies geometrically between $\langle\hat{P}\rangle$ and $\langle\check{P}\rangle$ it also decreases as seen in equation (5.28).

5.5 The Envelope of the Peaks and Troughs in Power Transmission to a Finite Beam $\hat{P}$ and $\check{P}$

The final quantities to be calculated, as seen in figure 5.3, are the envelope of the peaks and troughs in power transmission $\hat{P}$ and $\check{P}$, and also the maximum possible value of the $\hat{P}$. These quantities are calculated in Appendix 4, and the results are summarised as follows.

(i) At high frequencies when $t_d^2 < \cos\beta \cos\varepsilon$, the envelope of the peaks $\hat{P}$ is simply related to $\langle P\rangle$ in the same way as the peak value of receiver mobility $\hat{Q}$ is related to the frequency averaged value of Q in equation (2. 6), i.e.,

$$\hat{P} = \langle P\rangle. \frac{2}{\cos\beta}. \tag{5.29}$$

Likewise the envelope of the troughs $\check{P}$ is

$$\check{P} = \langle P\rangle. \frac{\cos\beta}{2}. \tag{5.30}$$

This is true even at the coupled resonances when $\sin(\phi - \gamma) = 1$, therefore the peak possible power in this regime is

$$\hat{P}_{max} = \langle P \rangle . \frac{2}{\cos \beta} \quad . \tag{5.31}$$

The reason for this simple relationship between $\hat{P}$ and $\langle P \rangle$ is that the source beam behaves as a velocity source driving the top of the isolator at constant velocity irrespective of the receiver mobility.

(ii) At lower frequencies when $t_d^2 > \cos \beta \cos \varepsilon$ the relationship between $\hat{P}$, $\breve{P}$ and $\langle P \rangle$ is illustrated in figure 5.3.

In the region of the troughs in $\langle P \rangle$, the relationship between $\hat{P}$ and $\langle P \rangle$ is as given before in equation (5.29), i.e.,

$$\hat{P} = \langle P \rangle . \frac{2}{\cos \beta} \quad .$$

However at either side of the peak in $\langle P \rangle$ when $\langle P \rangle = \frac{1}{2} \langle \hat{P} \rangle$ two peaks in $\hat{P}$ occur, both being of magnitude

$$\hat{P}_{max} = \frac{\langle \hat{P} \rangle}{2} . \frac{1}{\cos \beta} = \tfrac{1}{2} |F_1|^2 . \frac{\hat{S}}{4} . \tag{5.32}$$

Therefore, the maximum possible power transmission is limited by the source characteristics, and is equal to one quarter of the maximum possible power input to the uncoupled source structure. This is the same maximum value as was calculated for the semi-infinite beam receiver, in that instance this value could only occur at one frequency when $t^2 = 2 \cos \varepsilon$. However, for the finite beam receiver this maximum can occur in the region of every coupled resonance when $\sin(\phi - \gamma) = 1$, provided $t^2 > \cos \beta \cos \varepsilon$.

Although it has not been possible to include the effect of isolator damping into this analysis on account of the complexity of the problem, it can be estimated that the solution is approximately given from equation (5.32) as

$$\hat{P}_{max} = \frac{\langle \hat{P} \rangle}{2} . \frac{1}{\cos \beta} \tag{5.33}$$

where $\langle \hat{P} \rangle$ is given in equation (5.26).

5.6 Summary

When the receiver beam is finite, the frequency averaged power transmission at low frequencies is always less than that to the equivalent semi-infinite beam because finite beam resonances lead to beam vibration that tends to reduce the force transmitted by the isolator. In this frequency range the power transmission is governed by one of the two following factors.

(i) If the source beam damping is light and the isolator damping is high, most of the power input to the source beam is absorbed in the isolator. The frequency averaged power transmission to the receiver beam is governed by a parameter Q/Q_d, i.e.,

$$\text{Power input/Power transmitted} = Q/Q_d \tag{5.34}$$

where $Q_d^2 = Q^2 + \frac{\eta\omega}{K}.\hat{Q} + (\frac{\eta\omega}{K})^2$, $\hat{Q}$ is the peak receiver beam mobility, $\frac{\eta\omega}{K}$ is the real component of the isolator mobility. In these circumstances the source beam acts as a velocity source upon the isolator when

$$(\omega/K)^2 > \hat{S}Q_d. \tag{5.35}$$

(ii) If there is light isolator damping, the input power is partly dissipated in the source beam and partly in the receiver beam. For this to be so $\hat{S}/S$ must be of the same order as $\hat{Q}/Q$, i.e., the source beam must be heavily damped. Under this condition the source beam behaves as a velocity source upon the isolator when $(\omega/K)^2 > \hat{S}\hat{Q}$. (5.36)

At high frequencies when criteria (5.35) and (5.36) are both satisfied, the source beam behaves as a velocity source, i.e., it moves with the same velocity as if unconnected to the isolator. In this frequency region the frequency averaged power transmission to a finite beam is the same as to an equivalent infinite beam.

CHAPTER 6

EXPERIMENTAL MEASUREMENTS OF POWER TRANSMISSION FROM A SHORT SOURCE BEAM TO AN INFINITE OR FINITE RECEIVER BEAM

6.1 Introduction

This chapter describes measurements intended to experimentally verify the theoretical predictions made in the previous chapters, 4 and 5. The physical configurations for these experiments are shown in figures 6.1 and 6.2. The short 'source' beam was coupled, at end 2, to a long 'receiver' beam, at point 3, by a rubber isolator. Power was input at end 1 of the source beam by a force, provided by a coil and magnet arrangement. For the first experiment the uncoupled end of the long receiver beam was embedded in a sand box, providing an anechoic termination, thereby simulating a semi-infinite beam. In the second experiment the sand box was removed allowing the receiver beam to exhibit resonant behaviour associated with a finite beam.

The objectives of the experiments were: first, to measure the power input at point 1 on the source beam, and the power transmitted to the infinite and finite receiver beams at point 3. Second, to measure the source and receiver beam properties and thereby predict the input and transmitted power at points 1 and 3, respectively.

This chapter therefore may be divided into three parts: a description of the properties of the individual components and an account of the power measurements, and finally a discussion of the results.

6.2 Description of Components

6.2.1 The source beam

The source beam consisted basically of 50 cm x 3.2 cm x 6 mm aluminium alloy bar. These parameters were chosen to satisfy the requirements of (i) a structure mobile enough to admit a measurable quantity of power; (ii) a source beam with a low modal density compared

to the receiver beam, but with resonances in the range of interest, i.e., 100 Hz - 4 kHz. Both sides of the beam were covered with a constrained layer damping treatment, which was composed of a layer of Evostick 6508 rubber-based adhesive, sandwiched by a 1 mm thick steel sheet. The damping treatment was applied to limit the dynamic range of the input power, and also to go a small way towards modelling a heavily damped machine structure.

The total mass of the beam was 0.49 kg.

6.2.1.1 The measurement of the source beam inertances ωS, $\omega \hat{S}$ and $\omega \check{S}$.

The disconnected source beam was suspended by piano wires. An impedance head, B & K type 8001, was attached at end 1 to monitor the input force and acceleration, while the response at end 2 was to be monitored by an accelerometer, B & K type 4344. The point inertance at position 1, $\bar{I}_1$, and the transfer inertance to end 2, $\bar{I}_{12}$, were measured using the rapid swept sinewave method |26|. The imaginary component of the point inertance at end 1 is given in figures 6.3 and 6.4, while the $|\text{transfer inertance}|^2$ is shown in figure 6.5. Inertance rather than mobility was used for all measurements as it is a more convenient quantity when acceleration signals are used. The behaviour of the beam, as shown in figures 6.3-6.5, may be split into three frequency regions.

(i) From figure 6.5 it can be seen that, for frequencies less than 50 Hz, the beam moved as a rigid body. The point inertance at ends 1 and 2 of the rigid beam can be shown to be

$$\bar{I}_1 = \bar{I}_2 = \frac{4}{m} \quad \text{where } m \text{ is the mass of the beam.} \tag{6.1}$$

This is four times larger than the point inertance at the centre of the beam, because the beam rotates in addition to moving in translation. Likewise the transfer inertance is given as

$$\bar{I}_{12} = -\frac{2}{m} \tag{6.2}$$

and

$$|\bar{I}_{12}|^2 = \frac{4}{m^2}$$

where m is the mass of the beam.

(ii) From figure 6.5 it can be seen that at approximately 50 Hz

$$\frac{4}{m^2} = \omega^2 S^2 \quad , \tag{6.3}$$

which becomes

$$k\ell = 2 \tag{6.4}$$

on making the substitution

$$S = \frac{k}{\mu\omega} \tag{6.5}$$

to equation (6.3), μ is the mass/unit length.

Above this frequency the flexibility of the beam controls the energy content, and the beam model described in equation (4.1) is applicable. It is worth noting that this transition occurs below the first resonance frequency.

By using the measured resonance frequencies in conjunction with the approximate wavenumber for the n^{th} mode of vibration of a free-free beam, namely,

$$k_n = (n + \tfrac{1}{2})\frac{\pi}{\ell} \quad , \quad n \text{ is an integer} \tag{6.6}$$

the wavenumber of the source beam was calculated to be

$$k = 0.72 f^{\frac{1}{2}}. \tag{6.7}$$

By substituting this expression into equation (6.3) the frequency averaged value of the imaginary part of the inertance is given as

$$\omega S = 0.75 f^{\frac{1}{2}}. \tag{6.8}$$

This value is plotted on figures 6.3 and 6.4 and can be seen to be the geometric mean of the peaks and troughs. Applying the measured values of $\omega\hat{S}$ and ωS to equation (4.3) gives

$$\frac{\hat{S}}{S} = \frac{2}{\cos \varepsilon} = 10^4 f^{-1}. \qquad (6.9)$$

The loss factor of the beam, (which is not required for power measurements,) can be calculated from equation (6.9) by substituting for $\cos \varepsilon$ in equation (4.2)

$$\eta_b = 1.5 \times 10^{-3} f^{\frac{1}{2}}. \qquad (6.10)$$

From figures 6.3 and 6.4 it can be seen that at about 10 kHz the envelopes of the peaks and troughs in the real components of mobility coincide. This indicates that above this frequency the real component of mobility of the finite beam is equal to that of an infinite beam, having no resonant behaviour. The envelope of the peaks is given from equations (4.2) and (6.9) to be $\hat{S} = 4S/(\eta_b k\ell)$.

Therefore 'infinite' behaviour occurs when $4/(\eta_b k\ell) < 1$.

This criterion may be compared with that stated by Skudrzyk [18] who stated that 'infinite' behaviour occurred when the half power bandwidth of the resonance $(\eta_b \omega)$ was greater than the spacing between the modes $(\Delta\omega)$, i.e., $\Delta\omega < \eta_b \omega_n$. This equation can be applied to the specific example of a beam by using the relationship between wave numbers and frequencies, i.e.,

$$k_n = \omega_n^{\frac{1}{2}} \sqrt[4]{\mu/EI}$$

and equation (6.6). Skudrzyk's criterion for the onset of the infinite behaviour then becomes $1 > 2\pi/(\eta_b k\ell)$, which is close to that stated above.

A comparison of figures 6.4 and 6.5 verifies the simple proportionality relationship between the real component of the point mobility and the square of the transfer mobility modulus expressed in equation (5.3) and Appendix 3.

(iii) At 300 Hz, in figures 6.4 and 6.5 there is a "noisy" trough in the measured imaginary component of inertance and transfer inertance, when the measured response becomes very small. Above this frequency the average value of inertance became half that of the average at low frequencies.

This phenomenon is analysed in Appendix 5. It is a result of the rotational inertia of the impedance head at the end of the beam. At 800 Hz the rotational impedance of the impedance head about the attachment point was equal in magnitude to the rotational impedance of the beam at that point. This prevented any power input at this frequency. At frequencies above 800 Hz the high rotational impedance of the impedance head prevented the beam from rotating, thereby reducing the point inertance by a factor of two, i.e.,

$$\bar{I}_1 = \frac{\omega S}{2}(1 + i), \tag{6.11}$$

The power input was halved, as reflected in the transfer inertance, giving

$$|I_{12}|^2 = \frac{\omega^2 S}{2} . \hat{S}. \tag{6.12}$$

6.2.2 The receiver beam

The receiver beam was made of steel and measured 6.12 m x 5 cm x 6 mm. It was suspended by four piano wires and both ends were initially free. A semi-infinite beam was experimentally modelled when the end remote from the attachment point 3 was embedded in a sand box. Both sides of the beam were covered with AQUAPLAS free layer damping tape, which was added to control the resonant response when the beam was 'finite', i.e., without the sand box. The damping treatment gave the beam a frequency independent loss factor of 0.008 through the range of interest.

6.2.2.1 The measurement of the receiver beam inertances ωQ, $\omega \hat{Q}$, $\omega \check{Q}$.

The point inertance at position 3 on the receiver beam, in the semi-infinite configuration was measured using the rapid swept sine wave method |26|. Position 3 was one centimetre from the end of the beam. The real and imaginary components of the apparent mass are shown in figure 6.6. Below 1 kHz the imaginary component of apparent mass was equal to the predicted value for an unconstrained end of a semi-infinite beam, i.e.,

$$\frac{\mu}{2k} = 1.36f^{-\frac{1}{2}} \quad . \tag{6.13}$$

However, this prediction is grossly inaccurate at 2.5 kHz when there was a large trough in the measured characteristic. This departure from the predicted value occurred for the same reasons as given to explain the change of behaviour, noted at 800 Hz, in the source beam characteristics: i.e., it occurred because of an additional mass having translational and rotational inertia at the beam tip. This mass consisted of the combination of the monitoring transducers (a force transducer B & K type 8200 and an accelerometer type 4333) and approximately 2 cm of the beam tip. The tip of the beam acted as a redundant mass because the excitation was necessarily applied a finite distance from the end. Appendix 5 shows that, in these circumstances the measured real component of apparent mass is the sum of the real component of the beam apparent mass, the mass of the transducers and beam tip. From the high frequency asymptotic value on figure 6.6 it can be seen that this redundant mass is equal to approximately 100 gms.

The measured imaginary component of inertance shown in figure 6.7 is derived from the reciprocal of the apparent mass in figure 6.6. The additional mass at the beam tip causes the measured imaginary component of inertance to depart from the semi-infinite beam value at about 200 Hz. Therefore, the measured value rather than that predicted for a semi-infinite beam was used in the power predictions.

In figure 6.8 the imaginary components of apparent mass for the finite and semi-infinite beams are compared. As expected, the curve

for the semi-infinite beam was the geometric mean of the peak and trough values in the data for the finite beam. The peak and average values of imaginary apparent mass are related by equation (2.6), i.e.,

$$\frac{\omega\hat{Q}}{\omega Q} = \frac{2}{\cos\beta} = 10^{2}f^{-\frac{1}{2}}. \qquad (6.14)$$

6.2.3 The isolator

The isolator, inserted to couple the two beams between points 2 and 3, consisted of two adjacent blocks of natural rubber, each 1 cm deep by 1.2 x 1.2 cm cross section. Natural rubber was chosen because its properties did not vary rapidly over the frequency range of interest. This was confirmed experimentally, in that the static stiffness 'K' was measured as 10^5 N/m, but the dynamic stiffness had only increased to 1.2×10^5 N/m at 2 kHz. The first standing wave in the isolators occurred at about 3 kHz. The isolators were secured in position with cyranoacrylate cement, which provided a rigid bond.

6.3 Power Transmission Measurements

Having measured the source and receiver beam properties, the two beams were coupled together by the isolator. For the power measurements, the force input and the acceleration at position 1 (see fig. 6.2) were monitored by an impedance head B & K type 8001, while the acceleration response at point 3 on the receiver beam was monitored by a B & K accelerometer type 4333.

For ease of measurement and clarity in presentation, the results of the measurements were expressed in terms of power × ω, per unit force spectrum input, which have units of inertance. These quantities were calculated from a single rapid swept sine wave test in the following way:

The power × ω, for unit force spectrum input, at position 1, is

$$\frac{\text{power} \times \omega}{\frac{1}{2}|F_1|^2} = \mathrm{Im}\{\bar{I}_{1c}\}, \qquad (6.15)$$

where F_1 is the input force, and $\bar{I}_{1c}$ is simply the inertance at point 1 when the two beams are coupled.

The power × ω, for unit force spectrum, transmitted to the receiver beam at position 3 is

$$\frac{\text{power} \times \omega}{\frac{1}{2}|F_1|^2} = \frac{\frac{1}{2}|\bar{a}_3|^2}{\frac{1}{2}|\bar{F}_1|^2} \cdot \text{Im}\{\bar{A}_3\} = |\bar{I}_{13}|^2 . \text{Im}\{\bar{A}_3\}, \qquad (6.16)$$

where $|\bar{a}_3|$ is the modulus of the acceleration of position 3, $\bar{I}_{13}$ is the transfer inertance between points 1 and 3, and $\bar{A}_3$ is the apparent mass at position 3 measured previously and shown in figure 6.8.

The advantage of this method chosen to measure the transmitted power is that only modulus data is required in the measurement of $|\bar{I}_{13}|^2$. This was important in this case because the acceleration response at point 3 was very small and accurate phase information could not be provided due to the effects of background noise.

6.4 Presentation and Discussion of Results

6.4.1 Power input to the finite source beam and transmitted to the semi-infinite receiver beam

The power input to the source beam and that transmitted to the receiver beam are compared in figure 6.9, together with the predictions of frequency averaged power <<P>>.

First, at frequencies less than 50 Hz the source beam moved as a rigid body, absorbing no power, therefore the power input was equal to that transmitted to the receiver beam. By substituting the source beam properties of equations (6.1) and (6.2) into equation (3.8) the predicted power P in this region is given as

$$P = \frac{1}{2}|F_1|^2 . \frac{Q}{4}, \qquad (6.17)$$

which agrees well with the measurement.

For frequencies above 50 Hz the source beam behaved as a flexible beam. In this region the frequency averaged power input $\langle\langle P \rangle\rangle$ to the coupled beam was predicted in equation (4.6) to be the same as that input to the uncoupled beam. This was confirmed as the frequency averaged imaginary component of inertance for the coupled beam, figure 6.9, is the same as for the uncoupled beam, figure 6.3.

Therefore the frequency averaged power input is

$$\omega\langle\langle P \rangle\rangle = \tfrac{1}{2}|F_1|^2 .\omega S. \qquad (6.18)$$

Note the same change in level at 800 Hz in figure 6.9 as was observed in figure 6.4.

Figure 6.10 gives the result of dividing the transmitted power by the input power shown in figure 6.9. The result is a smooth function, demonstrating that the peak to trough variations of both input and transmitted power are the same. The ratio shown in figure 6.10 is therefore the ratio between the averaged power $\langle\langle P \rangle\rangle$ input and that transmitted, which is given in equation (5.19).

This equation has two regimes. First, at low frequencies, the ratio is controlled by the relative sizes of the real component of the isolator and receiver mobility, i.e.,

$$\frac{\text{Power transmitted}}{\text{power input}} = \frac{Q}{Q + \frac{\eta\omega}{K}} . \qquad (6.19)$$

In the case considered it can be seen that the isolator damping becomes significant at about 200 Hz when $Q = \eta\omega/K$, causing half the input power to be absorbed in the isolator and half in the receiver.

At about 400 Hz the important transition occurred when

$$\frac{t_d^2}{2\cos\varepsilon} = \frac{Q}{Q + \frac{\eta\omega}{K}} \qquad (6.20)$$

or

$$(\omega/K)^2 \simeq \hat{S}.(Q + \frac{\eta\omega}{K}).$$

t_d^2 is calculated from equation (5.13). For our prediction it was necessary to use the measured receiver properties from figure 6.7 rather than the theoretical value for a semi-infinite beam, Q. Note the trough, seen in figure 6.10 at about 2.5 kHz, which was caused by the dip in the receiver inertance, shown in figure 6.7. The source beam properties at end 2 of the beam were not affected by the presence of the impedance head at end 1, therefore the source beam inertance given in equation (6.8) was used over the whole frequency range.

Figures 6.11 and 6.12 show the power input to the source beam and transmitted to the receiver beam against the predictions of peak and trough power. The two regimes are clearly shown. First, for frequencies greater than 400 Hz, the source beam behaves as a velocity source, therefore the frequencies of the power flow peaks, and the ratio of peak to averaged power is the same as for the uncoupled beam. Second, for frequencies less than 400 Hz, the peak to average power was predicted to be

$$\frac{<\hat{P}>}{<<P>>} = \frac{4}{t_d^2} \cdot \left(\frac{Q}{Q + \frac{\eta\omega}{K}}\right)^2 \qquad (6.21)$$

and is seen to be in good agreement with the measurement data. At about 200 Hz, the peak to mean ratio in power is a minimum. This is the frequency of maximum coupling between the two beams when

$$(Q + S - \frac{\omega}{K}) = 0.$$

6.4.2 Power input to the source beam and transmitted to the finite receiver beam

The results from this experiment, together with predicted levels and comparative plots from the previous semi-infinite receiver case, are shown in figures 6.13-6.19.

Figure 6.13 compares the power input to the source beam with that transmitted to the finite receiver beam. The plot appears somewhat

confused on account of the peaks associated with the receiver resonances; however, two observations can be made. First, at low frequencies the power input is equal to the power transmitted, both exhibiting the large peak to trough variations in power, indicating that the power is mainly being absorbed in the receiver beam. Second, at high frequencies the source beam behaves as a velocity source, the resonance frequencies power input levels being almost identical to that of an uncoupled beam. The transmitted power at these frequencies was a fraction of that input to the source beam, and was mainly absorbed at the receiver beam resonances.

The power flow will now be discussed in greater detail; to aid this the behaviour is divided into three frequency regimes.

(i) Below 50 Hz the source beam moved as a rigid body. In this frequency region the source beam acted as a 'force source' that is, the mobility of the source beam was greater than that of the isolator and receiver beam, causing equation (3.8) to reduce to

$$P = \tfrac{1}{2}|F_1|^2 \cdot \frac{|M_{12}|^2}{|M_2|^2} \cdot \mathrm{Re}\{\bar{M}_R\},$$

which on substituting from equations (6.1) and (6.2), with the source beam properties, and equation (3.9), for the receiver beam mobility, reduces to

$$P = \tfrac{1}{2}|F_1|^2 \cdot \frac{Q_r}{4} \cdot \qquad (6.22)$$

Therefore the frequency averaged power is simply

$$\langle P \rangle = \tfrac{1}{2}|F_1|^2 \cdot \frac{Q}{4},$$

which is the same as the power transmitted to the semi-infinite receiver beam in this frequency range, as predicted in equation (6.17) and demonstrated in figures 6.15 and 6.16.

As all the power input was dissipated in the receiver beam, the ratio between the envelope of the peak $\hat{P}$ and the average power $\langle P \rangle$ is simply

$$\frac{\hat{P}}{\langle P \rangle} = \frac{2}{\cos \beta}$$

as can be seen from figure 6.15.

(ii) At high frequencies, most of the input power was dissipated in the source beam, and was the same as if the beam were uncoupled. As the source beam behaved as a velocity source of magnitude $|V_f|$ at the top of the isolator, the transmitted power was simply

$$P = \tfrac{1}{2}|V_f|^2 \cdot \frac{Q_r}{(\omega/K)^2} \cdot \qquad (6.23)$$

The frequency averaged power $\langle P \rangle$ was the same as that for the semi-infinite receiver beam, namely,

$$\langle P \rangle = \tfrac{1}{2} \cdot |V_f|^2 \cdot \frac{Q}{(\omega/K)^2} ,$$

as can be seen from figures 6.18 and 6.19.

The maximum power was transmitted at the source beam resonances when V_f is a maximum.

The ratio of the envelope of the peaks, to the frequency averaged power is again simply

$$\frac{\hat{P}}{\langle P \rangle} = \frac{2}{\cos \beta} .$$

(iii) It was only in the mid-frequency region, when the beams were well coupled, that a difference occurred between the average power transmission to the semi-infinite and finite beams.

By making the receiver beam finite, or alternatively less well damped, its ability to absorb power is reduced and so a greater proportion of the input power is absorbed by the source beam and isolator. If the isolator damping is light and the source beam damping relatively heavy, the power input to the source beam is shared between the source and

receiver beams as described in section 5.4 Pt. (i). Alternatively, if the source beam damping is light and the isolator is relatively heavily damped, the power is shared between the isolator and the receiver beam, as described in section 5.4, Pt. (ii). It is this latter case which occurred in experiments reported upon here, the criteria for such behaviour being described by the inequality in equation (5.25), namely,

$$(\frac{Q_d}{Q})^2 > \frac{\cos \varepsilon}{\cos \beta} \cdot \frac{4}{t_d^2},$$

where Q_d^2 from equation (5.7) is

$$Q_d^2 = Q^2 + \frac{\eta\omega}{K} \hat{Q} + (\frac{\eta\omega}{K})^2.$$

The frequency averaged power input to the source beam, $<<P>>$, is seen from figure 6.16 to be the same as for the uncoupled beam, i.e.,

$$<<P>> = \tfrac{1}{2}|F_1|^2.S,$$

despite the complicated end condition at point 2.

The frequency averaged power transmitted $<<P>>$ is given in equation (5.28) as

$$<<P>> = \tfrac{1}{2}|F_1|^2.S \sin \varepsilon. \frac{Q}{Q_d}. \qquad (6.24)$$

Note from equation (5.7) that Q_d^2 takes its minimum value when the receiver beam is semi-infinite, and increases with decreasing beam damping. Thus the average power transmitted to the finite beam was less than that transmitted to the semi-infinite beam.

Equation (6.24) is plotted on figure 6.16 below 500 Hz, and is seen to be a good estimate of the frequency averaged power transmission.

At 500 Hz the power dissipated in the source beam became as great as that dissipated in the isolator and receiver beam, occurring when

$$\frac{Q_d}{Q} = \frac{2 \cos \varepsilon}{t_d^2} .$$

Above this frequency the source beam behaved as a velocity source, and the prediction shown in Figure 6.16 between 500 Hz and 1 kHz is given by equation 6.23. This transition to velocity source behaviour occurred at a higher frequency for the finite beam than for the semi-infinite beam, on account of the increased isolator effectiveness.

Having looked at the averaged power over the broad frequency interval between two source beam resonances, i.e., $\langle\langle P \rangle\rangle$, the form of the power averaged over the narrow interval between two receiver beam resonances, i.e., $\langle P \rangle$, is considered together with the envelope of the peak power $\hat{P}$ (refer to figure 5.3 for the relationship between these quantities).

Figure 6.14 compares the power input to the source beam when the receiver beam was finite and semi-infinite. It can be seen that the frequency averaged power $\langle P \rangle$ input for the finite receiver beam case was almost the same as the power input for the semi-infinite beam case. The maximum ratio of the envelope of the power flow peaks $\hat{P}$ to the mean level $\langle P \rangle$ is $\hat{P}/\langle P \rangle = 2/\cos \beta$.

This is, however, only true at low frequencies, when all the power is dissipated in the receiver beam. The ratio decreases as an increasing amount of power is dissipated in the isolator and source beam.

Figures 6.15-6.17 show the measured values of the frequency averaged power $\langle P \rangle$, this quantity lies on the geometric mean of the peaks and troughs in power caused by the receiver beam resonances. From figure 6.15 it can be seen that the peak values of $\langle P \rangle$ at approximately 120 and 300 Hz were considerably less than the equivalent peaks of power transmission to the semi-infinite beam. At these peak values of $\langle P \rangle$ the fluctuations about the mean value were small because the power was mainly being dissipated in the isolator, the properties of which did not vary much with frequency. Note also the slight frequency shift in the peak of $\langle P \rangle$ at 300 Hz, compared with the semi-infinite beam case. This was caused by the increased size of Q_d^2 in the frequency equations (5.5)-(5.8).

The predicted peak and trough values of $\langle P \rangle$, namely $\langle \hat{P} \rangle$ and $\langle \check{P} \rangle$ taken from equations (5.26) and (5.27) are plotted in figure 6.17.

It is seen that the measured power is underestimated by a factor of two. This is partly because of the technique used to obtain the average value tends to smooth the data, but the main difference is probably because the theory developed in this thesis will always predict the power transmission for the maximum coupling, i.e., at the coincidence of the peaks in the real components of the source and receiver mobilities.

From figure 6.15 the envelope of the peaks in power transmission can be seen. In the trough between 120 and 300 Hz it can be seen that the envelope of the peaks $\hat{P}$ is related to the average power $\langle P \rangle$ by the relationship in equation (5.29). The maximum possible value of $\hat{P}$ occurring near the peaks in $\langle \hat{P} \rangle$ is given as

$$P = \frac{\langle P \rangle}{2} \cdot \frac{1}{\cos \beta}$$

in equation (5.33).

This value is plotted on figure 6.15 and appears to be a slight underestimate. A possible reason for this is that in this frequency region these particular beams become almost perfectly coupled, i.e., $S = Q_d$, as witnessed by the very shallow trough in $\langle P \rangle$ between 120 Hz and 300 Hz. The theory, as developed in Appendix 4, is not strictly applicable under these circumstances and so some inaccuracy could be expected.

6.5 Summary

A short source beam was coupled by an isolator to a long receiver beam. Power input to the source beam was measured along with the power transmitted to the long receiver beam. These measurements were compared with predictions of frequency averaged and peak power made using the frequency average and peak values of the source and receiver mobilities; satisfactory agreement was obtained. The following specific points arise:

(i) At low frequencies the source beam behaves as a rigid body. The transition from rigid body to flexural beam-like behaviour occurs when the real component of mobility of the beam, due to flexural motion, becomes comparable with the magnitude of the rigid beam mobility.

(ii) The real component of mobility at one end of a beam is proportional to the square of the modulus of the transfer mobility to the other end. This fact can be used to estimate the real component of mobility at a point. $Re(M_{11}) \propto |M_{12}|^2$

(iii) The frequency averaged power input to the free end of the source beam was independent of the termination at the other end, being the same for no coupling, a semi-infinite beam via an isolator, a finite beam via an isolator.

(iv) In the mid-frequency range, the power transmitted to the finite beam was slightly less than that to the semi-infinite beam. This was because the isolator absorbed more power in the former case.

(v) A frequency was reached at which

$$\hat{S}.(Q^2 + \frac{\eta\omega}{K}\hat{Q} + (\frac{\eta\omega}{K})^2) \leq (\frac{\omega}{K})^2,$$

then the source beam behaved as a velocity source acting on the top of the isolator. In this regime the frequency averaged power transmission to the finite and semi-infinite beams was identical.

PART 2

PRACTICAL MEASUREMENT CONSIDERATIONS

Part 1 presented a theoretical investigation into some of the parameters controlling the power transmission between coupled structures. However it is also necessary to be able to measure power transmission between coupled structures in order to confirm theoretical predictions or to take suitable vibration control measures in a practical situation. Therefore, three methods of measuring power input to a structure are presented. These methods involve the use of acceleration data and point and transfer frequency response data.

The power measurement methods require the frequency response data to be presented in the form of the real and imaginary component form. Measurements of this kind require greater accuracy and care than is necessary in making the modulus measurements more commonly made. Therefore, the sources of inaccuracies in the real and imaginary components of the point frequency response measurement are also considered here.

CHAPTER 7

THE MEASUREMENT OF POWER TRANSMITTED TO A STRUCTURE

7.1 Introduction

In marine engine installations, machines transmit power via their seatings to remote parts of the ship. It is of interest to measure this power, in order to determine the effectiveness of vibration isolation, or to quantify the amount of power that could cause unwanted sound radiation, or as input data for statistical energy analysis of the vibrational energy distribution around the ship [28].

The power input to a structure from multipoint excitation could easily be found from the time records of the force and acceleration at each point. However, it is difficult to measure the applied forces as it is necessary to interpose a force transducer between the machine foot and the seating, therefore alternative methods are presented here which only require the acceleration to be monitored when the machine is in operation.

The power is calculated using a digital computer to perform operations in the frequency domain. In all cases, the power is obtained from the product of the acceleration spectra and some structural frequency response data.

General expressions for the power input to a structure via multipoint excitation are derived using the force or velocity at each excitation point. However, these expressions are shown to be too unwieldy except for the simple case of very weak coupling between excitation points.

At the opposite extreme, it is shown that if the excitation points are strongly coupled by modal behaviour, then the power input can be measured using an alternative method which requires acceleration to be measured at only one, two or four points on the structure.

Finally, for the special case of a machine supported upon vibration isolators, a method is presented for measuring the power transmitted to the seating structure using the accelerations above and below each isolator.

Laboratory experiments confirm the validity of these methods.

7.2 General Expressions for Power Input by Multipoint Excitation

N forces $\bar{F}_1 \ldots \bar{F}_R \ldots \bar{F}_S \ldots \bar{F}_N$ are applied to a structure. The velocity response at each of the N driving points $\bar{V}_1$ to $\bar{V}_N$ can be written as:

$$[\bar{V}] = [\bar{M}][\bar{F}] \qquad (7.1)$$

where

$$[\bar{V}] = \begin{bmatrix} \bar{V}_1 \\ \vdots \\ \bar{V}_N \end{bmatrix}, \quad [F] = \begin{bmatrix} \bar{F}_1 \\ \vdots \\ \bar{F}_N \end{bmatrix},$$

$$[M] = \begin{bmatrix} M_{11} & \cdots & M_{1N} \\ \vdots & & \\ M_{N1} & & M_{NN} \end{bmatrix}$$

an N x N square matrix of point and transfer mobilities.

For harmonic excitation, the time averaged power input to the structure is given as the sum of the powers input at each point, i.e.,

$$\tfrac{1}{2}\mathrm{Re}\{[\bar{F}^*]^T[\bar{V}]\} = \tfrac{1}{2}\mathrm{Re}\{[\bar{F}^*]^T[\bar{M}][\bar{F}]\}, \qquad (7.2)$$

where ^{T} denotes the transpose matrix, and * denotes complex conjugate.

If reciprocity between points on the structure is assumed then

$$\bar{M}_{RS} = \bar{M}_{SR},$$

and equation (7.2) can be expanded to

$$\tfrac{1}{2}\sum_{R=1}^{N}\mathrm{Re}\{\bar{F}_R^*\bar{V}_R\} = \tfrac{1}{2}\sum_{R=1}^{N}|\bar{F}_R|^2.\mathrm{Re}\{\bar{M}_{RR}\} + \tfrac{1}{2}\sum_{R=1}^{N}\sum_{S=1}^{N}\mathrm{Re}\{\bar{F}_R^*\bar{F}_S\}\mathrm{Re}\{\bar{M}_{RS}\}. \qquad (7.3)$$

$R = S$ $\qquad$ $R \neq S$

Using the definition

$$[\bar{F}] = [\bar{Z}][\bar{V}]$$

where the impedance matrix $[\bar{Z}]$ is the inverse of the mobility matrix, i.e.,

$$[\bar{Z}] = [\bar{M}]^{-1},$$

the total time average power input for harmonic excitation can be written as,

$$\tfrac{1}{2}\mathrm{Re}\{[\bar{V}^*]^T[\bar{F}]\} = \tfrac{1}{2}\mathrm{Re}\{[\bar{V}^*]^T[\bar{Z}][\bar{V}]\}.$$

This may be expanded in the manner of equation (7.3) as

$$\tfrac{1}{2}\sum_{R=1}^{N}\mathrm{Re}\{\bar{V}_R^*\bar{F}_R\} = \tfrac{1}{2}\sum_{R=1}^{N}|V_R|^2.\mathrm{Re}\{\bar{Z}_{RR}\} + \tfrac{1}{2}\sum_{R=1}^{N}\sum_{S=1}^{N}\mathrm{Re}\{\bar{V}_R^*\bar{V}_S\}\mathrm{Re}\{\bar{Z}_{RS}\}. \quad (7.4)$$

$$R = S \qquad\qquad R \neq S$$

Equations (7.3) and (7.4) show three possible ways of measuring the power input to a structure.

(i) Using the left hand of equations (7.3) and (7.4)

$$\text{Power} = \tfrac{1}{2}\sum_{R=1}^{N}\mathrm{Re}\{\bar{F}_R^*\bar{V}_R\}.$$

The power is simply a sum of the powers input at each point. For random excitation the power/Hz is simply given as

$$\text{Power/Hz} = \sum_{R=1}^{N}\mathrm{Re}\{\bar{G}_{F_RV_R}\}, \quad (7.5)$$

where $\bar{G}_{F_RV_R}$ is the cross spectral density between the force and velocity at point R. This is the best way to measure power but the method is impractical because the force cannot usually be monitored.

(ii) The right hand side of equation (7.3) has theoretical interest but little practical use, as it is much more complicated than the left hand side of this equation.

(iii) The right hand of equation (7.4) gives a possible but impractical way of measuring power. There are two main objections. First, the impedance matrix requires many measurements, $N(N + 1)/2$. Secondly, the impedance matrix cannot be measured directly, but requires the inversion of the measured N x N mobility matrix $[\bar{M}]$. This process would create inaccuracies, unless perhaps modal analysis of the measured data could produce an appropriate mathematical model [12].

However, one simple case can be treated, i.e., weak coupling between excitation points, (which can occur on heavily damped marine engine seatings [29]). In this case the transfer impedance $\bar{Z}_{RS}$ becomes negligible and equation (7.4) reduces to

$$P = \tfrac{1}{2} \sum_{R=1}^{N} |V_R|^2 . \mathrm{Re}\{\bar{Z}_R\}, \qquad (7.6)$$

i.e., the sum of the powers independently measured at each point.

7.3 Using the Envelope of Resonance Peaks to Estimate Power Absorbed by a Finite Structure

The previous section outlined the difficulty in measuring power input to an arbitrary structure by multiple forces. However, a method is presented here for the special case of measuring the power input by an undefined excitation distribution, to a structure which is sufficiently lightly damped for the vibrations to be governed by modal behaviour. Subject to this condition, the power input to the structure can be equated to the sum of the powers absorbed by each vibrational mode. The power absorbed by each vibrational mode is calculated from the resonance peak value of the point or transfer inertance at selected positions on the structure, and the acceleration spectra at those points. In order to gain an estimate of the power levels between resonances, cubic spline curves are fitted through the resonance peak inertance values.

Experimental work was carried out on a damped plate in order to study the practibility and limitations of the method.

7.3.1 Theory

The purpose of this section is to provide some theoretical justification for the proposed method of measuring power absorbed by a structure. First the general relationships between forces and velocities on a multimodal structure are stated. These are used to derive the relationship between the power absorbed by a mode and the generalised force associated with that mode. The power absorbed is related to the product of two velocities on the structure. Finally, single point excitation is considered and the real component of mobility at a point is expressed in terms of the transfer mobility to another point.

(i) General relationships

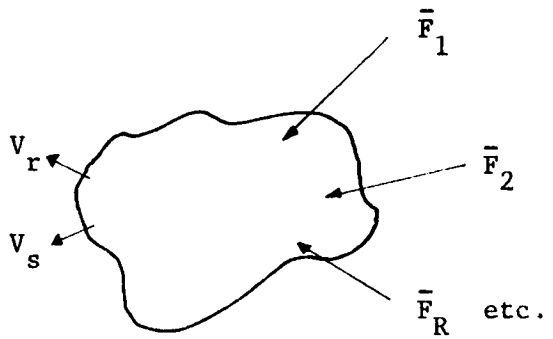

If a structure is excited by N forces, $\bar{F}_1 e^{i\omega t}$, $\bar{F}_2 e^{i\omega t}$ .... $\bar{F}_R e^{i\omega t}$ ... $\bar{F}_N e^{i\omega t}$, the generalised force to the p^{th} mode of the structure can be written as

$$f_p = \sum_{R=1}^{N} \bar{F}_R \psi_R^{(p)} \qquad (7.7)$$

where $\psi_R^{(p)}$ is the eigenvector of the pth mode at position R. The time dependence $e^{i\omega t}$ is suppressed.

The velocity at any point s, $\bar{V}_s$, is given by the sum of the modal contributions as

$$\bar{V}_s = \sum_{p=1}^{m} \bar{M}^{(p)} . \psi_s^{(p)} . \bar{f}_p, \qquad (7.8)$$

where $\psi_s^{(p)}$ is the eigenvector of the p^{th} mode at position s. $\bar{M}^{(p)}$ is the modal mobility of the p^{th} mode, defined by

$$\bar{M}^{(p)} = \frac{1}{m_p} \cdot \frac{\eta\omega\omega_p^{\,2} + i\omega(\omega_p^{\,2} - \omega^2)}{(\omega_p^{\,2} - \omega^2)^2 + (\eta\omega_p^{\,2})^2}\,, \qquad (7.9)$$

where m_p and ω_p are the generalised mass and angular natural frequency of the p'th mode, respectively, η is the hysteretic damping coefficient (loss factor).

For single point excitation at position s, the generalised force for the p'th mode is given from equation (7.7) as

$$\bar{f}_p = \bar{F}_s . \psi_s^{(p)} \,.$$

On substituting this into equation (7.8) the point mobility at position s is given as

$$\bar{M}_s = \frac{\bar{V}_s}{\bar{F}_s} = \sum_{p=1}^{m} \bar{M}^{(p)} . (\psi_s^{(p)})^2 . \qquad (7.10)$$

Likewise, the transfer mobility between points r and s is found by setting $\bar{f}_p = \bar{F}_r . \psi_s^{(p)}$ in eqn.(7.9), giving

$$\bar{M}_{rs} = \frac{\bar{V}_s}{\bar{F}_r} = \sum_{p=1}^{m} \bar{M}^{(p)} . \psi_r^{(p)} . \psi_s^{(p)} . \qquad (7.11)$$

From equation (7.9) an important relationship is derived, namely:- in the region of the p'th mode

$$|\bar{M}^{(p)}|^2 = \mathrm{Re}\{\bar{M}^{(p)}\} . \hat{M}^{(p)}, \qquad (7.12)$$

where $\hat{M}^{(p)}$ is the resonance peak value of $\bar{M}^{(p)}$ (when $\omega = \omega_p$).

Note that this statement for a single mode is similar to that derived for a set of equally spaced modes in Appendix 3 (equation (A3.9).

(ii) Power input in terms of generalised force

The total power input from N forces is given as the sum of the powers input at each position, R, i.e.,

$$P = \tfrac{1}{2} \sum_{R=1}^{N} \mathrm{Re}\{\bar{F}_R^* \bar{V}_R\} \tag{7.13}$$

where * denotes the complex conjugate.

Substituting for $\bar{V}_R$ using equation (7.8) gives

$$P = \tfrac{1}{2} \sum_{R=1}^{N} \mathrm{Re}\{\bar{F}_R \cdot \sum_{p=1}^{m} \bar{M}^{(p)} . \psi_R^{(p)} . \bar{f}_p\}; \tag{7.14}$$

changing the order of the summation,

$$P = \tfrac{1}{2} \sum_{p=1}^{m} \mathrm{Re}\{\bar{M}^{(p)} . \bar{f}_p \sum_{R=1}^{N} . \bar{F}_R^* . \psi_R^{(p)}\}, \tag{7.15}$$

which on substitution from equation (7.7) gives

$$P = \tfrac{1}{2} \sum_{p=1}^{m} |\bar{f}_p|^2 . \mathrm{Re}\{\bar{M}^{(p)}\}. \tag{7.16}$$

It can thus be seen that the total power input is equal to the sum of the power input to each mode.

(iii) The estimation of power input at resonances from the velocity at two points

Using equation (7.8) the product of the velocities at two arbitrary points r and s can be written as

$$\bar{V}_s \bar{V}_r^* = \sum_{p=1}^{m} \bar{M}^{(p)} . \psi_s^{(p)} . \bar{f}_p . \sum_{q=1}^{m} \bar{M}^{(q)} . \psi_r^{(q)} . \bar{f}_q^* \tag{7.17}$$

where q is an independent integer.

Expanding the summations into two parts,

$$\bar{V}_s \bar{V}_r^* = \sum_{p=1}^{m} |M^{(p)}|^2 . \psi_s^{(p)} \psi_r^{(p)} . |f_p|^2 + \sum_{p=1}^{m} \sum_{q=1}^{m} \bar{M}^{(p)} \bar{M}^{(q)*} . \bar{f}_p \bar{f}_q^* \psi_r^{(q)} \psi_s^{(p)} .$$

$$p = q \qquad\qquad p \neq q \qquad (7.18)$$

At frequencies near the p'th mode only the term from the left hand summation contributes significantly to the velocity product, provided the modes are well separated, i.e.,

$$V_s V_r^* = |M^{(p)}|^2 . \psi_s^{(p)} \psi_r^{(p)} \; |f_p|^2 . \qquad (7.19)$$

Now, substituting equation (7.12) gives

$$\bar{V}_s \bar{V}_r^* = |f_p|^2 . \mathrm{Re}\{M^{(p)}\} . \hat{M}_{rs}^{(p)} \qquad (7.20)$$

where $\hat{M}_{rs}^{(p)}$ is the resonance peak transfer mobility of the p'th mode between points r and s.

Therefore, using equation (7.16) the power to the p'th mode, P_p, can be written as

$$P_p = \tfrac{1}{2} \bar{V}_s \bar{V}_r^* . \frac{1}{\hat{M}_{rs}^{(p)}}$$

as the right hand side of equation (7.20) is real, this can be written as

$$P_p = \tfrac{1}{2} |\bar{V}_s \bar{V}_r^*| . \frac{1}{|\hat{M}_{rs}^{(p)}|} \; . \qquad (7.21)$$

Likewise, the power to mode p can be estimated from a single point measurement by substituting r = s in equation (7.21)

$$P_p = \tfrac{1}{2} |\bar{V}_s|^2 . \frac{1}{\hat{M}_s^{(p)}} \qquad (7.22)$$

where $\hat{M}_s^{(p)}$ is the peak real component of mobility of the p'th mode at point s.

Therefore, equations (7.21) and (7.22) both represent practical means of measuring power in the region of resonance of well-separated modes.

(iv) Estimation of power input between two resonances

Between two resonances when only the adjacent modes p and q contribute significantly, the power absorbed is given from equation (7.16) as

$$P = P_p + P_q, \tag{7.23}$$

where

$$P_p = \tfrac{1}{2}|f_p|^2.\mathrm{Re}\{M^{(p)}\}, \qquad P_q = \tfrac{1}{2}|f_q|^2.\mathrm{Re}\{M^{(q)}\}.$$

It can be seen that this is always non-zero and positive.

Equation (7.18) shows that there is no simple relationship between $\bar{V}_s\bar{V}_r^*$ and the power absorbed in this region. However, it is still useful to make an estimate of the power absorption. It is shown in Appendix 7 that between two modes, $\bar{V}_s\bar{V}_r^*$ may be approximated in the following way

$$\tfrac{1}{2}|\bar{V}_s\bar{V}_r^*| \simeq P_p.\hat{M}_{rs}^{(p)} + P_q\hat{M}_{rs}^{(q)}. \tag{7.24}$$

In practice it is possible for $\bar{V}_s\bar{V}_r^*$ to go to zero, or become twice the value given by (7.24). However, this expression gives a type of expected average value from which the power may be estimated.

Between the two modes, the power is to be estimated by an expression of the form of equation (7.21), i.e.,

$$E(P) = \tfrac{1}{2}|V_sV_r^*|^2 . \frac{1}{X} = (P_p\hat{M}_{rs}^{(p)} + P_q\hat{M}_{rs}^{(q)}) \frac{1}{X}, \tag{7.25}$$

where E denotes estimate, and X is the factor to be selected to provide an estimate of the true power P (equation (7.21). The ratio between estimated and true power is therefore

$$\frac{E(P)}{P} = \frac{1}{X} \cdot \frac{P_p \hat{M}_{rs}^{(p)} + P_q \hat{M}_{rs}^{(q)}}{P_p + P_q} \qquad (7.26)$$

For this ratio to be unity, X must take various values depending on the relative sizes of P_p, P_q, $\hat{M}_{rs}^{(p)}$, $\hat{M}_{rs}^{(q)}$. The following examples are taken

(a) when $P_p \hat{M}_{rs}^{(p)} > P_q \hat{M}_{rs}^{(q)}$, $P_p > P_q$, which is the example considered earlier, i.e., close to the p'th mode. Substitution of these values into equation (7.26) gives

$$X \simeq \hat{M}_{rs}^{(p)} \qquad (7.27)$$

as shown previously in equation (7.21).

(b) when $P_p = P_q = \frac{P}{2}$, i.e., at the trough of the input power when the contribution from the two modes are equal. Equation (7.26) yields

$$X = \tfrac{1}{2}(\hat{M}_{rs}^{(p)} + \hat{M}_{rs}^{(q)}) \qquad (7.28)$$

(c) when $P_p \hat{M}_{rs}^{(p)} = P_q \hat{M}_{rs}^{(q)}$, i.e., when velocities from the two modes are the same.

From equation (7.26)

$$\frac{1}{X} = \tfrac{1}{2} \cdot \left(\frac{1}{\hat{M}_{rs}^{(p)}} + \frac{1}{\hat{M}_{rs}^{(q)}}\right). \qquad (7.29)$$

Therefore if a function X(f) could be constructed which would satisfy equations (7.27) to (7.29) the power could be estimated at all frequencies using $\frac{1}{2}\bar{V}_s \bar{V}_r^*$. However, as most power is absorbed at resonance it is only necessary for X(f) to be accurate in that region, i.e., $X = \hat{M}_{rs}^{(p)}$. At frequencies between the resonances it can be shown from equations (7.28), (7.29), that

$$\hat{M}_{rs}^{(p)} > X > \hat{M}_{rs}^{(q)} \qquad \text{if} \qquad \hat{M}_{rs}^{(p)} > \hat{M}_{rs}^{(q)}, \qquad (7.30)$$

and in the particular case of

$$\hat{M}_{rs}^{(p)} = \hat{M}_{rs}^{(q)}$$

then

$$\hat{M}_{rs}^{(p)} = X = \hat{M}_{rs}^{(q)} \quad . \tag{7.31}$$

Therefore, between resonances it is sufficient to estimate the power by joining the points $X = \hat{M}_{rs}^{(p)}$ and $X = \hat{M}_{rs}^{(q)}$ with a line satisfying equation (7.30).

In practice, a cubic spline curve was fitted between the peaks. It was constrained to have zero slope at resonance as only the one mode is significant in that region. Between two peaks a cubic spline function will usually satisfy (7.30). This cubic spline function $X(f)$ will subsequently be referred to as the envelope of the peaks.

(v) Summary of proposed methods

In the light of the previous two sections, the following formulae for measuring power can be listed.

By setting $r = s$ in equation (7.25), the power may be estimated at a single point s from the velocity V_s, and the envelope of the peaks in the real component of mobility at this point, $\hat{M}_s$. This envelope $\hat{M}_s$ is best obtained from the real component of mobility as the coupling between modes is sometimes large enough to influence peaks in the mobility modulus. The estimated power is

$$E(P) = \tfrac{1}{2}|V_s|^2 . \frac{1}{\hat{M}_s} , \tag{7.32}$$

or if acceleration signals are used and the structure is subject to random excitation

$$\omega \times \frac{E(P)}{Hz} = G_{ss} . \frac{1}{\hat{I}_s} \tag{7.33}$$

where G_{ss} is the acceleration spectral density at point s, and $\bar{I}_s$ is the inertance at point s, and $\hat{I}_s$ is the envelope of the peaks in the imaginary component of the inertance.

Likewise the power may also be estimated using the velocities at two points r and s (using equations (7.25)),

$$E(P) = \tfrac{1}{2}|V_s V_r^*|. \frac{1}{|\hat{M}_{rs}|} \; ; \qquad (7.34)$$

or if acceleration is used and the structure is subject to random excitation

$$\omega \times E(P)/Hz = |\bar{G}_{rs}|. \frac{1}{|\hat{I}_{rs}|} \qquad (7.35)$$

where $\bar{G}_{rs}$ is the cross spectral density between acceleration at points r and s, and $|\hat{I}_{rs}|$ is the envelope of the peaks in the transfer inertance.

Some insight as to the meaning of the equations is gained by noting, from equation (7.9), that in the region of resonance

$$1/\hat{M}_s = Re\{\bar{Z}_s\},$$

where $\bar{Z}_s$ is the impedance at point s. Thus, in this region, the total power input to a structure with modal behaviour would be

$$E(P) \simeq \tfrac{1}{2}|V_s|^2.Re\{Z_s\}$$

which by comparison with equation (7.6) is seen to be an $1/N^{th}$ of the power that would be estimated in the assumption of weak coupling between excitation points.

(vi) Estimation of the real component of a point mobility from transfer measurements

If the system is excited by a single force $\bar{F}_R$ at point R then the power input is

$$P = \tfrac{1}{2}|F_R|^2.Re\{\bar{M}_R\} \qquad (7.36)$$

where $\bar{M}_R$ is the mobility at point R.

By substituting equation (7.36) into equation (7.32), the real component of mobility at point R is estimated as:-

$$E(\mathrm{Re}\{\bar{M}_R\}) = |\bar{M}_{sR}|^2 . \frac{1}{\hat{M}_s} \qquad (7.37)$$

where $|\bar{M}_{sR}|$ is the modulus of the transfer mobility between points R and s. Likewise, substituting equation (7.36) into equation (7.24)

$$E(\mathrm{Re}\{M_R\}) = |M_{sR}| . |M_{rR}| . \frac{1}{|\hat{M}_{rs}|} \quad . \qquad (7.38)$$

This procedure makes it possible to estimate the real component of mobility at a point without the use of phase information.

7.3.2 Experimental measurements

Some experimental measurements were performed upon the plate shown in figure 7.1. The objective of these experiments was to determine the validity of the procedures outlined in section 7.3.1.

Power was only input at one point, position 2, and measured using expressions (7.32) and (7.34) at points 1, 3, 4 and 5. As the measurement points were remote from the excitation position it was immaterial whether the excitation was single or multipoint.

All the power measurements were normalized to unit excitation force. Accelerometers were used to monitor the vibration; therefore, for convenience, the results are presented in terms of Power × ω per unit mean square force, i.e., effectively having the units of inertance.

As single point excitation was used, the results will effectively be testing the validity of equations (7.37) and (7.38).

(i) Description of the physical model

An aluminium plate, measuring 30 cm × 60 cm × 6 mm was suspended vertically, as shown in figure 7.1. One side of the plate was completely covered with AQUAPLAS, an unconstrained layer damping treatment. This gave the plate an almost frequency-independent loss factor of 0.012.

Input power was to be measured at point 2, force and acceleration were monitored by an impedance head, B & K type 8001. The accelerations were monitored at positions 1, 3, 4 and 5 by accelerometers, B & K type 4344. For point and transfer inertance measurements between these points the force gauges, B & K type 8200 were used. When not in use, they were left attached to the structure as masses. A coil and magnet arrangement forming an electrodynamic exciter was used to apply the necessary forces. The rapid swept sine method |26| was used for all tests.

(ii) Power experiments 0 - 1 kHz

First, the normalised power (imaginary component of inertance) input at point 2 was measured, i.e.,

$$\frac{\omega \times \text{power}}{|F|^2} = \text{Im}\{\bar{I}_2\} \tag{7.39}$$

where $\bar{I}_2$ is the inertance measured at point 2; it is shown in figure 7.2. This is the curve to be reproduced from measurements made at other points. Three estimates of input power were made, two using point measurements at positions 1 and 3 (equation (7.32) and a third using a transfer measurement between points 1 and 3 (equation (7.34). When only single point excitation is used the normalised power estimated from equation (7.37) becomes, for point 1,

$$\frac{E(\omega \times \text{power})}{|F|^2} = E(\text{Im}\{\bar{I}_2\}) = |\bar{I}_{12}|^2 . \frac{1}{\hat{I}_1} , \tag{7.40}$$

where E( ) denotes estimate. Likewise for point 3,

$$E(\text{Im}\{\bar{I}_2\}) = |\bar{I}_{23}|^2 . \frac{1}{\hat{I}_3} . \tag{7.41}$$

The normalised power estimated from the transfer measurement between points 1 and 3 becomes, from equation (7.38),

$$E(\text{Im}\{I_2\}) = |\bar{I}_{23}| . |\bar{I}_{21}| . \frac{1}{|\hat{I}_{13}|} . \tag{7.42}$$

The power estimates in these equations required $\hat{I}_1$, $\hat{I}_3$ and $\hat{I}_{13}$, which were obtained as follows:

The point and transfer inertances at points 1 and 3 were measured. The imaginary components of the point measurements were plotted in figures 7.3 and 7.4 and the modulus of the transfer measurement in figure 7.5.

The amplitude and frequency of the resonance peaks in the inertance data were obtained using a program called XPEAK (Appendix 8). The program also inserted data points, either side of the resonance point, with an amplitude equal to that of the resonance peak. A cubic spline curve was fitted through these points, the points at either side of the resonance peak ensured zero slope in this region. The fitted curves $(\hat{I}_1, \hat{I}_3, |\hat{I}_{13}|)$ had the same frequency increment between data points as the original inertance plots. Figures 7.3-7.5 show the curves $\hat{I}_1$, $\hat{I}_3$, $|\hat{I}_{13}|$ compared with the original inertance data.

Finally, in order to estimate the normalised power, the accelerations at points 1 and 3, normalised with respect to the input force at point 2, were measured, i.e., $|\bar{I}_{23}|$, $|\bar{I}_{21}|$. By inserting these values into equations (7.40)-(7.42), the three estimates of power were made and these are plotted in figures 7.6-7.8 together with the true input power at point 2.

(ii) Discussion of the results of power experiments 0 - 1 kHz

The comparative plots in figures 7.6-7.8 are now discussed in order.

Figure 7.6 shows the true power input at position 2, $(\mathrm{Im}\{\bar{I}_2\})$ compared with the estimate using data from position 1. Looking first at the form of $\mathrm{Im}\{I_2\}$, it can be seen that the resonances are well separated except for the two close resonances at about 230 Hz. The data in the region of the troughs are noisy, as is generally the case for this type of measurement, because the imaginary component of inertance is small compared with the real component in this region. Above 800 Hz the quality of the data is poor as a sampling rate of only 2 kHz was used during acquisition.

The estimated power is seen to be accurate in the region of the resonances, as would be expected from the theory. The two peaks at about 230 Hz are accurate despite the fact that the second peak is poorly excited, in $\mathrm{Im}\{\bar{I}_1\}$ (in figure 7.3).

However, the estimate in the regions of the troughs is rather poor. Sometimes the estimate goes to zero, e.g., at 300 Hz and 375 Hz. This is unavoidable since, for single point excitation, there is a 50% chance that the acceleration contributions to $|\bar{I}_{12}|$ from adjacent modes are of opposite phase and subtract (see equation (A7.5)). Alternatively, even when the troughs do not go to zero they are sometimes not accurate as seen in the region of 550 Hz and 700 Hz.

This inaccuracy occurred because a weakly excited mode is adjacent to a strongly excited mode, as seen in figure 7.3. The cubic spline functions therefore are unlikely to take the correct values when it goes through such a large level change between two points. It is only when two adjacent peaks in $\mathrm{Im}\{\bar{I}_1\}$ have a similar magnitude that the trough would be accurately estimated (e.g., see 100 Hz in figure 7.6).

Figure 7.7 shows the power estimated from point measurement at position 3. In this plot the resonance peaks at 230 and 360 Hz are underestimated. The reason can be seen in figure 7.4. First, the peak at 230 Hz is weakly excited in $\mathrm{Im}\{\bar{I}_3\}$, and being so close to the larger peak is likely to be in error. Second, the peak at 360 Hz was not located and so is not accounted for in $\hat{I}_3$. However, it is worth noting that any error due to close resonances or missing modes in the envelope $\hat{I}_3$ always leads to an underestimation of the true value. This means that by taking the larger value from a comparison of the power estimates at two points, e.g., 1 and 3, would lead to the estimate being closer to the true value.

The trough estimates are generally better in figure 7.7 than in figure 7.6. The overestimation at about 300 Hz occurred because, as shown in figure 7.4, $\hat{I}_3$ is in error on account of the cubic spline program being unable to accommodate the sharp change at 230 Hz.

Figure 7.8 shows the power estimated from the transfer inertance measurement $|\hat{I}_{13}|$. The peaks are fairly accurate except for that at 230 Hz which was entirely missed by $|\hat{I}_{13}|$, in figure 7.5.

Estimating power using a transfer measurement $|\hat{I}_{rs}|$ has certain advantages over the point method (using $\hat{I}_s$). The first is that on a practical structure, transfer measurements are more easily carried out, not requiring the use of impedance heads. Secondly, use of the transfer measurement for power flow estimation requires only modulus information,

whereas the point measurement method requires phase information which is difficult to obtain on heavy structures or in noisy environments. Finally, it can be seen from equation (7.10) that point measurements $(\hat{I}_s)$ contain a squared eigenvector term $(\psi_s^{(p)})^2$ from which it may be observed that modes tend to be either strongly or weakly excited. This means that if all modes are excited, a widely fluctuating envelope function $\hat{I}_s$ is produced, which causes errors in the trough regions; alternatively the strongly excited modes cause the weak modes to go undetected. However, the transfer measurement, $\bar{I}_{rs}$, is seen in equation (7.11) to contain cross terms $\psi_r^{(p)}\psi_s^{(p)}$. This causes modes to be more evenly excited and therefore $|\hat{I}_{rs}|$ fluctuates less, yielding a more useful function than $\hat{I}_s$.

Figure 7.9 shows the running integral under the two curves shown in figure 7.8, giving the sum of the power contributions from each mode. Apart from the 'missed' mode at 230 Hz, it is evident that the agreement between the two curves is quite good.

In summary it is shown that if resonances are well separated they can be readily detected by a point or transfer measurement and successfully used in the measurement of power absorbed by a vibrating structure.

(iii) Power experiments 1 kHz - 4 kHz

The power input in this region is shown in figure 7.2. It can be seen that the modal bandwidths increase with increasing frequency, the well excited modes tending to overlap and obscure those less well excited. As the proposed method of estimating power relies on being able to detect individual modal contributions, one would expect problems in this region.

From the observations made in the previous section, it was expected that the transfer method would be more effective than the point method, in this higher frequency region. This indeed proved to be the case and only the results from the transfer measurements are reported here. The point measurement method, although tried, did not detect enough modes.

The power input was estimated using the transfer inertance between points 1 and 3 (see figure 7.10). The estimated power compared with the true values is shown in figure 7.12. It can be seen that at frequencies above about 3500 Hz, the estimate becomes rather poor, because the modes are too heavily damped to be detected properly. However, the estimate is also very poor between about 1250 Hz and 2250 Hz. The cause of this is seen in

figure 7.10. This region is a broad anti-resonance, occurring because the transducers at points 1 and 3 are of the order of a quarter of a wavelength from the edge of the plate. Thus $|\hat{I}_{13}|$ tends to 'miss' some modes in this region. Such an anti-resonance would still be observed even if the transducers were placed on the very edge of the plate, on account of the rotary inertia of the transducers. However, below this anti-resonance frequency, all modes have an antinode.

It was decided to make another power estimate using points 4 and 5 (see figure 7.1) which are not so close to the edge. The transfer inertance between these points is shown in figure 7.11. The power estimate using $|\hat{I}_{45}|$ is shown in figure 7.13, and is seen to give moderately good agreement with the true value up to about 2500 Hz. There is a slight frequency shift from the true value on account of the additional masses of the transducers applied to points 4 and 5.

It is worth making a general observation that the envelope function $|\hat{I}_{45}|$ changes only slowly with frequency, implying that if there are slight structural changes causing a shift in resonance frequencies the method will still give a reasonable estimate of power.

The two power estimates, seen in figures 7.12 and 7.13 were compared using a simple computer routine, and at each frequency point the larger of the two estimates was selected to form a new data file. This new estimate is compared with the true value in figure 7.14, and can be seen to be in reasonable agreement up to about 3500 Hz.

It would be possible to improve this estimate further by comparing it with more measurements and selecting the larger values.

7.4 The Measurement of Power Transmitted Through an Isolator using the Accelerations at the ends of the Isolator

A method is presented here of measuring the power input to a structure from a machine, multisupported by vibration isolators. The total power input can be equated to the sum of the powers transmitted by each isolator, which is calculated with a knowledge of the isolator properties and the accelerations at each end of the isolator. A low frequency approach which neglects isolator damping or frequency dependence in the isolator properties is given in |30|.

The power transmitted through an isolator can be calculated with reference to the figure below, where the end faces of the isolator are permitted to move with the one degree of freedom shown. The dynamic properties of the isolator are described by the point and transfer apparent mass.

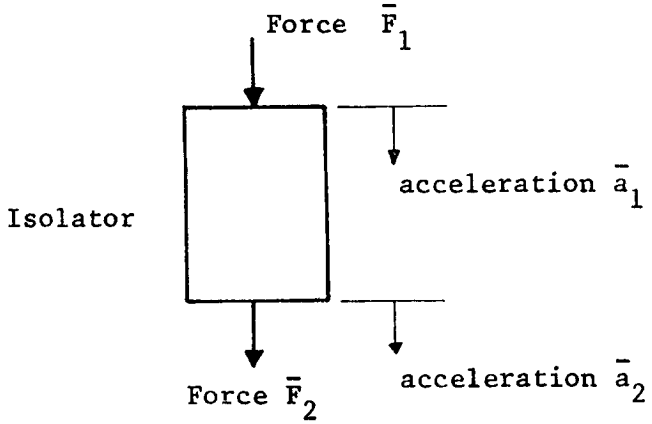

The transfer apparent mass is defined as

$$\bar{A}_{12} = \bar{A}_{21} = \frac{\bar{F}_2(\omega)}{\bar{a}_1(\omega)}\bigg|_{a_2=0} = \frac{\bar{F}_1(\omega)}{\bar{a}_2(\omega)}\bigg|_{a_1=0} \tag{7.43}$$

and the point apparent mass

$$\bar{A}_2 = \frac{\bar{F}_2(\omega)}{\bar{a}_2(\omega)}\bigg|_{\bar{a}_1=0},$$

where $\bar{F}_1$, $\bar{F}_2$ and $\bar{a}_1$, $\bar{a}_2$ are the forces and accelerations at the top and bottom of the isolator.

If accelerations are permitted at both ends of the isolator, for harmonic excitation, the force at the base of the isolator, $\bar{F}_2$, may be written as

$$\bar{F}_2 = \bar{A}_{12}\bar{a}_1 + \bar{A}_2\bar{a}_2 \,. \tag{7.44}$$

The time averaged power flow from the isolator, P_{tr}, is given from equation (1.12a) as

$$P_{tr} = \tfrac{1}{2}\mathrm{Re}\{\bar{F}_2\bar{V}_2^*\}$$

where $\bar{V}_2$ is the velocity at the foot of the isolator, defined as $i\omega\bar{V}_2 = \bar{a}_2$.

Therefore, by substitution into equation (7.43)

$$P_{tr} = \frac{1}{2\omega}\,\mathrm{Im}\{\bar{A}_{12}\bar{a}_1\bar{a}_2^* + \bar{A}_2|\bar{a}_2|^2\}. \qquad (7.45)$$

Likewise for random signals the 'power transmission spectral density' may be written as

$$P_{tr}/\mathrm{Hz} = \frac{1}{\omega}\,\mathrm{Im}\{\bar{A}_{12}\bar{G}_{a_2a_1} + \bar{A}_2G_{a_2}\}$$

where $\bar{G}_{a_2a_1}$ and G_{a_2} are the cross spectral densities and the acceleration spectral densities, respectively.

For a machine isolator, $\bar{a}_1$ is generally greater than $\bar{a}_2$, and the modulus of $\bar{A}_{12}$ is greater than the imaginary part of $\bar{A}_2$. Therefore, for harmonic excitation

$$P_{tr} \simeq \frac{1}{2\omega}\,\mathrm{Im}\{\bar{A}_{12}\bar{a}_1\bar{a}_2^*\} \qquad (7.46)$$

or, for random excitation,

$$P_{tr}/\mathrm{Hz} \simeq \frac{1}{\omega}\,\mathrm{Im}\{\bar{A}_{12}\bar{G}_{a_1a_2}\}.$$

For a simple spring with hysteretic damping,

$$\bar{A}_{12} = \frac{K}{\omega^2} + \frac{i\eta K}{\omega^2} \qquad (7.47)$$

where K is the dynamic stiffness (see, for example, figures 3.6 and 10.8).

The main advantages of using expressions (7.46) are

(i) only the isolator properties are required;

(ii) at frequencies below the first standing wave only the complex dynamic stiffness of the isolator is needed to describe the isolator properties;

(iii) the method accounts for acclerations at both ends of the isolator, including contributions to a_2 from other sources of vibration (see Chapter 10). Therefore, this method may be used to measure power from a machine supported upon many isolators, as the power flow through each isolator is measured independently. The total power transmitted from the machine is the sum of the individual contributions from each isolator.

The mathematics here describe vibration transmission via one degree of freedom only. However, provided an isolator is symmetric in construction (thereby eliminating cross terms), the power contribution from other degrees of freedom, such as shear or moment, could be simply included as independent contributions. Although this would involve measuring the transfer apparent mass in each of these components directly.

The use of equation (7.46) to measure power was demonstrated in section 3.5.3 part (iii) and in section 10.3.

7.5 Summary

Three practical methods for measuring the power input to a structure subject to multipoint excitation were presented. The methods required only acceleration data and premeasured frequency response data.

If there is weak coupling between excitation points, the power can be measured from the acceleration spectra and imaginary components of impedance at each of the excitation points; this method tends to over-estimate if the weak coupling assumption is incorrect.

If there is strong coupling between excitation points because of modal behaviour, the total power input can be found, for any excitation distribution, by summing the power absorbed by each mode of the structure. The power absorbed by each mode of the structure can be measured from acceleration data at one or two pairs of points on the structure.

If power is input to the structure via vibration isolators it can be measured using the accelerations above and below each isolator.

CHAPTER 8

MEASUREMENT ERRORS IN THE REAL COMPONENT OF MOBILITY

8.1 Introduction

It has been shown in the previous chapters that in order to predict or measure power transmitted to a structure it is necessary to measure the frequency response at driving or connecting points on the structure, and express it in complex notation (real and imaginary components). The frequency response function (see note 1(iii)) can take several forms, and the comments made in this chapter refer equally to all; however, for brevity, here reference will only be made to mobility and impedance.

Techniques for measuring the point mobility and impedance have long been established and are thoroughly described in |8, 9|. There are two basic approaches; steady state testing and transient testing, both with their merits. Steady state testing |9, 10| involves the use of continuous sinusoidal or random excitation, during which the structure responds in a 'steady state' manner. For transient testing excitation is applied for a brief duration and the structural response is then allowed to 'ring down' in free vibration. The frequency response is calculated from the Fourier transforms of the complete time histories, for forced and free motion of the excitation and response.

The test method chosen for the work reported here is a transient method, called, after the description of the excitation, the rapid frequency sweep method |31, 26|. It was chosen as it is very convenient to use if on line computer facilities are available as it requires only a short test time. The division of the Fourier transform of the velocity signal by that of the force, yields the complex mobility in the desired real and imaginary form.

The real component of mobility is of greatest interest as it is the component associated with the power transmission (see equation (1.12b)). However, it is a difficult measurement to make because, except at resonance, when it is dominant, the real component of mobility is much smaller than the imaginary component, and is accordingly prone to inaccuracies. The

purpose of this chapter is therefore to consider some errors that can occur when measuring the real component of mobility using a rapid frequency sweep technique. The three main areas are:

(i) extraneous noise in the force and response signals when the exciter has a finite impedance;

(ii) apparent noise due to a finite sampling rate;

(iii) the influence of the mechanical properties of the force and acceleration transducers.

8.2 Error in the Measurement of the Real Component at Mobility and Impedance Due to Extraneous Noise and Finite Exciter Impedance

The figure below shows a structure of point impedance $\bar{Z}$, which is driven with a rapid swept sine wave forcing function $f_1(t)$, by an exciter of mechanical impedance $\bar{Z}_e$ (this term also includes the back EMF damping effects). It is assumed that the exciter imposes no rotational restraint on the structure.

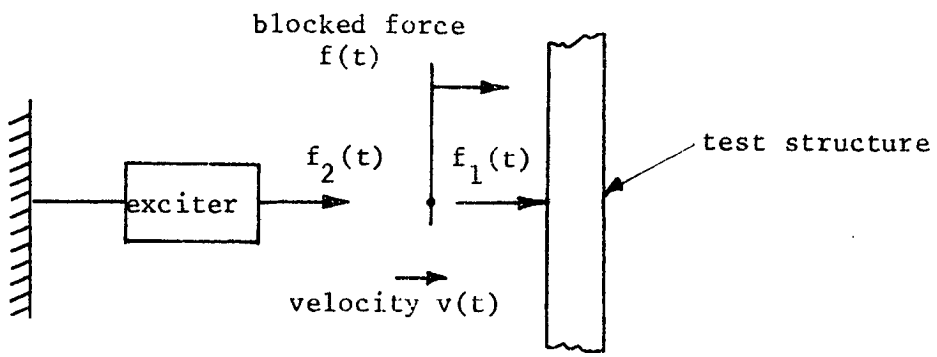

$f(t)$ is the ideal force which would be applied to a blocked structure ($v = 0$), as there would be no exciter impedance or back EMF effects. However, on account of the velocity response, $v(t)$, of the structure and exciter, the actual force applied to the structure, $f_1(t)$, is reduced to

$$f_1(t) = f(t) - f_2(t) \tag{8.1}$$

where $f_2(t)$ is the dynamic force responsible for the exciter motion. If the complete time histories of the transient forces and responses are Fourier transformed, equation (8.1) can be written as

$$\bar{F}(\omega) = \bar{F}_1(\omega) + \bar{F}_2(\omega) \tag{8.2}$$

where $\bar{F}(\omega)$, $\bar{F}_1(\omega)$ and $\bar{F}_2(\omega)$ are the Fourier transforms of $f(t)$, $f_1(t)$ and $f_2(t)$. As the exciter and structure have a common velocity $V(\omega)$ at the attachment point, equation (8.2) can be expressed in terms of the impedances,

$$\bar{F}(\omega) = \bar{V}(\omega)(\bar{Z} + \bar{Z}_e). \tag{8.3}$$

It can be seen that the attached exciter modifies the velocity response of the structure. If it is assumed that the exciter impedance includes a mechanical damping term (caused by the shaker suspension) and an electrical damping term (due to the back EMF caused by the movement of the coil in the magnetic field), then it is clear that the coupled exciter structure rings down more rapidly in free vibration than the uncoupled system.

For transient testing it is shown in |31| that to adequately describe a resonance peak in the frequency domain it is necessary to take a time record of length $T_o > \frac{1}{\Delta f}$ where $\Delta f = \xi f_n$, the bandwidth of the resonance of the uncoupled system. Therefore, if the structure-exciter system rings down rapidly due to large exciter damping, the remainder of the required time record, of length T, will mainly contain extraneous noise.

However, it is not only exciter damping that is a problem but also it is shown as follows that the mass and stiffness of the exciter can exacerbate noise corruption.

The mobility of the structure is given as $\bar{M}$,

$$\bar{M} = \bar{V}(\omega)/\bar{F}_1(\omega) \tag{8.4}$$

where $\bar{F}_1(\omega)$ is the Fourier transform of the force applied to the structure, which is measured by a force transducer. If extraneous noise $n(t)$ and $g(t)$ are added to the velocity and force signals, respectively, the measured mobility $\bar{M}_m$ becomes

$$\bar{M}_m = \frac{\bar{V}(\omega) + \tilde{N}(\omega)}{F_1(\omega) + \tilde{G}(\omega)} \tag{8.5}$$

where $\tilde{N}(\omega) = \frac{1}{2\pi}\int_o^{T_o} n(t)e^{-i\omega t}dt$, $\tilde{G}(\omega) = \frac{1}{2\pi}\int_o^{T_o} g(t)e^{-i\omega t}dt$, are the Fourier transforms of the noise signals. On substituting for $\bar{F}_1(\omega)$, using equations (8.2) and (8.3), the measured mobility becomes

$$\bar{M}_m = \frac{1 + (\tilde{N}(\omega)/\bar{F}(\omega)).(\bar{Z} + \bar{Z}_e)}{\bar{Z} + (\tilde{G}(\omega)/\bar{F}(\omega)).(\bar{Z} + \bar{Z}_e)} \tag{8.6}$$

The effects of the noise in the force and velocity signals are discussed separately:

(i) When $|\tilde{G}(\omega)/\bar{F}(\omega)|$ is comparable with $|\bar{Z}|/|\bar{Z} + \bar{Z}_e|$ the modulus of the measured mobility will have noise corruption, with values of $\pm\infty$ possible. This effect will be most noticeable at resonance, when $|\bar{Z}|$ is a minimum and the exciter impedance $\bar{Z}_e$ could be comparatively large. This type of noise corruption is therefore most likely when measuring the mobility of a light structure with small damping. It is clearly important to keep the exciter mass as small as possible, to minimise this problem. As this noise effect is in the denominator of equation (8.6), averaging of noisy mobility data will not yield the correct result.

(ii) If the factor $\tilde{G}(\omega)/\bar{F}(\omega)$ is negligible, then equation (8.6) reduces to the true mobility, influenced by the noise in the response, i.e.,

$$\bar{M}_m = Re\{\bar{M}\} + Im\{\bar{M}\} + (N(\omega)/F(\omega))(1 + \bar{Z}_e/\bar{Z}). \qquad (8.7)$$

It can be seen that errors in the real component of mobility occur when $Re\{\bar{M}\}$ is comparable with $|\tilde{N}(\omega)|/|\bar{F}(\omega)|$, which is most likely between resonances when $Re\{\bar{M}\}$ is small. Noise corruption of this sort is almost always found in practical measurements, particularly on heavier structures.

If it is assumed that the noise is random, then either ensemble averaging or averaging adjacent values in the frequency domain will accurately smooth out the noise contamination. This is possible as the noise term appears in the numerator in equation (8.7).

8.3 Sampling Rate Errors

When sampling continuous random data at discrete time intervals, for the purpose of spectral analysis, the minimum allowable sampling rate is twice the highest frequency of interest. This is known as the Nyquist criterion |32|. Accurate estimates of the spectral properties of random data require the averaging of many individual spectral records, each record formed from a Fourier transform of a finite length of signal |32|.

However, when calculating frequency response functions from transient test records, only one Fourier transform of each record (the force and response) is used. In this case, it has been found that the Nyquist criterion does not demand a high enough sampling rate to adequately describe the data for modulus and phase information.

An experimental investigation |31| found that, for transient testing, modulus data could be obtained with 5% accuracy at a frequency one-third of the sampling rate.

However, to accurately measure the phase, or the real and imaginary components, of the frequency response, is rather more demanding, as is shown in figure 8.1.

This figure shows the imaginary component of inertance, measured at point 1 of the source beam in the configuration shown in figure 5.1, using two different sampling rates, (a) 12,000 samples/sec; (b) 4,000 samples/sec. Plot (a) is inaccurate at low frequencies due to the short record length truncating the time record. Between 300 Hz and 1 kHz, (b) is very noisy. However, this noise appears to be attributable to 'sampling rate errors' as it is much reduced in (a) when a higher sampling rate was used.

These 'sampling rate errors' occur because a finite set of evenly spaced data points cannot perfectly describe a continuous data record. There is inevitably a measure of indeterminacy, decreasing with increasing sampling rate, which creates the effect of random 'noise' in the frequency response.

With reference to the previous section, the Fourier transforms of the noise in the force and response records due to sampling rate errors can be expressed as

$$\tilde{G}(\omega) = \tilde{\alpha}(\omega)F_1(\omega); \qquad \tilde{N}(\omega) = \tilde{\beta}(\omega)V(\omega). \tag{8.8}$$

This 'noise' is proportional to the signal size, the constants of proportionality $\tilde{\alpha}(\omega)$ and $\tilde{\beta}(\omega)$ are random variables of similar magnitudes. The magnitudes of $\tilde{\alpha}(\omega)$, $\tilde{\beta}(\omega)$ increase with increasing frequency, taking a maximum possible value of unity at the Nyquist frequency, when the sampling rate is twice that of the frequency of interest. In this case, it can be seen from the figure below that it is possible for the waveform to be undefined.

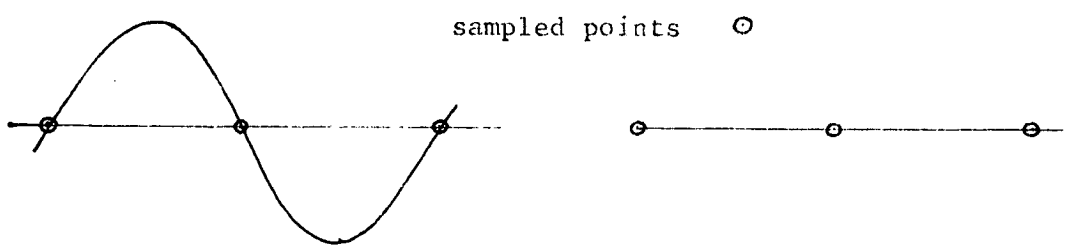

(a) waveform at Nyquist frequency

(b) possible interpretation of waveform

On substituting equation (8.8) into (8.5), the measured mobility becomes

$$\bar{M}_m = \frac{1 + \tilde{\alpha}(\omega)}{\bar{Z}(1 + \tilde{\beta}(\omega))} \qquad (8.9)$$

Therefore, when $|\tilde{\alpha}(\omega)|$ and $|\tilde{\beta}(\omega)|$ approach unity (i.e., at the Nyquist frequency) large errors will occur (as seein in figure 8.1). At lower frequencies when $|\tilde{\alpha}(\omega)|$ and $|\tilde{\beta}(\omega)|$ are small, the measured real component of mobility becomes, from equation (8.9),

$$Re\{M_m\} \simeq Re\{\bar{M}\} \pm |M|(|\alpha(\omega)| \mp \beta(\omega)|) \qquad (8.10)$$

Thus, there will be apparent random noise seen in the troughs between resonances, when $|M| > Re\{M\}$.

8.4 Relationships between the Dynamic Range in the Time Domain of the Response of a Single Degree of Freedom System, with the Dynamic Range in the Measured Inertance

In section 8.2, part (ii), the general relationship between measured mobility and the Fourier transform of the noise in the measured response was given. It is the intention here to replace these frequency domain terms with observable parameters in the time domain signals, for the simple case of a single degree of freedom system. Such an analysis has some usefulness because each mode of a multi-degree of freedom system can be regarded as responding in the time domain, in the manner of a single degree of freedom system.

As practical measurements generally use acceleration rather than velocity, inertance rather than mobility will be used and noise in the response $n(t)$ will refer to noise in the acceleration signal. The dynamic range in the frequency domain between the resonance peak value of the inertance $(1/2m\xi)$ (assuming viscous damping), is given from equation (8.7) as $(1/2m\xi).|\bar{F}(f)|/|\tilde{N}(f)|$. (8.11)

It is assumed that the exciter impedance may be neglected.

$\bar{F}(f)$ is the Fourier transform of a swept sine wave of amplitude F in the time domain which is given in |26| as

$$|\bar{F}(f)| = \frac{F}{2}\sqrt{\frac{T_f}{\Delta f}} \tag{8.12}$$

where T_f is the sweep time and Δf is the swept frequency range.

If it is assumed that the noise in the acceleration signal $n(t)$ is band limited white noise of standard deviation σ_n, then $\sigma_n^2 = G_n \Delta f$, where G_n is the magnitude of the noise spectral density and Δf is frequency range. G_n can be estimated from the Fourier transforms |32| as

$$G_n = \frac{2}{T_o} \cdot \text{expectation of } |\bar{N}(f).\bar{N}(f)^*|, \tag{8.13}$$

where T_o is the duration of the time history to be Fourier transformed.

Therefore, the magnitude of the Fourier transform of the noise can be expressed as

$$|N(f)| = \frac{\sigma_n}{\sqrt{2}}\sqrt{\frac{T_o}{\Delta f}} . \tag{8.14}$$

The resonance peak value of the inertance of the single degree of freedom system, $1/2m\xi$, can be expressed in terms of the time domain data.

It is shown in Appendix 6 that the mass m is related to the peak acceleration response a_{max} by

$$a_{max} = |\bar{F}(f)| . \frac{\omega_o}{m} . \tag{8.15}$$

(This is an interesting and useful result as the peak response level is exactly the same as that produced by an impulse I_o of Fourier transform modulus $|\bar{F}(f)|$.) After the acceleration reaches its peak value, it decays exponentially in free vibration; therefore the viscous damping ratio can be expressed in terms of the time, T_n, taken for the response to decay from a_{max} to noise level σ_n, i.e.,

$$e^{-\xi\omega_o T_n} = \frac{\sigma_n}{a_{max}} . \tag{8.16}$$

Substituting equations (8.12)-(8.16) into (8.11) gives the dynamic range in the frequency domain as

$$0.3.\frac{(a_{max}/\sigma_n)}{\log_{10}(a_{max}/\sigma_n)} \cdot T_n\sqrt{\frac{\Delta f}{T_o}} \qquad (8.17)$$

where if T_n is approximately equal to T_o, gives

$$\left[0.3.\frac{a_{max}/\sigma_n}{\log_{10}(a_{max}/\sigma_n)}\right] \cdot \sqrt{\Delta f.T_n}$$

The function in [ ] is plotted in the figure below.

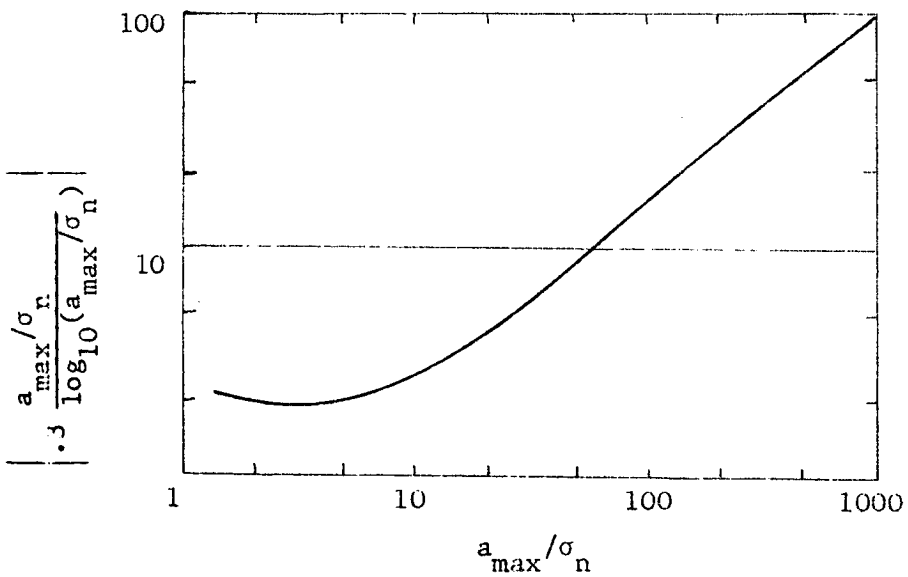

For example:- if in a test the sweep range (Δf) was 1000 Hz; the acquisition time (T_o) was 2.5 secs, and the dynamic range (a_{max}/σ_n) = 100. Then, using equation (8.17) the dynamic range in the frequency domain would be ≈ 1000.

8.5 The Use of Impedance Heads in Making Measurements of the Real and Imaginary Components of Inertance

It is well known that force and acceleration transducers add mass to a structure under test, thereby reducing the high frequency values of inertance. Impedance heads are carefully designed to have a minimal 'attached mass', typically 2-3 gm. However, other mechanical properties of the impedance heads still influence the measured data. These properties are the rotary inertia, the elasticity of the impedance head body and force crystal, the contact area with the structure.

Dealing first with the final two points, the accelerometer device is often located high in the body of the impedance head, above the force crystal, as seen in figure 8.2. Therefore, because of the elasticity of the impedance head body and the force crystal, the accelerometer is effectively mounted on a spring. This has the effect of creating an 'added stiffness' contribution to measured inertance data. This term is noticeable if the structure is heavy. However, it must be remembered that these spring effects only contribute to the imaginary component of mobility and do not affect the real component, which is the most important term, being associated with the power input. It has also been shown in |33| that the distortion of local material around the contact area of the impedance head causes an apparent stiffness term, K, in the measured inertance data of magnitude

$$K = 2aE/(1 - \nu^2)$$

where 'a' is the radius of the circular contact area, E is the modulus of elasticity, and ν is the Poisson's ratio. As before, this stiffness term is only noticeable on heavy structures in the high frequency region. Similar comments apply to this stiffness effect as to the previous one mentioned. Of course, on heavy stiffened structures, wavelengths are long (below the frequency when the structural element local to the excitation is able to resonate). Therefore, it is not necessary to use impedance heads but rather use an accelerometer adjacent to a force transducer, thereby avoiding these undesirable local distortion effects.

The rotary inertia of the impedance head reduces measured mobility data, and can cause anti-resonant behaviour, when the impedance head rotational impedance is comparable with the average rotational impedance of the structure. This effect is therefore only seen when point measurements are made towards the edge of structures, where vibration has a significant rotational component. Appendix 5 gives an analysis of this effect when an impedance head with mass and rotary inertia is placed at the end of a semi-infinite beam. This effect was mentioned in section 6.2.1.1, part (iii), and it is also observable in figures 10.4 and 10.5 at 4.5 kHz and 2.5 kHz, respectively.

8.6 Summary

Power input measurement requires accurate measurement of the real and imaginary components of the complex frequency response functions. Such measurements are subject to errors due to extraneous noise, the exciter and transducer mass and rotary inertia, the finite sampling rate of digitisation of time data.

(i) The exciter moving element mass or impedance exacerbates noise effects in the force signal. This causes noise corruption of data in the region of resonances.

(ii) Low response levels at the time of measurement can result in noisy frequency response measurements. If the noise is of a random nature, the frequency response measurements can be 'cleaned up' by averaging adjacent points in the frequency response measurement. This method is particularly appropriate if a large Fourier transform size is used, as averaging may not cause a serious loss of frequency resolution.

(iii) Frequency response measurements made using the division of single Fourier transforms are subject to 'random noise' type corruptions at frequencies approaching the Nyquist frequency. This effect is particularly noticeable in the real component of mobility as it is small relative to the modulus (except in the region of resonances). There is therefore some merit in keeping sampling rates high.

(iv) The rotational inertia of impedance heads or force transducers can cause anti-resonant behaviour and a lowering of values of point mobility measurements made near the edge of structures.

(v) Elastic deformation of the impedance head or local structure do not affect the measured values of the real component of mobility of the structure.

PART 3 APPLICATION OF TECHNIQUES TO PRACTICAL MEASUREMENTS OF POWER TRANSMISSION FROM A MACHINE TO A SEATING

CHAPTER 9

DISCUSSION OF THE APPROXIMATE BEHAVIOUR OF PRACTICAL MACHINE-ISOLATOR-SEATING CONFIGURATIONS

9.1 Introduction

The figure below shows a simplified diagram of a typical marine engine installation. It is composed of a heavily damped machine, which is

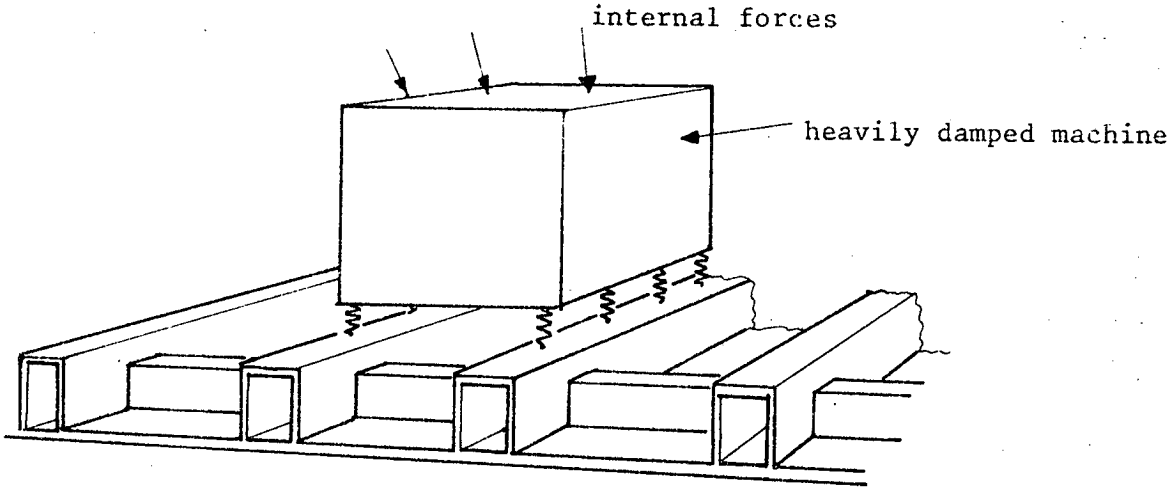

subjected to many internal forces and is multi-supported by vibration isolators upon a built-up stiff structure of plates and beams.

The main objective of this thesis has been to investigate the parameters which control power transmission between structures coupled by isolators. With this understanding, it is then possible to make simplifying assumptions of the practical situations, hence permitting approximate estimates of power transmission to be made.

In the simplest cases it is possible to represent the problem in terms of the free velocity V_f of the coupling points on the engine

structure, i.e., for single point coupling via a spring with complex stiffness, from equation (3.8),

$$P_{tr} = \tfrac{1}{2}|V_f|^2 . \frac{\mathrm{Re}\{\bar{M}_R\}}{|\bar{M}_2 + \frac{\omega}{K}(i + \eta) + \bar{M}_R|^2}$$

where $\bar{M}_2$ and $\bar{M}_R$ are the mobilities at the connection point on the machine and the seating. This expression is only useful for frequency averaged predictions of power transmission if the modulus of the denominator does not change rapidly with frequency, that is, if the isolator is very effective or the seating and structure are very heavily damped. This assumption is probably valid in the higher frequency region where the machine behaves as a velocity source above the isolator. In this frequency region, the vibrations at the different points on the seating are probably uncoupled and the total power transmission from N isolators would be simply the sum of the individual contributions, i.e.,

$$P_{tr} \simeq \tfrac{1}{2} \sum_{j=1}^{N} |V_j|^2 . \frac{\mathrm{Re}\ \bar{M}_R}{|\omega/K|^2} \qquad (9.2)$$

where V_j is the free velocity at point j on the machine. Although this particular case was not considered, some relevant measurements of engine velocity, and engine and seating mobilities are given by Ohlrich in [34]

An interesting attempt at accommodating the effects of multipoint supports has been made by Petersson and Plunt [29]. This method expresses the total power transmitted by the isolators in a form similar to equation (9.1), except that $|V_f|^2$ is the mean square space averaged velocity of the engine at the connection points and $\bar{M}_2$ and $\bar{M}_R$ are 'effective' mobilities or impedances, embracing the effect of the multi-point supports. The 'effective impedances' (as they are referred to) are obtained by experimental and computational procedures. A useful observation, which arose from experimental measurements on practical marine seatings made in this reference, is that the vibrations at adjacent mounting points do not appear to be strongly coupled (i.e., the local force input at a point is mainly responsible for the velocity at that point). This assumption greatly simplifies the analysis, but of course

the proposed procedures become unnecessary as the result reverts to a form similar to equation (9.2). However |29| appears to be the only recorded attempt to tackle the multipoint problem in a practical way.

These two approaches mentioned above are both most effective in the high frequency region where the machine tends to act as a velocity source above the isolators. However, the more novel feature of this thesis has been the attempt to make approximate power transmission predictions in the lower frequency region where it cannot be said that the source acts independently from the receiver. In this frequency region it is possible that the source and the receiver have marked resonant behaviour. Although the theory for the proposed approximation was derived using simple mass, beam and spring systems, the purpose of this chapter is to discuss how these results may be applied to the more complicated practical original installation. This involves a discussion of the approximate behaviour of practical machine and seating structures, which is a pre-requisite for power transmission estimates.

9.2 The Seating Structure

The seating in a marine engine installation is an extensive stiffened configuration made up of interconnected beams and plate elements.

For such a structure there are broadly two regions of behaviour; low frequency behaviour when the stiffening is effective, causing the built-up structure to vibrate in whole body modes, and high frequency behaviour when the individual plate or beam elements can resonate independently. The transition occurs when the element local to the excitation has its first resonance. Below this frequency, adjacent elements can be regarded as being well-coupled, but above this frequency there is weaker coupling.

9.2.1 The high frequency behaviour is considered first, when the seating behaves as a simple element, beam or plate. The theory developed in Chapters 2-6 assumed that the seating could be represented by an end-excited beam, but the results would hold equally rigorously to any structure with evenly spaced and equally excited modes, which would include a centre-excited beam and some centre excited plates.

However, in general the assumption of equally excited and evenly spaced modes is not true, which causes some difficulty in the choice of resonant peak value of point mobility $(\hat{Q})$ to be used in power transmission estimates (see table 2). It was therefore decided to investigate the form of the point mobility of a structure with unevenly spaced unequally excited modes, with a view to selecting an appropriate resonant peak value to use in the approximate seating mobility formula (equation (2.5)). Selected for this study was the simplest structure which satisfies these requirements, namely, a simply supported rectangular plate.

9.2.1 (i) The mobility of a simply supported rectangular plate

Equations (7.9) and (7.10) give the real component of mobility of the p'th mode at point s on an arbitrary structure. The frequency averaged value of the mobility at point s for a single mode is given in |21| as

$$\langle \mathrm{Re}\{M_s^{(p)}\} \rangle = \frac{\pi}{2m_p} (\psi_s^{(p)})^2 \qquad (9.3)$$

where m_p is the modal mass (plate mass/4 for a simply supported plate) and $\psi_s^{(p)}$ is the eigenvector for the p'th mode at point s. The resonance peak value of mobility of the mode at point s is

$$\hat{M}_s^{(p)} = (\psi_s^{(p)})^2 . \frac{1}{\eta \omega_p m_p} , \qquad (9.4)$$

where ω_p is the angular resonance frequency and η is the loss factor.

The frequency averaged value of the real component of mobility of a plate is given by summing the number a modal contribution, ΔN, in a given frequency band $\Delta\omega$. Therefore, using equation (9.3), the frequency

averaged value of the real component of mobility is

$$Q = \frac{\pi}{2m_p} \cdot \frac{1}{\Delta N} \cdot \sum_{p}^{p+\Delta N} (\psi_p^s)^2 \cdot \frac{\Delta N}{\Delta \omega} \qquad (9.5)$$

For a simply supported plate of area A_o

$$\Delta N/\Delta\omega = (\mu/EI)^{\frac{1}{2}} . A_o/(4\pi) \qquad (9.6)$$

and $\psi_s^{(p)} = \sin k_x x_s \sin k_y y_s$, where $x_s y_s$ are the coordinates of point s and k_x and k_y are the wavenumbers in the x and y directions. At any position the frequency averaged value of $(\psi_p^s)^2 = \frac{1}{4}$ (if measured over at least five modes |24|). Thus it can be shown from equations (9.5) and (9.6) that the frequency averaged mobility of a plate is

$$Q = 1/(8\sqrt{\mu EI}). \qquad (9.7)$$

Although the frequency averaged value at mobility Q is independent of position, the choice of $\hat{Q}$, the approximate resonance peak value, depends upon the excitation position and is related to the number of modes strongly excited, as is shown in the following two cases:

(i) For a centre excited plate, only symmetrical modes are excited, i.e., $\Delta N/\Delta\omega$ is a quarter of the value given in equation (9.6). The eigenvector for these modes is unity, therefore from equation (9.4), $\hat{Q}$ takes its maximum possible value of

$$\hat{Q} = 1/(\eta m_p \omega_p). \qquad (9.8)$$

(ii) If the plate were excited in such a position that all the modes were equally excited, i.e., $\Delta N/\Delta\omega$ is the value given in equation (9.6) then from equations (9.5) and (9.7) the eigenvector of each mode is $\frac{1}{2}$ and $\hat{Q}$ takes its minimum average value of

$$\hat{Q} = 1/(4\eta m_p \omega_p). \qquad (9.9)$$

For an arbitrary structure the modal density and the average resonance peak values will be between these two limits. Therefore to minimise errors in the choice of an approximate seating formula for a plate, it would be reasonable to assume that half the modes are excited, each mode with a resonant peak value $\hat{Q}$ of

$$\hat{Q} = \frac{1}{2\eta\omega_p m_p} . \tag{9.10}$$

The approximate plate mobility formula, in a form comparable with the beam formula in equation (2.5), is

$$\bar{Q} = \frac{Q(\cos(\beta/2) + i \sin(\beta/2) \cos(A_o k^2/4))}{1 - \sin(\beta/2) \sin(A_o k^2/4)} \tag{9.11}$$

where k is the flexural wave number and A_o the plate area. β is defined from the resonance peak value given in equation (9.10).

9.2.2 Marine engine seatings have the general appearance of plates stiffened periodically in either one direction or two orthogonal directions. As stated earlier, below the first resonance of the individual plate elements, the stiffening controls the vibration of the structure and hence the point mobility. It is worth noting here that stiffening is useful in reducing the low frequency mobility of structures, thereby reducing power transmission from any force source.

If the seating is stiffened in two orthogonal directions, the point mobility becomes that of an orthotropic plate, with modes fairly evenly distributed in frequency, and may therefore be modelled by an approximate expression of the form of equation (9.11).

If the seating is stiffened in only one direction, then there is periodic structural behaviour with 'stop bands' and 'pass bands' over broad frequency ranges |21|. Power can only be transmitted by the structure in the pass band region and so the averaged real component of mobility (related to the power input), is much larger in this frequency region than in the stop band. Thus, in developing approximate seating formulae, these two frequency areas must be considered separately. Some

insight into the behaviour of this type of seating resulting from measurements is given in the next chapter (see section 10.2).

The point mobility of one of the beams in a beam-stiffened plate tends to that of an uncoupled beam at high frequencies (i.e., frequencies greater than that of the first resonance of the intermediate plate elements).

In the low frequency region when the overall vibration of the seating is governed by the stiffening, the real component of mobility is the same on the plate or on the adjacent stiffening beams. The flexibility of the plate merely contributes a local stiffness term to the mobility, $i\omega/k_L$, which having a purely imaginary mobility, has no effect on power input to the seating, if it is excited by a force source, i.e.,

$$\bar{M}_{plate} = \frac{i\omega}{k_L} + \bar{M}_b . \qquad (9.12)$$

$\bar{M}_b$ is the mobility on the adjacent beam.

If, however, a machine is rigidly connected to the seating, this local stiffness could act as an isolator at low frequencies.

9.3 The Machine

The machine structure is rather complicated, consisting of a jointed, built-up casing, which is coupled to the internal moving parts by various types of bearing. The bearings, which rely upon the presence of oil films between moving parts, have accordingly a stiffness which is load and speed dependent, and tends to be non-linear |35|. When the machine is not running the oil films are not generated and so the coupling between the casing and the moving parts is reduced. This is seen in |36| where the measured loss factor on the running machine was twice that of the inactive machine. To be rigorous then in the measurement of machine mobilities, it would be necessary for the machine to be running during the test, as in |37|. These problems of the fluctuation in bearing coupling are of course most acute when considering the transmission of vibration through the bearings. However, in the approach adopted here, the inner workings of the machine are not deeply considered, but only the resulting velocities on the casing.

It is assumed therefore that the machine is a casing acted upon by internal force sources (from the combustion or bearings) which are independent of the casing vibration level.

The machine has three regions of behaviour. At low frequency it moves as a rigid body in translation and rotation. In the mid-frequency region the internal stiffening is effective and the casing vibrates in overall modes, in bending or twisting; for example in |13| in this mid-frequency region it was considered that an automotive diesel engine behaved as a beam. The real component of mobility is the same on the unstiffened or adjacent stiffened regions, the only difference between the two points being the local stiffness effect, as given in equation (9.12). Finally, at high frequencies, when individual casing elements can vibrate independently the point mobility tends to that of the local element. In this frequency region the structure does not vibrate in overall body modes but vibrations tend to propagate around the machine, causing the casing close to the internal excitation point to vibrate more than the casing remote from the internal excitation point.

9.4 Power Transmission Approximations

Power transmission estimates can be made in the light of the various simplifying assumptions based upon the known machine and seating behaviour. The three frequency regimes mentioned above in the discussion of the machine structure are maintained.

(i) At low frequencies the machine moves as a rigid body. Equation (3.16) gives the power transmitted by the vertical motion of the machine alone. In Appendix 10 the expression is derived for power transmission to a seating from a spring mounted rigid body. The rigid body is free to move in translation and rotation, and it can be seen that the power contributions of the two degrees of freedom are independent of each other. This decoupling arises because of symmetry in the seating and isolator arrangement, i.e., the point mobilities $\bar{M}_1$ at the two coupling points are the same. Expression (A10.11) could easily be extended in like manner to include the power transmission from the other four degrees of freedom

of the rigid body if necessary, provided that the assumption of symmetry in the machine and seating arrangement could be made. It is worth noting in equation (A10.11) that it is also necessary to know the transfer mobility between coupling points. However, at these low frequencies the flexural wavelength in the seating is long and so that carefully selected groups of isolators could be modelled as simple isolators at each corner of the machine.

(ii) It is in the mid-frequency range that there is the possibility of difficulty in predicting power transmission from the machine. This is because both the machine and the seating would be behaving in a resonant manner, and the isolator, if present, may not have large enough mobility to decouple the two systems.

This case was considered in principle in Chapters 5 and 6. In Appendix 9, it is shown how these results may be applied to estimate the power transmission between two arbitrary structures coupled by a spring. Equation (A9.6) gives the transmitted power by a single isolator to be

$$P_{tr} \simeq \hat{P}_{in} \cdot \frac{\mathrm{Re}\{\bar{M}_2\}\ \mathrm{Re}\{\bar{M}_R\}}{|\bar{M}_2 + \frac{\omega}{K}(i + \eta) + \bar{M}_R|^2}$$

where $\hat{P}_{in} = \frac{1}{2}|V_f|^2/\mathrm{Re}\{\bar{M}_2\}$, which is the maximum power that can be input to the uncoupled machine at any frequency, and must be measured on the machine in question. $\bar{M}_2$, $\bar{M}_R$ are the mobilities of the source and seating, for which the average resonant peak values $\hat{S}$ and $\hat{Q}$ and the frequency averaged values S and Q must be estimated in order to predict frequency averaged and peak power using table 2.

No account is made for multi-point coupling in the theory; and the effect must therefore be estimated. In the next chapter it is seen that reasonable estimates are obtained if it is assumed that if two isolators lie within half the flexural wavelength of the seating they act as a single isolator of twice the stiffness, while if the isolators are separated by a distance greater than half a wavelength the power transmission contributions can be regarded as independent and summed separately.

Finally, in the previous section it was noted that built-up machines and seatings have a local stiffness which varies depending on whether the point of interest is an unstiffened or stiffened region. It can be seen from the following expression that the local stiffness of the structure has no effect on the power transmission, P_{tr}.

$$P_{tr} = \tfrac{1}{2}|V_f|^2 \cdot \frac{\mathrm{Re}\{\bar{M}_R\}}{|\bar{M}_2 + i\omega(\frac{1}{K_2} + \frac{1}{K_R} + \frac{1}{K_I}) + \bar{M}_R|^2}$$

provided the isolator stiffness (K_I) is much less than the local stiffness of the seating, and source (K_R, K_2). However, if there is no isolator these local stiffnesses are largely responsible for any decoupling between the source and seating. In these circumstances, if some vibration isolation is desired, it is advisable therefore to couple stiffened parts of the source to unstiffened parts of the seating or vice-versa. This procedure would also ensure a measure of decoupling at high frequencies when the vibration is governed by the local behaviour of the source and seating.

(iii) In the high frequency region it is most likely that the machine behaves as a velocity source above the isolator. It was shown in equation (5.36) that this velocity source region begins when

$$(\frac{\omega}{K})^2 > \hat{M}_2 . \hat{M}_R$$

where ω/K is the isolator mobility, and $\hat{M}_2$ and $\hat{M}_R$ are the resonance peak values of the source and seating mobilities. At these high frequencies it is likely that the connection points on both the source and seating are uncoupled from each other and the total power transmission is given as a sum of the contributions from the individual isolators, i.e., for N isolators,

$$P_{tr} \simeq \tfrac{1}{2} \sum_{j=1}^{N} |\bar{V}_j|^2 . \frac{\mathrm{Re}\{\bar{M}_R\}}{(\omega/K)^2}$$

where $\bar{V}_j$ is the free velocity at point j on the machine.

CHAPTER 10

POWER TRANSMISSION EXPERIMENTS ON A SEMI-PRACTICAL MOTOR-ISOLATOR-SEATING ARRANGEMENT

10.1 Introduction

An experiment was set up to test some of the theoretical and experimental techniques developed in this thesis in a rather more realistic situation than considered earlier; the semi-practical model chosen consisted of a D.C. electric motor mounted with four rubber isolators upon a ship-like seating structure.

The D.C. motor was set in motion and the power transmitted by the isolators to the seating structure was measured using two techniques proposed earlier, namely, using the isolator transfer apparent mass, and using the seating apparent mass.

Although the motor was mounted on four isolators in the final configuration, initial tests were also conducted with only one isolator connected.

Three types of machine excitation were considered; first, an external rapid frequency sweep forcing function applied to the stationary motor; second, with the motor free running with all excitation provided by out of balance forces and brush noises, etc.; third, "impulsively" hammering on the motor casing in syncronization with the motor rotation. This was to simulate the vibration of a periodically excited machine such as a diesel engine.

The motor also radiated noise from the casing and from a cooling fan, which caused an acoustic 'short circuiting' path around the isolators to the seating structure, a situation that may not be uncommon in practice.

To permit theoretical predictions of power transmission the properties of the uncoupled motor, isolators and seating were measured.

10.2 Description of Components

(i) The seating

Figure 10.2 shows the seating structure; designed to be an approximation to a $\frac{1}{4}$ scale section of ship hull. The structure consisted of a 6 mm x 2.4 m x 1.2 m steel plate stiffened by five beams each of the section shown in figure 10.1, and spaced 17.8 cm apart. The adhesive joints at the top and base of the web consisted of a 50/50 by volume, mixture of Araldite Resin 2003 and aluminium powder. This mixture provided a hard and brittle bond between components. This adhesive was used as it was thought that welding would buckle the plate sections. The plate was supported upon 10.2 cm of plastic foam: tests made on an undamped plate indicated that the plate was well decoupled from the floor.

The circumference of the plate was embedded in sand to a distance varying between 30 and 60 cm, as seen in figure 10.2. This caused the finite plate to behave vibrationally as part of a much more extensive structure, as, for example, a ship's structure.

The point inertance was measured at the centre and edge of the top flange of the central beam (positions a and b), see figures 10.1, 10.2. The rapid frequency sweep method [26] was used, with excitation provided by a coil and magnet arrangement. Force and acceleration were monitored with a Force Transducer B & K type 8200 and Accelerometer B & K type 4333. Sampling rates of 2k samples/sec and 20 k samples/sec were used in all tests to provide data in the 0-1 kHz and 1 kHz-10 kHz ranges, respectively.

Figure 10.3 displays the imaginary component of inertance and modulus of inertance at the two measurement positions. Considering first the measurements made at the centre of the flange, it can be seen that above 400 Hz the inertance may be approximated to that of a single infinite T-sectioned beam, with the neutral axis taken about the bottom edge of the web (as it is assumed that the plate does not stretch). The beam inertance was calculated on this assumption to be $k/(4\mu) = 10^{-2} \times f^{\frac{1}{2}}$, where μ is the mass/unit length and the wave number is $0.85 \times f^{\frac{1}{2}}$.

The first flexural wave resonance of the beam cannot occur until above 600 Hz, therefore below this frequency it can be assumed that each beam moves as a rigid body. The point inertance of an equivalent system

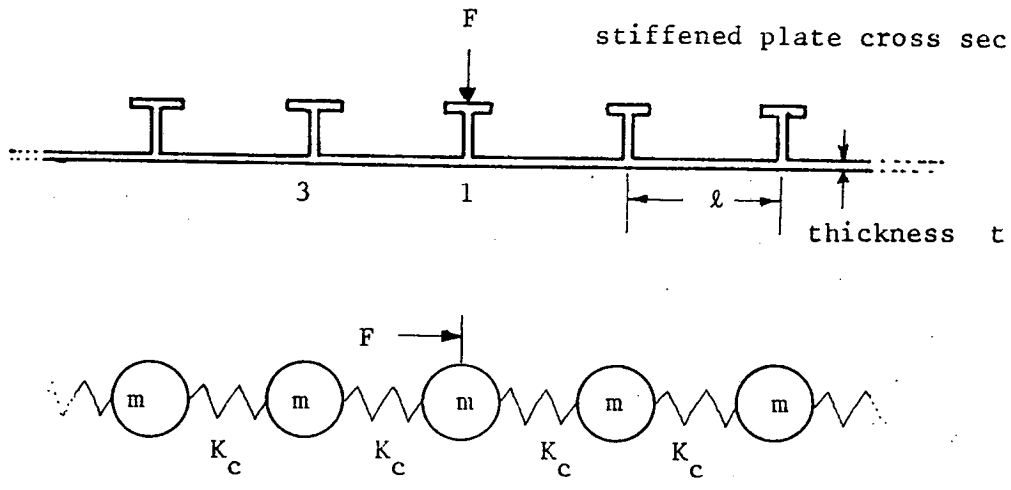

Model for low frequency behaviour of stiffened plate cross section

with an infinite number of parallel equi-spaced rigid beams can be found with consideration of the figures above, where m is the mass of one beam and one plate section, K_c is the stiffness of a cantilever of length ℓ and thickness t, i.e., $3EI/\ell^3$. Using the approach used in [21, Ch.], the point inertance on the beam can be shown by this representation to be

$$\bar{I}_s^{(1)} = \frac{i\omega}{2\sqrt{K_c m}} \cdot \frac{1}{(1 - \omega^2 M/(4K_c))^{\frac{1}{2}}} \qquad \omega^2 < \frac{4K_c}{m} \tag{10.1}$$

and the transfer inertance between adjacent beams

$$\bar{I}_s^{(13)} = \bar{I}_s^{(1)} e^{i\gamma} \tag{10.2}$$

where $\cos \gamma = 1 - \omega^2 M/(2K)$.

Below the cut-off frequency, which, using equation (10.1) is 120 Hz, the point inertance is purely imaginary, indicating that the power is readily transmitted through the structure, and the adjacent beams are well coupled. Below the cut-off frequency, equation (10.1) predicts $I_s^{(1)} = 2.7 \times 10^{-4} f \text{ kg}^{-1}$, and is shown in figure 10.3 to be a reasonable estimate of average behaviour. Above the cut-off frequency power cannot

be input to the seating system with this mode of behaviour and the point inertance becomes purely real, tending to that of the mass of a rigid beam.

As the plate is finite, with five beams rather than an infinite number, there should be five resonances below the cut-off frequency, it is possible that the three broad peaks in this region were associated with the three symmetrical modes 1, 3 and 5 (which would be excited by the force applied to the central beam).

The inertance of the edge of the flange was very similar to that at the centre until about 1 kHz. At about 3 kHz a broad resonance occurred which was identified as being the fundamental cantilever mode of the beam section about the root. This frequency was calculated using a first mode approximation based upon modelling the web as a free-pinned beam, mass loaded at the free end with the flange |38, Ch. 9|. The effect of the web root stiffness and top flange rotary inertance were negligible. The resonance frequency was given as

$$f^2 = \frac{f_o^{\,2} \times M_W/4}{M_W/4 + M_F(\phi(\ell))^2} \; ; \qquad f_o^{\,2} = \frac{2.45}{\ell^2}\sqrt{\frac{\rho A_o}{EI}} \qquad (10.3)$$

where M_W, M_F are the mass of the web and flange, respectively; $\phi(\ell)$, the eigenvector at the top of the web, is unity. f_o is the resonance frequency of a beam of length ℓ, the web length.

The resonance frequency, f_o, calculated on this basis was 3.09 kHz.

At very high frequencies the inertance at the edge of the flange approached that of a 6 mm plate.

(ii) The motor

The motor chosen for the experiment was a compound wound, 1.5 hp, D.C. electric motor, made by the Normand Electrical Company, frame size 7A. The motor casing was of cast iron, 6 mm thick, in the unstiffened sections. The output shaft was of $\frac{3}{4}$ inch diameter and was located by deep groove ball bearings, type RLS 62Z. The motor weighed 32.7 kg, and can be seen in figures 10.6, 10.9 and 10.10.

The point inertance of the motor was measured at the front left foot (position 1) and, the selected point for external excitation, at the front of the top of the motor (position 5). The imaginary component of inertance and modulus of inertance at these two points are shown in figures 10.4 and 10.5. Below 300 Hz it can be seen that the machine behaved as a rigid mass. The inertance at points 1 and 5 were approximately the same value of 0.1 kg^{-1}. The point inertance of a body free to rotate is given as

$$\frac{1}{m} + \frac{a^2}{I} \qquad (10.4)$$

where 'a' is the distance from the centre of gravity to the excitation point, and I the moment of inertia about centre of gravity and m is the mass of the motor. The moment of inertia can therefore be deduced from the measured data to be

$$I \simeq m \frac{a^2}{2} . \qquad (10.5)$$

Between 300 Hz and 3 kHz the real component of the point inertance was controlled by the local stiffness of the structure, while the imaginary component of inertance governed the power absorbed by the motor vibrating in its overall modes of vibration. For force source excitation the local stiffness of the motor does not affect the power input to the structure (see section 9.4(ii)).

At about 4 kHz the resonance of the structure local to the driving point occurred. Above this frequency the imaginary component of inertance became the dominant component in the modulus, thus indicating the frequency above which machine-like structures begin to behave as structures of infinite extent, without strongly resonant behaviour. The high frequency inertance at point 5, as seen in figure 10.5, approached that of a 6 mm cast iron plate, where 6 mm was the thickness of the local structure.

The broad troughs observed at 4.5 kHz at point 1, and at 2.5 kHz at point 5 were associated with antiresonant behaviour at the measurement position, exacerbated by the rotary inertia of the transducers, as discussed in section 8.4.

(iii) The isolators

Four isolators, 1-4 (see figure 10.6) were used to mount the motor, one beneath each foot. Each isolator was a piece of natural rubber, 3 cm x 3 cm x 1 cm, sandwiched between two 3 cm x 3 cm x 5 mm aluminium plates. The rubber was bonded to the aluminium with cyanoacrylate cement.

The power transmission through each isolator can be measured with a knowledge of the isolator transfer apparent mass (Section 7.4). The arrangement used to measure these quantities is shown in figure 10.7. Rapid frequency sweep excitation was used, and the acceleration above each isolator and the resulting blocked force below each isolator were monitored. The isolators were mounted in pairs for stability, and suspended weights were used to apply a static preload comparable with that which would be imposed by the motor. The transfer apparent mass of the isolator to be used under the front left foot, $\bar{A}_I^{(1)}$ is shown in figures 10.8(a) and (b). The low frequency behaviour, 0-1 kHz, in figure 10.8(a), was that of a hysteretically damped spring, i.e.,

$$\bar{A}_I^{(1)} = (\omega^2/K).(1 + i\eta) \qquad (10.6)$$

where $K = 4.43 \times 10^5$ N/m, $\eta = 0.08$.

The cross coupling effects, particularly noticeable in the imaginary component, were probably associated with resonant behaviour of the static loading arrangement. To avoid these imperfections, the modelled data, equation (10.6) and figure 10.8(a), was actually used in the power transmission experiments.

The high frequency behaviour data, 1 kHz-10 kHz, shows that the spring-like behaviour ceased at the natural frequency of the isolator at about 2.2 kHz. Thereafter the modulus of the transfer apparent mass is approximately 4×10^{-3} kg.

10.3 Power Input to and Transmitted from a Motor Mounted upon Four Isolators when Subjected to a Rapid Swept Sinewave Forcing Function

The motor was mounted on the seating structure using the four isolators. Figure 10.10 shows the arrangement for only one isolator. Each isolator was attached to the seating structure via a 1.5 cm diameter washer, at points mid-way between the edge and centre of the beam flange. Cyanoacrylate cement was used for the bonding.

A Ling exciter type 406, shown in figure 10.10, was attached via a short flexible drive rod to position 5 at the front of the motor. The applied force was monitored using a B & K force transducer type 8200, and the acceleration by an adjacent accelerometer B & K type 4333. Accelerometers were positioned above and below each isolator as shown in figure 10.10.

The objective of the experiment was to excite the stationary motor with a rapid frequency sweep between 0-1 kHz and measure the energy* input

---

* It must be noted here that when a structure is subjected to continuous excitation, the power, (or rate of energy dissipation,) is the quantity of interest. For random excitation $\omega \times$ power/Hz was given in equation (1.13b) as

$$\omega \times P_{in}/Hz = G_{FF}.I_m\{\bar{I}_s\},$$

where G_{FF} is the force spectral density, having units of F^2/Hz. However, if the structure is excited by a transient force, the total energy dissipated E_{in} becomes the quantity of interest, where

$$E_{in} = \int_0^\infty P(t)dt$$

where $P(t)$ is the instantaneous power. The spectral content of the energy is expressed in a similar manner to equation (1.13b), i.e.,

$$\omega \times E_{in}/Hz = |\bar{F}(f)|^2.I_m\{\bar{I}_s\}$$

where $|\bar{F}(f)|$ is the modulus of the transient force Fourier transform, with units of F/Hz. It can be seen from the above expressions that the same relationship is derived if, for continuous excitation the power is normalised by the force spectral density, or, for transient excitation the energy is normalised by the square of the force Fourier transform modulus, i.e.,

$$\frac{\omega \times P_{in}/Hz}{G_{FF}} \equiv \frac{\omega \times E_{in}/Hz}{|\bar{F}(f)|^2} \equiv I_m\{\bar{I}_s\}$$

Likewise similar relationships exist between the energy transmitted and the power transmitted.

at position 5 and the energy transmitted via the four isolators.

The energy input, E_{in}, was normalised to the force input and was therefore equivalent to the imaginary component of inertance at point 5 of the coupled systems.

$$\frac{\omega \times E_{in}/Hz}{|\bar{F}(f)|^2} = I_m\{\bar{I}_5\}$$

where $\bar{F}(f)$ is the Fourier transform of the applied force.

The total energy transmitted, E_{tr}, was the sum of the energies transmitted through each isolator, and when normalised to the force input is given from section 7.4 as

$$\frac{\omega.E_{tr}/Hz}{|\bar{F}(f)|^2} = \frac{1}{|\bar{F}(f)|^2} \sum_{n=1}^{4} I_m\{\bar{a}_M^{(n)}(f).\bar{a}_S^{*(n)}(f).\bar{A}_I^{(n)}\} \qquad (10.7)$$

where $\bar{a}_M^{(n)}(f)$ and $\bar{a}_S^{(n)}(f)$ are the Fourier transforms of the accelerations above and below the n^{th} isolator, $\bar{A}_I^{(n)}$ is the transfer apparent mass of the n^{th} isolator.

Figure 10.11 shows the normalised power $\times \omega$[†] transmitted by each of the n isolators. As the excitation was applied on the central axis of the motor the front two isolators transmitted similar quantities of normalised power and likewise did the back two isolators. However, apart from at the resonance at 320 Hz the front pair of isolators transmitted at least three times as much normalised power as the back pair. To understand this it is necessary to look at a model of the experimental system shown on the following page. The rigidity of the beams at low frequencies permits the low frequency behaviour to be modelled as a two dimensional system as shown. The relevant expression of power transmission in a more general case is given in Appendix 10. The power transmitted is the sum of the torque (F × a) and the direct force (F) contributions. At the front of the motor

---

[†] As the normalised energy is equivalent to the normalised power, the discussion of results will refer only to the normalised power to conform with the bulk of the text.

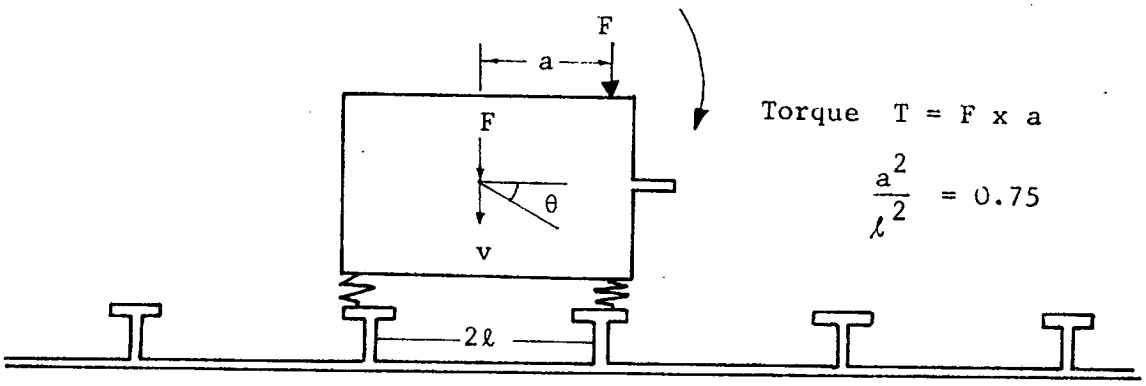

Two-dimensional model of coupled motor seating.

the torque and direct force are in phase, giving large power transmission to the seating, whereas at the back, the contributions tend to cancel. It is interesting to note that below 100 Hz (the region of the cut-off frequency, equation (10.1)) the normalised power tends to flow in the negative direction up the back isolators. This was verified with steady state measurements. Such negative power flows are likely when the seating moves in phase at the mounting points while the motor is being excited in the rocking mode, or vice versa.

Figure 10.12 shows the normalised power input at point 5 and the sum of the normalised powers transmitted by the four isolators. Below the first resonance of the motor, 320 Hz, the normalised power input was closely related to that transmitted. The imaginary component of inertance at point 5 could not be measured between 50 Hz and 300 Hz as it was very small compared with the real component.

In this low frequency there were two peaks in normalised power transmission. The first peak is the fundamental vertical resonance of the motor upon the four isolators with resonance frequency $f_o = 2\pi\sqrt{4K/m} =$ 37.5 Hz. It can be shown from equation (A9.4) that, at resonance, the normalised peak power transmission becomes

$$\frac{I_m\{\bar{I}_s^{(1)}\}}{m^2.(I_m\{\bar{I}_s^{(1)}\} + \eta\omega^2/(4K))^2} = 6.1 \times 10^{-2}\ kg^{-i} \qquad (10.8)$$

where $\bar{I}_s^{(1)}$ is the seating inertance at point 1 ($4 \times 10^{-3} kg^{-1}$). The imaginary component of the isolator inertance ($\eta\omega^2/(4K)$) was comparable with $I_m\{I_s^{(1)}\}$ causing half of the normalised power input to be dissipated in the isolators (equation (3.29)).

The second peak was the resonance of the rocking mode of the motor, which using equation (10.5), was calculated to be $f_2 = 2\pi\sqrt{8K/m} = 53$ Hz. The peak can only be estimated using equations (10.1) and (10.2), as $\bar{I}_s^{(13)}$ was not measured. The estimated peak height, assuming the seating was an infinite array of beams, was 0.15 kg^{-1}, which as expected, is an overestimation.

The power transmission at frequencies above these two resonances can be estimated using high frequency approximations to equation (A9.4), where it could be assumed that the motor behaved as a velocity source above the isolators. With reference to the previous figure in the text, equation (A9.4) becomes

$$\frac{P}{\frac{1}{2}|F|^2} \simeq I_m\{I_s^{(1)}\}(2 - \cos\gamma).(\frac{f_o}{f})^4 \qquad (10.9)$$

where $f_o = 2\pi\sqrt{4K/m}$, and $\cos\gamma$ is given in equation (10.2).

On average this equation (10.9) becomes simply

$$\frac{P}{\frac{1}{2}|F|^2} = I_m\{I_s^{(1)}\}.2.(\frac{f_o}{f})^4. \qquad (10.10)$$

which is exactly twice the power transmission that would occur if the rotation of the motor had been neglected. Equation (10.10) was plotted in figure 10.12 using the straight line approximation to the point seating inertance, shown in figure 10.3. The agreement was quite good even in the resonant region between 300 Hz and 1 kHz. This was because these resonances were heavily damped and the rigid body motion of the motor could still be a dominant component of the motor foot vibration.

10.4 Power Transmission to the Seating Via a Single Isolator from the Free-running Motor

For this experiment only the front left isolator (no. 1) was connected (see figures 10.9, 10.10), while the remainder of the motor was supported by three nylon cords. The motor was run at 40 cycles/sec. and the power transmitted to the seating was measured using two comparative methods:

(i) using the cross spectral density of the accelerations above and below each mount, $G_{a_m^{(1)} a_s^{(2)}}$ and the isolator transfer apparent mass, $\bar{A}_I^{(1)}$ (see figures 10.8a and b).

$$\omega \times \text{P/Hz} = I_m\{\bar{G}_{a_m^{(1)} a_s^{(1)}} \cdot \bar{A}_I^{(1)}\} \qquad (10.11)$$

(ii) Using the spectral density of the acceleration on the seating $G_{a_s^{(1)}}$ and the imaginary component of the seating apparent mass $\bar{A}_s^{(1)}$

$$\omega \times \text{P/Hz} = G_{a_s^{(1)}} \times I_m\{\bar{A}_s^{(1)}\}. \qquad (10.12)$$

Apart from providing a confirmation of the measured power, using the two methods provide useful information about the strength of the acoustic coupling between the motor and the seating: the isolator transfer mass method (equation (10.11)) rigorously measured the power which was transmitted by the isolator, but the estimate of power obtained using the seating apparent mass (equation (10.12)) was derived only from the acceleration at one point on the seating and was therefore insensitive to the origin of the vibration, whether in the isolator or acoustic excitation.

The power transmitted measured using the two methods is shown in figure 10.13. The acceleration spectral densities were estimated with 78 statistical degrees of freedom, and the transform size of each estimate was 1024 points, giving a 2 Hz resolution for the 0-1 kHz frequency data and 20 Hz resolution for the 0-10 kHz data.

Figure 10.13 shows that between 3 kHz and 7 kHz the two methods were in agreement, indicating that in this region the power was transmitted by the isolator. However, below this frequency, particularly between 200 Hz and 2 kHz the bulk of the power appears to have been transmitted by acoustic excitation, as the isolator transfer apparent mass method measured much lower values than the seating apparent mass method, (equation (10.12)). This result is confirmed from figure 10.13,which shows that in this frequency region the acceleration level at the connecting point on the seating was unchanged when the isolator was disconnected,while the running motor was suspended in the same position. This was not a surprising result as the motor was cooled by a rather noisy internal fan.

Figure 10.14 shows that at 80 Hz, 120 Hz and 160 Hz the acceleration levels were the same above and below the connected isolator, which would appear strange; however, it can be seen from figure 10.13 that the acoustic path is dominant at these frequencies by an order of magnitude.

At the fundamental rotation frequency the power was transmitted by the isolator as the two methods gave results which were in moderately good agreement.

10.5 Power Transmission to the Seating Via a Single Isolator from the "Impulsively" Excited Running Motor

In the previous section it was observed that at many frequencies the noise radiated by the motor was responsible for more power transmission to the seating than the vibration isolators. It was therefore decided to increase the vibration level of the motor by exciting it impulsively in synchronisation with the rotation frequency. Impulsive excitation of this sort has a broad frequency spectrum, not unlike that of the combustion forces in a diesel engine.

The configuration used in this test is shown in figure 10.9 and 10.10. A circular aluminium plate with a slot in the circumference was mounted on the motor output shaft. With each rotation, the slot passed through a detection device which output a voltage pulse, which after amplification

caused the shaker hammer fixture (see figure 10.10) to impact the motor casing at position 5. The hammer fixture was a mild steel cylinder, which in its inactive position was about 1 mm above the casing.

The motor was run at 40 cycles/sec. and the hammering amplification adjusted to give a steady sound. The input was monitored at position 5 with an adjacent accelerometer, B & K type 4333. Figures 10.16a and b show the acceleration time history of one impact at the excitation (point 5) and the foot (point 1), when the motor was freely suspended by four nylon cords. Figures 10.17a and b give the spectral densities of these two signals between 0-1 kHz, resolution 2 Hz. The side bands around each harmonic in the excitation spectrum indicate some kind of amplitude modulation of the impacting, perhaps associated with the natural frequencies of the hammer upon the shaker suspension. The spectral density of the motor foot acceleration is also shown for a 20 Hz **resolution.** Figure 10.18 displays the spectral densities of the accelerations at these two positions for the 1 kHz-10 kHz frequency range. It can be seen that the spectral density at point 1 has a similar form to the imaginary component of inertance at point 1 (see figure 10.4), and the spectral density at point 5 is of a similar form to the modulus of the inertance at point 5. Low pass filtering at 7 kHz was responsible for the decrease in the spectral densities (figures 10.18a and b) at high frequencies.

Figure 10.19 compares the power transmitted to the seating measured by the two methods, using the isolator transfer apparent mass and the seating point apparent mass. The two measurements agreed well below 500 Hz, which confirms that the power was transmitted by the isolator in this frequency region. Between 500 Hz and 1 kHz it can be seen that the seating apparent mass method (equation (10.12)) gave a slightly larger answer than the isolator transfer apparent mass method (equation (10.11)), which indicates that sound radiation from the casing and the isolator vibration were responsible for similar quantities of power transmission to the seating.

Figure 10.20 compares the power measured using the two methods between 1 kHz and 10 kHz. There is excellent agreement until about 7 kHz. Above this frequency it could be that the seating point apparent mass method is in error as the isolator was not connected at the edge of the flange (as was assumed in applying equation (10.12)), but rather mid-way between the edge and centre of the flange.

Figure 10.21 shows the power transmitted to the seating measured using the isolator transfer apparent mass method (equation (10.11)). This was measured using 20 kHz sampling rate, giving a 20 Hz frequency resolution. Between 0 and 240 Hz the power transmitted was predicted using equation (A9.4), adapted for single point transmission, i.e.,

$$\omega P/Hz = G_{a_m}(1) \cdot \frac{I_m\{\bar{I}_s^{(1)}\}}{(\frac{1}{m} - \frac{\omega^2}{K})^2 + (I_m\{\bar{I}_s^{(1)}\} + \frac{\eta\omega^2}{K})^2} \qquad (10.13)$$

The predicted points were calculated by using the measured value of the seating imaginary component of inertance $Im\{\bar{I}_s^{(1)}\}$ (figure 10.3) at each of the harmonics of 40 Hz, and values of $G_{a_s}(1)$ in figure 10.17. The agreement is seen to be reasonable.

In the higher frequency region the motor moved as a velocity source above the isolator, and this was confirmed by calculating the transmitted power using the acceleration at the foot of the free motor, as below

$$\omega P/Hz = G_{a_s}(1) \cdot |\bar{A}_I^{(1)}|^2 . Im\{\bar{I}_s^{(1)}\} \qquad (10.14)$$

where $G_{a_s}(1)$ is shown in figure 10.18b, and $|A_I^{(1)}|$ is the modulus of the isolator transfer apparent mass. These multiplications were performed using the measured data files on the computer, and can be seen to give good agreement with the power measured using the transfer apparent mass method. The exception to this is in the trough region around 2 kHz, where there was significant acoustic excitation of the seating. In this region, equation (10.14) predicts power assuming that there are no other sources of vibration acting on the seating, giving a positive value. However, the measured values are sometimes greater than these values or negative (which may have little meaning with such low signal levels) which is possible if a seating has a source of vibration in addition to a single isolator.

10.6 Power Transmitted to the Seating Via Four Isolators, from the Impulsively Excited Running Motor

The motor with all four isolators connected was run, as before, at 40 cycles/sec. The power was measured through each isolator with equation (10.11), using the cross spectrum between accelerations above and below each mount.

Figure 10.22 shows the power transmitted by the four isolators between 0-1 kHz compared with the one isolator result discussed earlier. It can be seen that the power transmitted at the fundamental rotation frequency, 40 Hz, was unchanged. At higher frequencies more power was transmitted by the four isolators than the single isolator. The bulk of it was transmitted by the front two isolators.

Figure 10.23 compares the power transmitted by the front and back pairs of isolators in the 1 kHz-10 kHz frequency range. The front two isolators, being closer to the excitation point, were responsible for the majority of the power.

Figure 10.24 gives the comparison of the power transmitted by the single isolator with that transmitted by the four isolators over the whole frequency range, resolution 20 Hz. The power transmitted at the fundamental rotation 40 Hz is given using a modification of equation (10.13).

$$\omega P/Hz = (G_{a_m^{(1)}}/9).\ \frac{Im\{\bar{I}_s^{(1)}\}}{(\frac{1}{m} - \frac{\omega^2}{4K})^2 + (Im\{\bar{I}_s^{(1)}\} + \frac{\eta\omega^2}{4K})^2} = .09 \qquad (10.15)$$

The term $G_{a_m^{(1)}}/9$ arises on account of the acceleration being one third at the centre of gravity of the motor, compared with that at the end where the excitation was applied (equations (10.4) and (10.5)).

Between 40 Hz and 300 Hz the motor moved as a rigid body and the power is given using equation (10.10), i.e.,

$$\omega P/Hz = (G_{a_m^{(1)}}/9).\ \frac{2.\{\bar{I}_s^{(1)}\}}{(\frac{\omega^2}{4K})^2} \qquad (10.16)$$

and can be seen to be approximately 4 times the single isolator value. Between 300 Hz and 2 kHz, when the motor moved in the overall modes of vibration (see figure 10.11, 300-500 Hz), the power was equally transmitted from the front and back of the motor. Therefore,

$$\omega P/Hz \simeq G_{a_m^{(1)}} .2. \frac{\{I_s^{(1)}\}^2}{(\frac{\omega}{2K})^2} \qquad (10.17)$$

which is eight times that of the single isolator case.

In the high frequency region between 3 kHz-10 kHz, the local modes of the motor vibration dominated the behaviour and only the front end of the motor, nearer to the excitation, contributed significantly to the power transmission (figure 10.23). Above 3 kHz the seating tended to resonate locally (see figure 10.3) and so the power was transmitted independently through the front two isolators. Therefore

$$\omega P/Hz = 2.G_{a_m^{(1)}} \cdot |A_I^{(1)}|^2 . Im\{\bar{I}_s^{(1)}\} \qquad (10.18)$$

and can be seen in figures 10.24 and 10.25 to be, on average, a factor of two greater than the single isolator case. Figure 10.27 shows a very similar expression to equation (10.18), namely,

$$\omega P/Hz = (\sum_{n=1}^{4} .G_{a_m^{(n)}}) . |A_I^{(1)}|^2 . Im\{I_s^{(1)}\}, \qquad (10.19)$$

where $G_{a_m^{(n)}}$ is the acceleration spectral density at the n^{th} foot of the freely suspended motor. It is assumed in this equation that the power transmission from each of the isolator feet was independent. As can be seen from the figure (10.27) this assumption is vindicated for frequencies greater than 3 kHz. However, at lower frequencies this assumption tends to cause the predicted power to underestimate the true value by a factor varying between two and four. This would probably be because at lower frequencies each pair of isolators on the same beam would be very closely coupled, due to the long wavelengths of the beam vibration.

Figure 10.26 compares the averaged power transmitted between 1 kHz and 10 kHz, measured using the two alternative methods (equations (10.11) and (10.12)) at each of the connecting points. The application of equation (10.12) in this manner assumes that the vibrations at the connecting points on the seating are uncoupled, i.e.,

$$\omega P/Hz = \sum_{n=1}^{4} G_{a_s^{(n)}} . \mathrm{Im}\{A_s^{(1)}\} \qquad (10.20)$$

where $G_{a_s^{(n)}}$ is the acceleration spectral density at the n^{th} coupling points a_s on the seating. It can be seen that this assumption causes an overestimation of the true power by a factor of two between 3 kHz and 4 kHz, but thereafter provides a good answer.

Finally, figure 10.28 compares the power input to the motor at point 5 (measured using the acceleration and 'imaginary' component of apparent mass at that point) with the total power transmitted by the four isolators. The two curves have a similar form, which above 3 kHz can be seen to be associated with the resonant peaks in the point inertance at the excitation point (figure 10.5). Thus for this type of structure, as for the simpler ones considered earlier, the power is input and transmitted at the resonance frequencies.

10.7 Summary

(i) The seating structure was a beam stiffened plate. The inertance at a point on the beam had three significant regimes of behaviour. At low frequencies the beams moved as rigid masses interconnected by the plate sections with stiffness-like behaviour. In the mid and high frequency range the point inertance on the centre of the beam was on average that of a single uncoupled beam. The point inertance at the edge of the top flange of the T-section beam became an order of magnitude greater than that of the centre, for frequencies above the first resonance frequency of the beam section.

(ii) The D.C. motor, a compact built-up construction, had three regimes of behaviour: first, rigid body motion below 300 Hz. Second, between 300 Hz and 3 kHz the structure moves in the whole body modes of vibration, while the structure local to the excitation point behaved as a pure stiffness. Lastly, above 3 kHz the individual components of the structure could resonate and the local structural characteristics dominated the point inertance measurement. These modes of vibration were heavily damped and not strongly coupled around the motor.

The motor coupled to the seating with the isolators had three types of excitation applied: a rapid frequency sweep, internal forces due to the free running motor and, external impacting applied to the motor casing. These yielded the following results:-

(iii) With the rapid frequency sweep excitation it was seen that the power was transmitted to the seating mainly by the resonances of the fundamental rigid body modes of the motor, namely, the fundamental vertical mode, and the rocking mode of the motor; these transferred similar quantities of power. Above these resonance frequencies the behaviour was straightforward, with the motor acting as a velocity source above the isolators. Power was successfully measured through the individual isolators, and in some cases negative values occurred.

(iv) When the motor was run without any additional external exitation it was found that below 3 kHz the acoustic radiation from the motor was responsible for much of the power transmission to the seating, rather than the isolator vibration. However, it was found that the isolator transfer apparent mass method of measuring power was successful in measuring the power through the isolator alone, despite the significant additional acoustic excitation of the seating.

(v) The motor was impulsively excited with each revolution; and power measured through each of the four isolators was compared with simple predictions made using the acceleration on the feet of the freely suspended motor. These predictions never became difficult, as the effect of increasingly complicated behaviour at high frequencies was mitigated by increased decoupling between mounting points on the seating structure.

CHAPTER 11

CONCLUSIONS

The thesis is presented in three parts. The first part gave a theoretical investigation of the parameters which controlled power transmission via spring-like isolators between machine sources and seating structures. The second part was concerned with practical issues, namely, the measurement of power input to a seating, and the accuracy with which the point frequency response of structures could be measured. The final part discussed the application to the practical situation of the theory developed earlier. This was culminated in an experiment on a semi-practical machine-seating configuration.

The results of these three sections were summarised at the end of each section but are briefly restated here for completeness.

11.1 Theoretical Considerations

The first section dealt with the parameters controlling power transmission between simplified machine sources and seatings, and produced the following results:

(i) For force source excitation to a structure the power is input at resonance. However, the frequency averaged power input is the same to a finite structure as that to an equivalent structure of infinite extent. This fact enables simple estimates of power input to be made from readily available mobility data of infinite structures.

(ii) At low frequencies a machine moves as a rigid body. The power transmitted from such a source to a finite seating via an isolator was considered and simple algebraic formulae for frequency averaged and peak power transmission were developed. Maximum frequency averaged power is transmitted at the resonance of the mass-spring and equivalent infinite seating. The isolator damping is an important parameter in controlling power transmitted at this resonance frequency. Less power is transmitted, at this resonance, to a finite seating than to an equivalent seating of

infinite extent. For frequencies above and below this resonance, the frequency averaged power transmitted to a finite seating is the same as that transmitted to an equivalent structure of infinite extent.

For practical machines the rigid body motion in each of the degrees of freedom can transmit power to the seating. Provided there is symmetry in the mounting arrangement each of these contributions can be considered separately, using the theory presented for the single degree of freedom case.

(iii) The power transmission via an isolator from a resonant source of vibration, namely, a short beam, to a long receiver beam, was analysed. A useful point that arises in characterising the source structure is that for a beam the real component of mobility at one end is proportional to the square of the modulus of the transfer mobility to the other end. This statement only holds in an average sense for general structures, but is a useful approximation.

The frequency averaged power input to the source structure was found to be independent of the coupling to the seating structure. Furthermore, the peak power that could be input at resonance increased with decreasing coupling between machine and seating. This means that if a machine is isolated from the seating the vibrational power that has to be absorbed internally is increased, thereby increasing noise radiation and allowing the possibility of damage occurring.

The formulae were derived expressing the peak and frequency averaged power input to the machine source, and the peak and frequency averaged power transmitted to the seating structure. These formulae, which provided no resonance frequency information, required only knowledge of the frequency averaged point mobility and the resonance peak value of mobility of the machine source and the seating. In practice, it is hoped that these two quantities could be obtained theoretically or estimated from experience.

At low frequencies all the power input to the machine source is transmitted to the seating. This represents the worst case from the transmission viewpoint. A frequency is reached when the modulus squared of the isolator transfer mobility is equal to the product of the resonant

peak values of the source and seating mobilities. Above this frequency the machine behaves as a velocity source above the isolators. From theoretical and experimental work it was found that the frequency averaged power to a finite seating structure was the same as that to an equivalent infinite structure except at the low frequency resonances of the coupled source seating system when slightly less power was transmitted to the finite seating.

11.2 The Measurement Methods

Three potentially useful methods for measuring the power input to a seating structure were proposed, the use of which was verified experimentally.

(i) Power measured through isolators, using accelerations above and below each isolator. This method successfully measures the power to a seating via one isolator in the presence of vibration contributions to the seating from other sources such as noise or other vibration inputs.

(ii) Power absorbed by a structure with modal behaviour, can be measured using accelerations at one, two or four points. This method would be particularly useful at low frequencies when modes are well-separated in frequency.

(iii) Power can be measured using the acceleration spectral density at uncoupled input points on the seating structure. This method is only useful at high frequencies if there is multipoint excitation.

Caution must be exercised in the measurement of the real component of mobility of a structure. If the structure is heavy then the background noise, the finite sampling rate of digital data and structural, local stiffness, can all degrade the accuracy of measured data. Alternatively, if the structure is light, the exciter moving element mass, the transducer rotational inertance and the sampling rate of digital data can cause denegration of the measured data.

11.3 The Practical Experiment

The seating structure, which consisted of a very heavily damped periodically-stiffened plate, had three zones of behaviour which could be characterised by approximate mobility formulae. At low frequencies the stiffening was effective and this particular structure behaved as a periodic mass-spring arrangement, the masses associated with the beams and the springs with the intermediate plate sections. The point mobility was very low; stiffening is therefore a useful way of reducing low frequency power transmission. In the mid frequency range,(the lower limit was defined as when the intermediate plate had its first resonance,) the beams tended to be vibrationally uncoupled and the point mobility on a beam tended to the value of an uncoupled beam. At high frequencies the point mobility tended to that of the local beam flange.

The machine structure, likewise, had three zones of behaviour, which may be characterised by approximate mobility formulae. At low frequencies there was rigid body motion. In the mid-frequency range the real component of mobility was dominated by the overall modes of the machine. The modulus of the mobility tended to be dominated by the local flexibility of the structure (which incidentally only has an influence on power transmission to the seating if there is no isolator). At high frequencies the local elements of a machine could resonate independently. This fact, in combination with the heavy damping of the machine, resulted in poor transmission of vibration around the machine and the vibrations of the mounting points became uncoupled.

For the chosen experimental parameters,the behaviour of the coupled system was very straightforward. There were similar power transmission contributions at low frequencies involving the translational and rocking resonances of the rigid machine upon the isolators. Although the power level of the translational resonance was well estimated, the level from the rocking resonance was not well judged. In practice a low frequency transfer measurement between the two sets of mounting points on the seating is necessary in order to take power transmission by rocking into account. Incidentally, the measurements in this frequency region showed that although the net power transmission from the sum of the isolators was positive, two isolators were actually transmitting power in the negative direction,back into the machine.

Above these low order resonances the machine behaved as a velocity source above the isolators. It seemed to be possible to estimate the effect of the multiple isolators by assuming that if they were positioned within a spacing of half a flexural wavelength on the seating they were coupled as a single isolator, but if there was at least half a wavelength spacing then the power contributions were independent. This of course only holds if the seating does not have strong resonant behaviour.

Useful topics for further work would be to experimentally examine, using the power flow techniques, the power transmission via multi-supports to resonant and non-resonant seatings. Also to experimentally examine, or by using finite element methods, the low frequency mobility of built up structures (i.e., when the stiffening is effective), with a view to compiling a list of approximate formulae.

REFERENCES

1. Snowdon, J.C. Vibration and shock in damped mechanical systems. John Wiley & Sons Inc., 1968.

2. Snowdon, J.C. Resilient mounting of machinery on plate-like and modified plate-like structures. J.A.S.A. 61(4), pp. 986-994, April 1977.

3. Soliman, J.I. and Hallam, M.G. Vibration Isolation between non rigid machines and non rigid foundations. Journal of Sound and Vibration 8(2), 1968, pp. 329-351.

4. Munjal, M.L. A rational synthesis of vibration isolators. Journal of Sound and Vibration 39(2), 1975, 247.

5. Ungar, E.E. and Dietrich, C.W. High frequency isolation. Journal of Sound and Vibration 4(2), 1966, 224-241.

6. Sykes, A.O. Isolation of vibration when machinery and foundation are resilient and wave effects occur in the mount. Noise Control, 1960, 6, 115.

7. Smollen, L.E. Generalised matrix method for the design and analysis of vibration isolation systems. J.A.S.A. 40, 1966, 195-209.

8. Massoud, M. and Pastarel, H. Impedance methods for machine analysis. Shock and Vibration Digest, vol. 10, No. 4, 1970.

9. Ewins, D.J. Measurement and application of mechanical impedance data. Journal of the Society of Environmental Engineers, June 1976 (3 parts).

10. Ewins, D.J. and Sainsbury, M.G. Mobility measurement for the vibration analysis of connected structures. Shock and Vibration Bulletin 42(1), 1972, 105.

11. Goyder, H.G.D. Methods and applications of structural modelling from measured frequency response data. Journal of Sound and Vibration 68(2), 1980, 209-230.

12. Ewins, D.J. On predicting point mobility plots from measurements of other mobility parameters. Journal of Sound and Vibration 70(1), May 8 (1980).

13. Lalor, N. and Petyt, M. Modes of engine structure vibration as a source of noise. Diesel Engine Conference, Milwaukee, 1975, SAE Paper 75 0833.

14. Petyt, M. Finite element methods for the response of structures to random excitation. Proc. World Conference on Finite Element Methods in Structural Mechanics, Bournemouth 1975.

15. Lyon, R.H. Statistical energy analysis of dynamical systems. The MIT Press, Cambridge, Massachusetts, London.

16. F.J. Fahy. Statistical energy analysis, a critical review. The Shock and Vibration Digest, Vol. 6, No. 7.

17. Davies, H. Exact solutions for the response of some coupled multi-modal systems. J.A.S.A. Vol. 51, No. 1, Pt. (2), Jan. 1972.

18. Skudrzyk, E. Vibrations of a system with a finite or an infinite number of resonances. J.A.S.A. Vol. 30, 1958, 1140.

19. Goyder, H.G.D. and White, R.G. Vibrational power flow from machines into built-up structures, Pt. 1: Introduction and approximate analysis of beam and plate-like foundations. Journal of Sound and Vibration 68(1), 8 Jan. 1980.

20. Goyder, H.G.D. and White, R.G. Vibrational power flow from machines into built-up structures. Pt. 2: Wave propagation and power flow in beam stiffened plates. Journal of Sound and Vibration 68(1), 8 Jan. 1980.

21. Cremer, L, Heckl, M.A. and Ungar, E.E. Structure-borne sound. Springer Verlag: Heidelberg, Berlin, New York. 1973.

22. Heckl, M.A. The different ways of sound transmission in and around resilient mounts. International Symposium of Shipboard Acoustics, 1976.

23. Goyder, H.G.D. and White, R.G. Vibrational power flow from machines into built-up structures. Pt. 3: Power flow through isolation systems. Journal of Sound and Vibration 68(1), 8 Jan. 1980.

24. Smith, P.W. and Lyon, R.H. Sound and structural vibration. NASA Contractor Report CR-160, March 1965.

25. Shock and Vibration Handbook, Vol. II, Ch. 36, p. 161. Material and interface damping.

26. White, R.G. Spectrally shaped transient forcing functions for frequency response testing. Journal of Sound and Vibration 23(3), 1976, 307-318.

27. Carrier, G.F., Krook, M. and Pearson, C. Functions of a complex variable. McGraw-Hill Book Co., New York, 1966, pp. 86, 3-31.

28. Odegaard-Jensen, J. Calculation of structure-borne noise transmission in ships using the "statistical energy analogy" approach. Proc. of Int. Symposium on Ship Acoustics, Janssen (Ed.), Elsevier, 1977.

29. Petersson, B. and Plunt, J. Structure-borne sound transmission from machinery to foundations. Chalmers University of Technology, Report 80-19.

30. Pavic, G. and Oreskuvic, G. Proceedings of the 9th International Congress on Acoustics, 1977, Paper G3. Energy flow through elastic mountings.

31. Holmes, P.J. and White, R.G. Data analysis criteria and instrumentation requirements for the transient measurement of mechanical impedance. Journal of Sound and Vibration, 25(2), 1972, 217-243.

32. Bendat, J.S. and Piersol, A.G. Measurement and Analysis of Random Data. John Wiley, New York, 1966.

33. Timoshenko, S.P. and Goodier, J.N. Theory of Elasticity. McGraw-Hill Book Co., 1934, 51, 70.

34. Ohlrich, M. On the transmission of audio frequency vibration from multi-point mounted engines to ship bottom structures. Int. Conference on Recent Advances in Structural Dynamics, 1980, University of Southampton.

35. White, M.F. Vibration transmission characteristics of bearings related to machinery condition monitoring. ISVR Technical Report No. 96, Dec. 1977.

36. Abideen, K. Structural damping of a running engine. M.Sc. Thesis, University of Southampton, 1976.

37. Kinns, R. The deduction of bearing forces in rotating machinery. Euromech 122, Paris, Sept. 1979.

38. Thomson, W.T. Vibration theory and applications, Ch. 9. George Allen & Unwin Ltd., 1966, 69, 71, London.

39. Handbook of Mathematical Functions. Eds. M. Abramowitz and J.A. Segan, Dover Publications.

APPENDIX 1

Calculation of the Average Value of the Real Component of Mobility

The real component of the cantilever mobility, excited at the free end, may be written in the form of equation (2.5)

$$\mathrm{Re}\{\bar{M}\} = \frac{\omega}{EIk^3} \cdot \frac{\cos\beta}{1 - \sin\beta\sin\theta} . \qquad (A1.1)$$

The average value of this expression over the frequency interval $\omega_1 < \omega < \omega_2$, corresponding to $2n\pi < \theta < 2(n+1)\pi$ in the θ plane, is

$$\langle \mathrm{Re}\{\bar{M}\} \rangle = \frac{1}{\omega_2 - \omega_1} \int_{\omega_1}^{\omega_2} D\omega^{-\frac{1}{2}} \cdot \frac{\cos\beta}{1 - \sin\beta\sin\theta} \, d\omega \qquad (A1.2)$$

$$D\omega^{-\frac{1}{2}} = \frac{\omega}{EIk^3} .$$

The θ and ω planes are related by the definition given in equation (2.1).

$$\theta = \varepsilon - C\omega^{\frac{1}{2}}$$

where

$$C = 2\ell \left(\frac{\mu}{EI}\right)^{\frac{1}{4}} \qquad (A1.3)$$

therefore

$$d\omega = -\frac{2}{C}\omega^{\frac{1}{2}} \, d\theta. \qquad (A1.4)$$

If we name the centre value of the θ interval, θ_c, i.e.,

$$\theta_c = (2n + 1)\pi$$

then the corresponding value of ω, from equation (A1.3) is

$$\omega_c = \left(\frac{\varepsilon - \theta_c}{C}\right)^{\frac{1}{2}}. \qquad \text{(A1.5)}$$

Using equation (A1.5), ω_1 and ω_2 can be written in terms of ω_c, which gives rise to the following relationship,

$$\frac{1}{\omega_2 - \omega_1} = - \frac{C}{4\pi\omega_c^{\frac{1}{2}}} . \qquad \text{(A1.6)}$$

By making substitutions from equation (A1.6) and (A1.4) into equation (A1.2) gives

$$\langle \mathrm{Re}\{M\} \rangle = \frac{D}{2\pi\omega_c^{\frac{1}{2}}} \int_0^{2\pi} \frac{\cos\beta}{1 - \sin\beta \sin\theta} \, d\theta. \qquad \text{(A1.7)}$$

To solve this integral it must be assumed that αr, hence β, change slowly compared to θ. In this event, by making use of a standard integral (see, for example, reference |27|), namely,

$$\int_0^{2\pi} \frac{a}{b - c\sin\theta} \, d\theta = \frac{2\pi a}{(b^2 - c^2)^{\frac{1}{2}}}, \qquad b > c \qquad \text{(A1.8)}$$

a, b and c are constants,

equation (A1.7) becomes

$$\langle \mathrm{Re}\{M\} \rangle = \frac{D}{\omega_c^{\frac{1}{2}}} . \qquad \text{(A1.9)}$$

This result is equal to the average value of the real component of mobility of a semi-infinite beam integrated over the same frequency interval, i.e.,

$$\frac{1}{\omega_2 - \omega_1} \int_{\omega_1}^{\omega_2} D_\omega^{-\frac{1}{2}} d\omega = \frac{D}{\omega_c^{\frac{1}{2}}} . \qquad \text{(A1.10)}$$

Therefore, for frequency average calculations, the real component of mobility of a finite beam may be represented by that of an infinite beam.

APPENDIX 2

Determination of the Reflection and Transmission Coefficients at the Termination of a Beam

If a beam is coupled to an arbitrary structure, as below

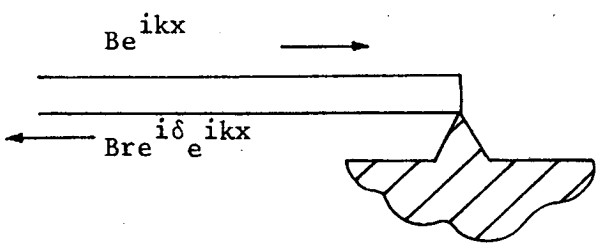

with continuity of shear force and velocity across the boundary, but no continuity of slope (i.e., a hinged connection). Then the reflection coefficient at the boundary is given by

$$re^{i\delta} = \frac{\bar{M}_2^* - \bar{M}_3}{\bar{M}_2 + \bar{M}_3} \cdot \frac{\bar{M}_2^*}{\bar{M}_2} \qquad \text{(A2.1)}$$

where $\bar{M}_2$ is the point mobility of a semi-infinite beam and $\bar{M}_3$ is the point mobility of an arbitrary receiving structure. (* denotes complex conjugate.)

Hence the modulus of transmission coefficient defined by

$$t^2 = 1 - r^2$$

is

$$t^2 = 4 \frac{\mathrm{Re}\{\bar{M}_2\} \cdot \mathrm{Re}\{\bar{M}_3\}}{|\bar{M}_2 + \bar{M}_3|^2} \quad . \qquad \text{(A2.2)}$$

When two structures are coupled by a hysteretically damped spring, the mobility term in equation (A2.2) can be replaced by

$$\bar{M}_3 = \frac{\omega}{K}(i + \eta) + \bar{M}_R$$

giving

$$|t|^2 = \frac{4\mathrm{Re}\{M_2\}.(\frac{\eta\omega}{K} + \mathrm{Re}\{\bar{M}_R\})}{|\bar{M}_2 + \frac{\omega}{K}(i + \eta) + \bar{M}_R|^2} . \qquad \text{(A2.3)}$$

where $(\omega/K)(i + \eta)$ is the spring mobility, and $\bar{M}_R$ is the mobility at the attachment point on the receiving structure.

APPENDIX 3

Calculation of $|M_{12}|^2$ for a Free-free Beam

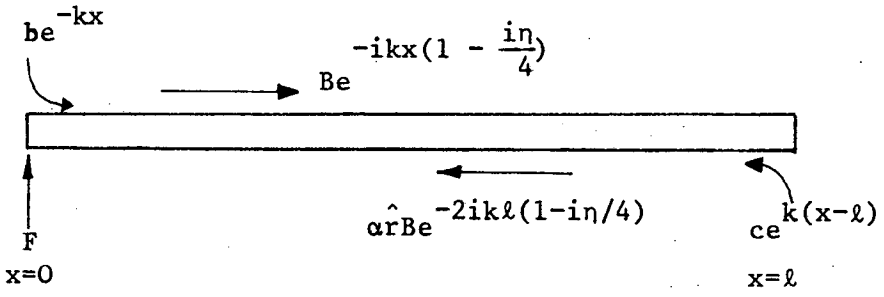

The displacements along a free-free beam are given, with reference to the figure above, as

$$y = Be^{-ikx(1 - i\frac{\eta}{4})} + be^{-kx} + \hat{\alpha r}.B.e^{ikx(1 - i\frac{\eta}{4})} + ce^{k(x - \ell)} \qquad \text{(A3.1)}$$

where $\hat{r} = re^{i\delta}.e^{-2ik\ell}$.

By setting the boundary conditions at $x = \ell$

$$\frac{\partial^2 y}{\partial x^2} = 0 \Big|_{x=\ell} \quad \text{and} \quad \frac{\partial^3 y}{\partial x^3} = 0 \Big|_{x=\ell}$$

and assuming that $k\ell > 2$, manipulation of equation (A3.1) yields

$$re^{i\delta} = e^{-i\frac{\pi}{2}} \quad \text{and} \quad c = \alpha^{\frac{1}{2}}B(1 - i)e.^{-ik\ell}. \qquad \text{(A3.2)}$$

Inserting the boundary conditions at $x = 0$, namely,

$$F = EI \frac{\partial^3 y}{\partial x^3} \Big|_{x=0} \qquad \frac{\partial^2 y}{\partial x^3} = 0 \Big|_{x=0}$$

gives $b = B(1 - i\alpha e^{-2ik\ell})$, (A3.3)

and

$$B = \frac{F}{EIk^3} \cdot \frac{1}{(1 + \alpha e^{-2ik\ell})(i - 1)} \quad \text{(A3.4)}$$

Now by setting $x = 0$ in equation (A3.1) gives

$$y|_{x=0} = 2B(1 - i\alpha e^{-2ik\ell}). \quad \text{(A3.5)}$$

Likewise, by setting $y = \ell$ in equation (A3.1), gives

$$y|_{x=\ell} = 2B\alpha^{\frac{1}{2}}(1 - i)e^{-ik\ell}. \quad \text{(A3.6)}$$

Using the relationship between velocity and displacement

$$V = i\omega y,$$

the real component of the point mobility at $x = 0$, can be found from equations (A3.5) and (A3.4) to be

$$\text{Re}\{\bar{M}_1\} = \frac{\omega}{EIk^3} \cdot \frac{1 - \alpha^2}{1 + \alpha^2 + 2\alpha \cos 2k\ell}. \quad \text{(A3.7)}$$

In the same manner $|\bar{M}_{12}|^2$ can be found from equations (A3.6) and (A3.5)

$$|M_{12}|^2 = \frac{\omega^2}{(EIk^3)^2} \cdot \frac{4\alpha}{1 + \alpha^2 + 2\alpha \cos 2k\ell}.$$

Therefore it can be seen that $\mathrm{Re}\{\bar{M}_1\}$ and $|\bar{M}_{12}|^2$ are related by

$$|\bar{M}_{12}|^2 = \mathrm{Re}\{M_1\}.\ \frac{\omega}{EIk^3} \cdot \frac{4\alpha}{1-\alpha^2} \qquad \text{(A3.8)}$$

Using the convention of Chapter 4, equations (4.2), (4.3),

$$|\bar{M}_{12}|^2 = S_r.\hat{S}.\sin\,\varepsilon. \qquad \text{(A3.9)}$$

APPENDIX 4

Power Transmission between a Long and a Short Finite Beam Coupled by a Damped Spring

(i) General relationships

The power transmission from the short to the long finite beam, shown in Figure 5.1, is to be calculated. The purpose of this section is to cover the analysis in greater detail than the summary in Section 5.2.

The short end of the beam is driven by a force of magnitude F_1. End (2) of the beam is connected by a damped spring, of complex stiffness $K(1 + i\eta)$, to the receiver beam.

The power transmission between two arbitrary structures is given by the expression in equation (3.8).

$$P_{tr} = \tfrac{1}{2}|F_1|^2 \cdot \frac{|M_{12}|^2}{|\bar{M}_2 + \bar{M}_R + \frac{\omega}{K}(1 + i\eta)|^2} \cdot \mathrm{Re}\{\bar{M}_R\}. \quad \text{(A4.1)}$$

The mobility at end (2) of the short source beam, $\bar{M}_2$, is given from equation (4.1) as

$$\bar{M}_2 = S_r - iS_i - iS, \quad \text{(A4.2)}$$

where

$$S_r = \frac{S \cos \varepsilon}{1 - \sin \varepsilon . \sin \phi}, \qquad S_i = \frac{S \sin \varepsilon . \cos \phi}{1 - \sin \varepsilon . \sin \phi}, \quad \text{(A4.3)}$$

S is the real component of mobility of a semi-infinite beam, ε and ϕ are the source beam damping and frequency parameters respectively, as defined in equations (4.2) and (4.3).

The transfer mobility $\bar{M}_{12}$ between points (1) and (2) is shown in Appendix 3 to be defined by

$$|M_{12}|^2 = \hat{S} . S_r . \sin \varepsilon, \quad \text{(A4.4)}$$

where $$\hat{S} = \frac{2S}{\cos \varepsilon}, \qquad (A4.5)$$

which is the peak value of mobility if the damping is light.

Equation (A4.4) illustrates the simple relationship between the real component of the point mobility and the square of the modulus of the transfer mobility.

The two quantities are closely related because S_r is proportional to the power input, and $|\bar{M}_{12}|^2$ to the energy content. The ratio between energy content and power input is expressed in the relationship |21|, power = $\eta\omega$.(energy content), for a modal single DOF model.

The mobility of the receiver beam $\bar{M}_R$ is given in equation (2.5) as

$$\bar{M}_R = Q_r - iQ_i - iQ, \qquad (A4.6)$$

where

$$Q_r = \frac{Q \cos \beta}{1 - \sin \beta \sin \theta}, \qquad Q_i = \frac{Q \sin \beta \cos \theta}{1 - \sin \beta \sin \theta}, \qquad (A4.7)$$

θ and β are the frequency and damping parameters of the receiver beam. The damping parameter is defined by the peak value of the real component of mobility $\hat{Q}$ in equation (2.6),

$$\hat{Q} = \frac{2Q}{\cos \beta}. \qquad (A4.8)$$

(ii) <u>The average power from the receiver beam resonances, <P></u>

Power transmission occurs between the two beams on account of resonances in both systems. The receiver is much larger than the source, causing $\theta >> \phi$. This means that for each source beam resonance, that is, an interval of $0 < \phi < 2\pi$, there are many receiver beam resonances, see Figure 5.3. It is therefore assumed that for each receiver resonance, (i.e., an interval $0 < \theta < 2\pi$,) ϕ, and hence the source mobility, remains constant. The average power transmission due to each receiver resonance <P>, which is shown in Figure 5.3, can be found by averaging P_{tr} over an interval of $0 < \theta < 2\pi$, as follows.

First, substituting equation (A4.6) and (A4.2) into (A4.1) gives

$$P_{tr} = \tfrac{1}{2}|F_1|^2 \cdot \frac{|M_{12}|^2 . Q_r}{(S_r + \frac{\eta\omega}{K} + Q_r)^2 + (S_i + C + Q_i)^2} \qquad (A4.9)$$

where $C = (S + Q - \frac{\omega}{K})$.

By substituting from equation (A4.7) for Q_r and Q_i, and by making use of the identity

$$Q_r^2 + Q_i^2 = Q^2 . \frac{1 + \sin\beta \sin\theta}{1 - \sin\beta \sin\theta} , \qquad (A4.10)$$

enables equation (A4.9) to be written in terms of θ and β

$$P_{tr} = \tfrac{1}{2}|F_1|^2 \times$$

$$\frac{|M_{12}|^2 . Q \cos\beta}{u_1^2 + 2Q(S_r + \frac{\eta\omega}{K})\cos\beta - \sin\beta[(u_1^2 - 2Q^2)\sin\theta - 2Q(S_i + C)\cos\theta]} \qquad (A4.11)$$

where

$$u_1^2 = (S_r + \tfrac{\eta\omega}{K})^2 + (S_i + C)^2 + Q^2 .$$

Using the two-angle formula

$$\sin(A - B) = \sin A . \cos B - \cos A \sin B \qquad (A4.12)$$

in equation (A4.11), gives

$$P_{tr} = \tfrac{1}{2}|F_1|^2 \times$$

$$\frac{|M_{12}|^2 . Q \cos\beta}{u_1^2 + 2Q(S_r + \frac{\eta\omega}{K})\cos\beta - \sin\beta[u_1^4 - 4Q^2(S_r + \frac{\eta\omega}{K})^2]^{\frac{1}{2}}\sin(\theta - \gamma)} , \qquad (A4.13)$$

where $$\tan \gamma = \frac{2Q(S_i + C)}{u_1^2 - 2Q^2} . \qquad (A4.14)$$

Now as θ varies over an interval $0 < \theta < 2\pi$, all the other terms in equation (A4.13) remain approximately constant being functions of either ϕ or ω. There is a peak in power transmission associated with a receiver mode whenever $\sin(\theta - \gamma) = 1$. The average power transmission from each of these peaks $\langle P \rangle$, is formed by averaging equation (A4.13) over an interval $0 < \theta < 2\pi$, i.e.,

$$\langle P \rangle = \frac{1}{2\pi} \int_0^{2\pi} P_{tr} . d\theta .$$

This integral is solved using a standard solution, see for example |27|,

$$\frac{1}{2\pi} \int_0^{2\pi} \frac{d}{b - c \sin x} dx = \frac{d}{(b - c)^{\frac{1}{2}}} , \qquad (A4.15)$$

a, b, c are constants; $b > c$.

Therefore,

$$\langle P \rangle = \tfrac{1}{2} |F_1|^2 . \frac{|M_{12}|^2 . Q}{u_1^2 + (S_r + \frac{\eta\omega}{K}) \hat{Q}} . \qquad (A4.16)$$

Substituting for $|M_{12}|^2$ and u_1^2 in terms of S_r and S_i using equations (A4.2) and (A4.4), respectively, gives

$$\langle P \rangle = \tfrac{1}{2} |F_1|^2 . \frac{2S . S_r . \tan \varepsilon . Q}{(S_r^2 + S_i^2) + S_r(\hat{Q} + \frac{2\eta\omega}{K}) + 2S_i C + C^2 + Q_d^2} , \qquad (A4.17)$$

where $$Q_d^2 = Q^2 + \frac{\eta\omega}{K} \hat{Q} + (\frac{\eta\omega}{K})^2 . \qquad (A4.18)$$

By making use of the identity

$$S_r^2 + S_i^2 = \frac{S^2(1 + \sin\varepsilon \sin\phi)}{1 - \sin\varepsilon \sin\phi} \quad , \tag{A4.19}$$

and substituting for S_r and S_i in terms of ϕ, from equation (A4.3), $\langle P \rangle$ becomes, after some manipulation,

$$\langle P \rangle = \tfrac{1}{2}|F_1|^2 \times$$

$$\frac{S \sin\varepsilon . 2SQ}{u_2^2 + S\cos\varepsilon\{\hat{Q} + \frac{2\eta\omega}{K}\} - \sin\varepsilon\left[(u_2^2 - 2S^2)\sin\phi - 2SC\cos\phi\right]} \quad , \tag{A4.20}$$

where $$u_2^2 = S^2 + Q_d^2 + C^2.$$

Using the identity in equation (A4.12), the term in [ ] becomes, after some manipulation,

$$|u_2^4 - 4S^2Q_d^2|^{\frac{1}{2}} \sin(\phi - \gamma),$$

where

$$\tan\gamma = \frac{2SC}{u_2^2 - 2S^2} \quad . \tag{A4.21}$$

$\langle P \rangle$ therefore becomes

$$\langle P \rangle = \tfrac{1}{2}|F_1|^2 \times$$

$$\frac{S \sin\varepsilon . 2SQ}{u_2^2 + S\cos\varepsilon(\hat{Q} + \frac{2\eta\omega}{K}) - \sin\varepsilon\left[u_2^4 - 4S^2Q_d^2\right]^{\frac{1}{2}} \sin(\phi - \gamma)} \quad . \tag{A4.22}$$

Calculation of the peak $\langle\hat{P}\rangle$, trough $\langle\check{P}\rangle$ and mean $\langle\langle P \rangle\rangle$ values of $\langle P \rangle$

$\langle P \rangle$, as expressed in equation (A4.22), is of the same form as the real component of the source beam mobility S_r, equation (A4.3), except that $\langle P \rangle$ is a function of $\phi - \gamma$ rather than ϕ. This means that the maximum power is, in this case, input and transmitted at the resonant frequencies of the coupled system when $\phi - \gamma = 1$, rather than at the uncoupled resonance frequency when $\phi = 1$.

The properties of $\langle P \rangle$ can be summarised in terms of its maximum value $\langle\hat{P}\rangle$, when $\sin(\phi - \gamma) = 1$, its trough value $\langle\check{P}\rangle$, when $\sin(\phi - \gamma) = -1$, and its frequency averaged value $\langle\langle P \rangle\rangle$.

(i) Calculation of $\langle\hat{P}\rangle$

The maximum value of $\langle P \rangle$ is found from equation (A4.22) by making the following three steps. First, set $\sin(\phi - \gamma) = 1$. Second, it is assumed that the damping of the source beam is light, allowing $\sin \varepsilon$ to be written as $1 - \frac{\cos^2\varepsilon}{2}$. Third, if it is assumed that $S \neq Q_d$ at the frequency of maximum coupling (when $(S + Q - \frac{\omega}{K}) = 0$) then it can be said that

$$u_2^4 > 4S^2Q_d^2.$$

If it is further assumed that

$$u_2^4 >> 4S^2Q_d^2$$

then the following approximation can be made

$$[u_2^2 - 4S^2Q_d^2]^{\frac{1}{2}} \simeq u_2^2 - \frac{2S^2Q_d^2}{u_2^2}.$$

On making these substitutions into equations (A4.22), the peak value of $\langle P \rangle$ becomes

$$\langle\hat{P}\rangle = \tfrac{1}{2}|F_1^2| \cdot \frac{(\hat{S})^2 Q \sin\varepsilon . u_2^2}{u_2^4 + u_2^2 . \hat{S}[\hat{Q} + 2\eta\omega/K] + [\hat{S}^2 - 2S^2]Q_d^2} \qquad (A4.23)$$

(ii) Calculation of $\langle\check{P}\rangle$

The trough value of $\langle P\rangle$ is found by setting $\sin(\phi - \gamma) = -1$ in equation (A4.22) and making the same two assumptions as stated for the calculation of $\langle\hat{P}\rangle$. Then

$$\langle\check{P}\rangle = \tfrac{1}{2}|F_1|^2 . \frac{S^2.Q \sin \varepsilon . u_2^2}{u_2^4 + u_2^2 \check{S}\left[\hat{Q} + \frac{2\eta\omega}{K}\right] - S^2 Q_d^2} , \qquad \text{(A4.24)}$$

where $\check{S} = \frac{S \cos \varepsilon}{2}$, the trough value of the source beam mobility.

(iii) Calculation of $\langle\langle P\rangle\rangle$

The frequency averaged value of $\langle P\rangle$ can be found by integrating $\langle P\rangle$ over an interval $0 < \phi - \gamma > 2\pi$, that is across the range shown in Figure 5.3, i.e.,

$$\langle\langle P\rangle\rangle = \frac{1}{2\pi} \int_0^{2\pi} \langle P\rangle d\phi .$$

It is assumed that all other variables, u_2, S, Q_d which are functions of ω do not change rapidly compared to ϕ.

This integral is solved using the standard solution given in equations (A4.15), giving

$$\langle\langle P\rangle\rangle = \tfrac{1}{2}|F_1|^2 \times$$

$$\frac{S \sin \varepsilon . \hat{S}Q}{\left[u_2^4 + u_2^2 \hat{S}\left(\hat{Q} + \frac{2\eta\omega}{K}\right) + S^2\hat{Q}^2 + \hat{S}^2 Q_d^2 - 4S^2Q^2\right)]^{\frac{1}{2}}} . \qquad \text{(A4.25)}$$

Calculation of $\hat{P}$ the Envelope of Power Transmission Peaks Caused by the Receiver Resonances

The final quantities to be calculated can be seen in Figure 5.3. They are the envelope of the peaks in transmission caused by the receiver resonances, $\hat{P}$, and also the peak possible value of $\hat{P}$.

Equation (A4.13) gives the power transmission as a function of $(\theta - \gamma)$. The peak power transmission $\hat{P}$ is found by making the substitution $\sin(\theta - \gamma) = 1$, giving

$$\hat{P} = \tfrac{1}{2}|F_1|^2 \times \frac{|M_{12}|^2 . Q \cos\beta}{u_1^2 + 2Q(S_r + \frac{\eta\omega}{K})\cos\beta - \sin\beta\left[u_1^4 - 4Q^2(S_r + \frac{\eta\omega}{K})^2\right]^{\frac{1}{2}}} . \quad \text{(A4.26)}$$

If it is assumed that the receiver damping is light then $\sin\beta$ can be expanded as

$$\sin\beta \simeq 1 - \frac{\cos^2\beta}{2} . \quad \text{(A4.27)}$$

Also, subject to the condition that $u_1^2 > 2Q(S_r + \frac{\eta\omega}{K})$, the expression in [ ] can be expanded as

$$u_1^2 - \frac{2Q^2(S_r + \frac{\eta\omega}{K})}{u_1^2} . \quad \text{(A4.28)}$$

This condition is always met, except when $u_1^2 = 2Q(S_r + \frac{\eta\omega}{K})$, in the unlikely event of both

$$S_r + \frac{\eta\omega}{K} = Q \quad \text{and} \quad S_i + C = 0$$

being simultaneously satisfied.

On making the substitutions from equations (A4.27) and (A4.28) into equations (A4.26), and substituting for $|M_{12}|^2$ from equations (A4.4), $\hat{P}$ becomes

$$\hat{P} = \tfrac{1}{2}|F_1|^2 \cdot \frac{S \sin\varepsilon\, S_r \hat{Q}.u_1^2}{|u_1^2 + \hat{Q}(S_r + \frac{\eta\omega}{K})|^2} \qquad \text{(A4.29)}$$

or by substituting from equation (A4.16)

$$\hat{P} = \langle P \rangle . \frac{2}{\cos\beta} \cdot \frac{u_1^2}{u_1^2 + \hat{Q}(S_r + \frac{\eta\omega}{K})} . \qquad \text{(A4.30)}$$

From equation (A4.30) it can be seen that there are two zones of behaviour depending on the relative magnitudes of u_1^2 and $\hat{Q}(S_r + \frac{\eta\omega}{K})$. The following analysis therefore determines when each of these two terms dominates or when

$$u_1^2 > \hat{Q}S_r . \qquad \text{(A4.31)}$$

For ease of analysis it is necessary to ignore the isolator damping. Substituting for u_1^2 from equation (A4.11) gives

$$S_r^2 + S_i^2 + Q^2 + 2CS_i + C^2 > S_r\hat{Q} . \qquad \text{(A4.32)}$$

Then substituting for S_r and S_i from equation (A4.3), and making use of the angle difference formula in equation (A4.12) enables the inequality in equation (A4.31) to be expressed as

$$u_2^2 - \sin\varepsilon \left[u_2^4 - 4S^2Q^2\right]^{\frac{1}{2}} \sin(\phi - \gamma) > \hat{Q}S\cos\varepsilon , \qquad \text{(A4.33)}$$

where

$$\tan\gamma = \frac{2SC}{u_1^2 - 2S^2} .$$

Dividing by u_2^2 gives

$$1 - \sin\varepsilon \left[1 - \frac{t^2}{4}\right] \sin(\phi - \gamma) > \frac{t^2}{2} \cdot \frac{\cos\varepsilon}{\cos\beta} . \qquad (A4.34)$$

When $\sin(\phi - \gamma) = 1$ (the frequency when $< P >$ is a maximum) the left hand side of the inequality is a minimum; hence at this frequency the inequality is least likely to be satisfied. Therefore, by substituting $\sin(\phi - \gamma) = 1$, the condition for the inequality to be satisfied for all values of $(\phi - \gamma)$ can be found. It is when

$$t^2 < \cos\beta \cos\varepsilon, \qquad (A4.35)$$

which is the condition for the source beam to behave as a 'velocity source' at the top of the spring.

There are therefore two regions of behaviour. First at high frequencies when equation (A4.35) is satisfied, $u_1^2 > \hat{Q}S_r$ for all values of $(\phi - \gamma)$ and so the peak power is given from equation (A4.30),

$$\hat{P} = <P>. \frac{2}{\cos\beta} . \qquad (A4.36)$$

Secondly, at lower frequencies when $t^2 > \cos\beta \cos\varepsilon$, equation (A4.34) shows that the value of $\sin(\phi - \gamma)$ determines whether $u_1^2 > \hat{Q}S_r$. There are three possibilities, illustrated in Figure 5.3. First, when $\sin(\phi - \gamma) << 1$ at the troughs of the $<P>$ functions, $u_1^2 > \hat{Q}S_r$ and the peak power $\hat{P}$ is

$$\hat{P} = <P>. \frac{2}{\cos\beta} ,$$

which means that the source beam behaves as a velocity source in these regions. Second, as $\sin(\phi - \gamma)$ increases, two frequencies are reached, at either side of the peak in $<P>$, at which $u_1^2 = \hat{Q}S_r$. By making this substitution into equation (A4.30) the peak power is

$$\hat{P}_{max} = \tfrac{1}{2}|F|^2 . \frac{\hat{S}}{4} = \frac{<\hat{P}>}{4} . \frac{2}{\cos\beta} .$$

This is the peak possible power transmission under any circumstances, it is only dependent on the source characteristics, and it can occur in the region of each coupled source receiver resonance, $(\sin(\phi - \gamma) \simeq 1)$.

Finally, as shown in Figure 5.3, between the two peaks a trough in the $\hat{P}$ envelope occurs when $\sin(\theta - \gamma) = 1$, when $\langle P \rangle$ is a maximum. At this frequency $u_1^2 < \hat{Q}S_r$ and the peak power becomes

$$\hat{P} = \tfrac{1}{2}|F|^2 . \hat{S} \sin \varepsilon . \frac{u_1^2}{\hat{Q}S_r} .$$

APPENDIX 5

Real and Imaginary Components of Impedance of a Rigid Element, With Translational and Rotational Inertia, Connected to a Semi-infinite Beam

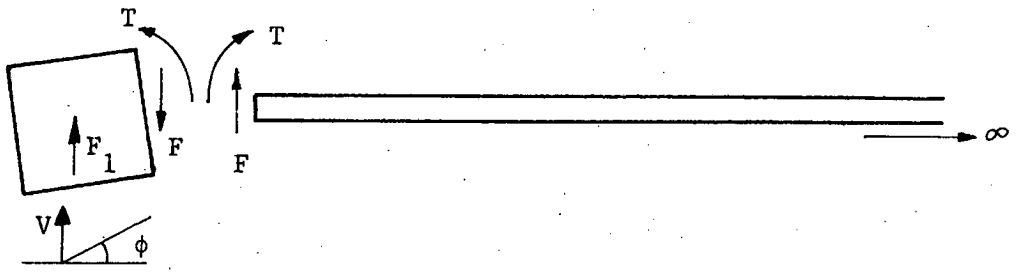

In the figure above, the velocity V and angular velocity $\dot{\phi}$ of the rigid element and the semi-infinite beam, when disconnected, are related to the applied force F and moment T by their respective impedance matrices $[A]$ and $[B]$, i.e.,

(i) For the rigid element

$$\begin{bmatrix} F \\ T \end{bmatrix} = [A] \begin{bmatrix} V \\ \dot{\phi} \end{bmatrix}$$

where

$$[A] = \begin{bmatrix} a_{11} & a_{12} \\ a_{21} & a_{22} \end{bmatrix} = \begin{bmatrix} i\omega m & 0 \\ 0 & i\omega I \end{bmatrix} \qquad (A5.1)$$

m and I are the mass and rotational inertia.

(ii) For the semi-infinite beam

$$[B] = \begin{bmatrix} b_{11} & b_{12} \\ b_{21} & b_{22} \end{bmatrix} = \frac{EIk^3}{\omega} \begin{bmatrix} 1 + i & \frac{1}{k} \\ \frac{1}{k} & \frac{1-i}{k^2} \end{bmatrix} \qquad (A5.2)$$

k is the wavenumber.

On rigidly connecting the two elements, they each move with the same velocity and angular velocity, therefore the impedance of the coupled system is simply the sum of that of the two components, i.e.,

$$\begin{bmatrix} F \\ T \end{bmatrix} = [A + B] \begin{bmatrix} V \\ \dot{\phi} \end{bmatrix}. \tag{A5.3}$$

The point impedance when a force, but no moment, is applied is found by setting $T = 0$ in equation (A5.3), giving

$$\frac{F}{V} = a_{11} + b_{11} - \frac{(b_{12} + a_{12})^2}{b_{22} + a_{22}},$$

which on substituting from equations (A5.1) and (A5.2) reduces to

$$\frac{F}{V} = \bar{Z} = \frac{EIk^3}{\omega} \left[\frac{(1 - \gamma)^2}{1 + (1 - \gamma)^2} + i \left[1 + \beta - \frac{(1 - \gamma)^2}{1 + (1 - \gamma)^2} \right] \right], \tag{A5.4}$$

where the rotational impedance ratio γ is

$$\gamma = \frac{\omega^2 I}{EIk}$$

and the point impedance ratio β is

$$\beta = \frac{\omega^2 m}{EIk^3}.$$

This equation has three regions of behaviour.

(i) At low frequencies when $\gamma << 1$, the rotational impedance of the mass is unimportant and

$$\bar{Z} = \frac{EIk^3}{2\omega} (1 + i) + i\omega m$$

which is simply the sum of the two point impedances.

(ii) When $\gamma = 1$, the moment impedance of the beam is of the same magnitude as that of the mass, giving

$$\bar{Z} = i\left(\frac{EIk^3}{\omega} + \omega m\right).$$

At this frequency the real component of impedance goes to zero.

(iii) When $\gamma >> 1$, the rotational impedance of the mass is so great as to prevent the end of the beam from rotating, i.e.,

$$\bar{Z} = \frac{EIk^3}{\omega}(1 + i) + i\omega m.$$

The real component of impedance is now twice the low frequency value.

APPENDIX 6

The Response of a Single Degree of Freedom System to a Swept Sine Wave

The response of a single degree of freedom system of mass, m, and stiffness K, to a rapid swept sine wave is found by evaluating the convolution integral.

The impulse response h(t) of a lightly damped single degree of freedom system is

$$h(t) = \left(\frac{1}{m\omega_d}\right) e^{-\zeta\omega_o t} \sin \omega_d t \qquad \text{(A6.1)}$$

where $\omega_d = \omega_o\sqrt{(1 - \zeta^2)}, \qquad \omega_o = \sqrt{\frac{K}{m}}$.

The forcing function of a swept sine wave is

$$f(t) = F \sin(at^2 + bt) \qquad 0 < t < T \qquad \text{(A6.2)}$$

where b is the starting frequency when $t = 0$ and 2a is the rate of change of angular frequency with time.

The displacement response may be written as the convolution integral.

$$x(t) = \int_o^t f(t - \tau)h(\tau)d\tau \qquad \text{(A6.3)}$$

substituting equations (A6.1) and (A6.2) into the above expression leads to

$$x(t) = \frac{F}{m\omega_d} \int_o^t \sin(a(t - \tau)^2 + b(t - \tau)) \sin \omega_d\tau . e^{-\zeta\omega_o\tau} d\tau .$$

This expression may be rearranged to give

$$x(t) = \frac{F}{m\omega_d} \int_o^t \sin(a\tau^2 - \omega(t)\tau + \phi(t)) \sin \omega_d\tau . e^{-\zeta\omega_o\tau} d\tau , \qquad \text{(A6.4)}$$

where $\phi(t) = at^2 + bt$ (the phase of the force at any instant), and $\omega(t) = d\phi/dt = 2at + b$ (the instantaneous angular frequency). Using the identity that $2 \sin A \sin B = \cos(A - B) - \cos(A + B)$, equation (A6.4) may be rewritten as

$$x(t) = \frac{F}{2m\omega_d} \int_o^t \cos(a\tau^2 - (\omega(t) + \omega_o)\tau + \phi(t)).e^{-\zeta\omega_o\tau} d\tau \qquad (A6.5)$$

$$- \frac{F}{2m\omega_d} \int_o^t \cos(a\tau^2 + (\omega_o - \omega(t))\tau + \phi(t)).e^{-\zeta\omega_o\tau} d\tau.$$

The second of these two terms contains the difference frequency $\omega_o - \omega(t)$, which will hereafter be referred to as $\Delta\omega(t)$. Only this term contributes significantly at frequencies in the resonance region, when $\Delta\omega(t)$ becomes small. Therefore only the second term will be included in subsequent analysis. If (A6.5) is rewritten in complex exponential form to include the damping ratio

$$x(t) = - \frac{F}{2m\omega_d} \text{Re} \int_o^t \exp\{-i(a\tau^2 + (\Delta\omega(t) - i\zeta\omega_o)\tau + \phi(t))\}d\tau. \qquad (A6.6)$$

This integral may be solved using 'error functions', but first it must be put in a form compatible with the standard solutions.

Firstly, writing

$$\Delta\omega(t) - i\zeta\omega_o = \bar{W}.$$

Then rearranging the argument of the integrand

$$x(t) = - \frac{F}{2m\omega_d} \text{Re} \int_o^t \exp\{-i\left[a(\tau + \frac{\bar{W}}{2a})^2 + \phi(t) - (\frac{\bar{W}}{2a})^2 a\right]\}d\tau. \qquad (A6.7)$$

If the substitutions

$$X = e^{i\frac{\pi}{4}} \sqrt{a}(\tau + \frac{\bar{W}}{2a})$$

where $t_o = \frac{\omega_o - b}{2a}$, the time to reach resonance frequency,

and $\alpha = \frac{(\omega_o + b)^2 - (\zeta\omega_o)^2}{4a} - \frac{\pi}{4}$.

The response of a single degree of freedom system to a rapid sweep is expressed as the product of four terms: a magnitude, dependent upon the force and the sweep rate, an exponential decay term due to damping, a harmonic oscillation at the natural frequency, and a modulating term defined by the "error functions".

(i) Discussion of the form of the modulating function

Error functions can only be evaluated using tables (see, for example, reference [39]). However, the approximate response of the single degree of freedom system may be estimated from asymptotic values of the "error function", which are given as follows.

For large values of z

$$\begin{aligned} &\text{erf}(z) \to 1 && z >> 1 \\ &\text{erf}(z) \leftarrow -1 && z << -1 \\ &\text{erf}(z) = 0 && z = 0 \end{aligned} \qquad \text{(A6.12)}$$

For small values of z the series form is useful

$$\text{erf}(z) = \frac{2}{\sqrt{\pi}} \{z - \frac{z^3}{3} + \frac{z^5}{10} \ldots\ (-1)^n \frac{z^{2n+1}}{n!(2n+1)}\}$$

therefore

$$\frac{d}{dz}(\text{erf}(z)) = \frac{2}{\sqrt{\pi}} \{1 - z^2 + \frac{z^4}{2} \ldots\ (-1)^n \frac{z^{2n}}{n!}\} \qquad \text{(A6.13)}$$

It is assumed that the initial sweep frequency 'b' is well below the natural frequency ω_o and that the sweep continues to a final frequency well above the resonance frequency. This being the case the first "error function" term in equation (A6.11) is approximately unity, provided that $\sqrt{a}\, t_o >> 1$. The second "error function" term is a

$$d\tau = \frac{e^{-i\frac{\pi}{4}}}{\sqrt{a}}\, dX$$

are made, and the limits are altered accordingly, as

$$X_1 = e^{i\frac{\pi}{4}}\sqrt{a}\,\frac{\bar{W}}{2a}$$

$$X_2 = e^{i\frac{\pi}{4}}\sqrt{a}\,(t + \frac{\bar{W}}{2a})$$

equation (A6.7) becomes

$$x(t) = -\frac{F}{2m\omega_d\sqrt{a}}\,\mathrm{Re}\,\exp\{-i(\frac{\pi}{4} + B(t))\}\int_{X_1}^{X_2}\exp(-X^2)dX \qquad (A6.8)$$

where

$$B(t) = \phi(t) - (\frac{\bar{W}}{2a})^2 a.$$

The solution to the integral may now be expressed in terms of the 'error function', which is defined as

$$\mathrm{erf}(z) = \frac{2}{\sqrt{\pi}}\int_0^z \exp(-X^2)dX \qquad (A6.9)$$

(see, for example, reference [39]), giving

$$x(t) = \frac{F}{4m\omega_d}\,\mathrm{Re}\{e^{-i(B(t) + \frac{\pi}{4})}.\sqrt{\frac{\pi}{a}}.[\mathrm{erf}(X_2) - \mathrm{erf}\,(X_1)]\}. \qquad (A6.10)$$

By substituting for $B(t)$, X_2 and X_1 in terms of a, b, ω_o and ζ the solution for $x(t)$ becomes

$$x(t) = -\frac{F}{4m\omega_d}\sqrt{\frac{\pi}{a}}\,\mathrm{Re}\{e^{\zeta\omega_o(t_o - t)}\,.e^{i(\omega_o t + \alpha)} \times$$

$$\times\,[\mathrm{erf}(e^{i\frac{\pi}{4}}.\sqrt{a}(t_o - \frac{i\zeta\omega_o}{2a})) - \mathrm{erf}(e^{i\frac{\pi}{4}}.\sqrt{a}\,(\frac{\bar{W}}{2a}))]\} \qquad (A6.11)$$

function of $\frac{\bar{W}}{2a}$ (the time for the frequency to sweep from the instantaneous value to the resonance frequency). This time is positive and at its maximum at the start of the sweep, zero at resonance, and large and negative at the end of the sweep.

Therefore from (A6.12) it may be deduced that at the beginning of the sweep the response is small. As the sweep frequency approaches the resonance frequency the amplitude increases, and at the resonance frequency it becomes

$$x = \frac{F}{4m\omega_d}\sqrt{\frac{\pi}{a}}\Bigg|_{\omega = \omega_o}.$$

The amplitude continues to increase as the sweep goes above resonance until it reaches its maximum value of

$$x_{max} = \frac{F}{2m\omega_d}\sqrt{\frac{\pi}{a}}\Bigg|_{\omega > \omega_o} \qquad \text{(A6.14)}$$

If there is no damping, the response amplitudes remain at this value.

The response amplitude at the resonance frequency is therefore only half the maximum value. However, at the resonance frequency the rate of increase of amplitude is a maximum. The rate of increase may be calculated from equation (A6.13) by substituting $z = 0$ and using the identity

$$z = e^{i\frac{\pi}{4}}\sqrt{a}.t + \text{const.}$$

$$dz = e^{i\frac{\pi}{4}}\sqrt{a}\,dt$$

giving

$$d\,\frac{erf(z)}{dt} = \frac{2}{\sqrt{\pi}}e^{i\frac{\pi}{4}}\sqrt{a}\,.$$

By substituting this expression into equation (A6.11) the maximum rate of change of the amplitudes is given as

$$\frac{dx}{dt} = \frac{F}{2m\omega_d} \cdot \qquad \text{(A6.15)}$$

It is seen that the rate of increase of amplitude is independent of sweep rate, and in fact is equal to that of an undamped single degree of freedom system excited by a steady harmonic force at its resonance frequency.

The time over which the amplitude increase may be approximated to being simply the maximum amplitude divided by the maximum increase rate

$$= \sqrt{\frac{\pi}{a}} \cdot$$

Hence it is seen that a faster sweep rate gives less time for the amplitude to increase.

The overall approximate envelope of the response for a single degree of freedom system is shown below:

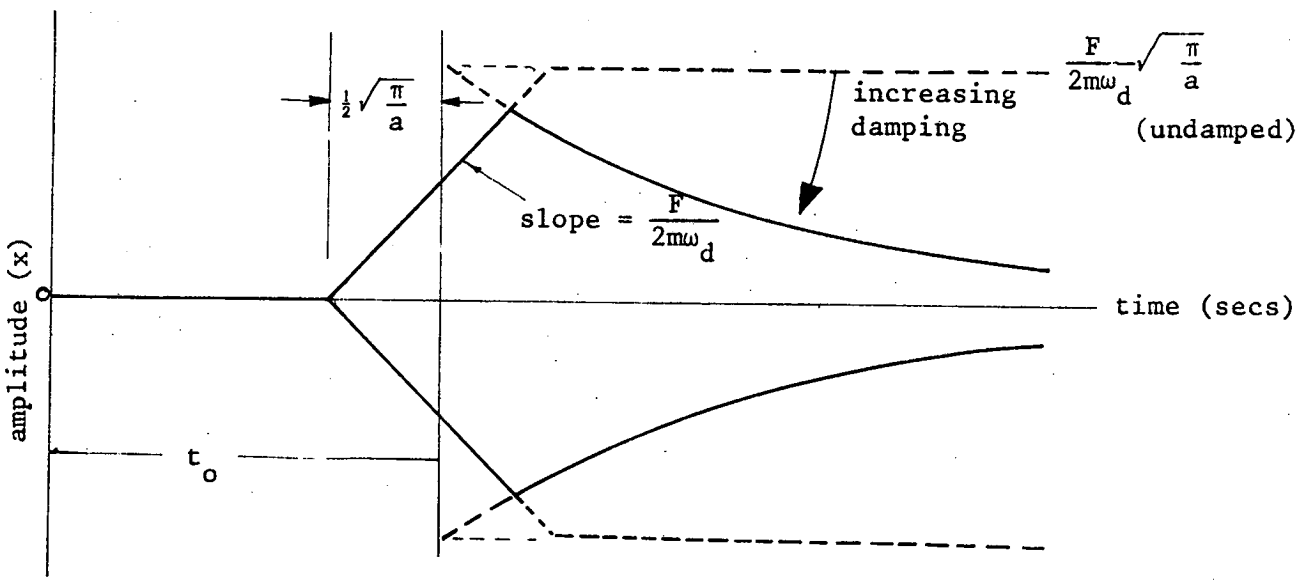

(ii) The effect of damping

The effect of the damping on the response of the single degree of freedom system is expressed in the experimental decay term in equation (A6.11). It is seen that for time greater than 't_o' the response decays at the same rate as that of our impulsively excited single degree of freedom system, namely,

$$e^{-\zeta\omega_o t}$$

as shown in the figure on the previous page.

It can also be seen from this figure that, for time greater than t_o, the damping could limit the maximum amplitude obtained if

$$\zeta\omega_o > 2\sqrt{\frac{a}{\pi}} . \qquad \text{(A6.16)}$$

(iii) Comment on the magnitude of the peak amplitude

If criterion (A6.16) is satisfied, equation (A6.14) gives the maximum response amplitude of a single degree of freedom system excited by a swept force of magnitude F.

$$x_{max} = \frac{F}{2m\omega_d}\sqrt{\frac{\pi}{a}} .$$

This is the same as would be produced by an impulse I of magnitude

$$I = \frac{F}{2}\sqrt{\frac{\pi}{a}} ;$$

that is,

$$x_{max} = \frac{I}{m\omega_d} .$$

However, it may be observed that the magnitude of the equivalent impulse 'I' above is exactly the size of the Fourier Transform modulus of the swept sine wave forcing function, |26|

$$F(\omega) = \frac{F}{2}\sqrt{\frac{\pi}{a}} .$$

This has the significant implication that the maximum response of a system is independent of the shape of the forcing function, but only dependent upon the modulus of the Fourier transform in the region of the resonance frequency.

APPENDIX 7

Investigation of Cross Terms in Velocity Product

The purpose of this section is to investigate the magnitude of the cross terms in equation (7.18) relative to the squared terms. When only two modes p and q contribute to the vibration at points s and r, equation (7.18) becomes

$$V_s V_r^* = |f_p|^2 . |M^{(p)}|^2 . \psi_s^{(p)} . \psi_r^{(p)} + |f_q|^2 . |M^{(q)}|^2 . \psi_s^{(q)} . \psi_r^{(q)}$$

$$+ (\bar{f}_p \bar{f}_q^* \bar{M}^{(p)} \bar{M}^{(q)*}) . \psi_s^{(p)} \psi_r^{(q)} + (f_p^* f_q M^{(p)} M^{(q)*}) . \psi_s^{(p)} \psi_r^{(p)} . \quad (A7.1)$$

Above the p^{th} natural frequency the modal mobility becomes mainly mass controlled, therefore,

$$I_m\{M^{(p)}\} \simeq -|M^{(p)}| . \quad (A7.2)$$

Likewise, below the q^{th} resonance frequency the modal mobility becomes stiffness controlled, therefore,

$$I_m\{M^{(q)}\} = |M^{(q)}| . \quad (A7.3)$$

In this region if $\bar{f}_p$ and $\bar{f}_q$ are the result of uncorrelated forces the second pair of terms in equation (A7.1) will be small compared with the first pair, and so only the first pair contribute to $V_s V_r^*$. If, however, the forces $\bar{f}_p$ and $\bar{f}_q$ are in or out of phase, as would be the case for single point excitation, the second pair of terms achieve their maximum value, and equation (A7.1) becomes

$$V_s V_r^* = |V_s V_r^*| = |f_p|^2 . |M^{(p)}|^2 . \psi_s^{(p)} \psi_r^{(p)} + |f_q|^2 . |M^{(q)}|^2 . \psi_s^{(q)} \psi_r^{(q)}$$

$$+ |f_p| |f_q| |M^{(p)}| |M^{(q)}| (\psi_r^{(q)} \psi_s^{(p)} + \psi_s^{(q)} \psi_r^{(p)}) \quad (A7.4)$$

From this equation it can be seen that when $|f_p||M^{(p)}| = |f_q||M^{(q)}|$ the third term is comparable with the sum of the first and second, and so it is not possible to have great confidence in power estimates made at this point. However, if the first two terms are used, a rough estimate is obtained. If $s = r$, equation (A7.4) becomes

$$|V_s|^2 \simeq (|f_p||M^{(p)}|\psi_s^{(p)} + |f_q||M^{(q)}|\psi_s^{(q)})^2. \qquad \text{(A7.5)}$$

If the power is being estimated from the squared terms in the expansion of equation (A7.5), i.e.,

$$|V_s|^2 \simeq |f_p|^2|M^{(p)}|^2 \psi_s^{(p)} + |f_q|^2|M^{(q)}|^2\psi_s^{(q)} \qquad \text{(A7.6)}$$

then by comparison of equations (A7.6) and (A7.5) it can be seen that the estimated value will be at worst, twice that of the true value. Although there is one equal likelihood of the estimated value going to zero if $\psi_s^{(p)}$ is of opposite sign to $\psi_s^{(q)}$.

APPENDIX 8

Program to Detect Peaks in Mobility, XPEAK

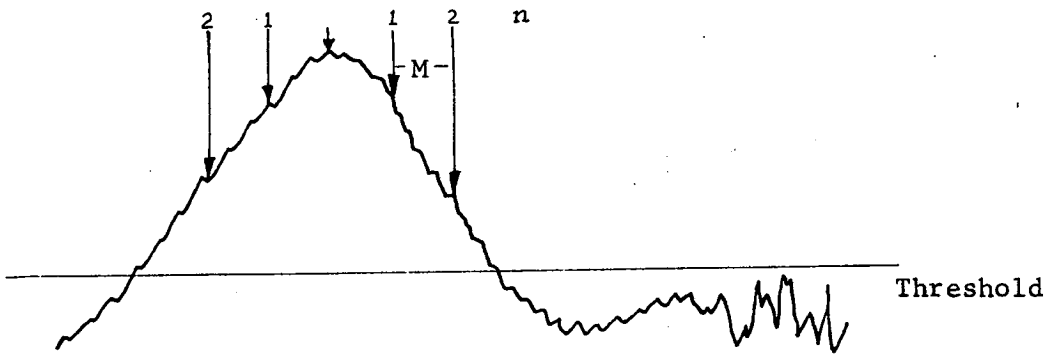

The main problem in detecting peaks is the noise and unevenness in the surrounding data, see Figure above. The sensitivity of the program can be varied in the following ways:

(i) A threshold can be imposed to ignore all data of lower value.

(ii) The local maximum is found, simply when one point is greater than the two surrounding points.

(iii) n steps, each of M points are made away from the local peak in each direction (higher and lower in frequency). A peak is only registered if the level at each step decreases. It was found that only two or three steps are necessary, i.e., n = 2, 3 and M can vary between 1 - 100 data points, depending on the width of the peak.

APPENDIX 9

Power Transmitted via a Spring to a Seating Structure from a General Source Structure Excited by Multiple Forces

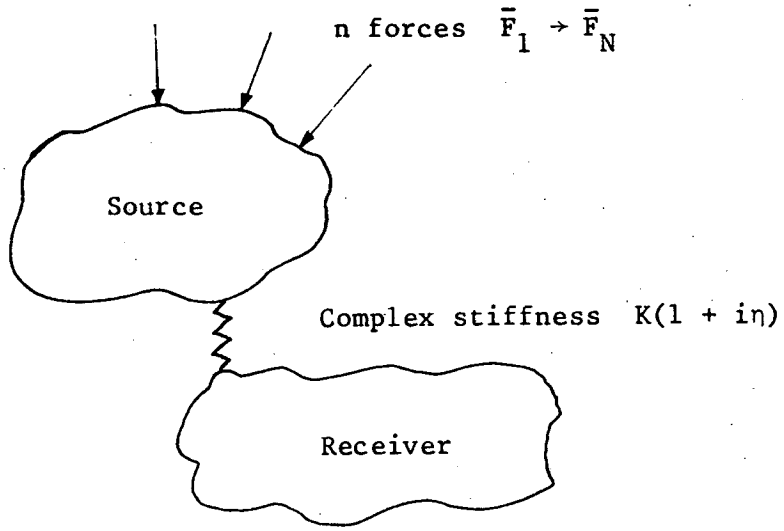

The power transmitted via a spring from a source structure to a passive receiving structure is given in equation (3.8) as

$$P_{tr} = \tfrac{1}{2}|V_f|^2 . \frac{Re\{M_R\}}{|\bar{M}_s + \frac{i\omega}{K}(1 + i\eta) + \bar{M}_R|^2} \qquad (A9.1)$$

where V_f is the velocity of the attachment point on the machine, prior to attachment of the spring, $\bar{M}_s$ and $\bar{M}_R$ are the mobilities at the attachment points on the source and receiving structures, respectively.

If the machine is sufficiently lightly damped for the vibration to be governed by modal behaviour, then, from equations (7.20) and (7.18), the mean square velocity can be given as the sum of the modal contributions,

$$\tfrac{1}{2}|V_f|^2 \simeq \tfrac{1}{2} \sum_{p=1}^{n} |\bar{f}_p|^2 . Re\{M^{(p)}\} . \hat{M}^{(p)} . (\psi_s^{(p)})^2 \qquad (A9.2)$$

where $\bar{f}_p$ is the generalised force for the p'th mode, i.e.,

$$\bar{f}_p = \bar{F}_1 \psi_1^p + \bar{F}_2 \psi_2^p \ \ldots \ \bar{F}_N \psi_N^p \qquad (A9.3)$$

$\psi_s^{(p)}$ is the eigenvector of the p'th mode at points $\bar{M}^{(p)}$ and $\hat{M}^{(p)}$ are the modal mobility and resonant peak values of the modal mobility respectively (equation (7.9)). Equation (A9.2) does not hold true between two resonances when two modes make similar velocity contributions (Appendix 7).

Now, in practical machines, there can be heavy damping, causing significant attenuation of vibration from the excitation region of the source structure to the coupling point. (Although this feature is only likely to be important when individual machine elements can resonate independently.) This effect can be allowed for, although without mathematical rigour, using a modal attenuation term $\sin(\varepsilon_s^{(p)})$, notated thus by way of comparison with the beam studies earlier (equation (5.3)).

The mean square velocity contribution from the p'th mode at the coupling point on the unconnected source structure, $\frac{1}{2}|V_f^{(p)}|$ may therefore be written from equation (A9.2) as

$$\tfrac{1}{2}|V_f^{(p)}|^2 = \tfrac{1}{2}|f_p|^2.\hat{M}^{(p)}.\sin(\varepsilon_s^{(p)}).\mathrm{Re}\{\bar{M}_s^{(p)}\} \qquad \text{(A9.3)}$$

where $\bar{M}_s^{(p)} = (\psi_s^{(p)})^2\,\bar{M}^{(p)}$ is the mobility of the p'th mode at the connecting point of the source structure.

On making this substitution into equation (A9.1), the power transmitted to the seating structure is given in general as

$$P_{tr} = \tfrac{1}{2}\sum_{p=1}^{n}|f_p|^2.\hat{M}^{(p)}.\sin(\varepsilon_s^{(p)}).\frac{\mathrm{Re}\{\bar{M}_s^{(p)}\}.\mathrm{Re}\{\bar{M}_R\}}{|\bar{M}_s + \frac{i\omega}{K}(i+\eta) + \bar{M}_R|^2} \qquad \text{(A9.4)}$$

If the particular case of the two coupled beams in Chapters 5 and 6 is considered, with multipoint excitation rather than single point excitation,

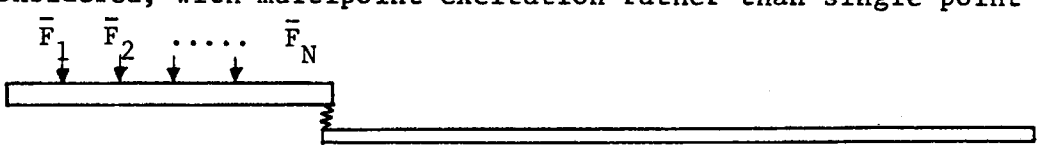

then equation (A9.4) becomes:

$$P_{tr} = \tfrac{1}{2}|f_p|^2 \cdot \frac{\hat{S} \sin\varepsilon . S_r . \mathrm{Re}\{\bar{M}_R\}}{|\bar{M}_2 + \frac{\omega}{K}(i + \eta) + \bar{M}_R|^2} \qquad \text{(A9.5)}$$

where it is assumed that $|f_p|^2$ does not change rapidly for different modes, $S_r = \sum_{p=1}^{n} \mathrm{Re}\{\bar{M}_2\}$ and $\hat{S} = \hat{M}^{(p)}$. Equation (A9.5) has an identical form as the single point excitation case considered earlier in equations (5.1)-(5.3), except that F_1 is replaced by f_p. Therefore, the expressions in table 2 hold approximately true for multipoint excitation of the source structure.

Now, in general, for a vibrating source, such as a machine, $\bar{f}_p$, $\hat{M}^{(p)}$ and $\sin(\varepsilon_s^{(p)})$ are not known, but their product can be found from the free velocity on the surface and the real component of mobility at that point, as can be seen from equation (A9.3).

$$\frac{\tfrac{1}{2}|V_f^{(p)}|^2}{\mathrm{Re}\{M_s^{(p)}\}} = \tfrac{1}{2}|f_p|^2 . \hat{M}^{(p)} . \sin(\varepsilon_s^{(p)}) = \hat{P}_{in}^{(p)} \qquad \text{(A9.6)}$$

Thus $\hat{P}_{in}^{(p)}$, which is the maximum power that can be input to the source by the p'th mode, is the only quantity that can be determined from the surface, but it is all that is necessary to make power transmission estimates. For a single mode, equation (A9.4) becomes

$$P_{tr}^{(p)} \simeq \hat{P}_{in}^{(p)} \cdot \frac{\mathrm{Re}\{\bar{M}_2^{(p)}\}\mathrm{Re}\{\bar{M}_R\}}{|\bar{M}_2^{(p)} + \frac{\omega}{K}(i + \eta) + \bar{M}_R|} \qquad \text{(A9.7)}$$

For estimates of power over a broad frequency range, these modal contributions can be summed so that $P_{tr} = \sum_{p=1}^{n} P_{tr}^{(p)}$, so

$$P_{tr} \simeq \hat{P}_{in} \cdot \frac{\mathrm{Re}\{\bar{M}_2\}\mathrm{Re}\{\bar{M}_R\}}{|\bar{M}_2 + \frac{\omega}{K}(i + \eta) + \bar{M}_R|^2} \cdot \qquad \text{(A9.8)}$$

where the function $\hat{P}_{in}$ is measured as $\tfrac{1}{2}|V_f|^2/\mathrm{Re}\{\bar{M}_2\}$. (A9.9)

This term, $\hat{P}_{in}$, is independent of the measurement position, and can therefore be estimated from more than one point on the machine. The estimates of this term can be in error when two modes interfere destructively at a point on the surface. However, this will always lead to an under-

estimation, which could be corrected from an additional measurement elsewhere. At high frequencies, for example greater than 2 kHz, on 6 mm thick steel panels, the mass and inertia of point mobility measurement transducers could seriously affect the measured value of $Re\{\bar{M}_2\}$ (as described in section 8.5), and would therefore lead to unreliable values of $\hat{P}_{in}$.

$\hat{P}_{in}$ can only be measured if no power is being absorbed by the machine seating, but this would permit measurements to be made on a machine mounted by isolators on a rigid foundation.

The form of the second group of terms in equation (A9.8) is the same as that which are in the analysis of the two coupled beams, equations (A4.4) and (A4.9). Therefore, if straight line approximations of the frequency averaged and resonant peak values of $\bar{M}_2$ and $\bar{M}_R$ were made, the equations given in table 2 could be used to make estimates of power, if divided by $\hat{S} \sin \varepsilon$. For example, for the velocity source region

$$(a_2^2 > \hat{S}\hat{Q}), \langle\langle P \rangle\rangle = \hat{P}_{in}.SQ/a_2^2$$

where $S = \langle Re\{\bar{M}_2\}\rangle$

$Q = \langle Re\{M_R\}\rangle$

$a_2^2 \simeq (\omega/K)^2$

$\hat{P}_{in}$ is measured for the particular machine.

APPENDIX 10

Power Transmission to a Symmetrical Seating Via Springs from a Rigid Machine Moving in Rotation and Translation.

The free machine

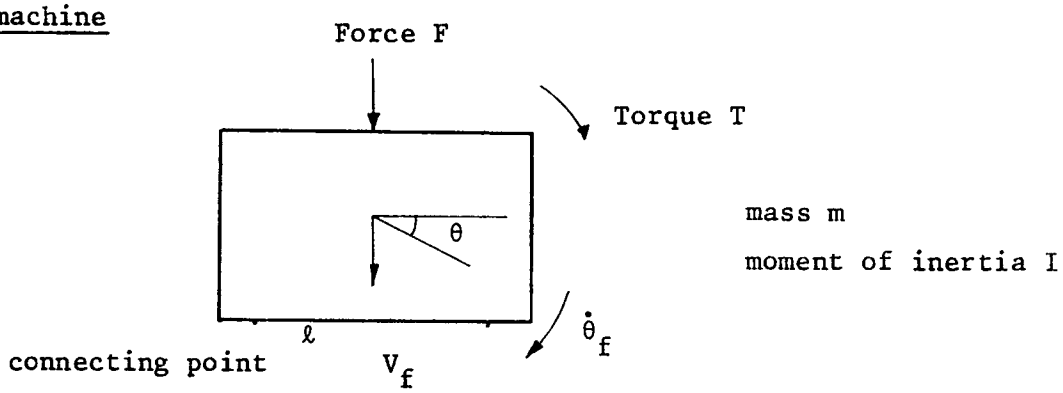

For the free machine, the velocity of the centre of gravity V_f is given as

$$\tfrac{1}{2}|V_f|^2 = \tfrac{1}{2}\frac{|F|^2}{(\omega m)^2} \quad . \qquad \text{(A10.1)}$$

Likewise, the velocity at the connecting points due to the angular velocity $\dot{\theta}_f$ is

$$\tfrac{1}{2}|\dot{\theta}_f|^2.\ell^2 = \tfrac{1}{2}\frac{|T|^2}{(\omega I)^2}.\ell^2. \qquad \text{(A10.2)}$$

The connected system

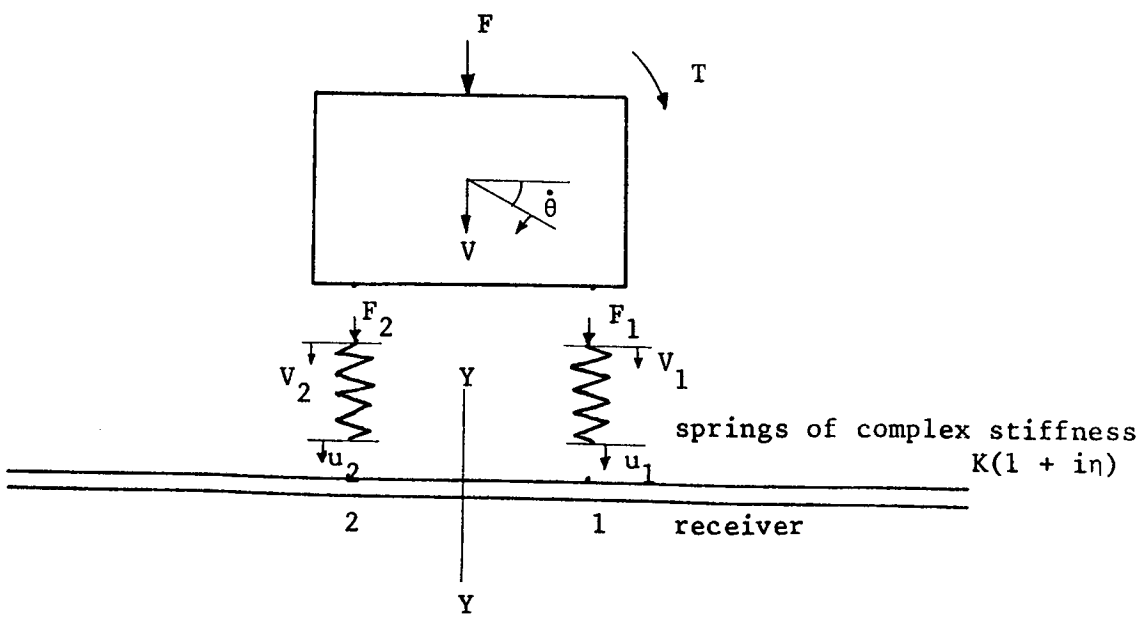

If it is assumed that the receiver is symmetrical about axis Y-Y then the receiver mobility matrix can be written as

$$\bar{M} = \begin{bmatrix} \bar{M}_1 & \bar{M}_{12} \\ \bar{M}_{12} & \bar{M}_1 \end{bmatrix}, \tag{A10.3}$$

where $\bar{M}_1$ is the mobility at points 1 and 2 and $\bar{M}_{12}$ is the transfer mobility between points 1 and 2.

The velocity V and angular velocity $\dot{\theta}$ of the mass can be expressed in terms of the velocities at the tops of the springs V_1 and V_2.

$$\begin{bmatrix} V \\ \dot{\theta} \end{bmatrix} = \tfrac{1}{2} \begin{bmatrix} 1 & 1 \\ \frac{1}{\ell} & -\frac{1}{\ell} \end{bmatrix} \begin{bmatrix} V_1 \\ V_2 \end{bmatrix}. \tag{A10.4}$$

The equation of motion of the mass is

$$\begin{bmatrix} V \\ \dot{\theta} \end{bmatrix} = \begin{bmatrix} V_f & 0 \\ 0 & \dot{\theta}_f \end{bmatrix} - [P] \begin{bmatrix} F_1 \\ F_2 \end{bmatrix} \tag{A10.5}$$

where $$[P] = \begin{bmatrix} 1/i\omega m & 1/i\omega m \\ \ell/i\omega I & -\ell/i\omega I \end{bmatrix}.$$

The velocity response of the receiver u_1 and u_2 of points 1 and 2, respectively, is

$$\begin{bmatrix} u_1 \\ u_2 \end{bmatrix} = [\bar{M}] \begin{bmatrix} F_1 \\ F_2 \end{bmatrix}. \tag{A10.6}$$

The forces in the isolator are given as

$$\begin{bmatrix} F_1 \\ F_2 \end{bmatrix} = \frac{\bar{K}}{i\omega} \begin{bmatrix} V_1 \\ V_2 \end{bmatrix} - \frac{\bar{K}}{i\omega} \begin{bmatrix} u_1 \\ u_2 \end{bmatrix} \tag{A10.7}$$

Using equations (A10.1) to (A10.7), the forces applied to the receiver F_1 and F_2 can be expressed in terms of the force and torque applied to the mass

$$\begin{bmatrix} F \\ T \end{bmatrix} = \begin{bmatrix} a & a \\ -b & b \end{bmatrix} \begin{bmatrix} F_1 \\ F_2 \end{bmatrix} \qquad \text{(A10.8)}$$

where

$$a = \frac{i\omega m}{2} (\bar{M}_1 + \frac{i\omega}{\bar{K}} + \bar{M}_{12}) + 1$$

$$b = - \frac{i\omega I}{2\ell} (\bar{M}_1 + \frac{i\omega}{\bar{K}} - \bar{M}_{12}) - \ell$$

Now, from equation (7.3) the power transmitted by two forces F_1 and F_2 is

$$P_{tr} = \tfrac{1}{2}\left[|F_1|^2 + |F_2|^2\right]\mathrm{Re}\{M_1\} + \tfrac{1}{2}\left[2.\mathrm{Re}\{F_1 F_2^*\}.\mathrm{Re}\{\bar{M}_{12}\}\right] \qquad \text{(A10.9)}$$

On substituting for F_1 and F_2 from equation (A10. 9), the power transmission becomes

$$P_{tr} = \tfrac{1}{2}|V_f|^2 . \frac{\mathrm{Re}\{(\bar{M}_1 + \bar{M}_{12})/2\}}{|(\bar{M}_1 + \bar{M}_{12})/2 + \frac{i\omega}{2\bar{K}} - \frac{i}{\omega m}|^2}$$

$$+ \tfrac{1}{2}|\dot{\theta}_f|^2 . \frac{\ell^2.\mathrm{Re}\{(\bar{M}_1 - \bar{M}_{12})/2\}}{|(\bar{M}_1 - \bar{M}_{12})/2 + \frac{i\omega}{2\bar{K}} - \frac{i\ell^2}{\omega I}|^2} \qquad \text{(A10.11)}$$

Thus it can be seen that the power transmitted by the translation and rotation of the mass are independent. These expressions are identical to the single coupling point expression (given by $\bar{M}_1 = \bar{M}_{12}$) except that the seating is characterised by a $(\bar{M}_1 \pm \bar{M}_{12})/2$ term as compared to $\bar{M}_1$ for single point coupling (or $\bar{M}_R$ in equation (9.1).

Table 1. Power input to and transmitted from a finite beam coupled to an arbitrary structure, for unit mean square force input.

		$r < \alpha$ or $\frac{t^2}{4} > \frac{S}{\hat{S}}$	$r = \alpha$ or $\frac{t^2}{4} = \frac{S}{\hat{S}}$	$r > \alpha$ or $\frac{t^2}{4} < \frac{S}{\hat{S}}$
INPUT	$\langle\hat{P}\rangle$	$S\frac{1+r}{1-r}$	$\hat{S}/2$	$\hat{S}$
	$\langle\langle P\rangle\rangle$	S	S	S
	$\langle\check{P}\rangle$	$S\frac{1-r}{1+r}$	$2\check{S}$	$\check{S}$
TRANSMITTED	$\langle\hat{P}\rangle$	$S\frac{1+r}{1-r}$	$\hat{S}/4$	$\frac{(\hat{S})^2}{S}\cdot\frac{t^2}{4}$
	$\langle\langle P\rangle\rangle$	S	$S/2$	$\hat{S}.\frac{t^2}{4}$
	$\langle\check{P}\rangle$	$S\frac{1+r}{1-r} \simeq \frac{St^2}{4}$	$S.\frac{t^2}{4}$	$S.\frac{t^2}{4}$

Legend for Table 1

$\langle \hat{P} \rangle$	envelope of peak power
$\ll P \gg$	frequency average power
$\langle \check{P} \rangle$	envelope of trough power
r	reflection coefficient modulus
t	transmission coefficient modulus related by $1 - r^2 = t^2$
	attenuation in wave amplitude travelling twice the length of the beam
$\frac{\hat{S}}{S}$	ratio between peak and average real component of mobility
$\hat{S}$	peak value of real component of mobility
S	frequency average value of real component of mobility
$\check{S}$	trough value of real component of mobility

note 1. $\frac{1 + r}{1 - r} \simeq \frac{4}{t^2} - 2$ if $t^2 < \frac{1}{2}$.

Table 2. $\langle\hat{P}\rangle$, $\langle\check{P}\rangle$, $\langle\langle P\rangle\rangle$ for power transmission between a short source beam and a long receiver beam

Zone	$\langle P\rangle$	$\langle\langle P\rangle\rangle$	$\langle\check{P}\rangle$
$u_2^2 > \hat{S}\hat{Q}$ Note:- High frequencies, source beam acts as 'velocity source'	$\frac{\hat{S}^2.Q \sin\varepsilon}{u_2^2}$ or $\frac{(\hat{S})^2}{S}.\frac{t_d^2}{4}.\sin\varepsilon$	$\frac{\hat{S}.SQ \sin\varepsilon}{u_2^2}$ or $\hat{S}.\frac{t_d^2}{4}.\sin\varepsilon$	$\frac{S^2Q \sin\varepsilon}{u_2^2}$ or $S.\frac{t_d^2}{4}\sin\varepsilon$
$\hat{S}\hat{Q} > u_2^2 > \check{S}\hat{Q}$ $+ \hat{S}(\check{Q} + \frac{\eta\omega}{K})$ Note:- Mid-frequencies, when $\hat{S}/S$ is comparable to $\hat{Q}/Q$	$\hat{S}.\frac{Q}{\hat{Q}}\sin\varepsilon$ or $S\frac{\cos\beta}{\cos\varepsilon}.\sin\varepsilon$	$\frac{S\hat{S}Q \sin\varepsilon}{[u_2^2\hat{S}\hat{Q}]^{\frac{1}{2}}}$ or $S.\frac{t_d}{2}\left[\frac{\cos\beta}{\cos\varepsilon}\right]^{\frac{1}{2}}\sin\varepsilon$	$\frac{S^2Q \sin\varepsilon}{u_2^2}$ or $S.\frac{t_d^2}{4}.\sin\varepsilon$
$S\hat{Q} + \hat{S}(\check{Q} + \frac{\eta\omega}{K}) > u_2^2$ (i) $S\hat{Q} > \hat{S}(\check{Q} + \frac{\eta\omega}{K})$ Note:- Very heavy *source damping*	$S.\frac{\cos\beta}{\cos\varepsilon}.\sin\varepsilon$	$S.\frac{\cos\beta}{\cos\varepsilon}.\sin\varepsilon$	$S.\frac{\cos\beta}{\cos\varepsilon}.\sin\varepsilon$
(ii) $\hat{S}(\check{Q} + \frac{\eta\omega}{K}) > \check{S}\hat{Q}$ Note:- Light source damping and heavy isolator damping:- same as for infinite beam receiver	$S.\frac{4}{t_d^2}(\frac{Q}{Q_d})^2\sin\varepsilon$	$S.\frac{Q}{Q_d}.\sin\varepsilon$	$S.\frac{t_d^2}{4}.\sin\varepsilon$

Legend for Table 2

- see Figure 5.3 for definitions of $\langle\hat{P}\rangle$, $\langle P\rangle$, $\langle\langle P\rangle\rangle$

$\langle\hat{P}\rangle$ envelope of peak power

$\langle\langle P\rangle\rangle$ frequency average power

$\langle\check{P}\rangle$ envelope of trough power

$\hat{S}$ peak value of source real component of mobility

S frequency average value of source real component of mobility

$\check{S}$ trough value of source real component of mobility

$\hat{Q}$ peak value of receiver real component of mobility

Q frequency average value of receiver real component of mobility

$\check{Q}$ trough value of receiver real component of mobility

$\sin\epsilon$ is the decrease in vibration level between the two ends of the source beam ($\sin\epsilon = 1/\cosh \eta k\ell/2$)

$\cos\epsilon$ is the source beam damping parameter

$\hat{S} = 2.S/\cos\epsilon$ as $\cos\epsilon \simeq 2\eta k\ell$

$\cos\beta$ is the receiver beam damping parameter

$\hat{Q} = 2Q/\cos\beta$

$\frac{\omega}{K}(1 + i\eta)$ is the isolator complex mobility

$$u_2^2 = S^2 + (Q + S - \frac{\omega}{K})^2 + Q_d^2$$

where $$Q_d^2 = Q^2 + \frac{\eta\omega\hat{Q}}{K} + (\frac{\eta\omega}{K})^2$$

$t_d^2 = \frac{4QS}{u_2^2}$ is the transmission coefficient from the source beam to the isolator and receiver beam

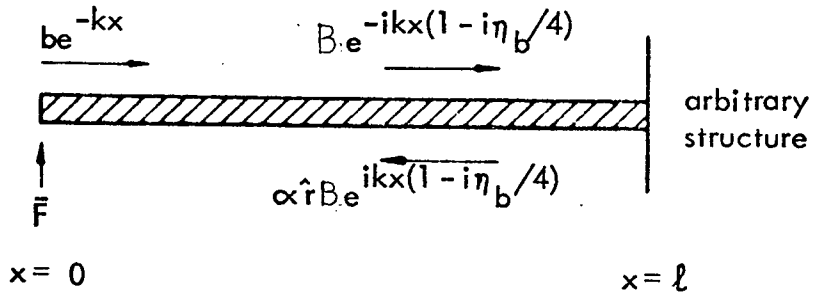

Fig. 2.1 Model of end excited beam.

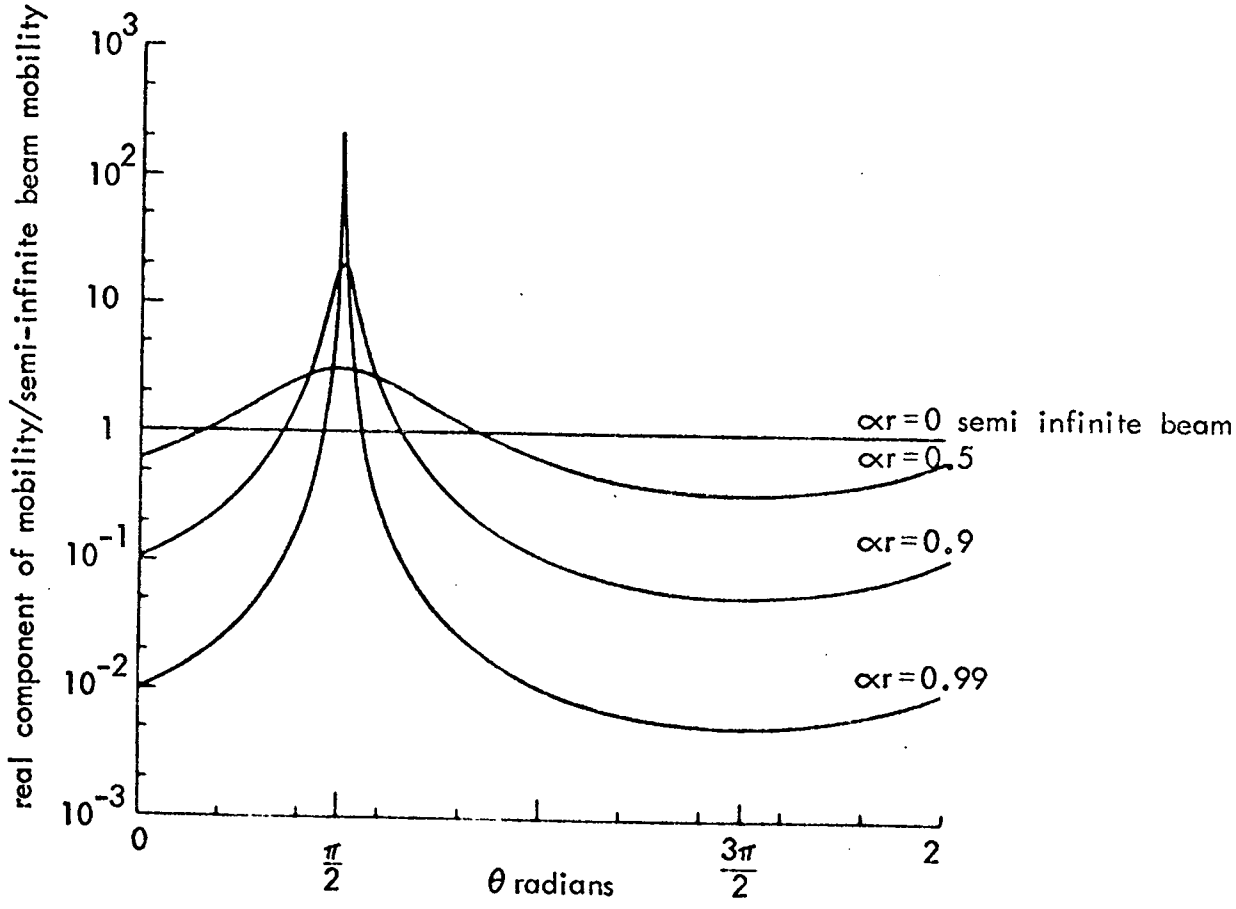

Fig. 2.2 Real component of mobility as a function of reflection coefficient, r, and damping attenuation 'α'.

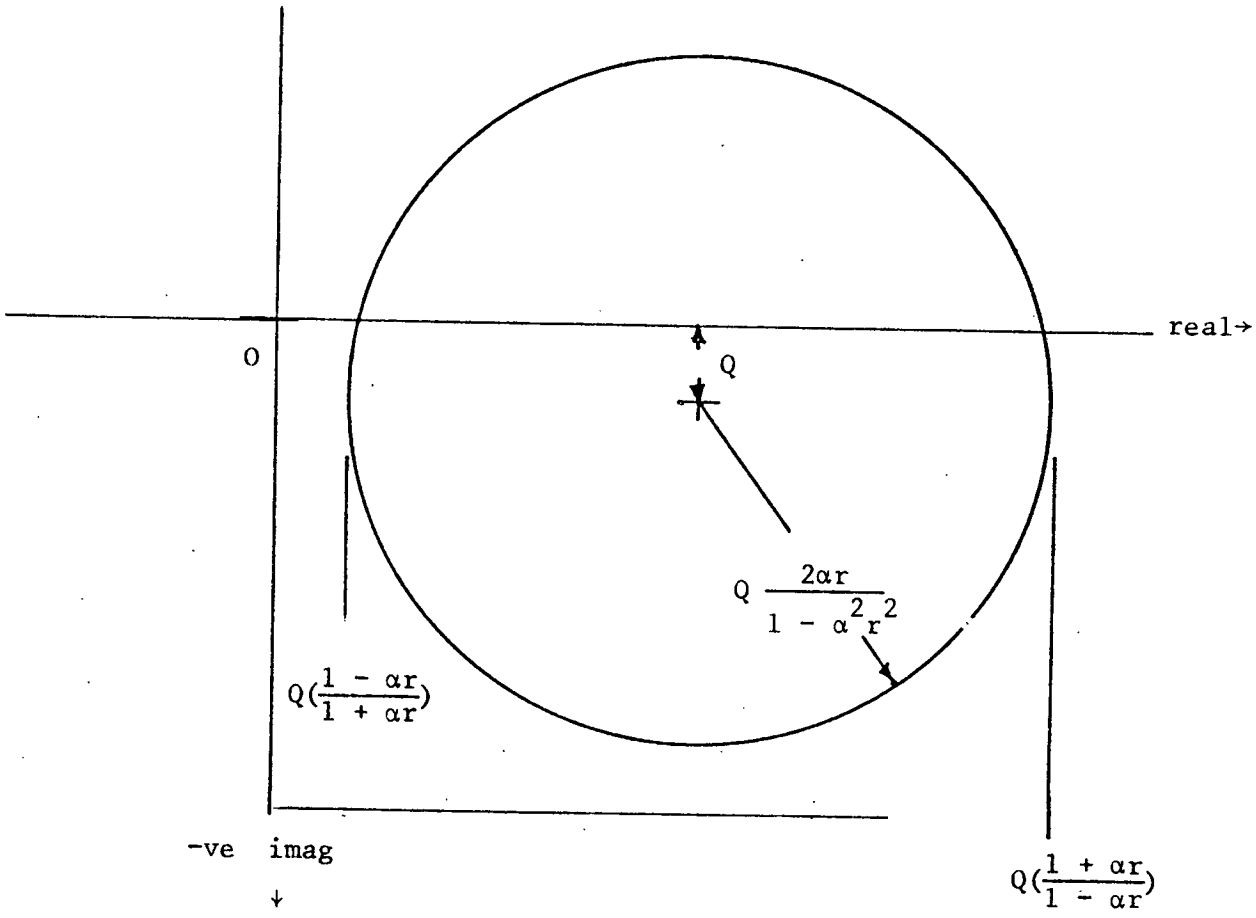

Fig. 2.3 Vector diagram of beam mobility $0 < \theta < 2\pi$

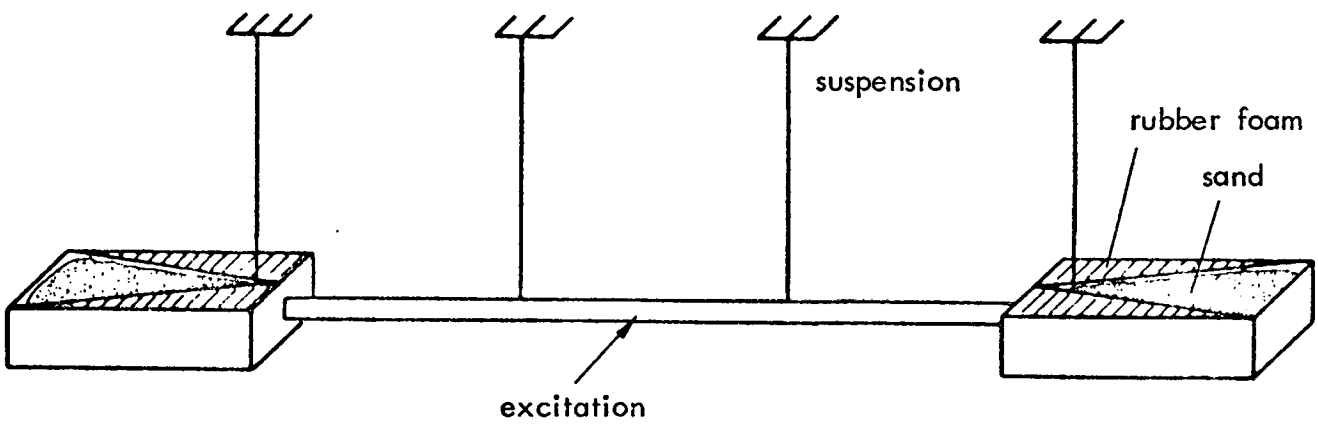

Fig. 2.4 Experimental infinite beam model.

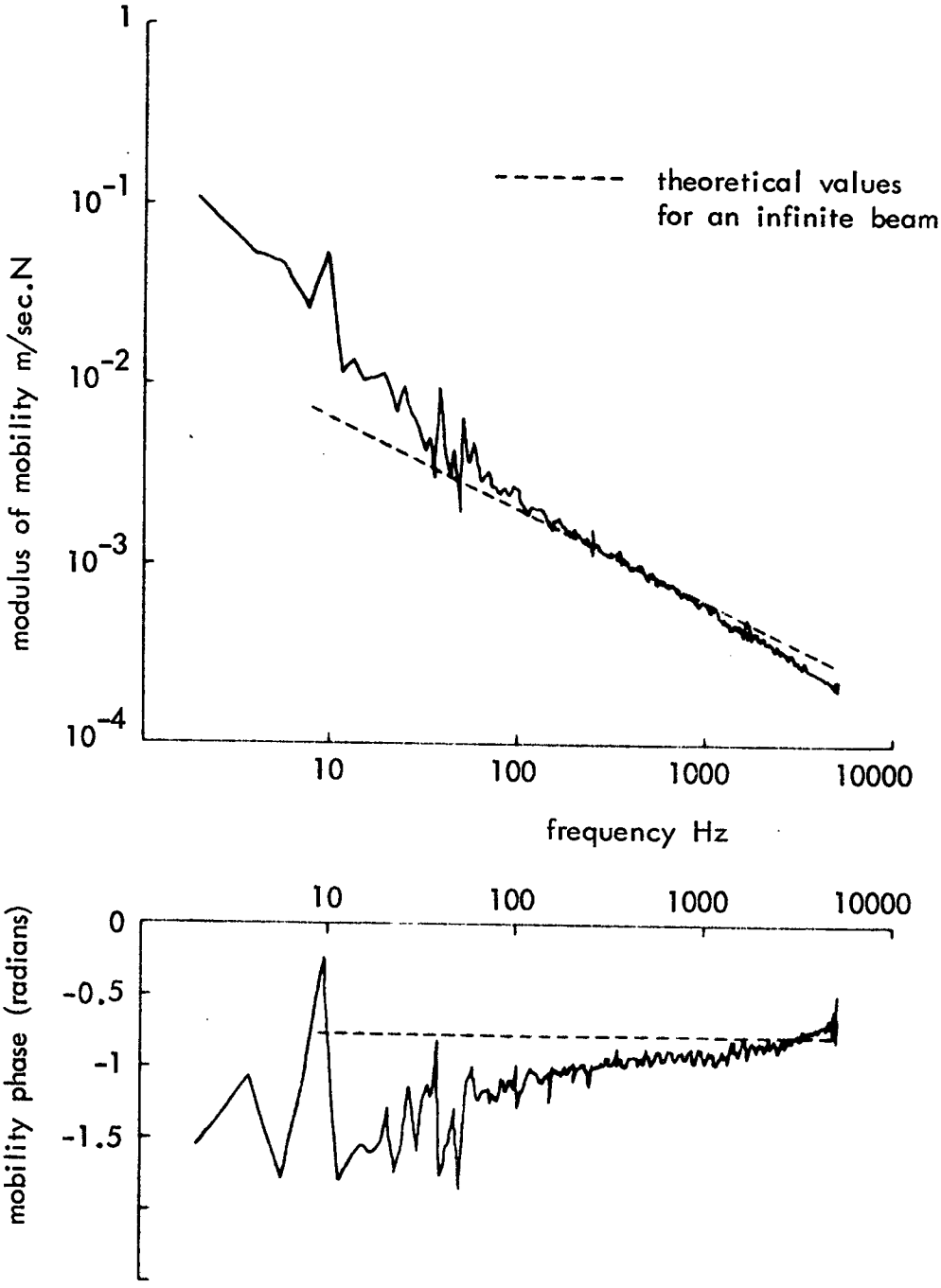

Fig. 2.5 Measured values of mobility modulus and phase of an experimental infinite beam.

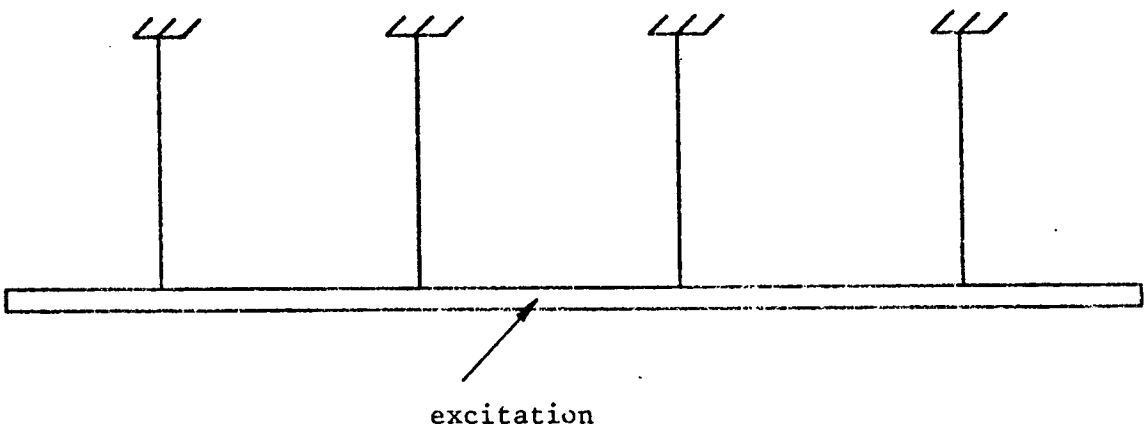

Fig. 2.6 Experimental finite beam

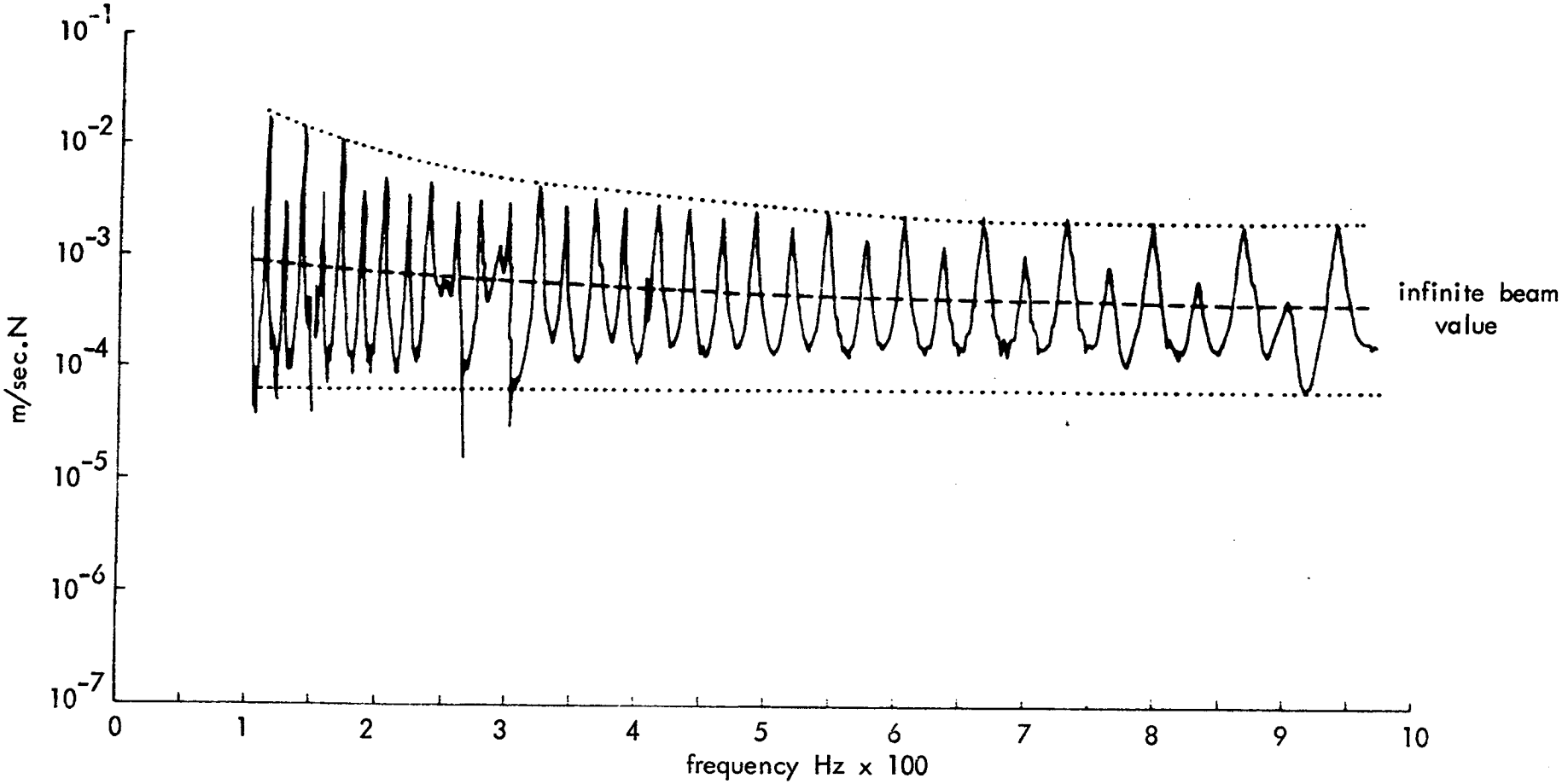

Fig. 2.7 Real component of finite beam point mobility.

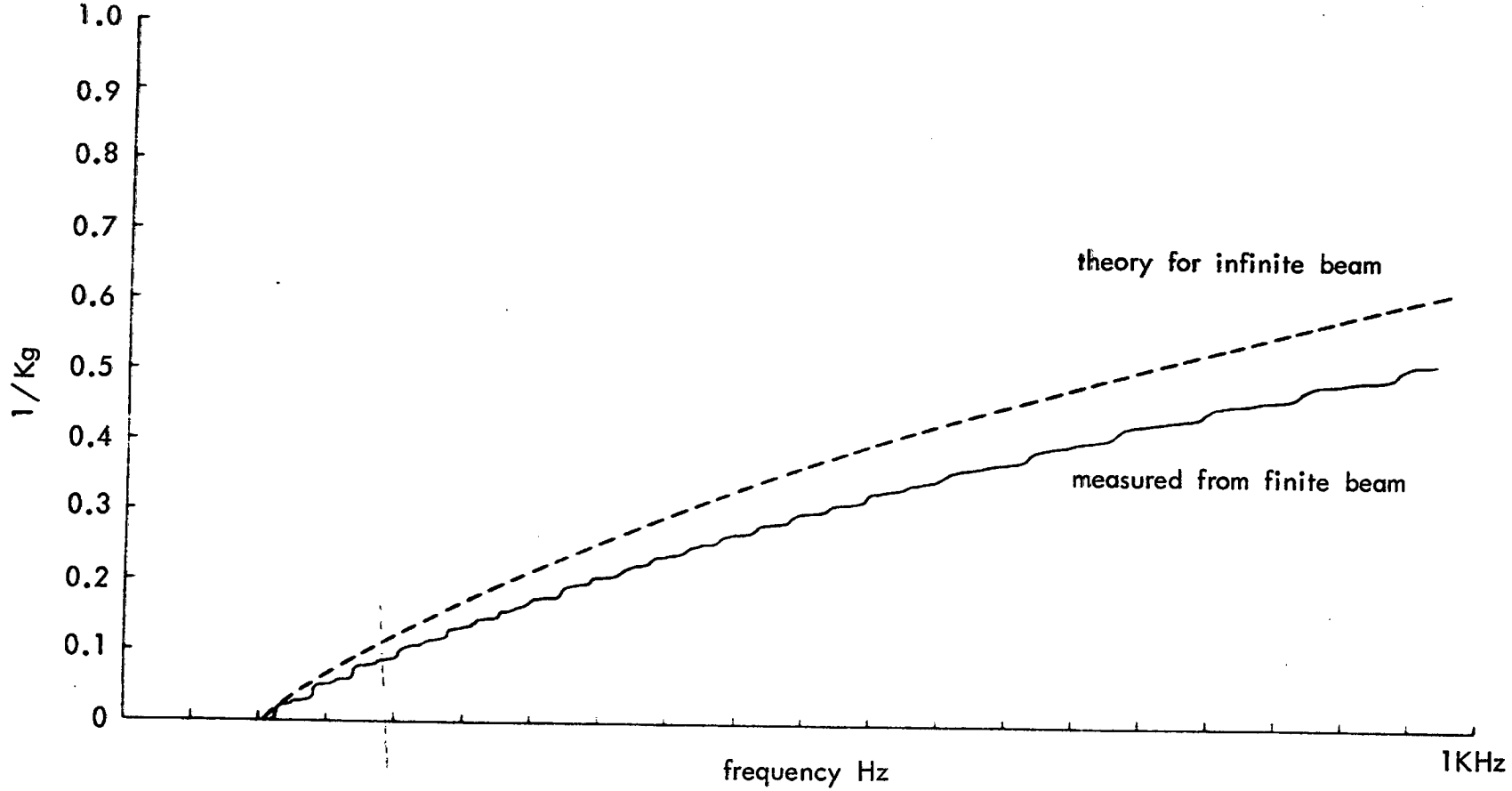

Fig. 2.8 Running integral across fig. 2.7.

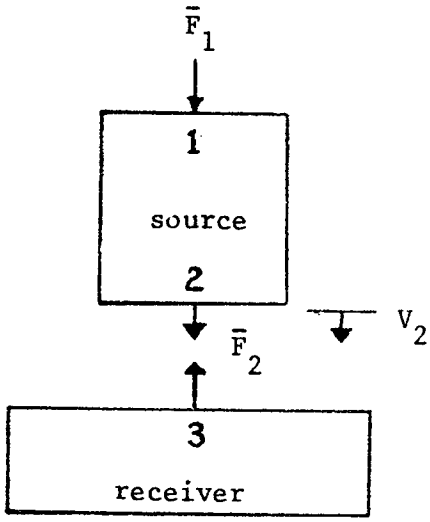

Fig. 3.1 Two coupled systems, no moment coupling.

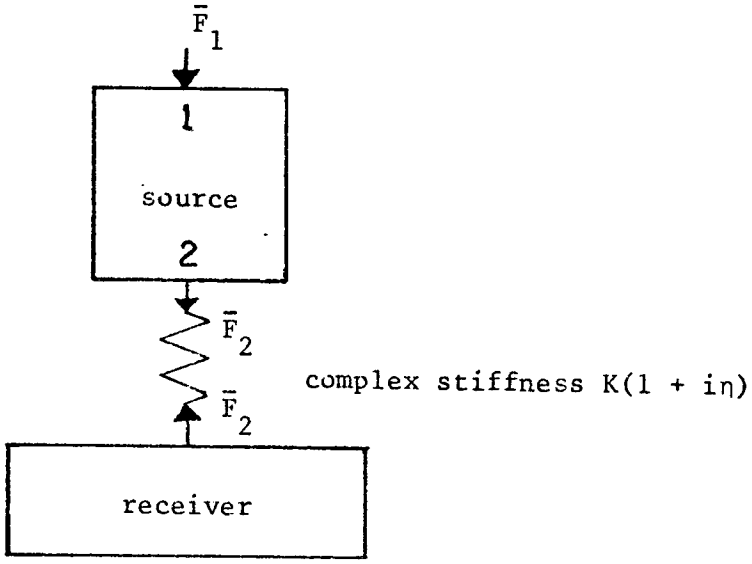

Fig. 3.2 Two systems coupled by a damped spring.

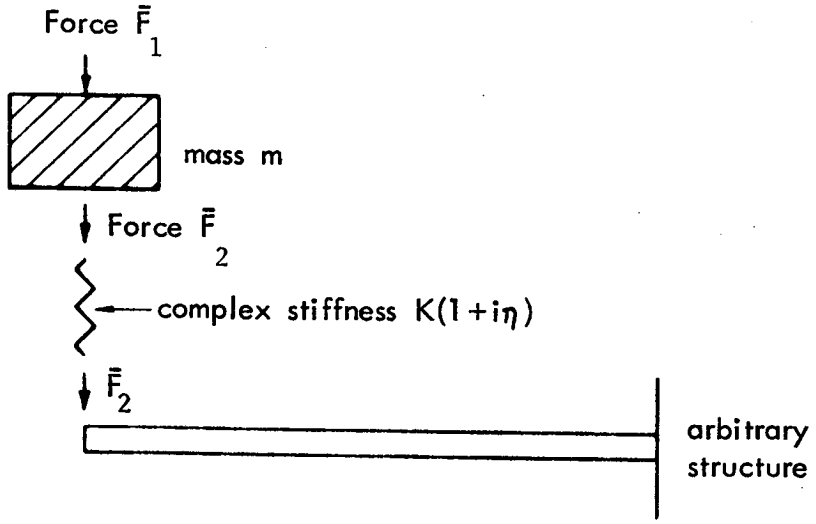

FIG. 3.3 Model of connected mass, spring and finite beam.

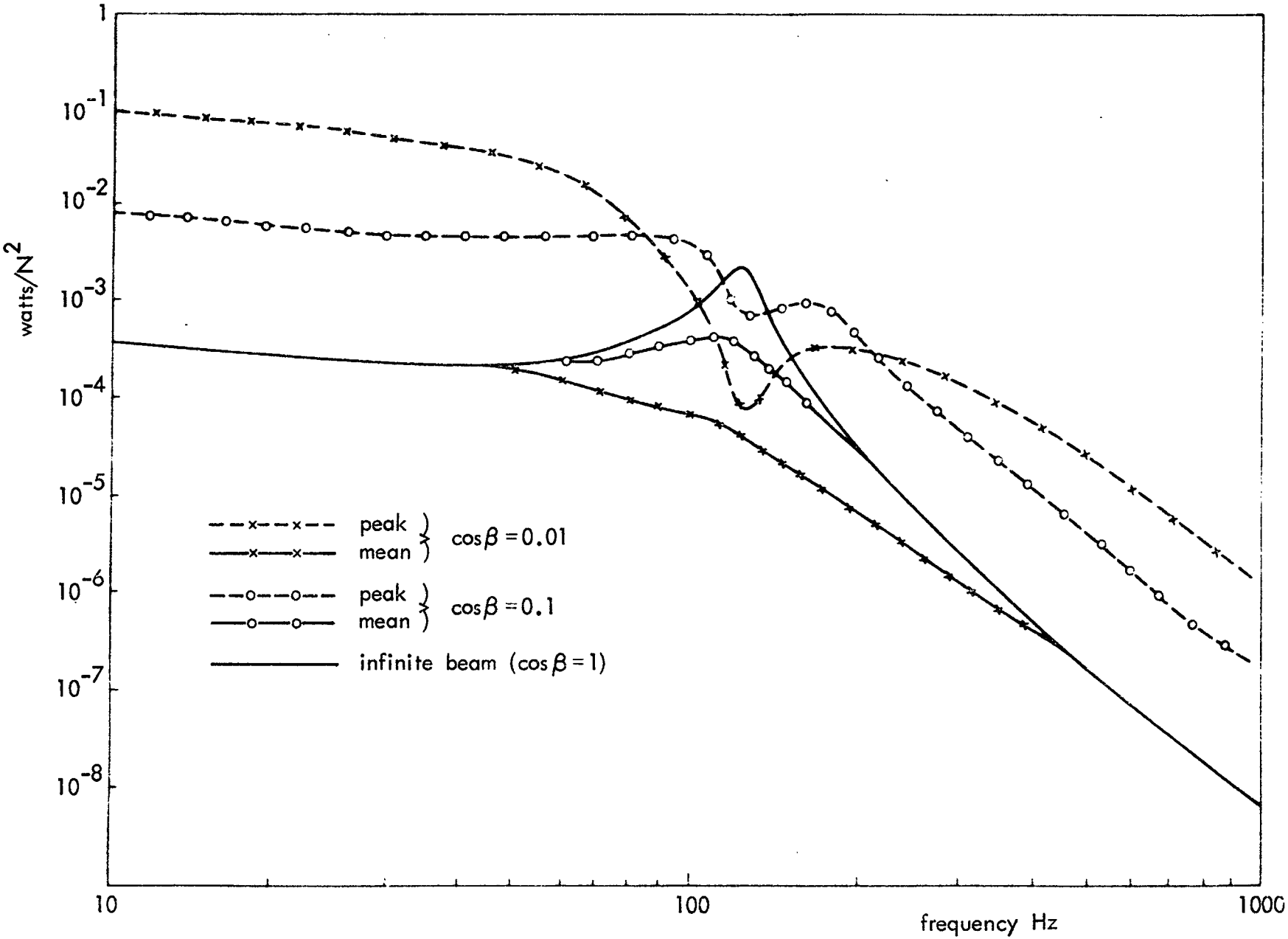

Fig. 3.4 Peak and mean power/<force>^{2} to finite and infinite beam seating via a mass and spring (same parameters as the experimental model)

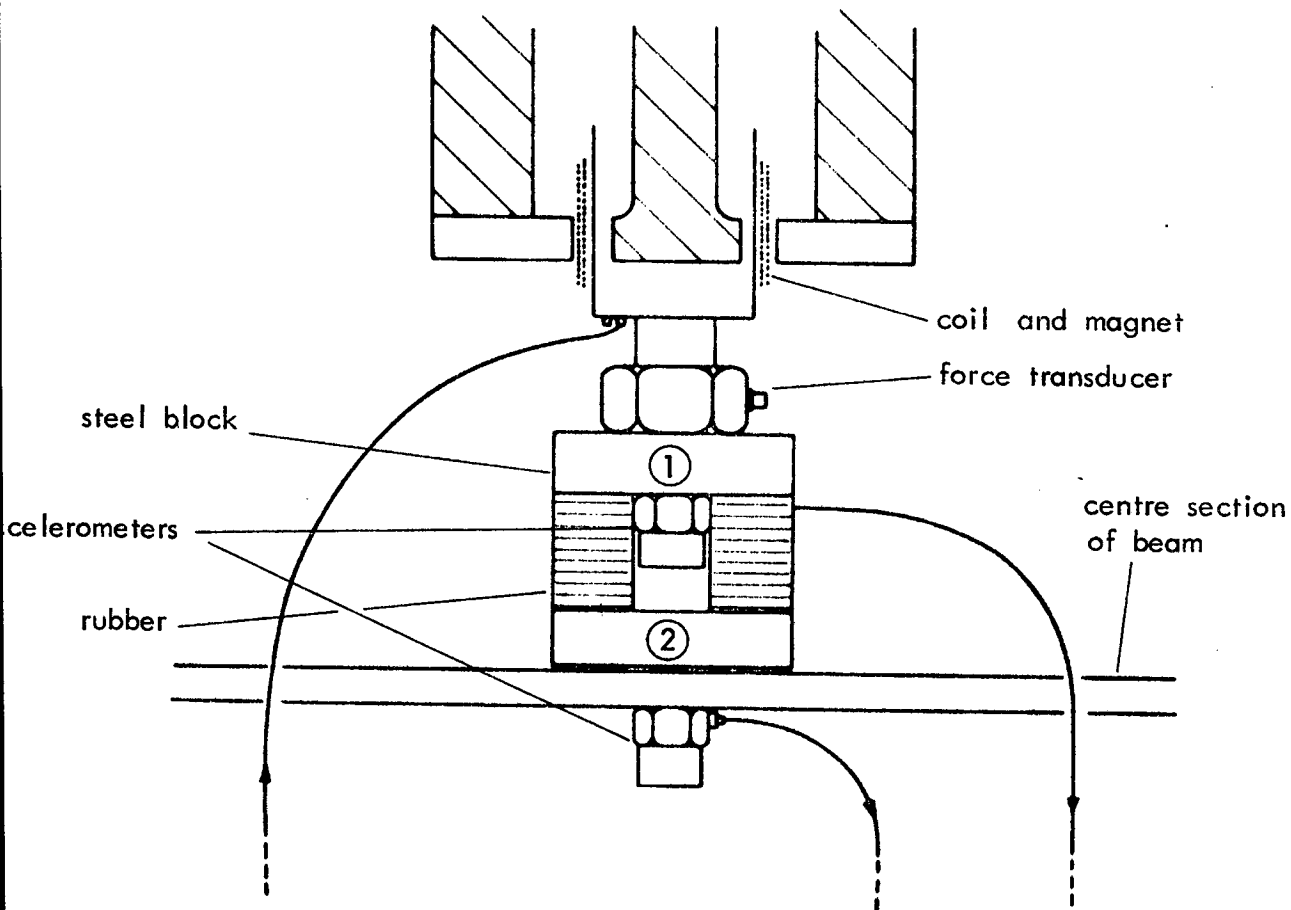

FIG. 3.5 Experimental layout.

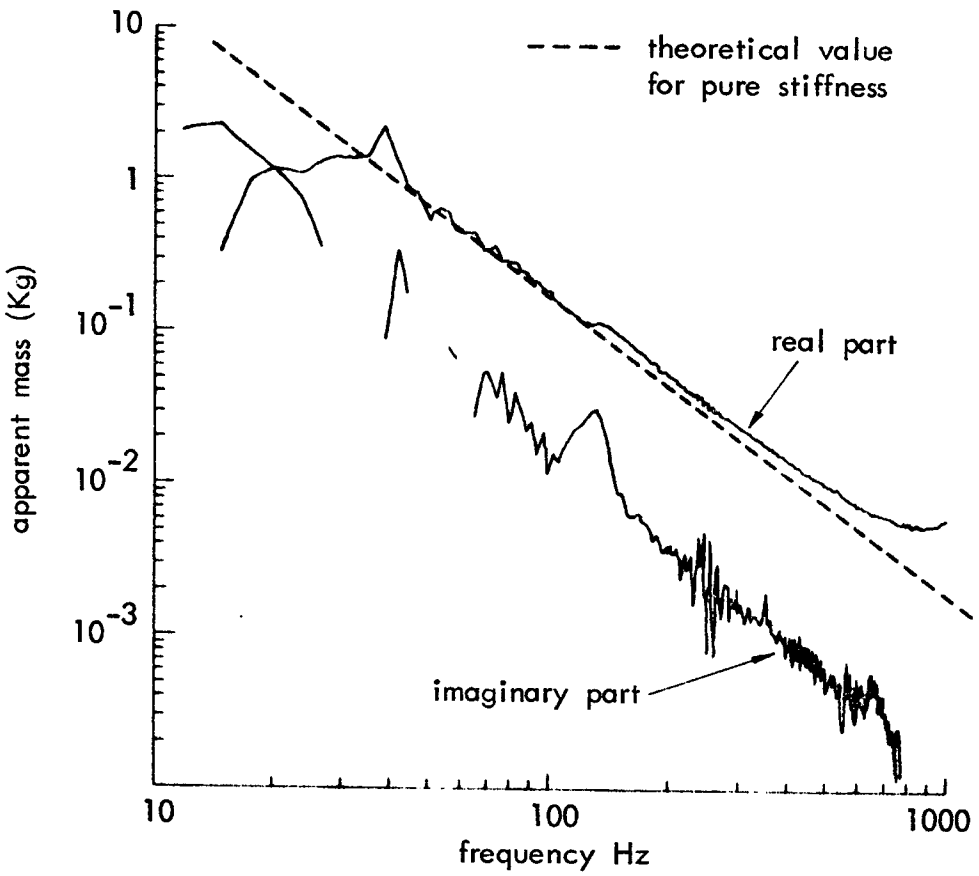

FIG. 3.6 Real and imaginary components of isolator transfer apparent mass.

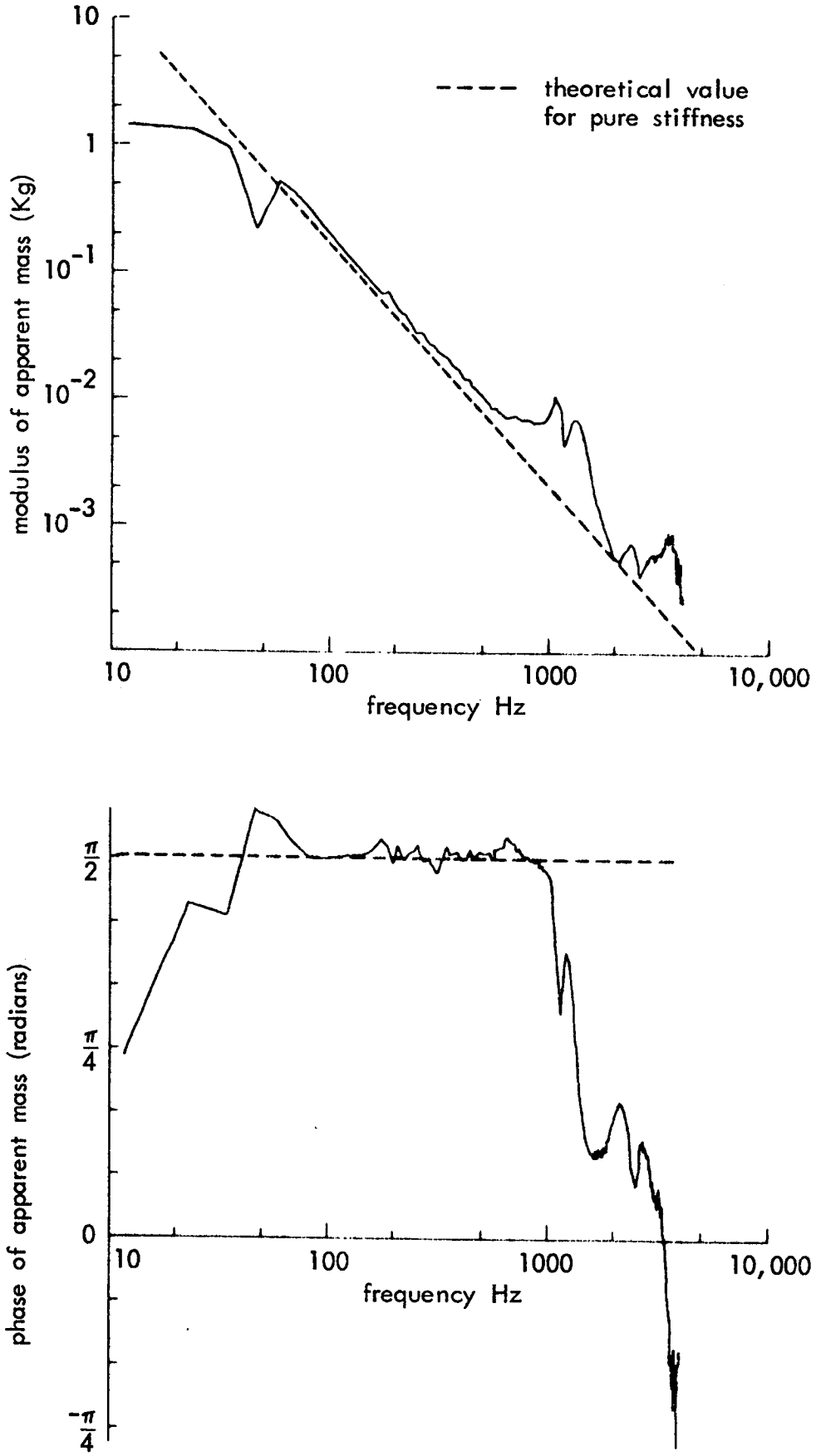

FIG. 3.7 Modulus and phase of isolator transfer apparent mass 0-4 kHz.

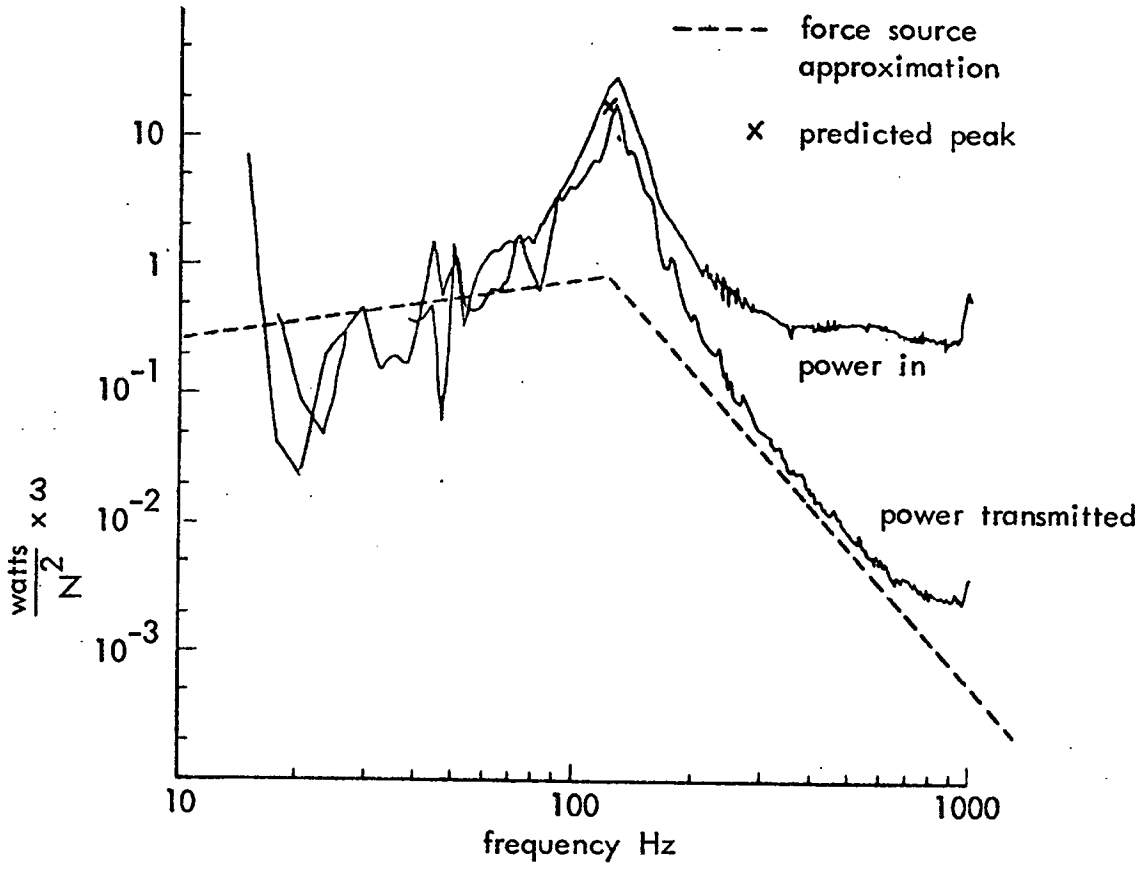

Fig. 3.8 Exp. 1. Power × ω, input to isolator and transmitted to the infinite beam, for unit force spectral density.

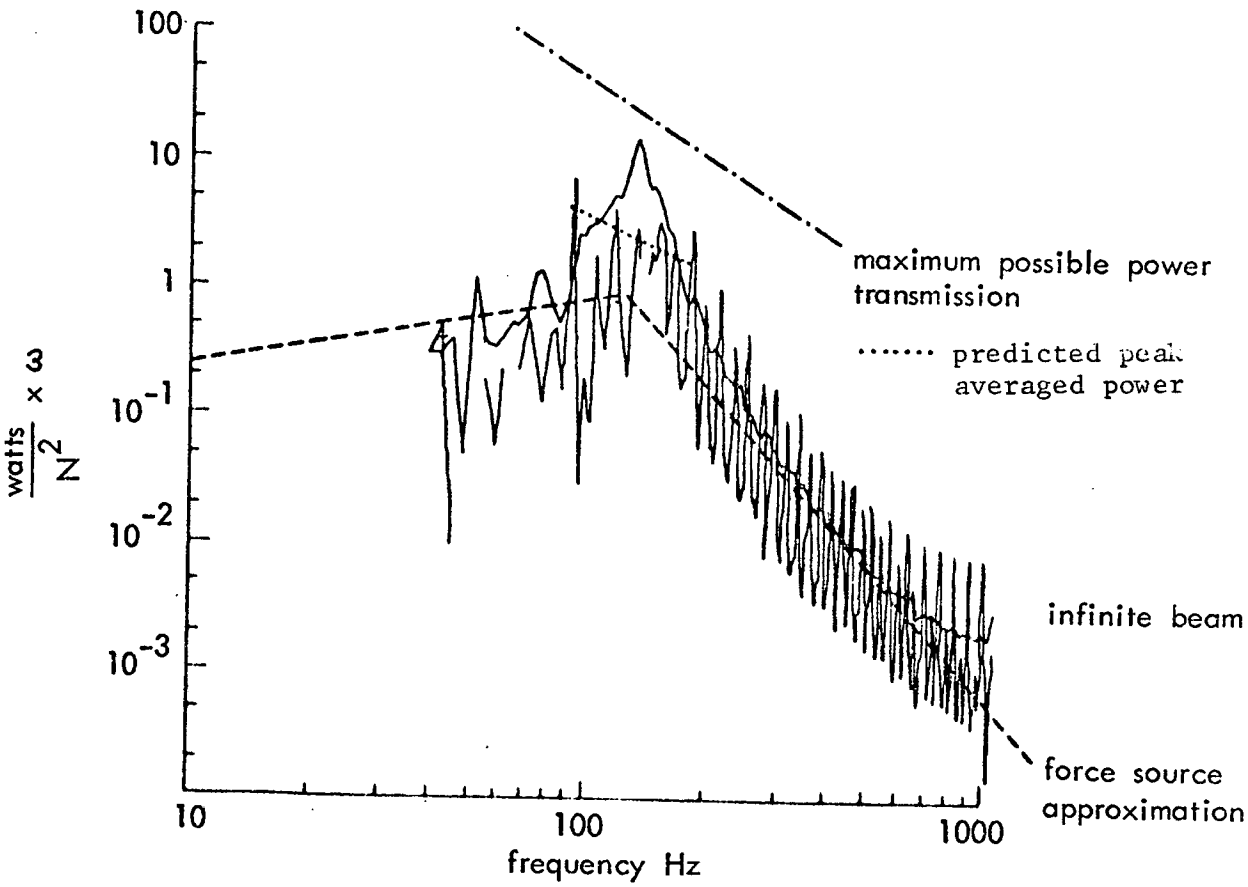

Fig. 3.9 Comparison between ω × power transmitted to the finite beam and the infinite beam for unit force spectral density input 0-1 kHz.

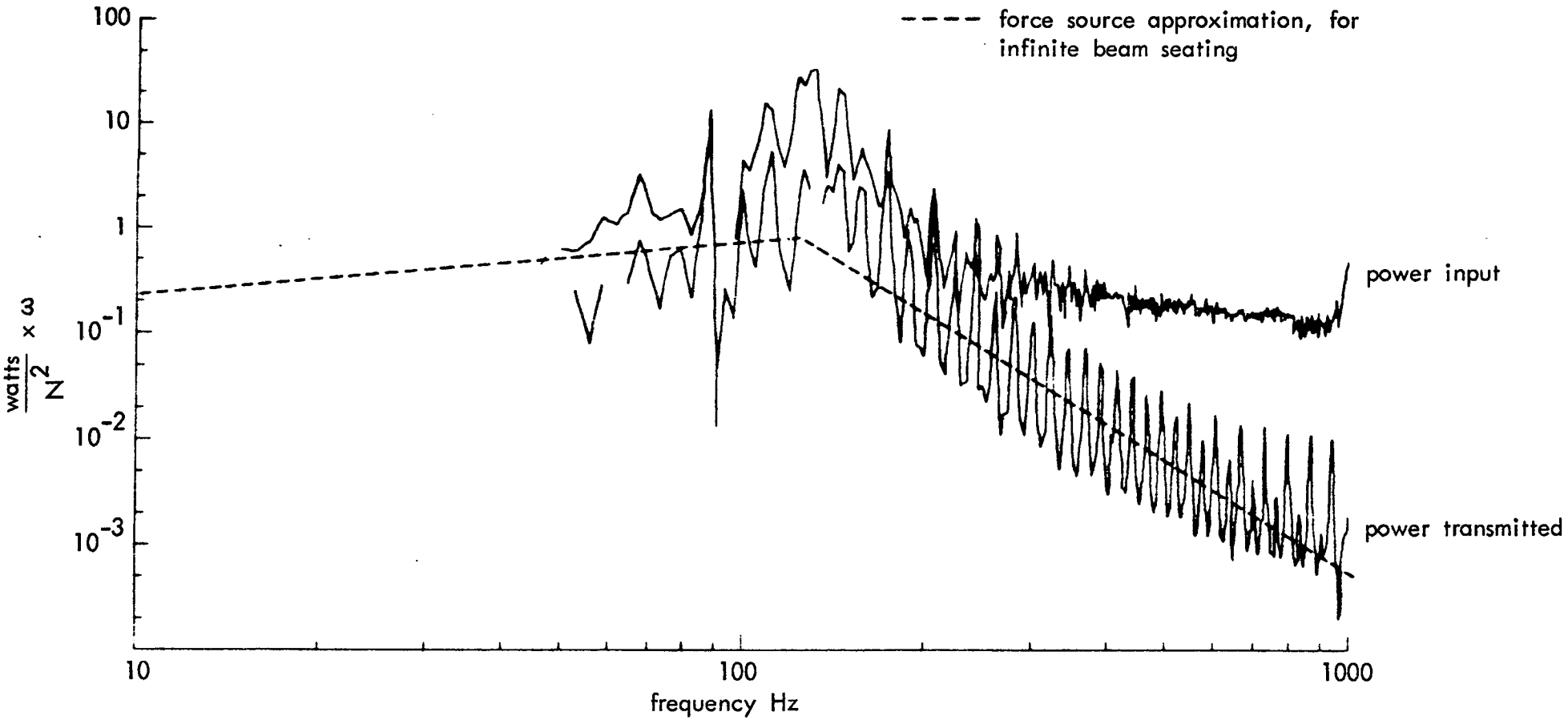

Fig. 3.10. Exp. 2. ω × Power. Input to isolator and transmitted to the finite beam, for unit force spectral density input. 0-1 kHz.

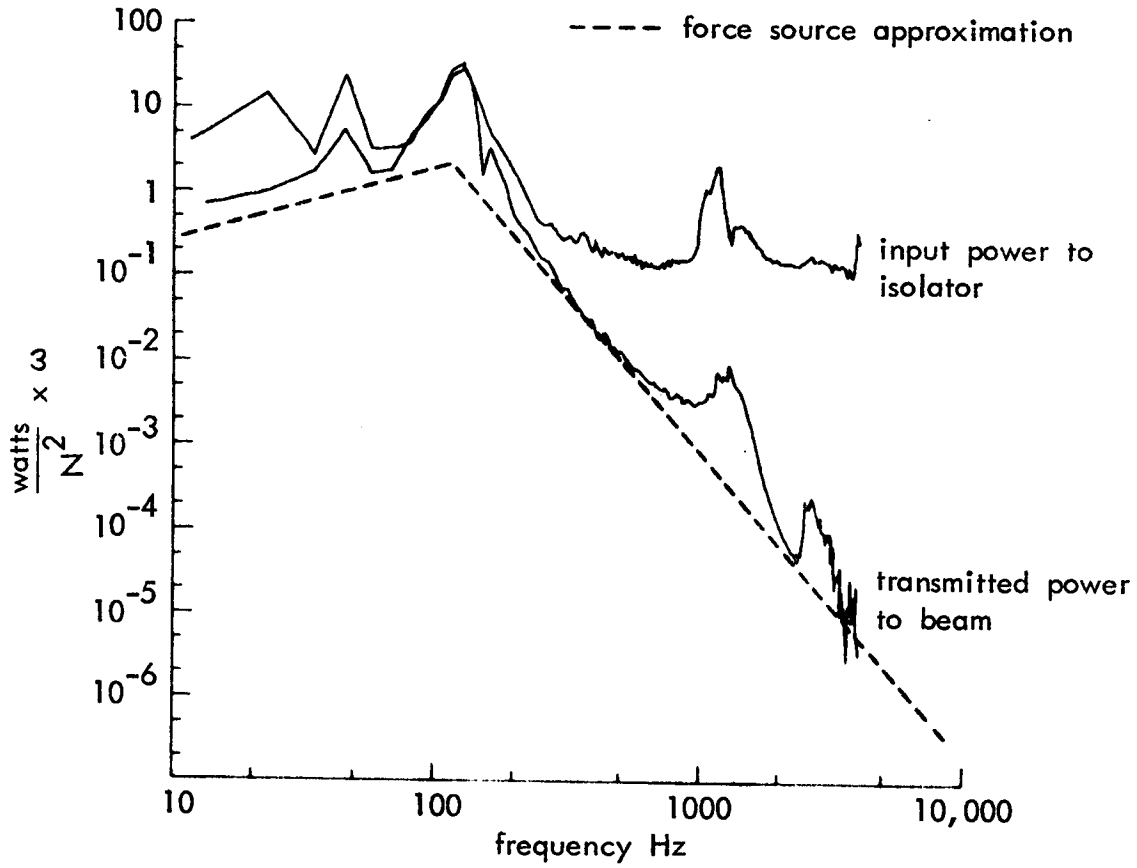

Fig. 3.11. Exp. 3, Power × ω Input to isolator, and transmitted to the infinite beam for unit force spectral density, 0-4 kHz.

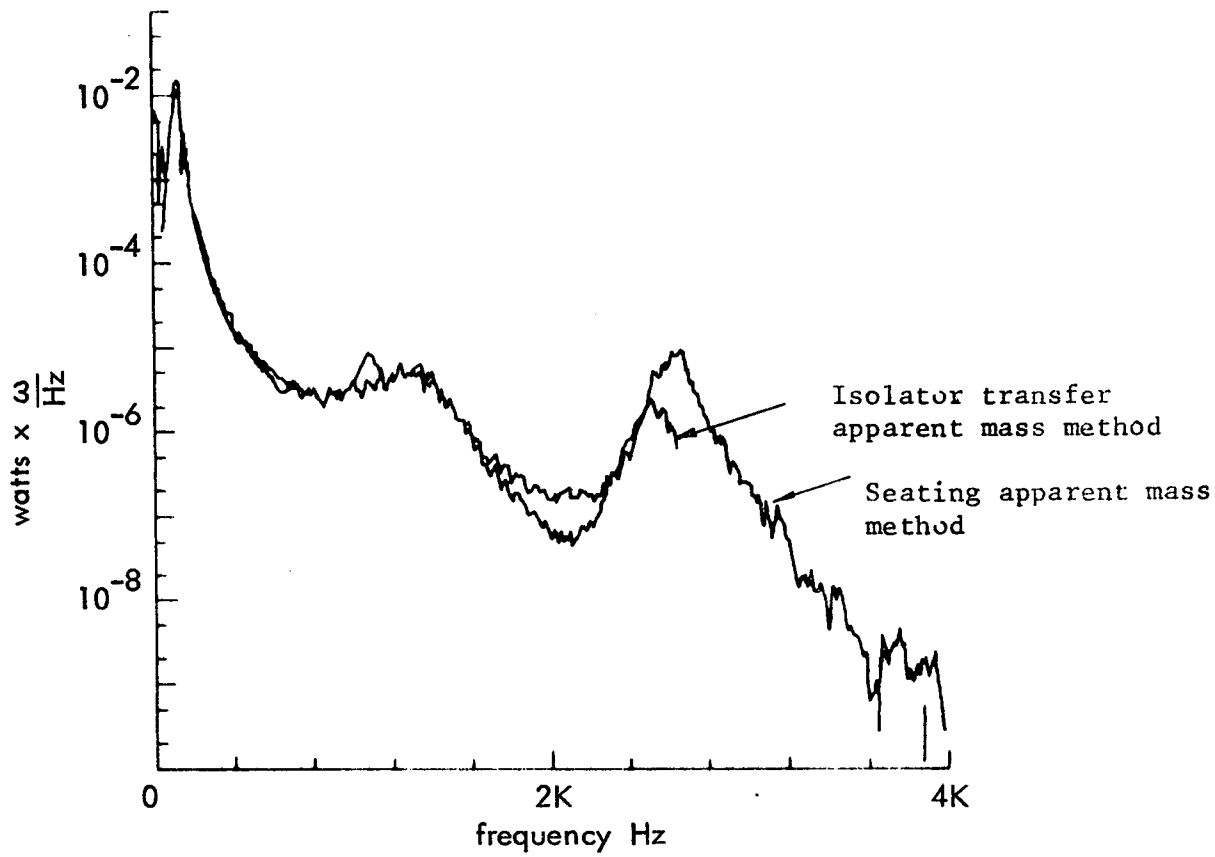

Fig. 3.12. Comparison of $\omega \times$ power/Hz measured using the isolator transfer apparent mass method, and the seating apparent mass method.

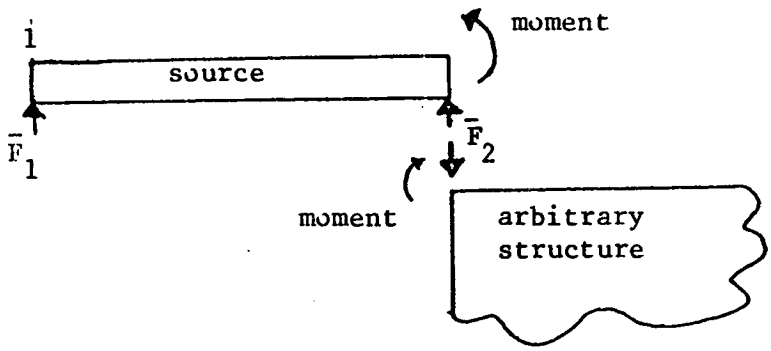

Fig. 4.1 Source beam coupled to an arbitrary structure.

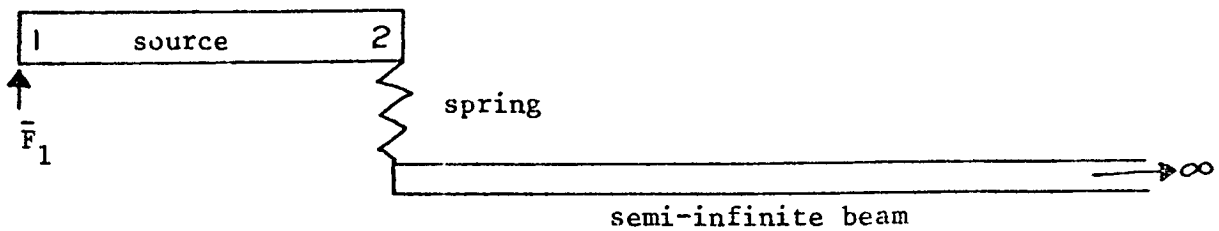

Fig. 4.2 Finite source beam coupled to a semi-infinite beam by a spring.

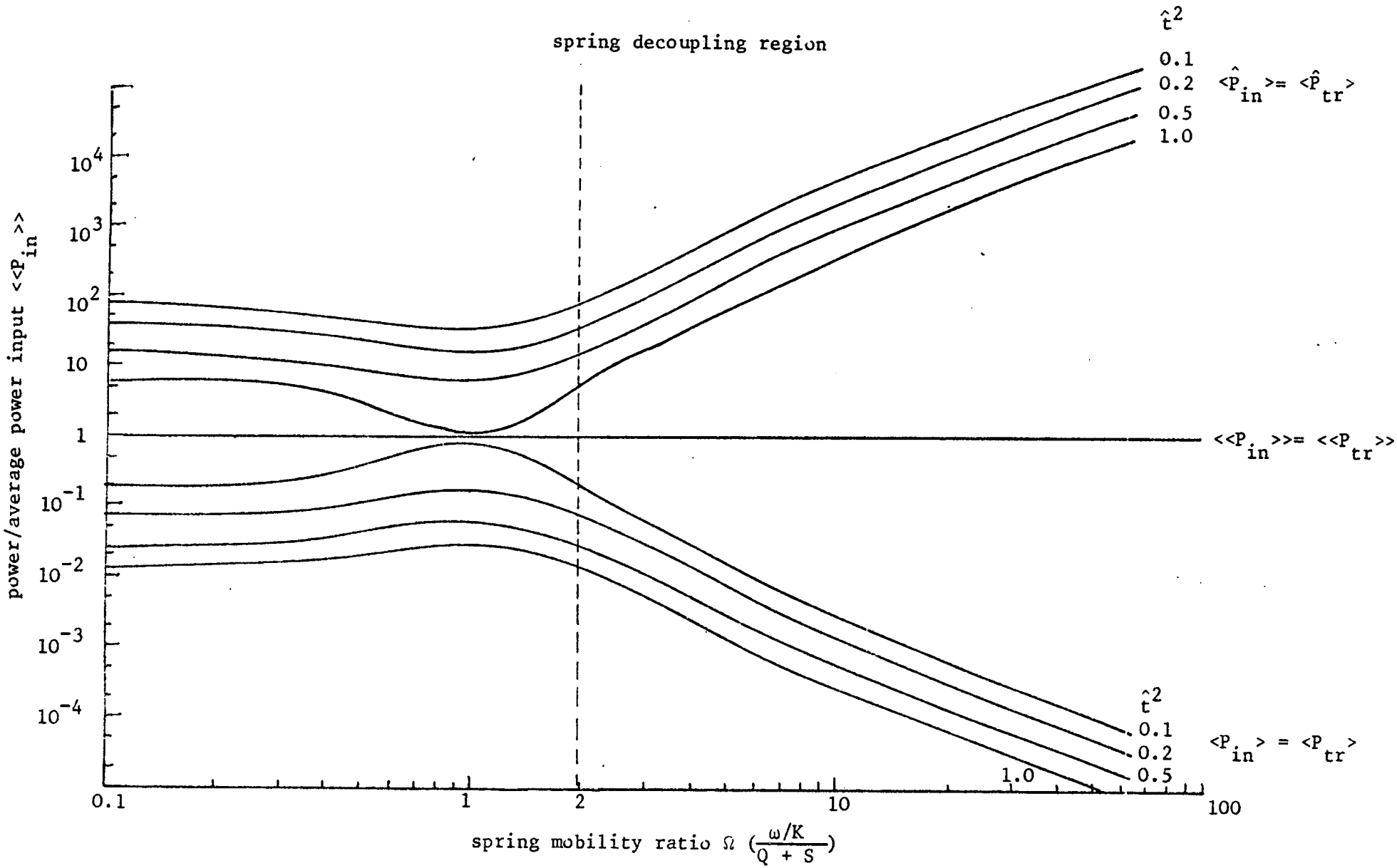

Fig. 4.3 Peak $\langle\hat{P}\rangle$, trough $\langle\check{P}\rangle$ and frequency averaged power $\langle\langle P\rangle\rangle$, input and transmitted from an undamped source beam, coupled to a semi-infinite beam by a spring.

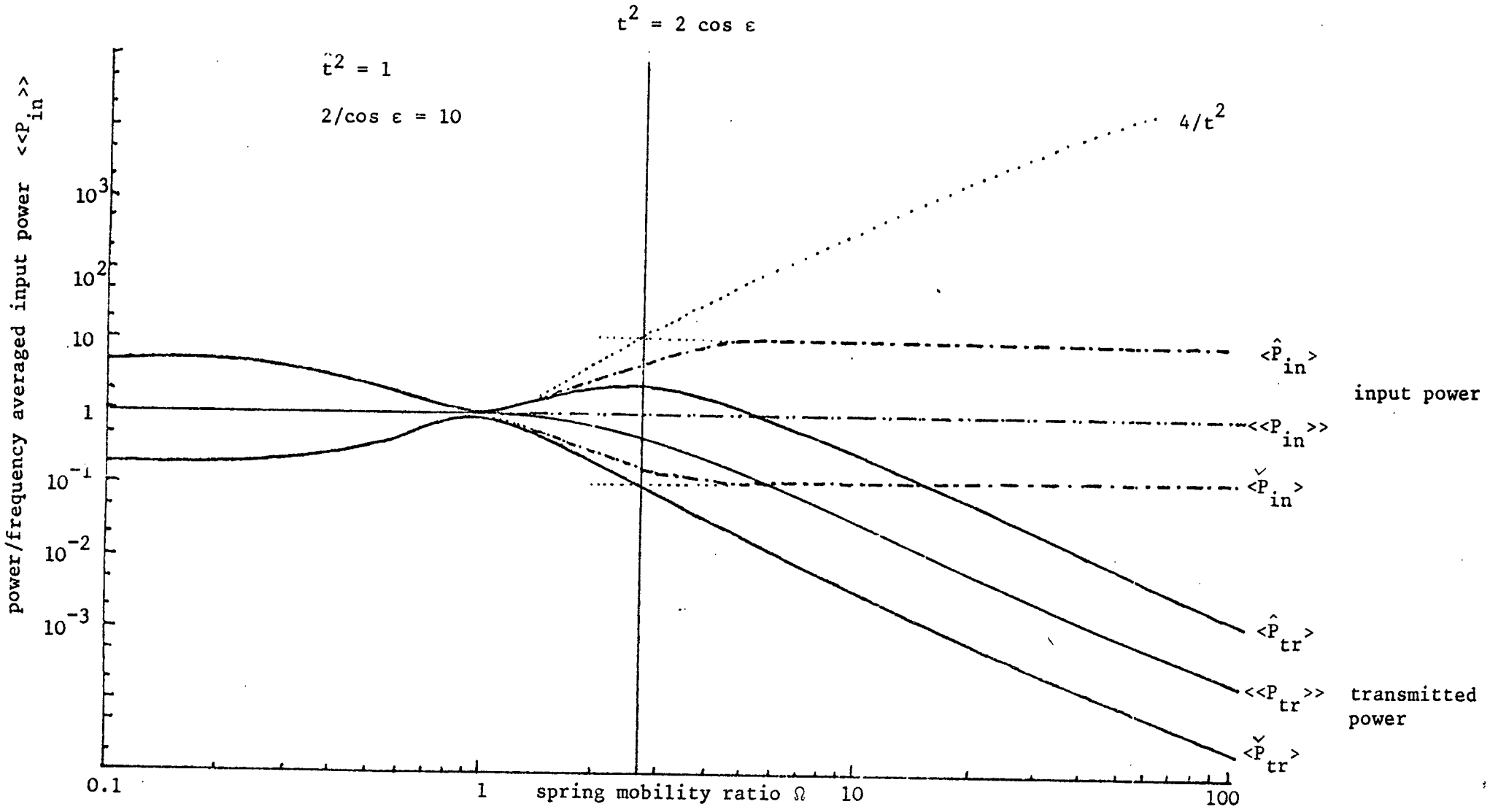

Fig. 4.4 Power input and transmitted from a damped finite beam coupled to a semi-infinite beam by a spring.

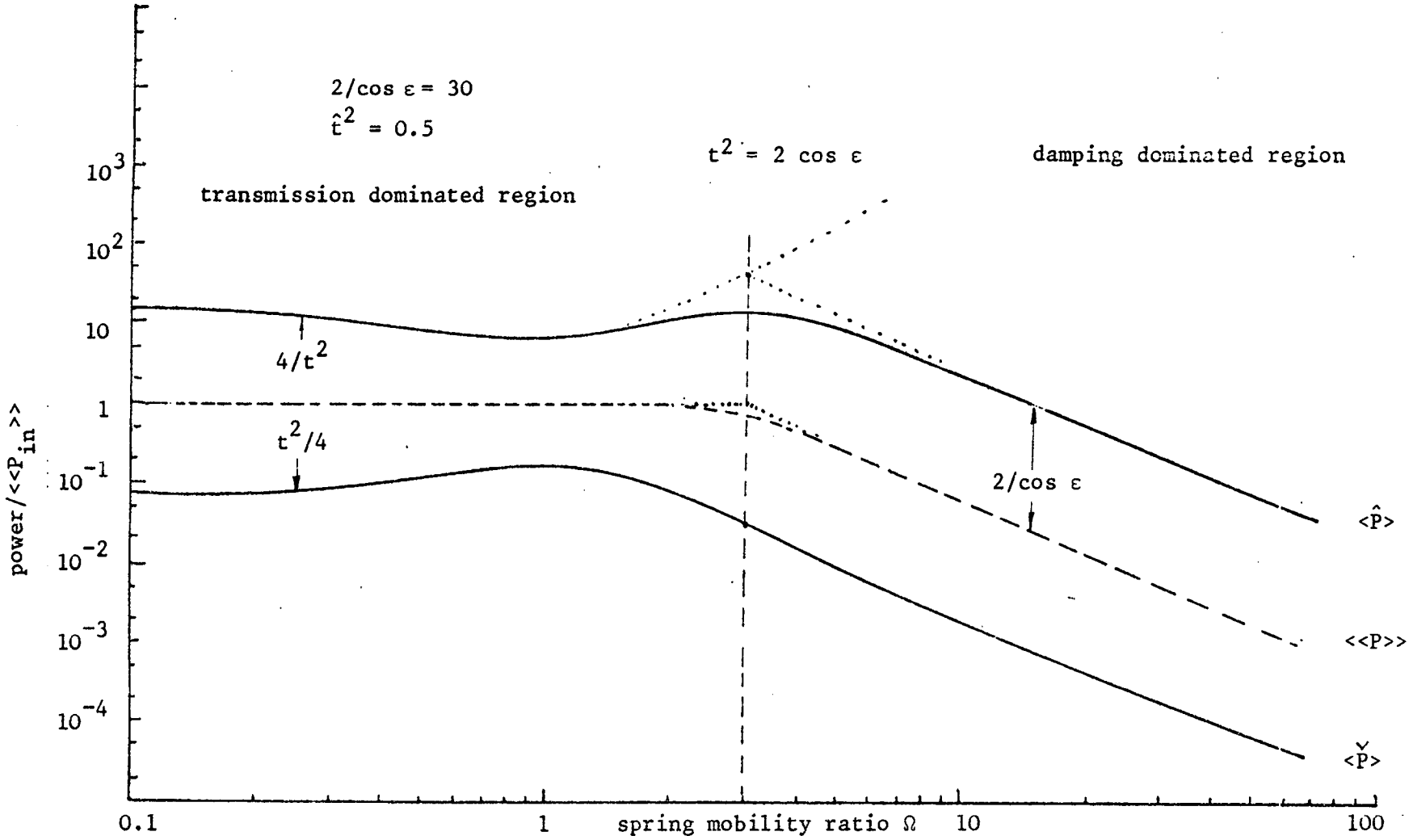

Fig. 4.5 Peak <$\hat{P}$>, trough <$\check{P}$> and mean power <<P>> transmitted to a semi-infinite beam from a damped source beam via a spring.

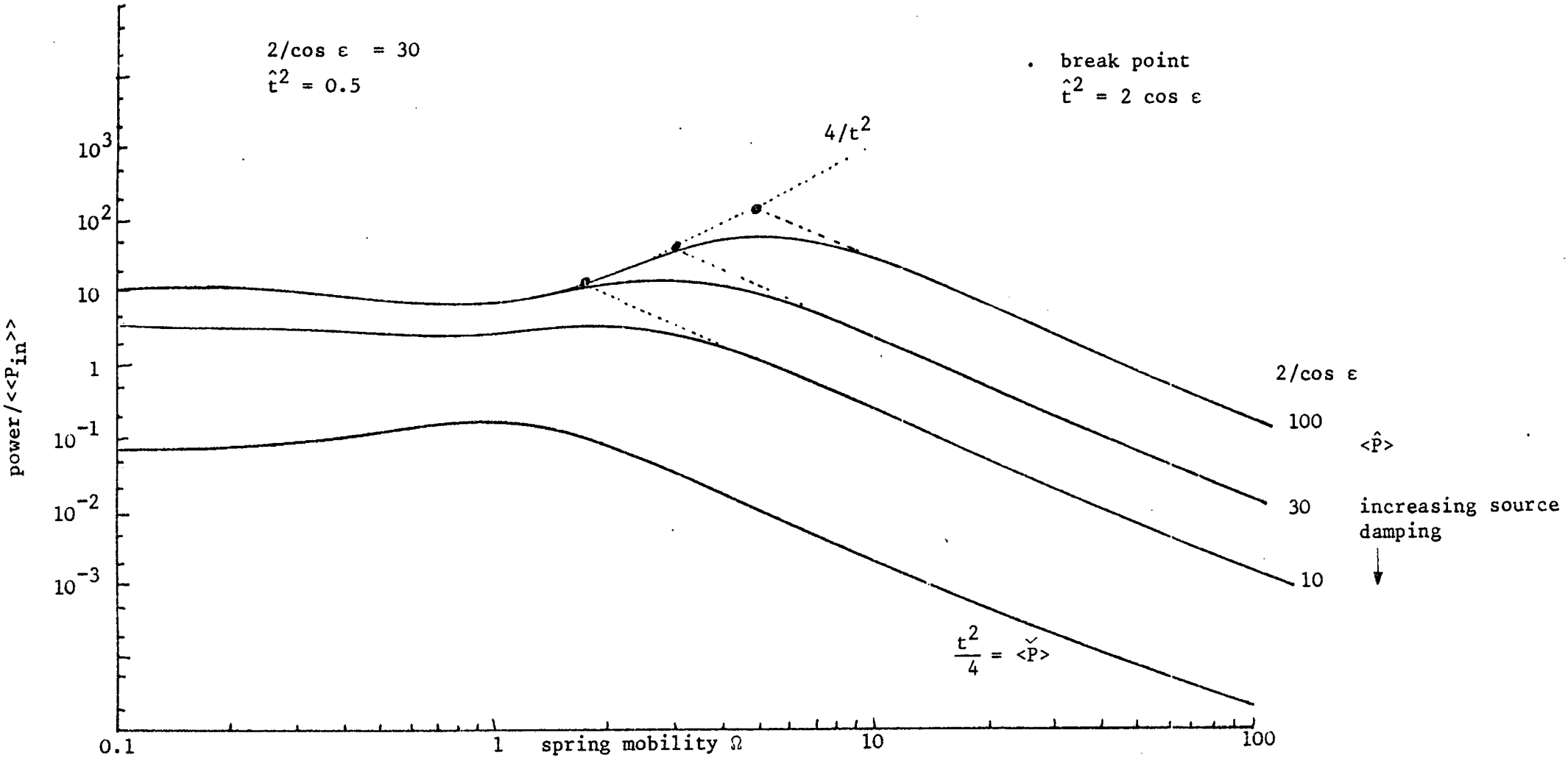

Fig. 4.6 The effect of source beam damping upon the peak <$\hat{P}$> and trough <$\check{P}$> transmitted power.

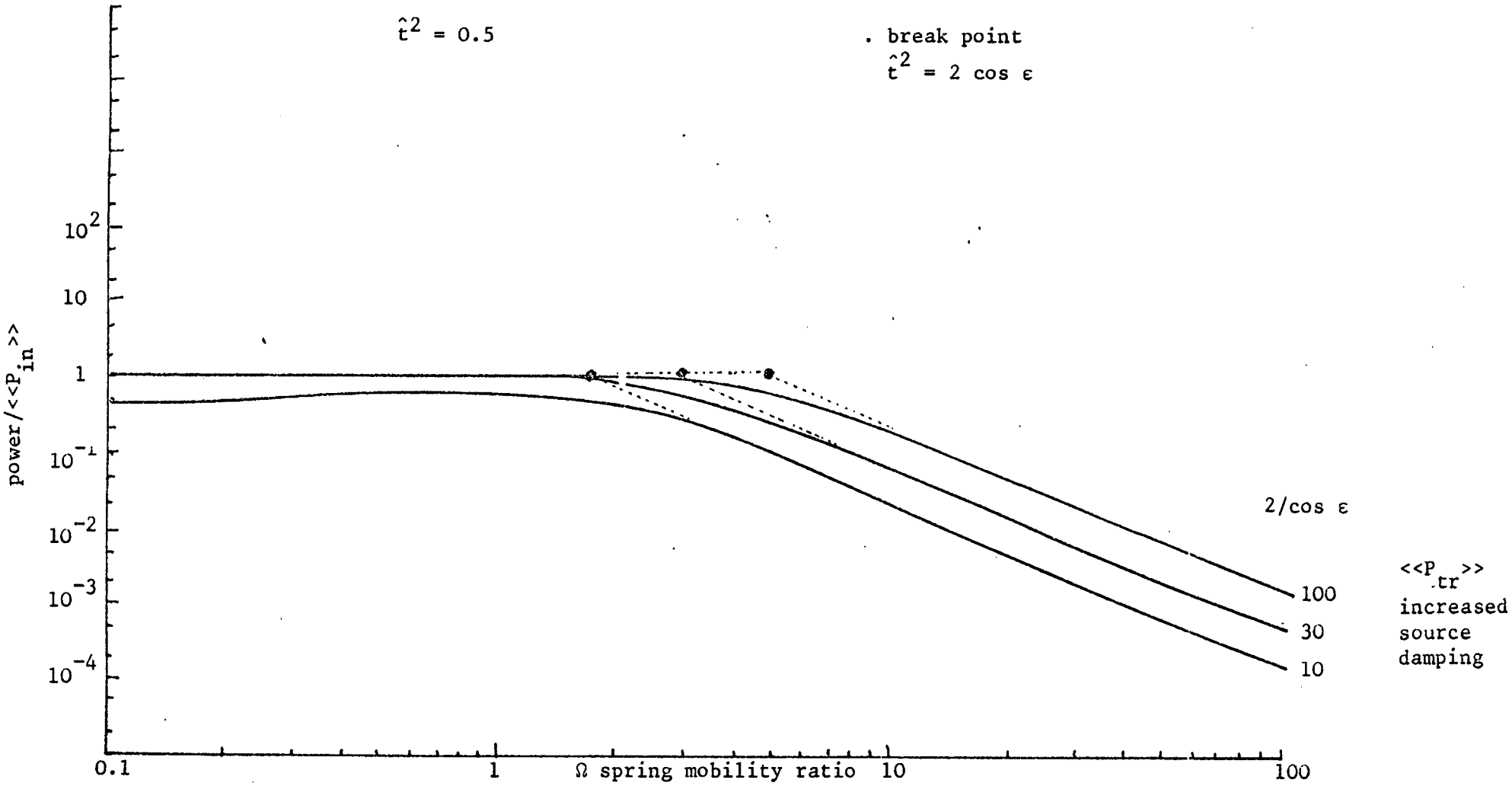

Fig. 4.7 The effect of source beam damping upon the frequency averaged transmitted power <<P_{tr}>> to the semi infinite beam receiver.

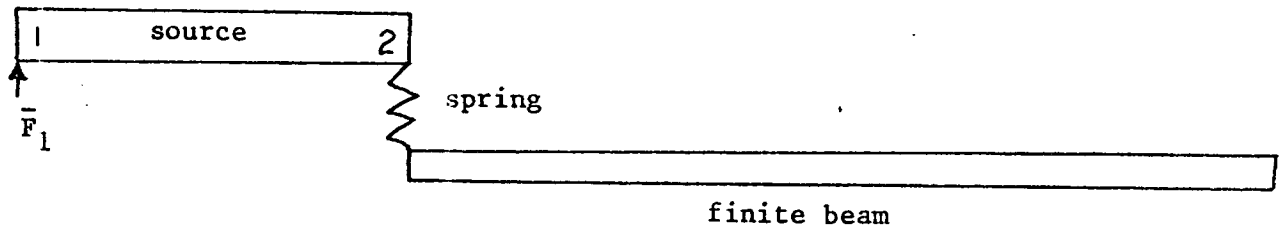

Fig. 5.1 Finite source beam coupled to a long receiver beam by a spring

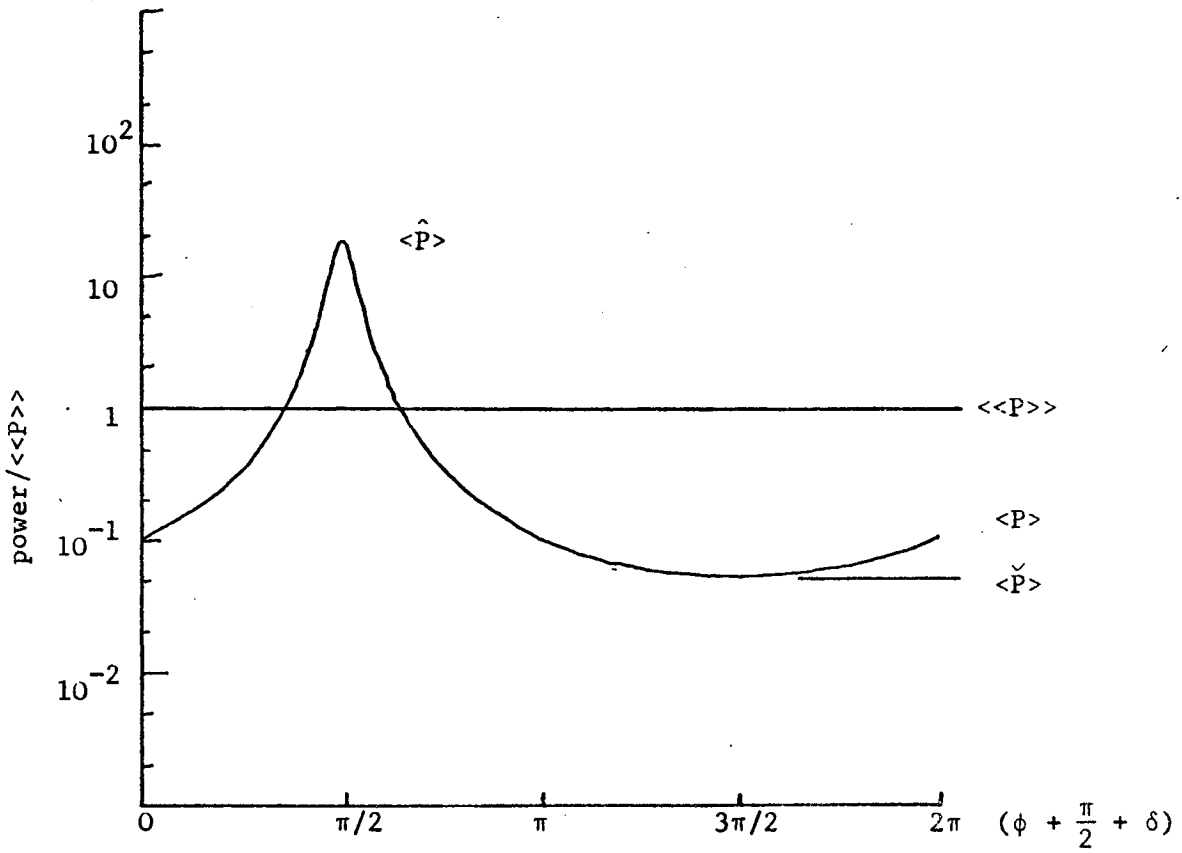

Fig. 5.2 Power transmitted to infinite beam, for one source beam mode $0 < \phi + \frac{\pi}{2} + \delta < 2\pi$

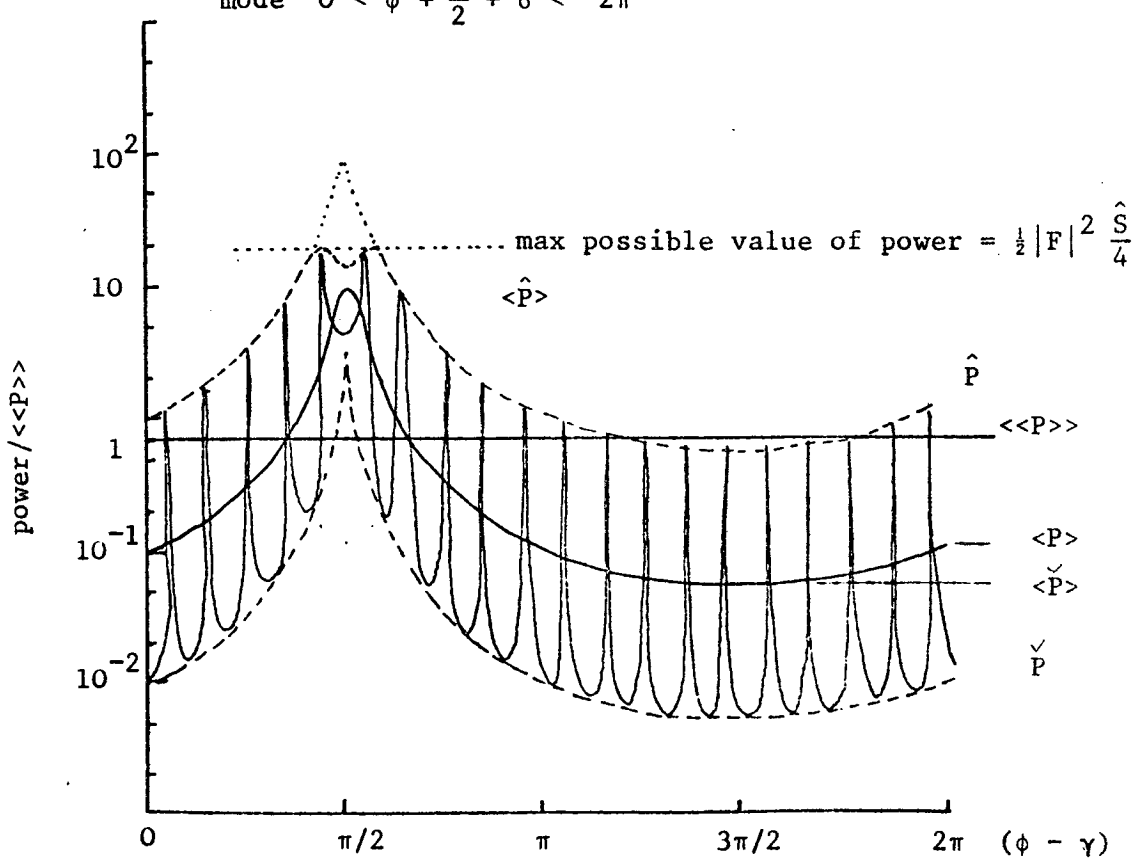

Fig. 5.3 Power transmitted to a finite beam, for one source beam mode $0 < \phi - \gamma < 2\pi$, and 20 receiver beam modes $0 < \theta < 20\pi$

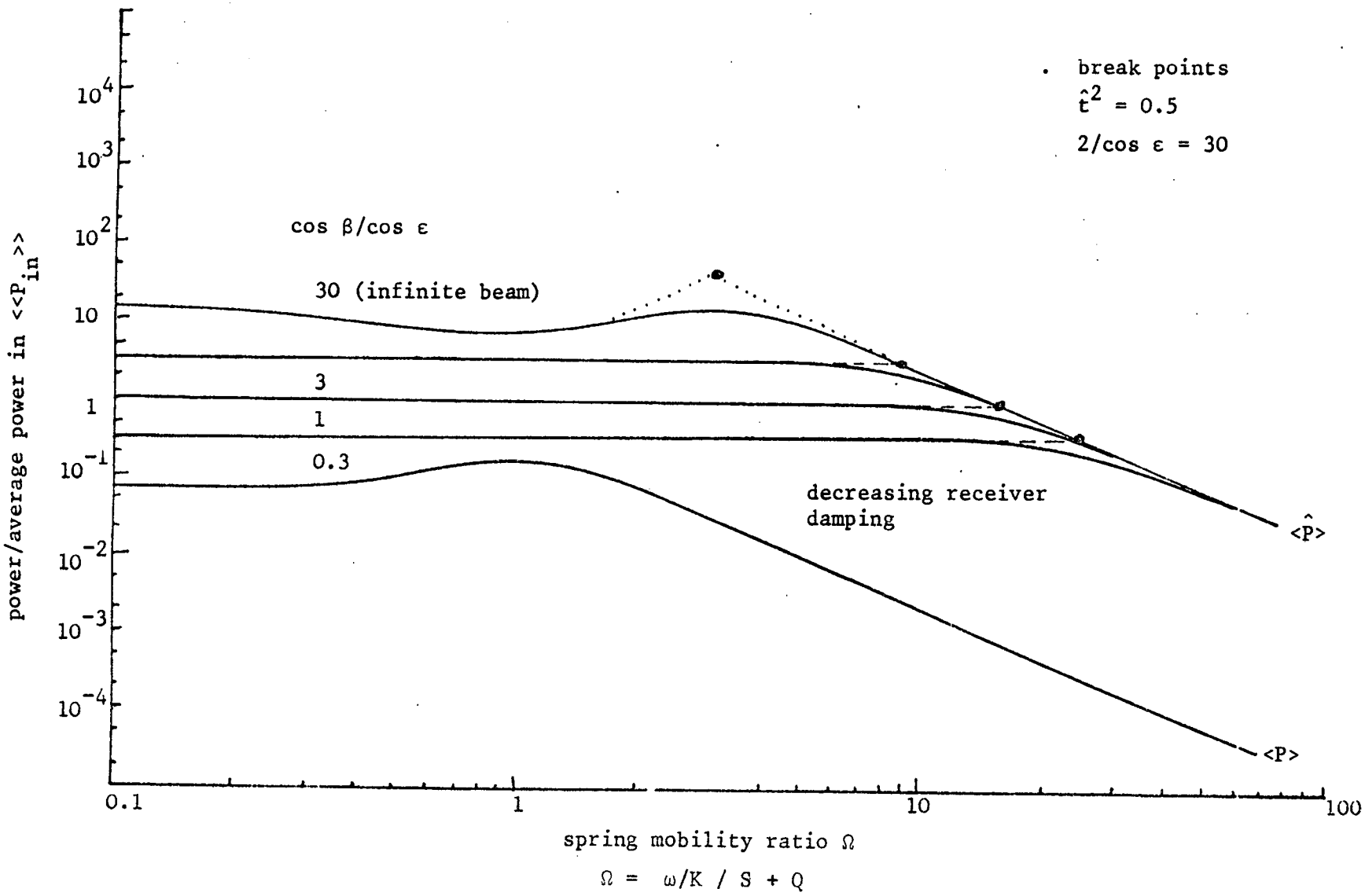

Fig. 5.4 The effect of the source-receiver damping ratio (cos β/cos ε) on peak $\langle\hat{P}\rangle$ and trough $\langle P\rangle$ power transmission.

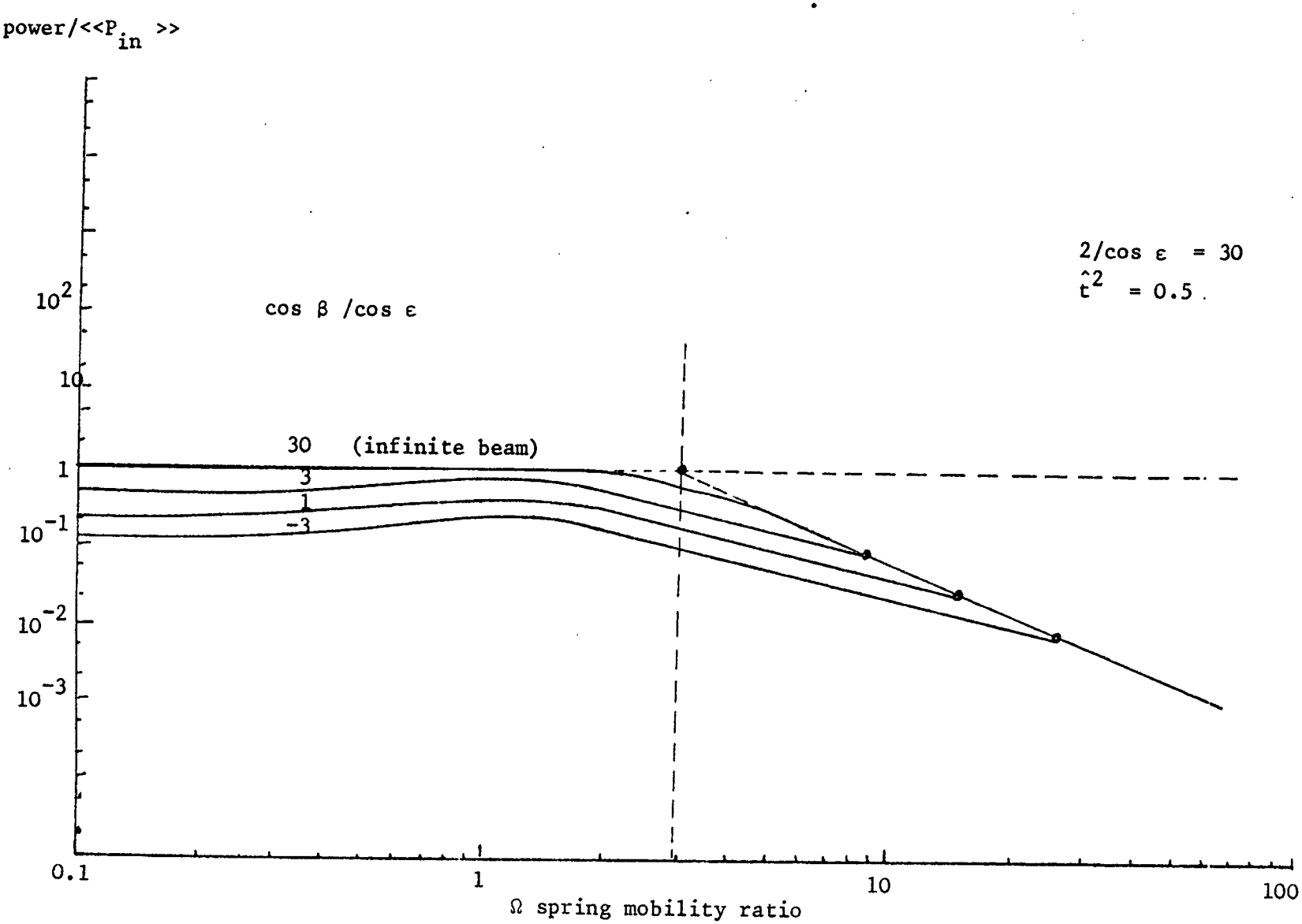

Fig. 5.5 The effect of the source-receiver damping ratio (cos β/cos ε) upon mean transmitted power <<P>>

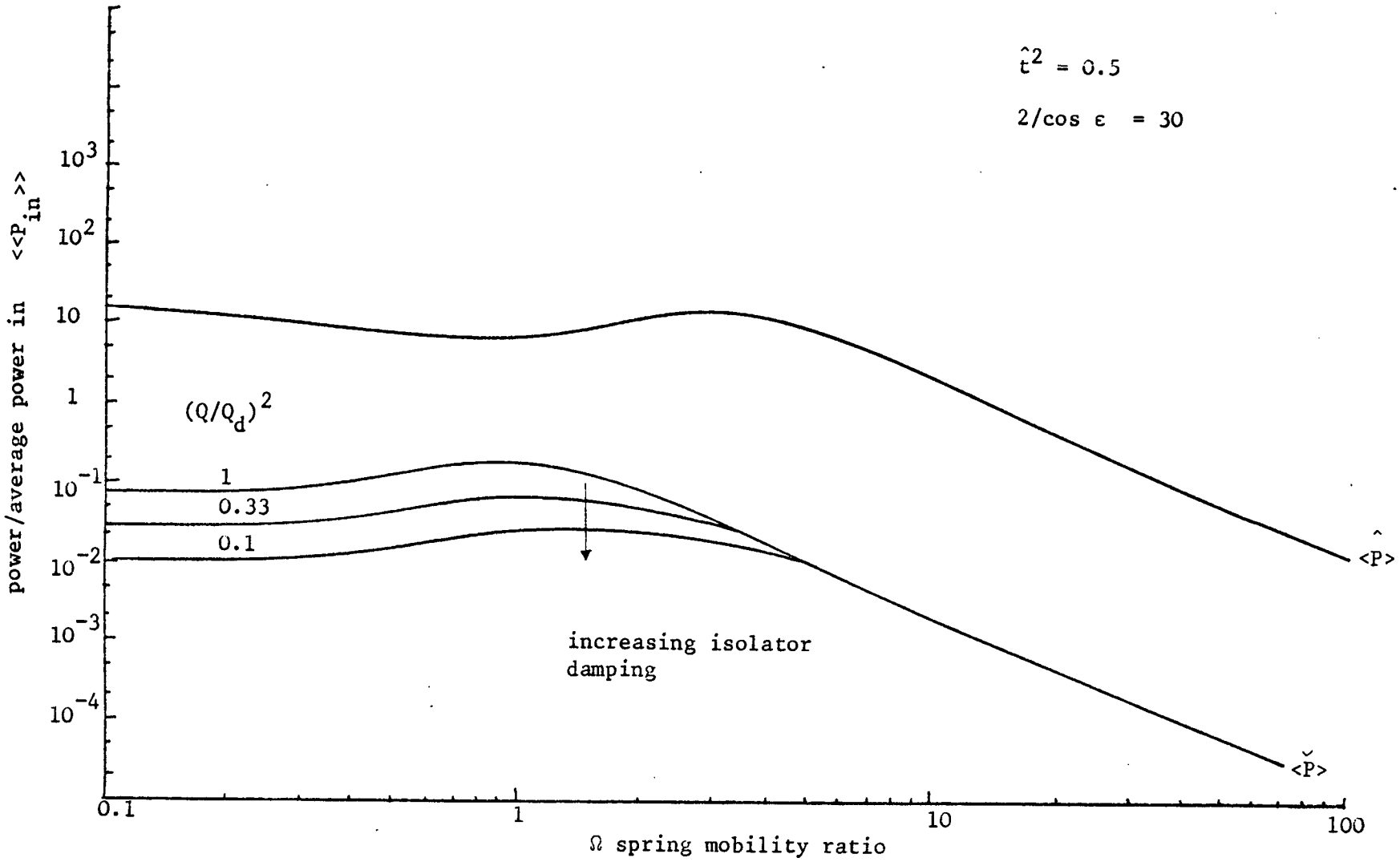

Fig. 5.6 The effect of increasing the isolator damping on $\hat{\langle P \rangle}$ and $\check{\langle P \rangle}$ when the source mobility is less than the receiver mobility, i.e., $S < Q$.

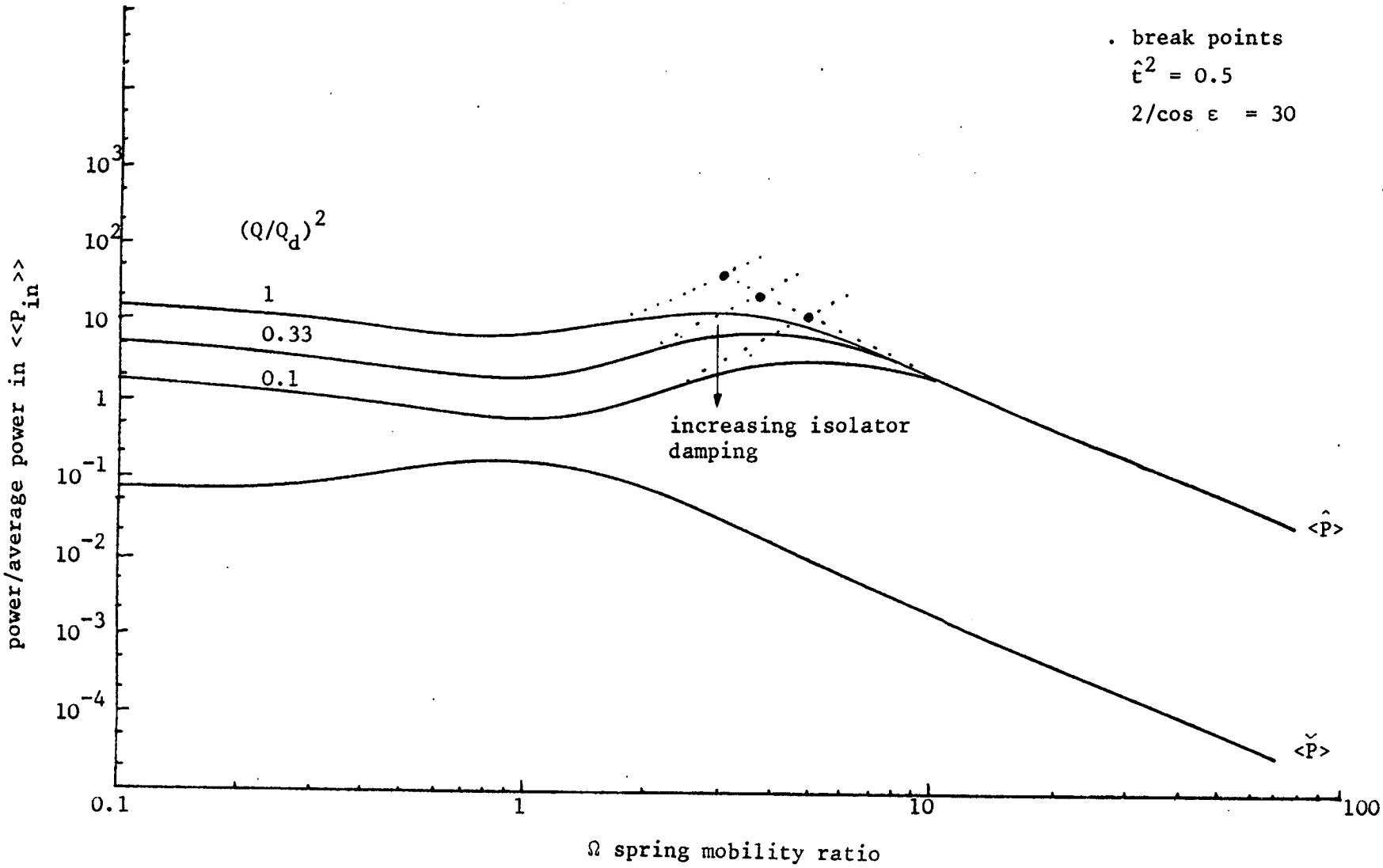

Fig. 5.7 The effect of increasing the isolator damping on $\langle\hat{P}\rangle$ and $\langle\check{P}\rangle$ when the source mobility is greater than the receiver mobility, i.e., S > Q.

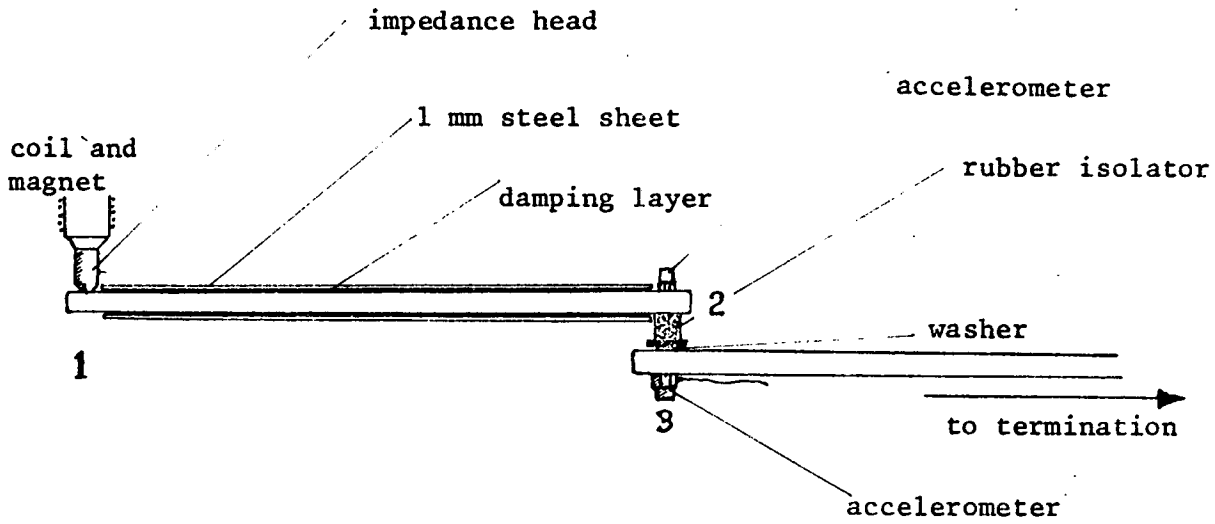

Fig. 6.1 Top view of experimental layout

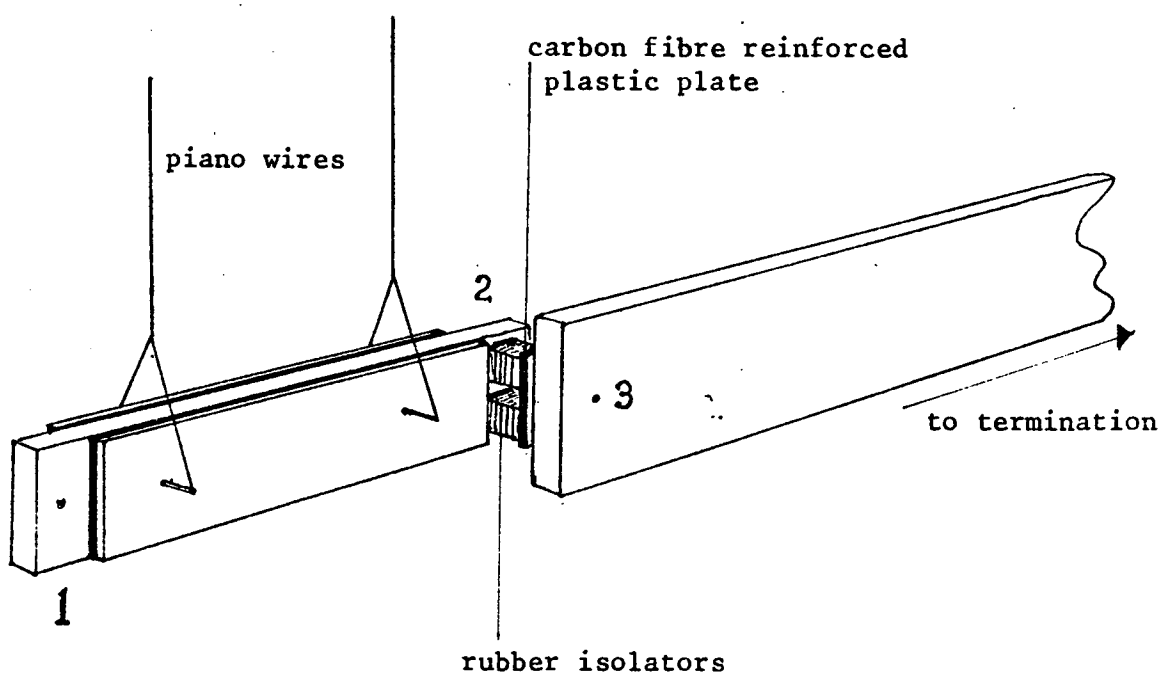

Fig. 6.2 Experimental layout

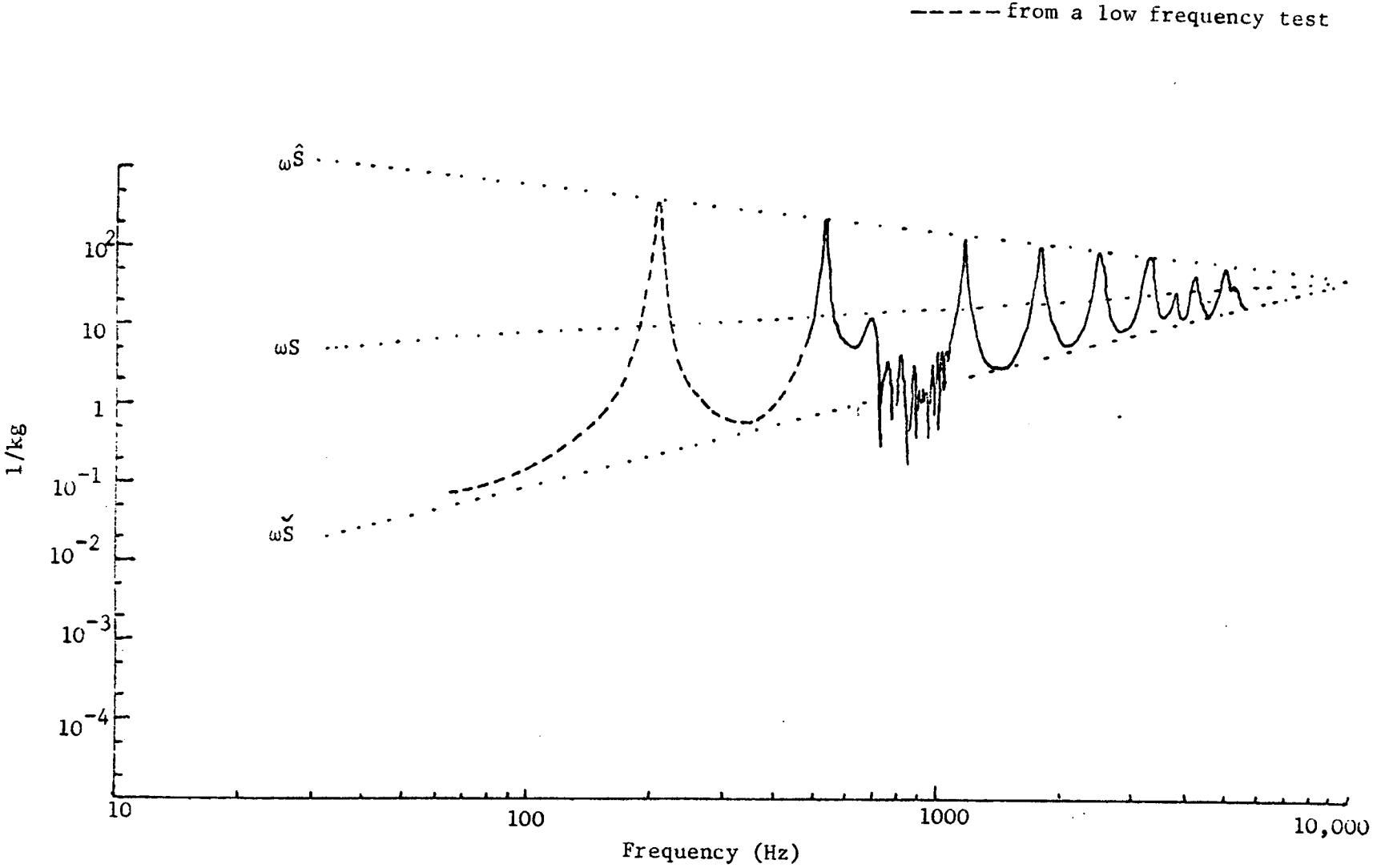

Fig. 6.3 Imaginary component of inertance at end 1 of the source beam

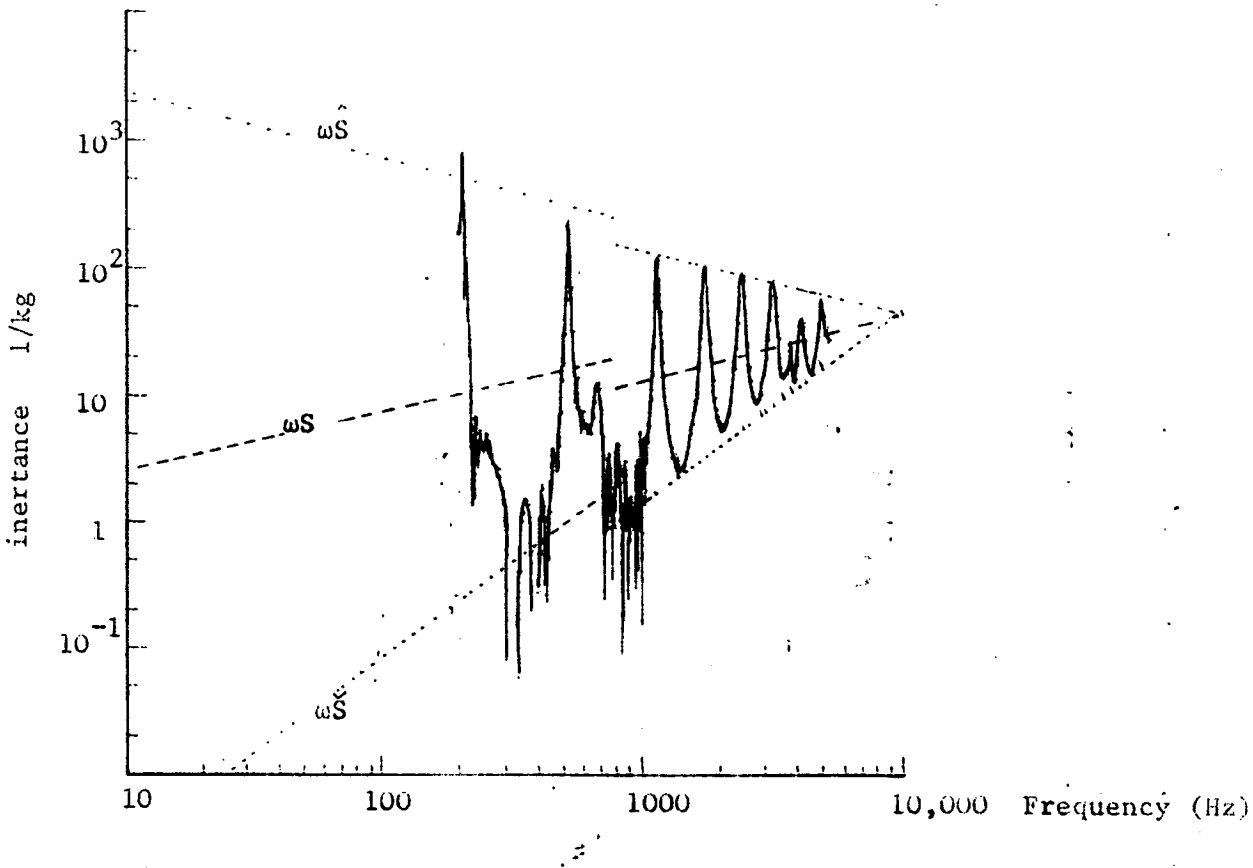

Fig. 6.4 Imaginary component of inertance at end 1 of the source beam

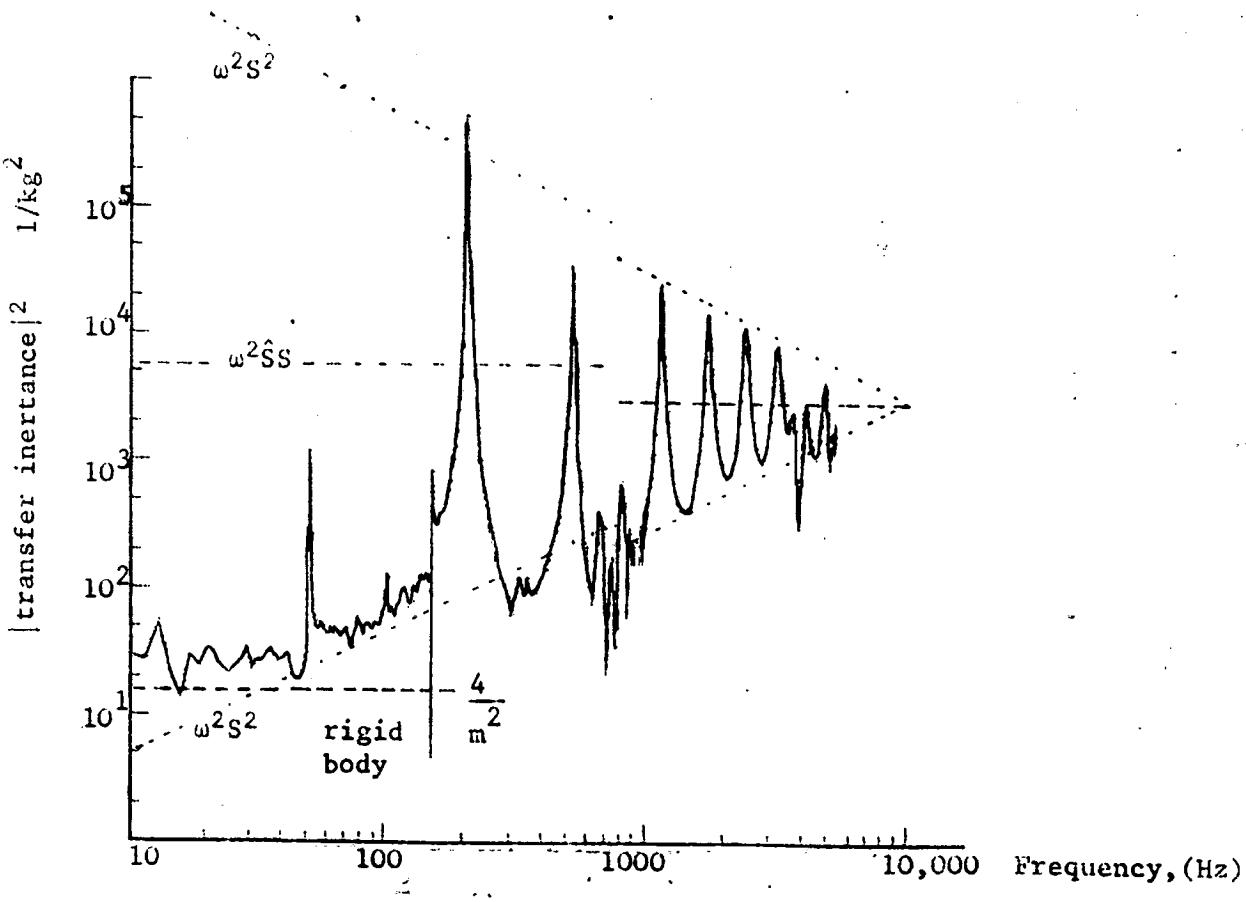

Fig. 6.5 |transfer inertance|² between ends 1 and 2 of the source beam

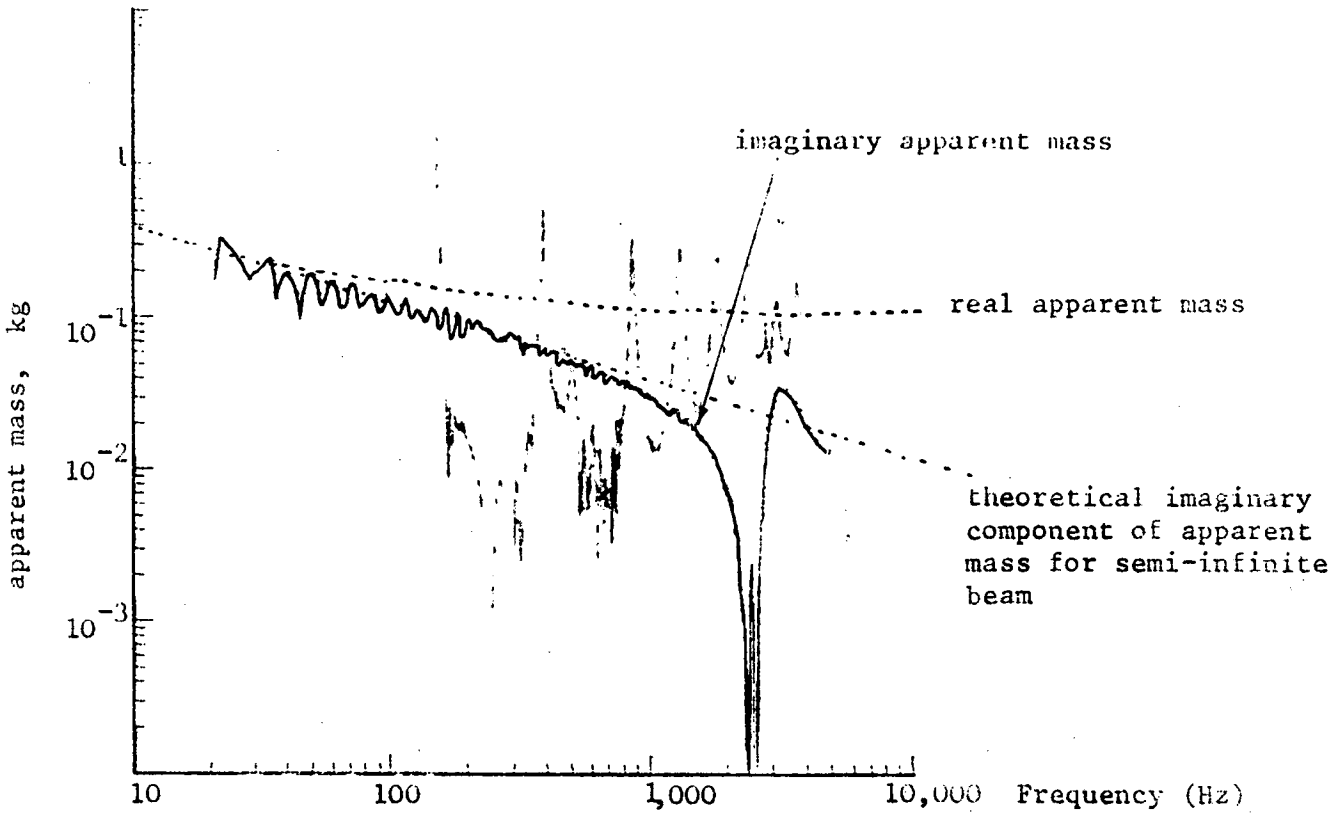

Fig. 6.6 Real and imaginary components of semi-infinite receiver beam apparent mass

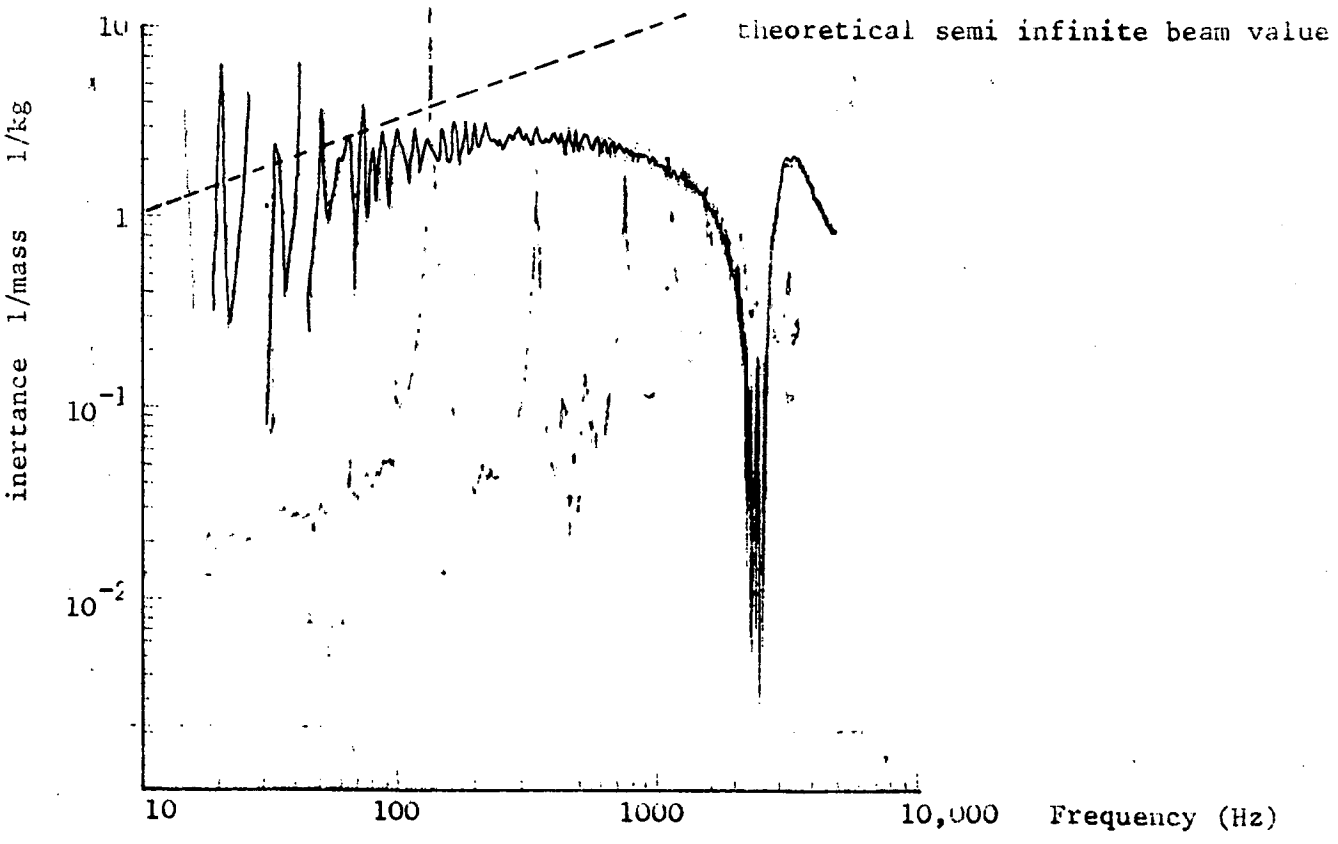

Fig. 6.7 Imaginary component of semi-infinite receiver beam inertance.

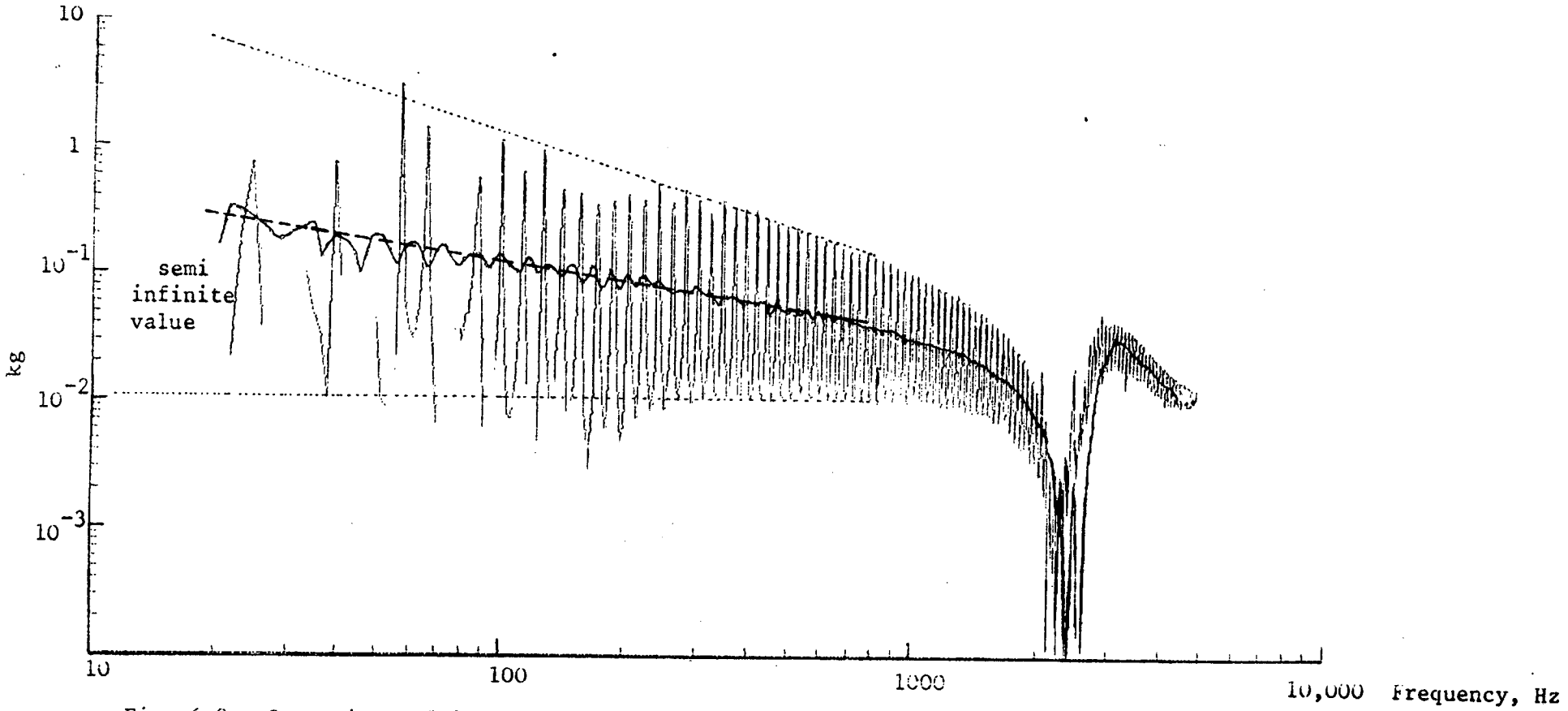

Fig. 6.8 Comparison of imaginary components of apparent mass for semi-infinite and finite beam receivers.

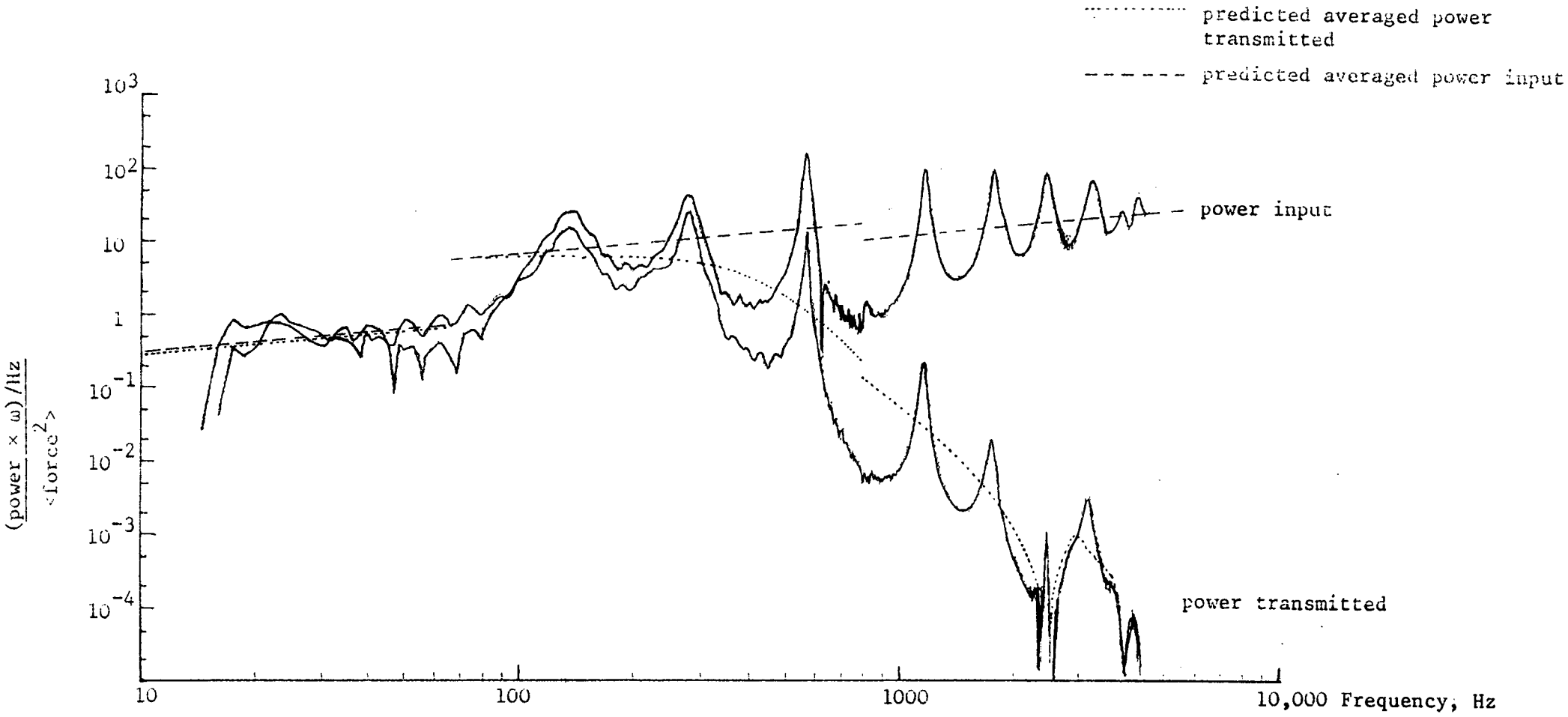

Fig. 6.9 Power × ω input to source beam and transmitted to the semi-infinite receiver beam, unit force spectral density input, 10 Hz - 4 kHz.

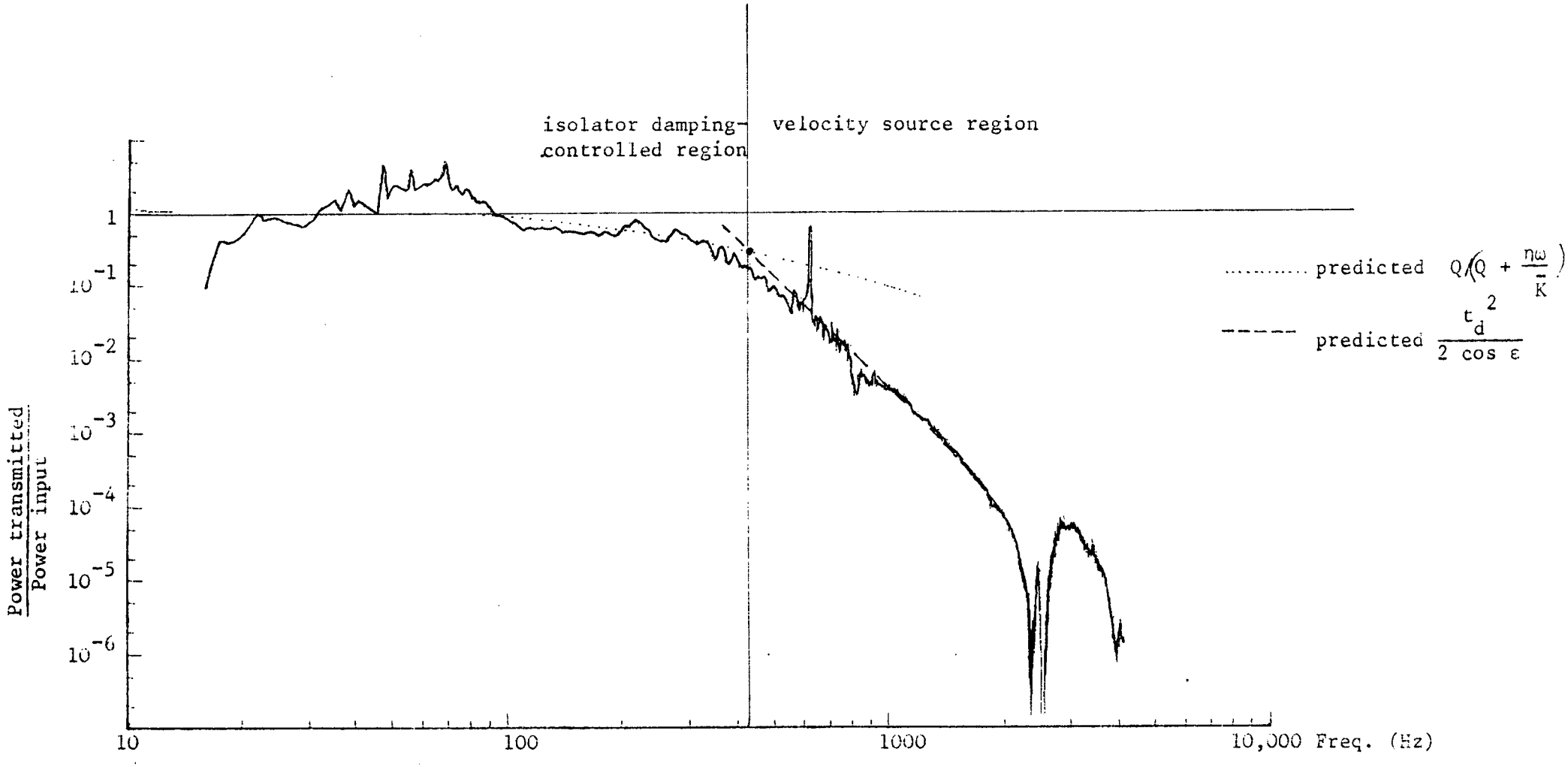

Fig. 6.10 $\frac{\text{Power transmitted to semi-infinite beam receiver}}{\text{Power input to source beam}}$

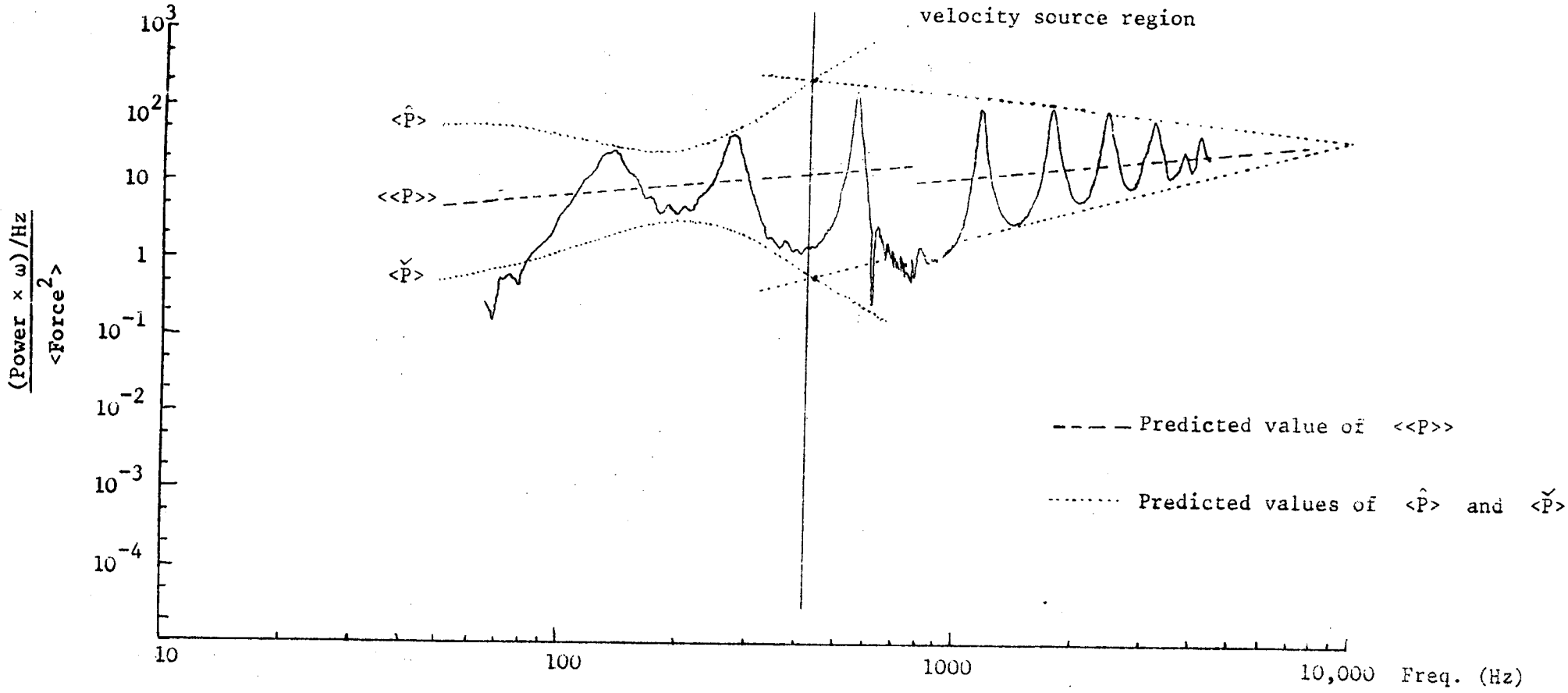

Fig. 6.11 Power × ω input to source beam for semi-infinite receiver beam, unit force spectral density input, 10 Hz - 4 kHz.

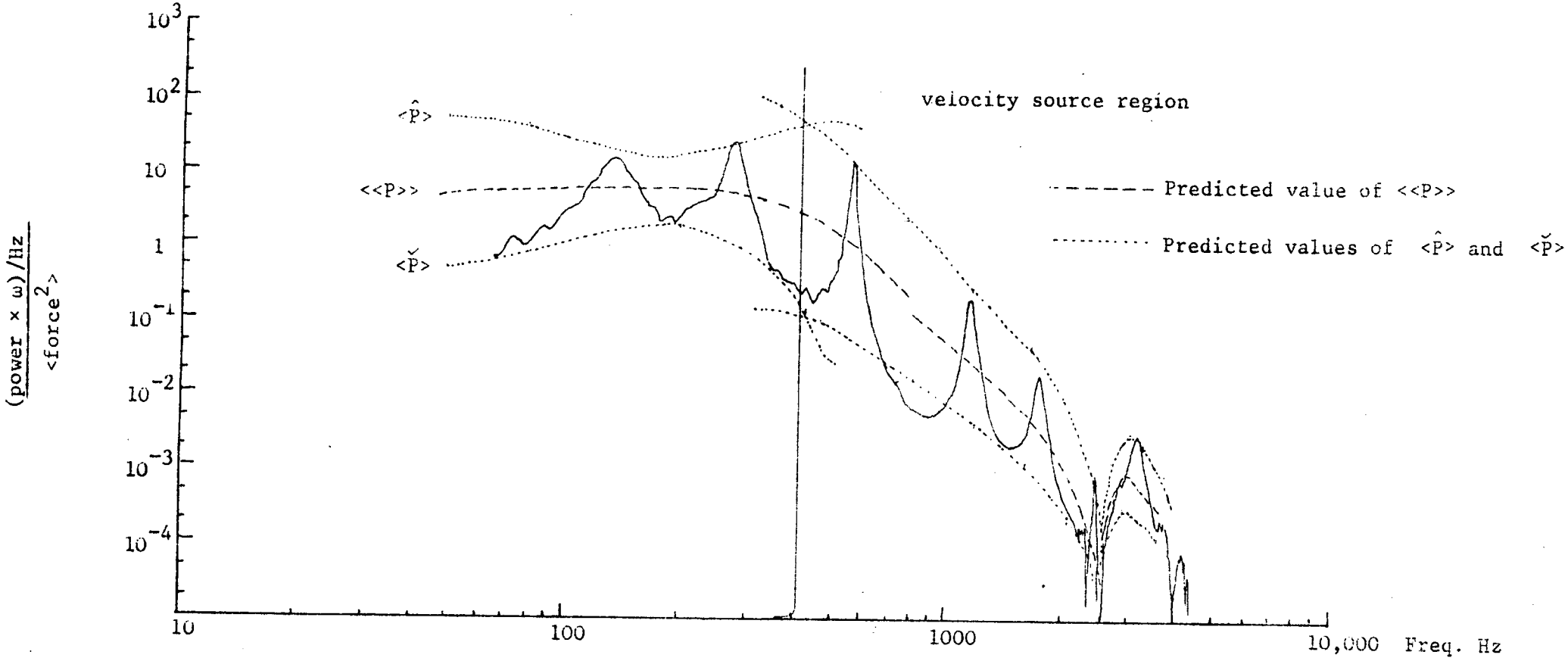

Fig. 6.12 Power × ω transmitted to the semi-infinite receiver beam unit force spectral density, 10 Hz - 4 kHz.

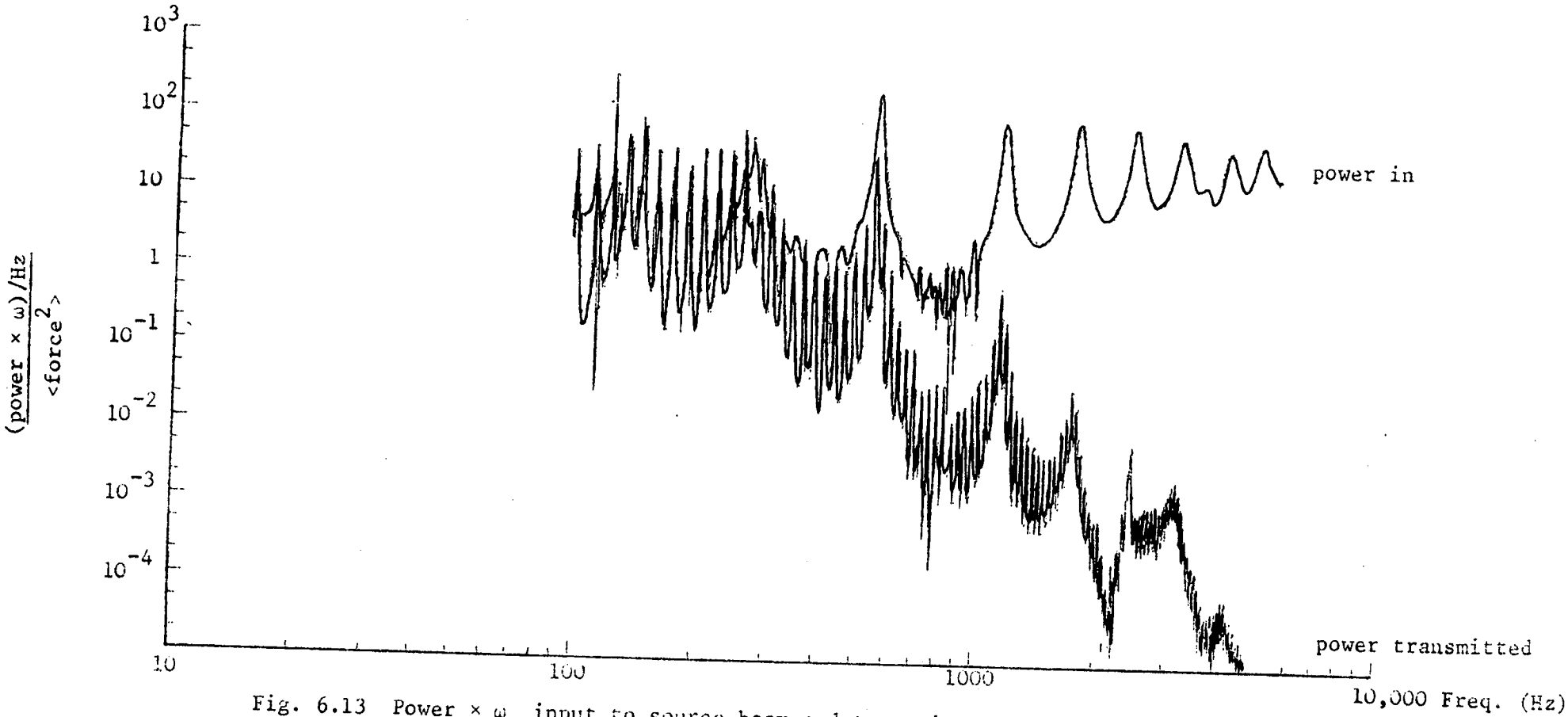

Fig. 6.13 Power × ω input to source beam and transmitted to finite receiver beam for unit input force spectral density, 100 Hz - 4 kHz.

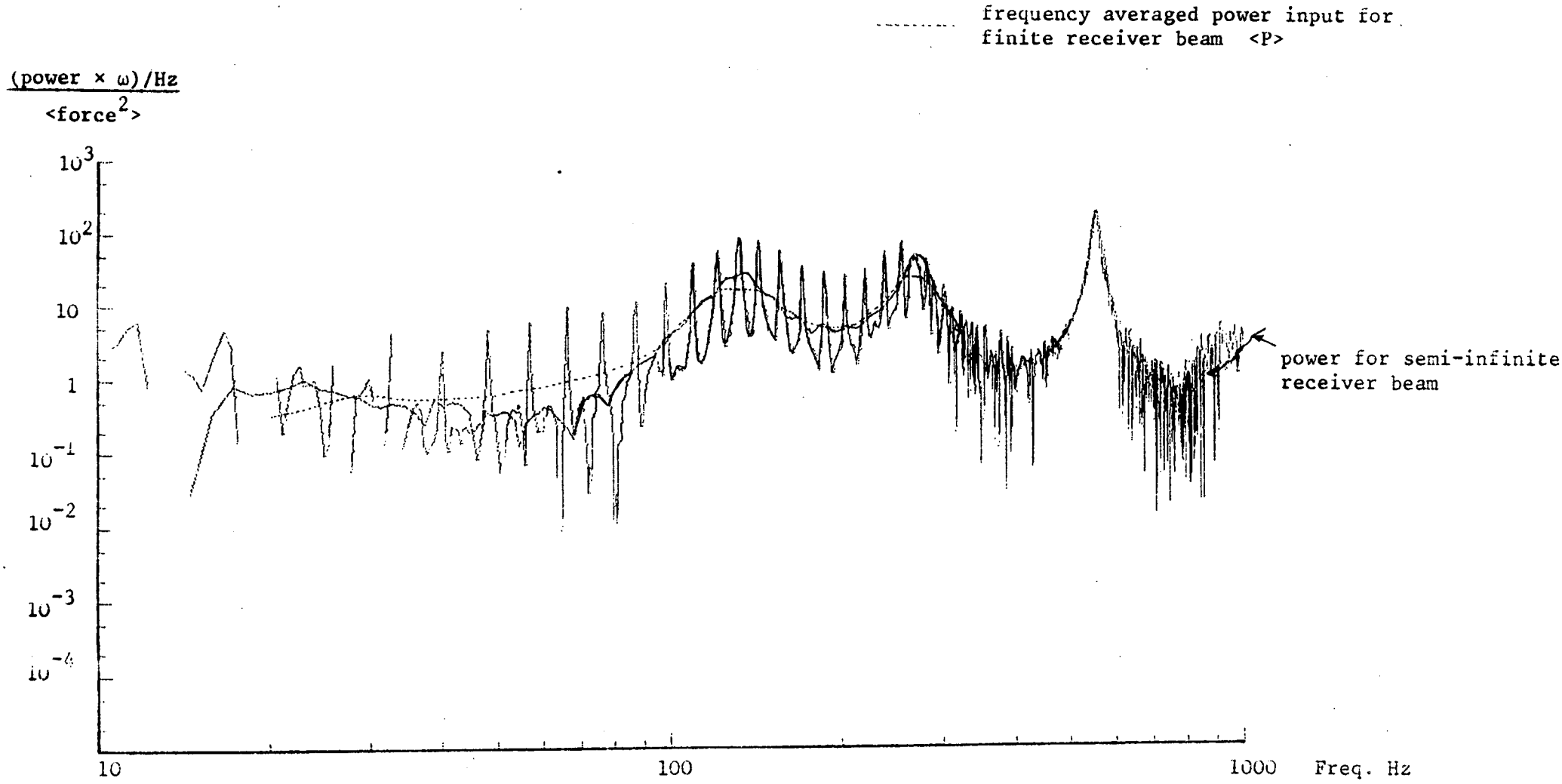

Fig. 6.14 Comparison of power × ω input to finite source beam, for semi-infinite and finite receiver beam, for unit force spectral density input, 10 Hz - 1000 Hz.

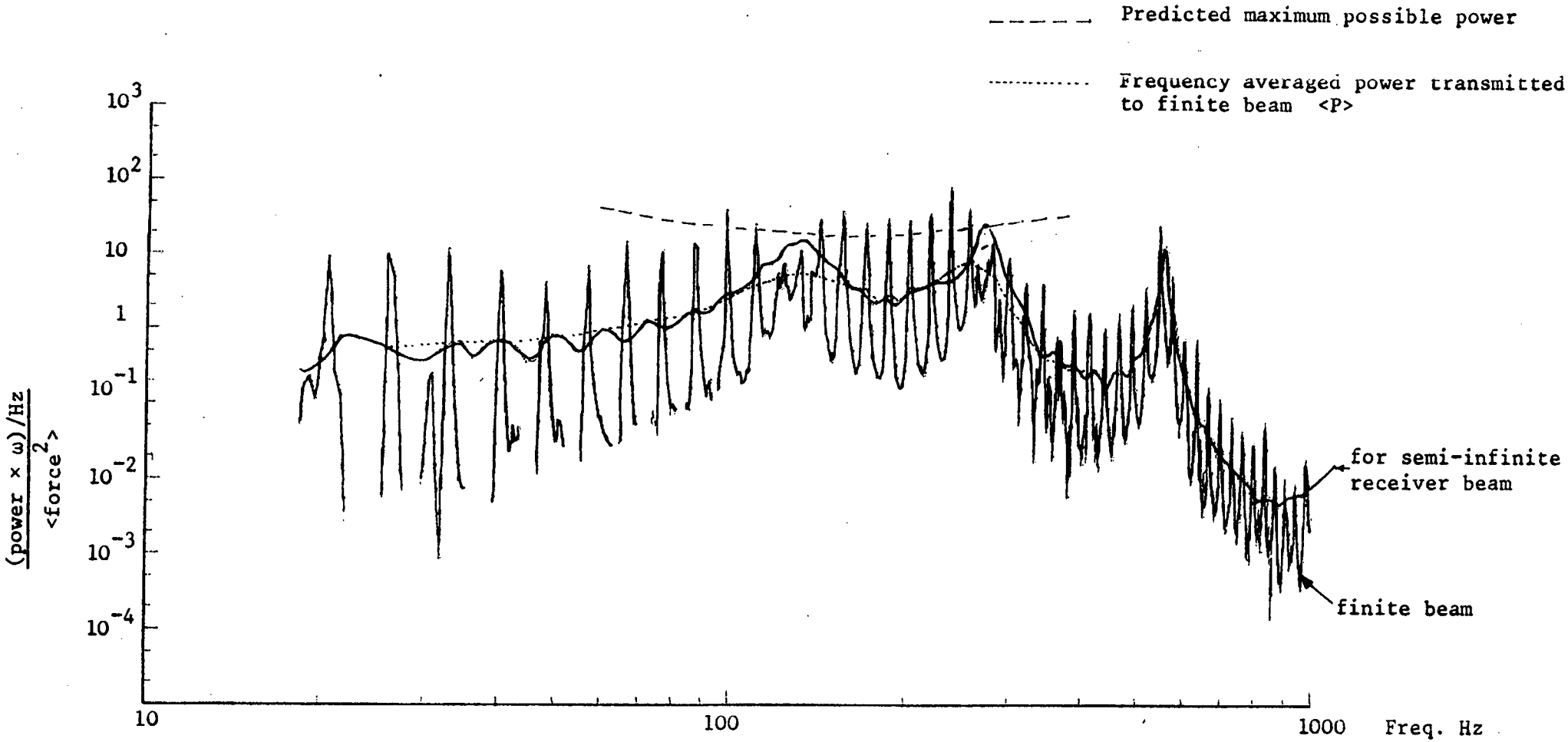

Fig. 6.15 Comparison of power $\times \omega$ transmitted to finite and semi-infinite beam receivers, for unit force spectral density input, 10 Hz - 1000 Hz.

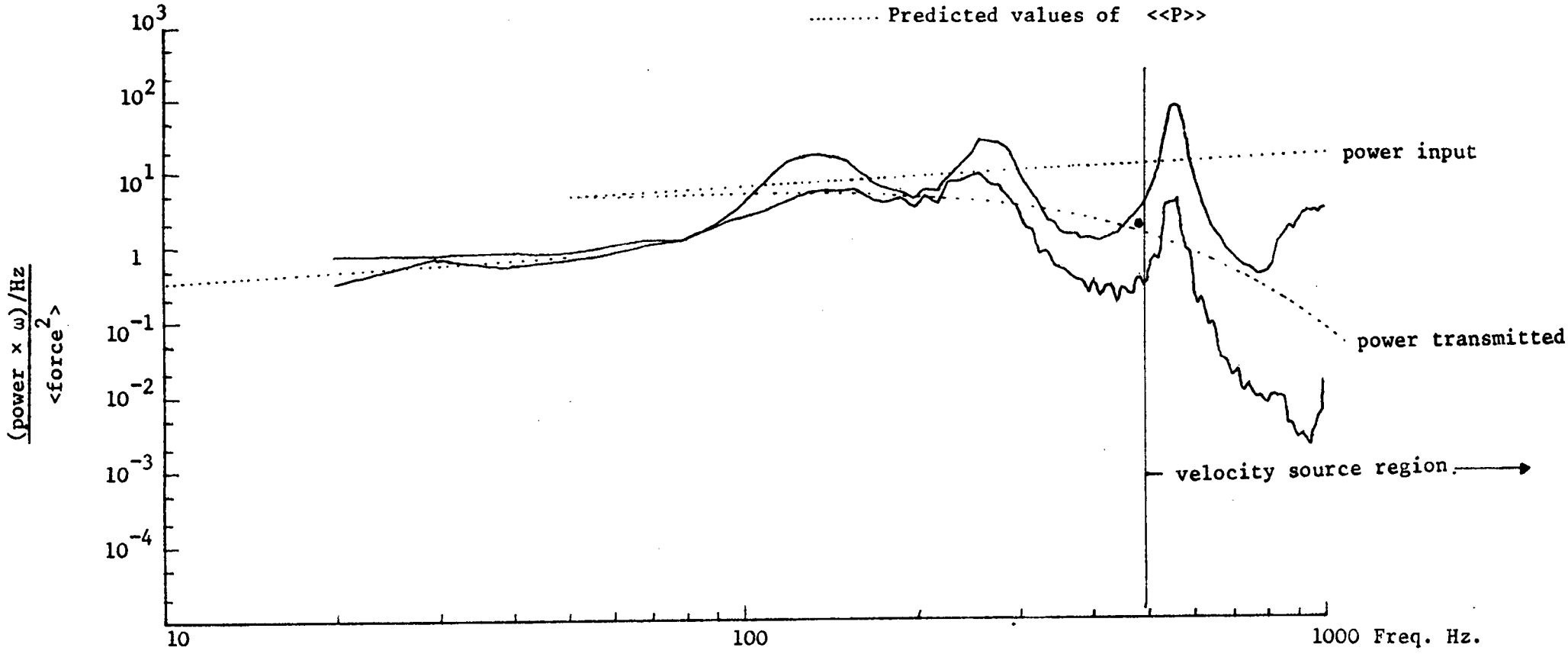

Fig. 6.16 Frequency averaged power × ω input to source beam and transmitted to the finite receiver beam <P>, unit force spectral density input, 10 Hz - 1 kHz.

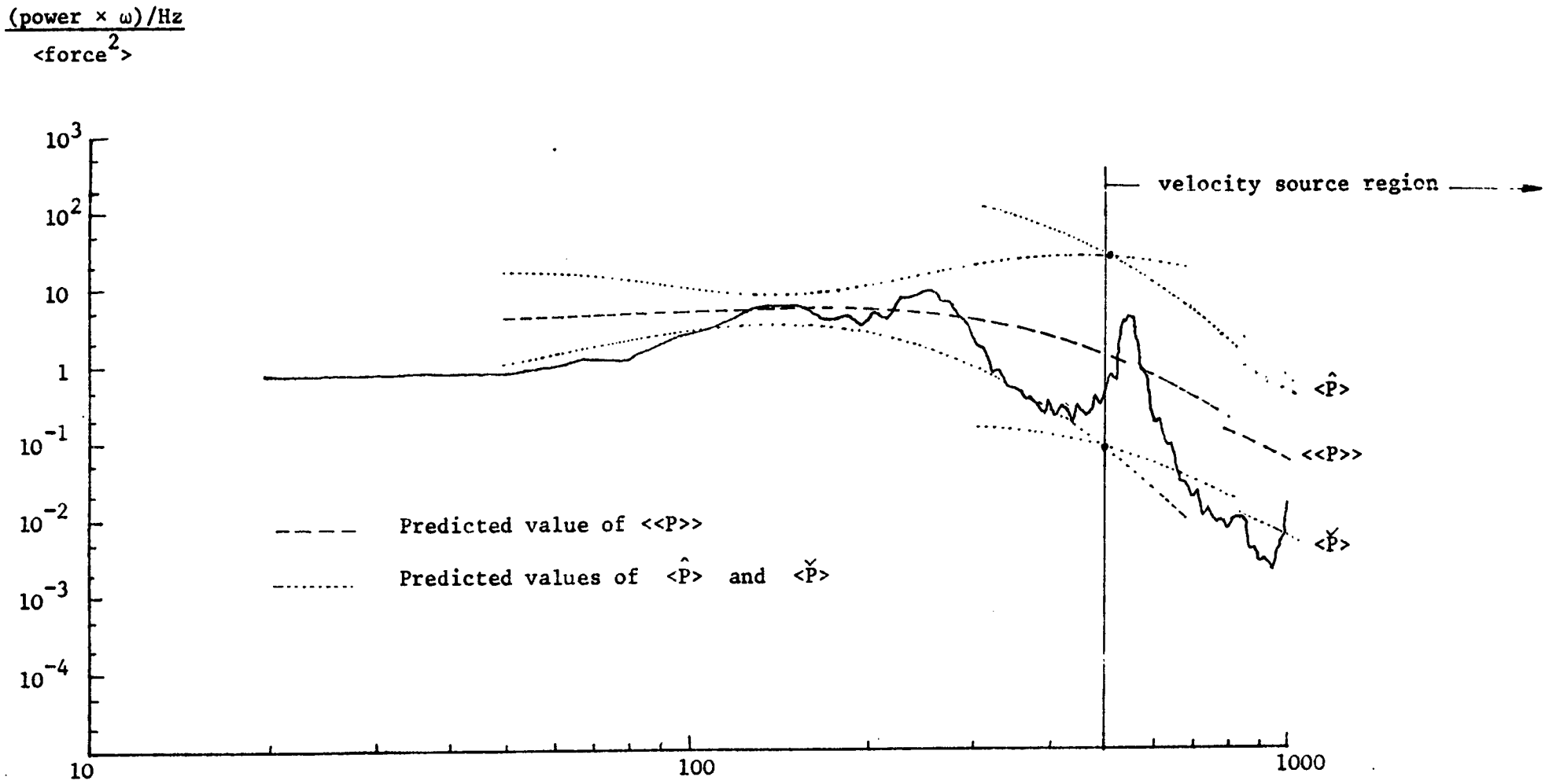

Fig. 6.17 Measured and predicted values of frequency averaged power transmission <P> to the finite beam, unit force spectral density input, 10 Hz - 1 kHz.

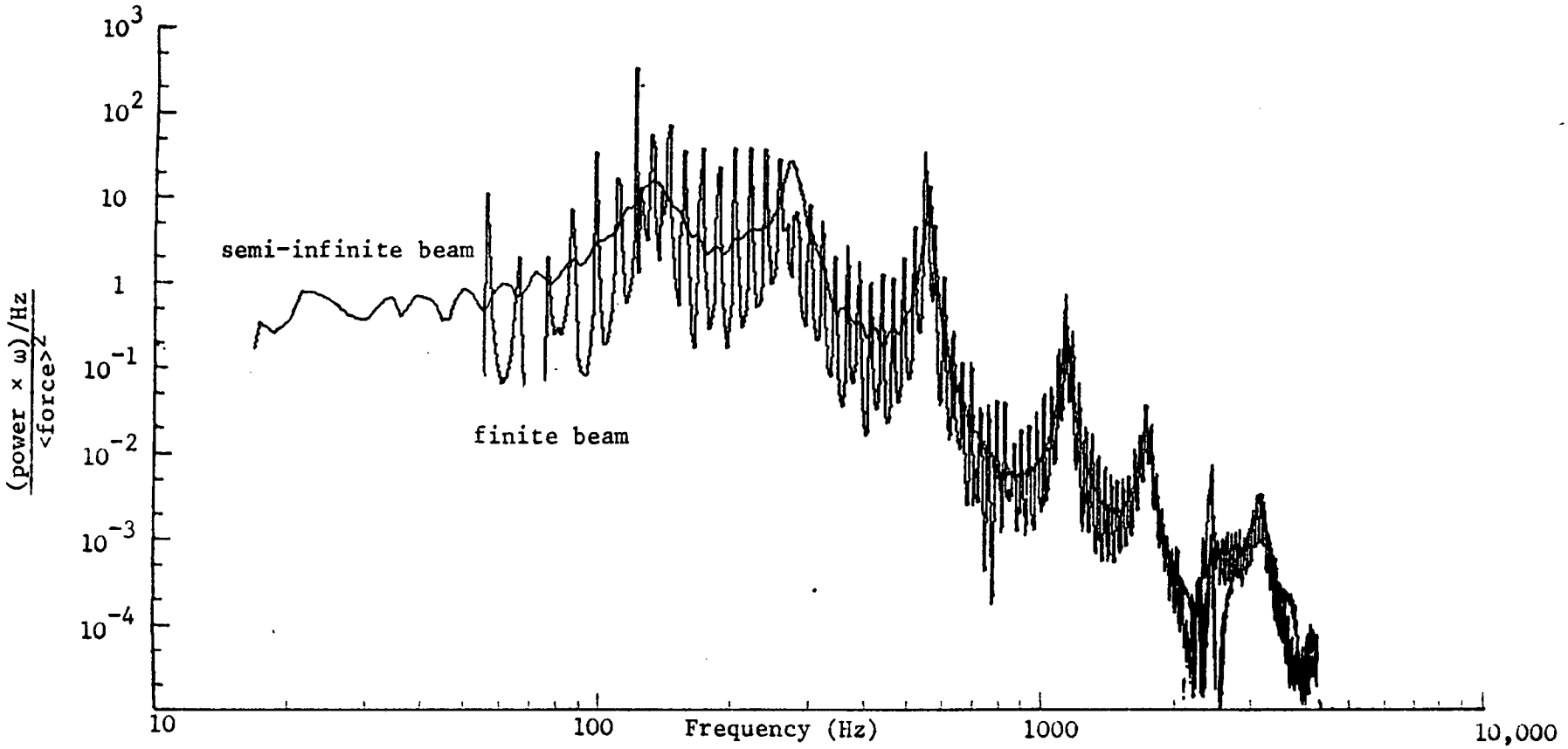

Fig. 6.18 Comparison of power × ω transmitted to finite and semi-infinite beam receivers for unit force spectral density input, 50 Hz - 4 kHz.

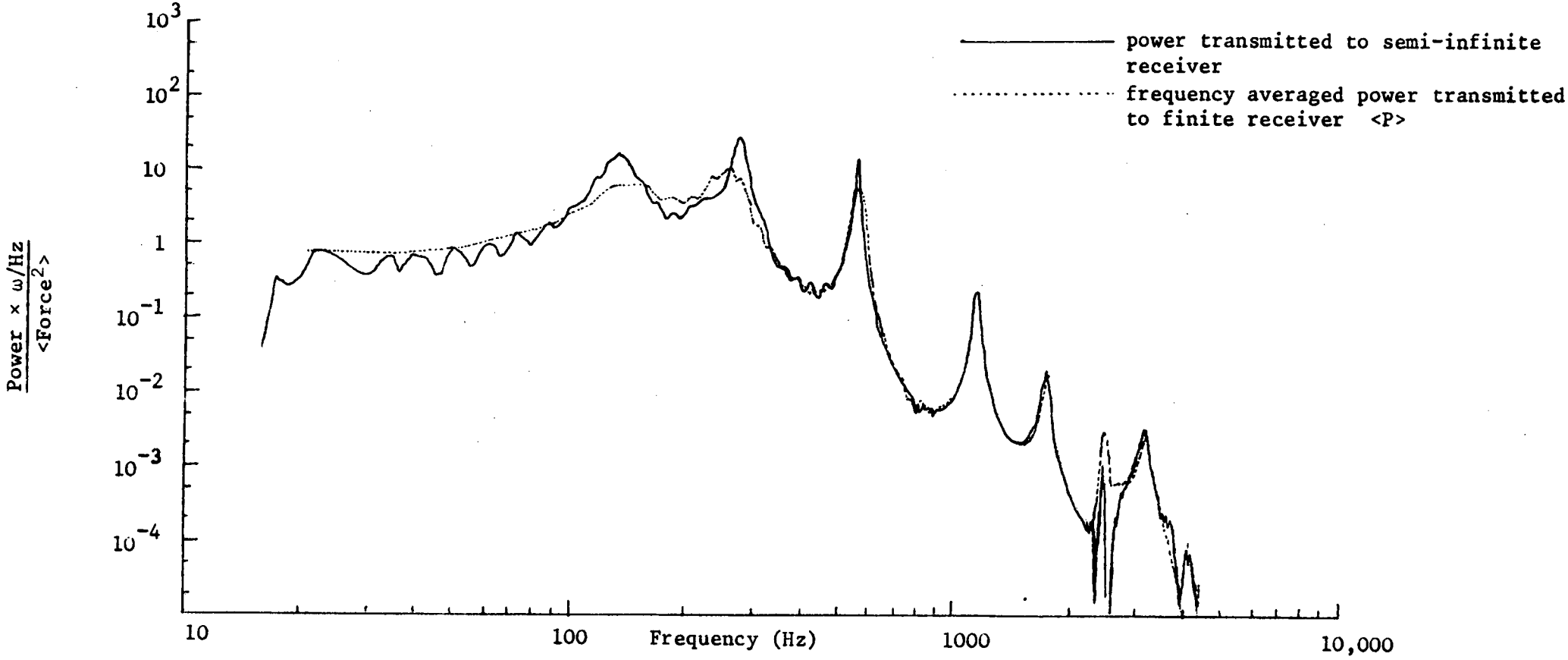

Fig. 6.19 Comparison of power × ω transmitted to a semi-infinite beam and the frequency averaged power × ω transmitted to a finite beam, for unit force spectral density input, 10 Hz - 4 kHz.

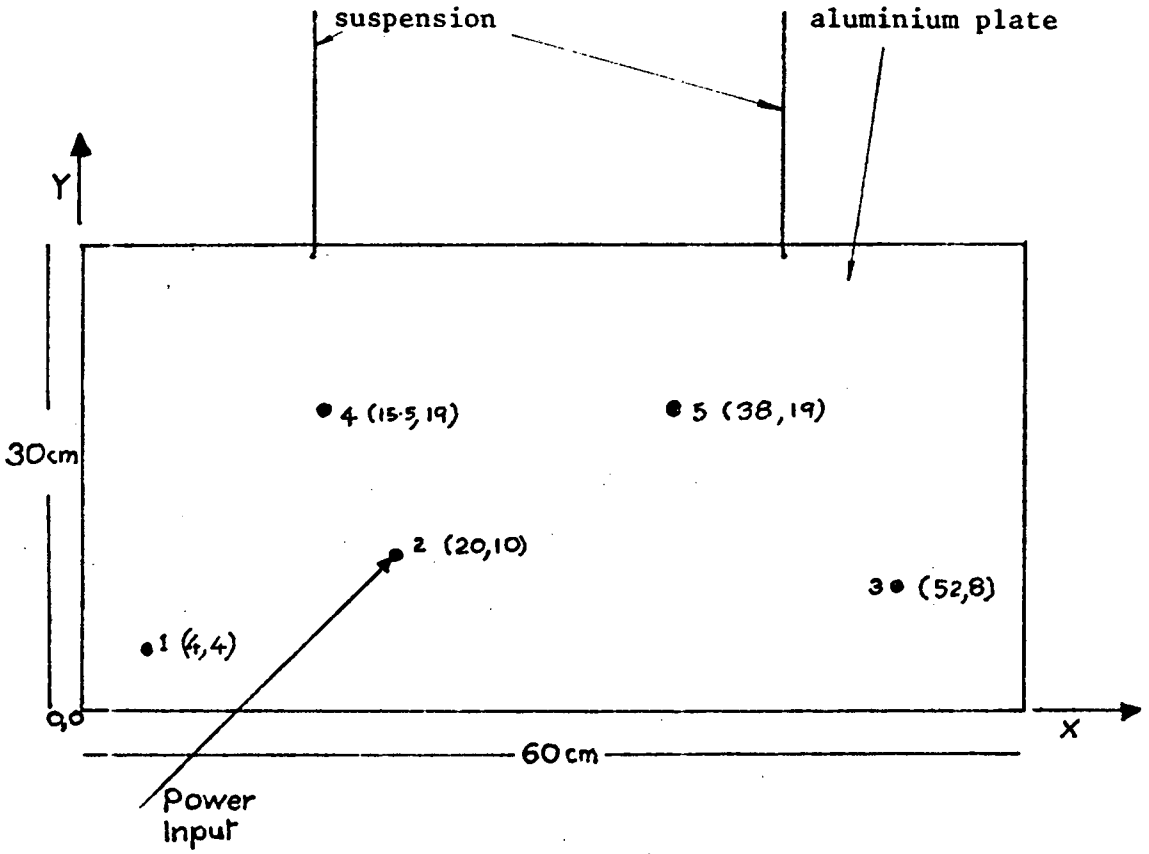

Figure 7.1 Diagram of plate

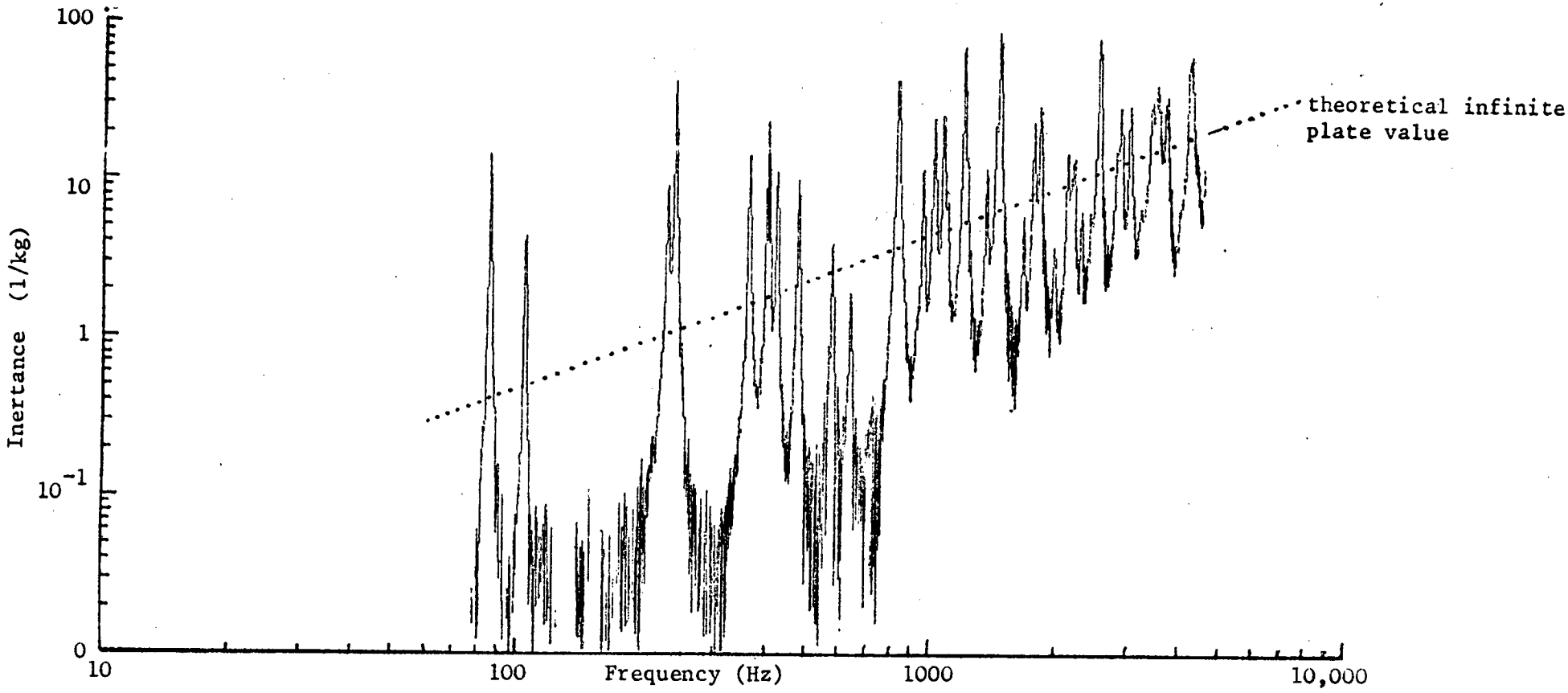

Fig. 7.2 Imaginary component of inertance at point 2, $I_m\{\bar{I}_2\}$.

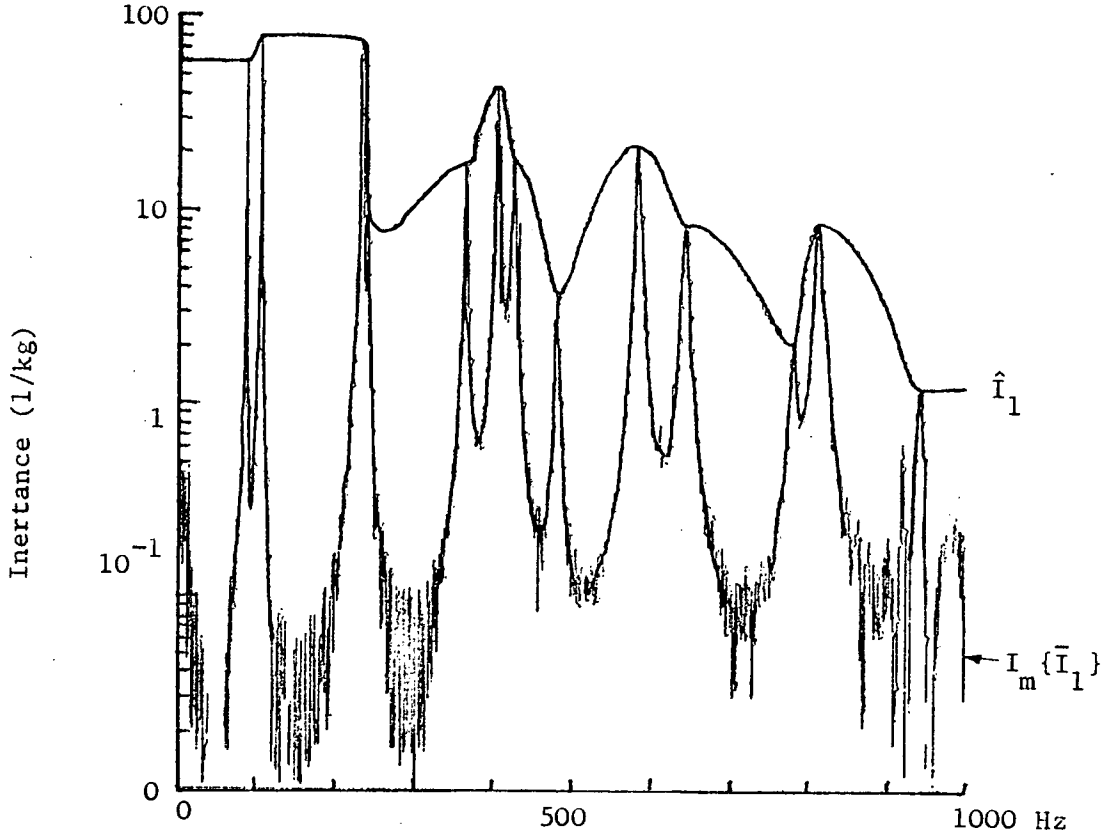

Fig. 7.3 Imaginary component of inertance, $\mathrm{Im}\{\bar{I}_1\}$, and envelope of peaks at point 1, $\hat{I}_1$.

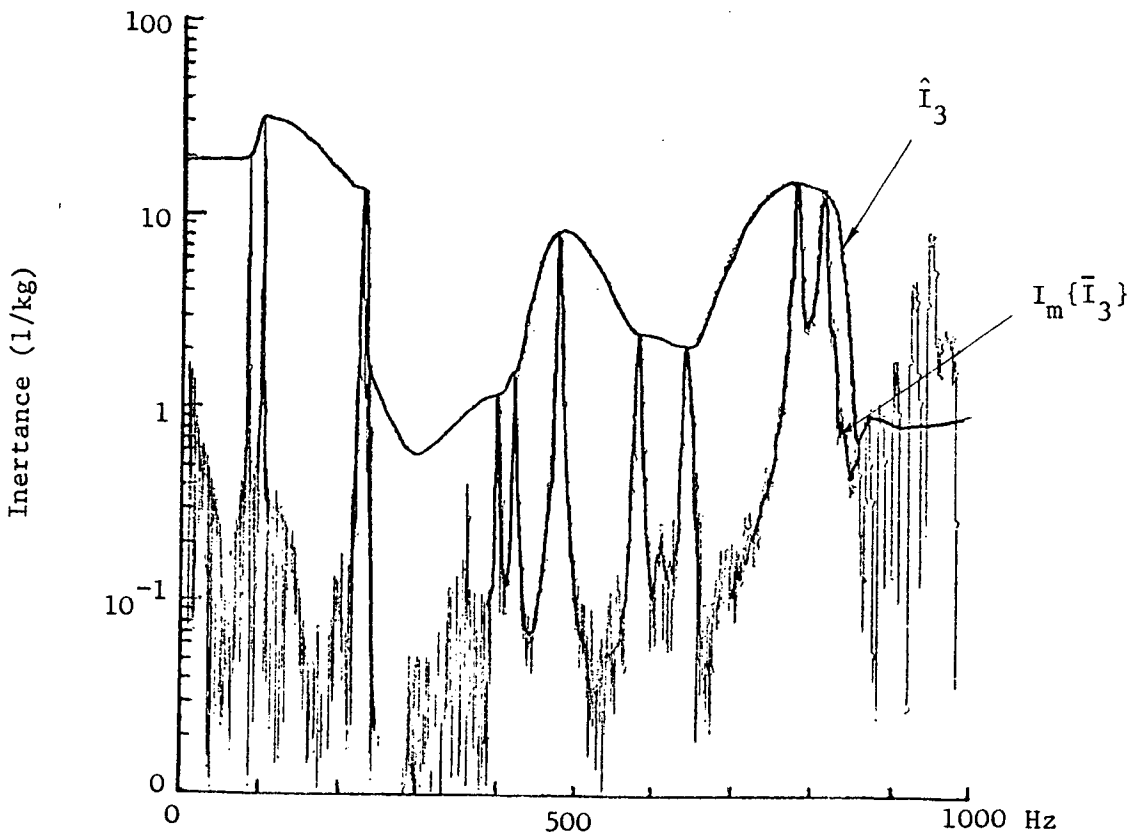

Fig. 7.4. Imaginary component of inertance $I_m\{\bar{I}_3\}$ and envelope of peaks $\hat{I}_3$.

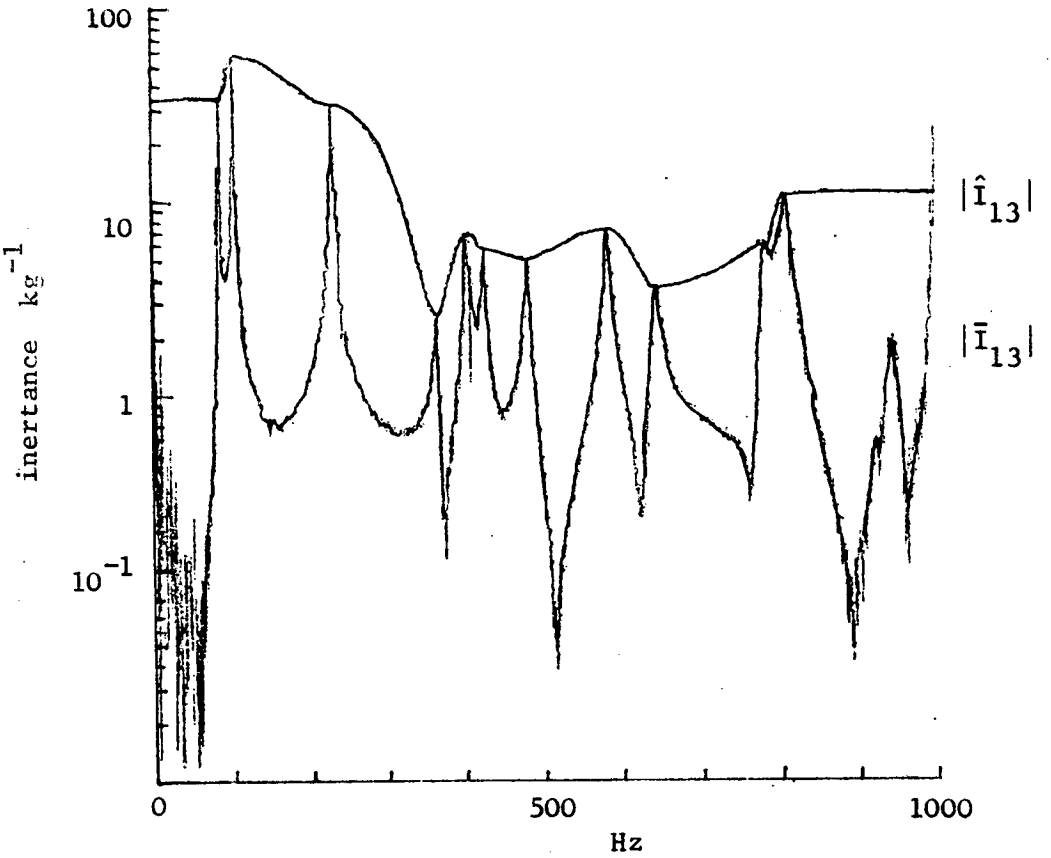

Fig. 7.5 Modulus of transfer inertance between points 1 and 3, $|I_{13}|$, and envelope of peaks $|\hat{I}_{13}|$

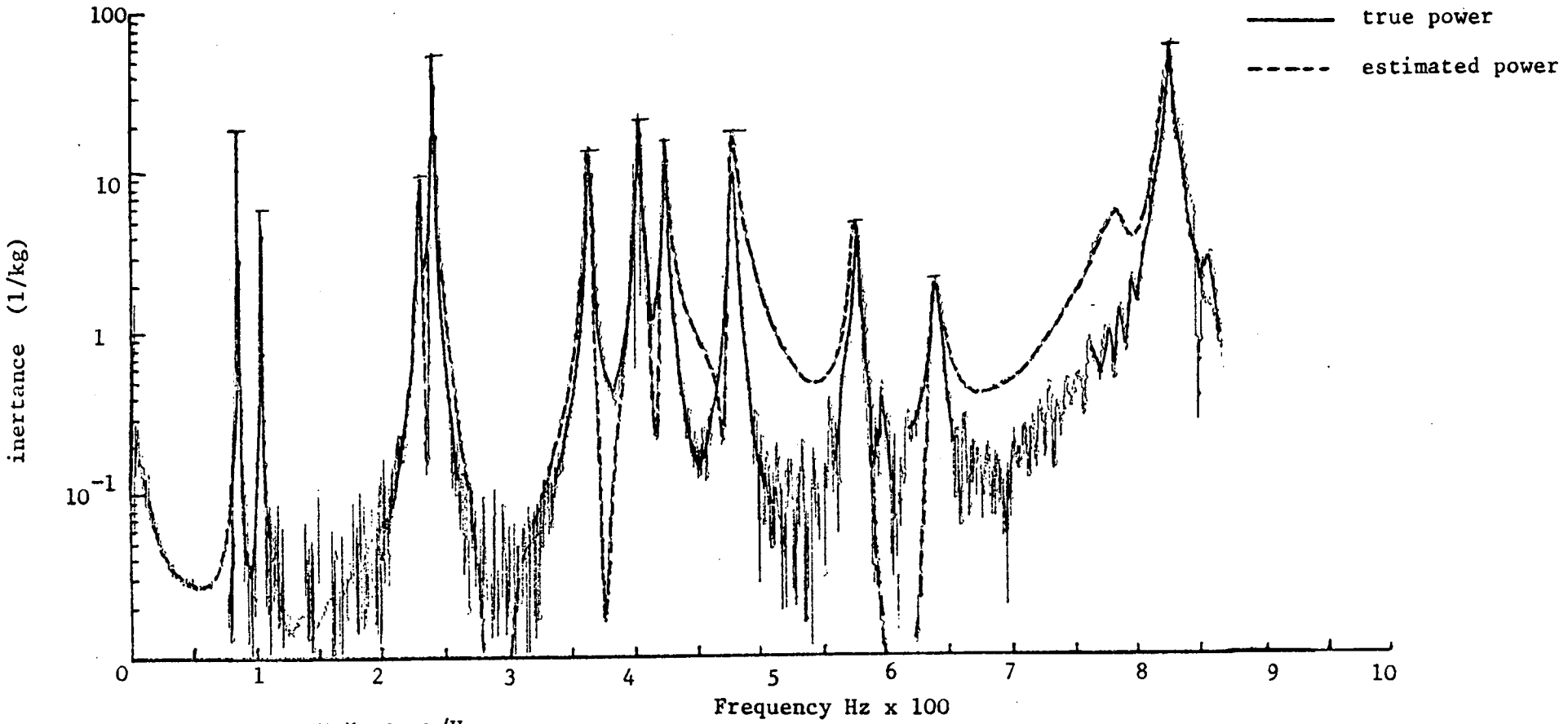

Figure 7.6 $\frac{\omega \times \text{power/Hz}}{\langle \text{Force} \rangle^2}$ input at point 2 compared with the estimated value using $\hat{I}_1$.

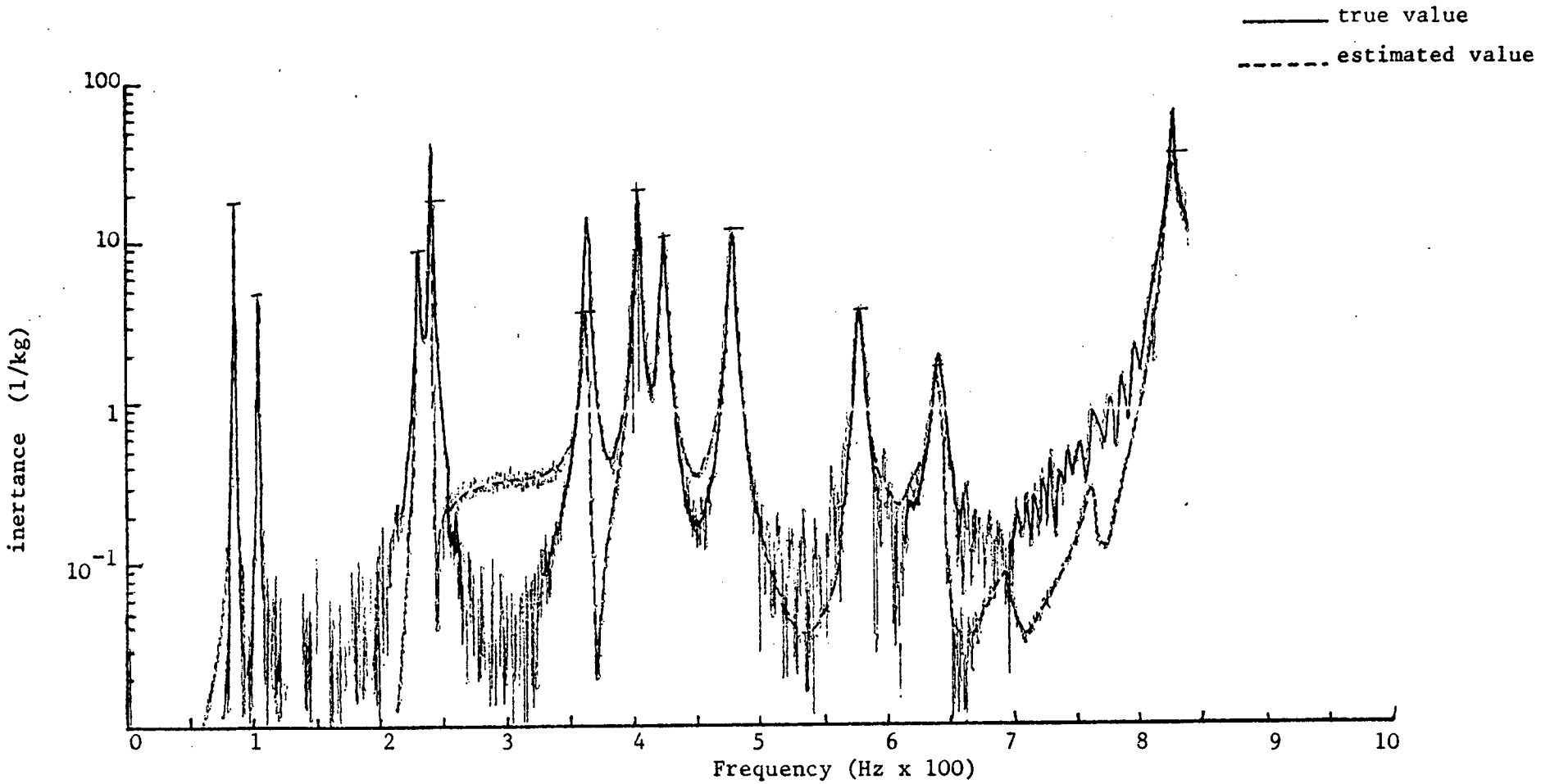

Fig. 7.7 $\frac{\omega \times \text{power/Hz}}{\langle \text{Force} \rangle^2}$ input at point 2 compared with the estimated value using $\hat{I}_3$

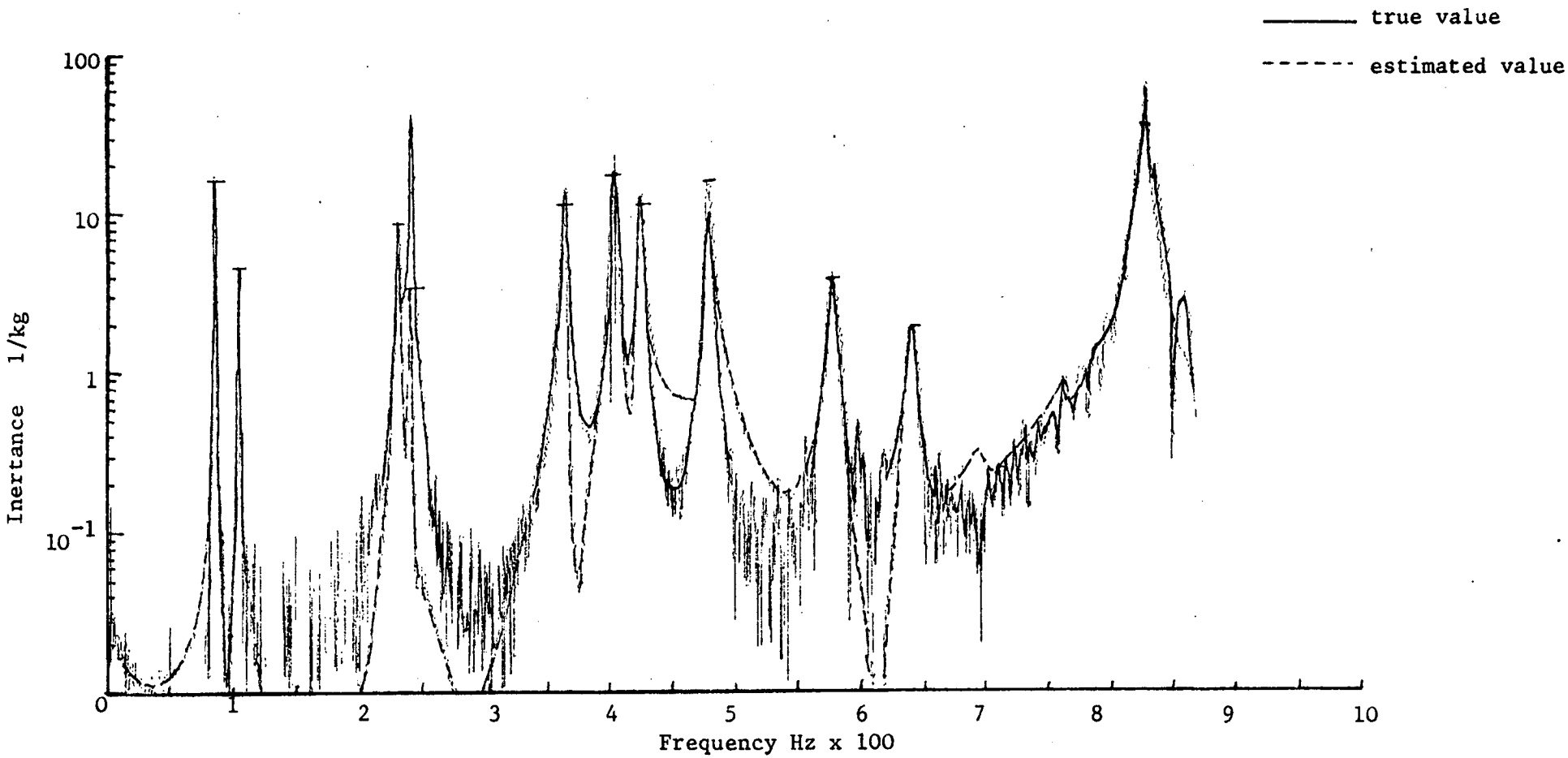

Figure 7.8 $\frac{\omega \times \text{power/Hz}}{\langle \text{Force} \rangle^2}$ input at 2 compared with estimate using $|\hat{I}_{13}|$.

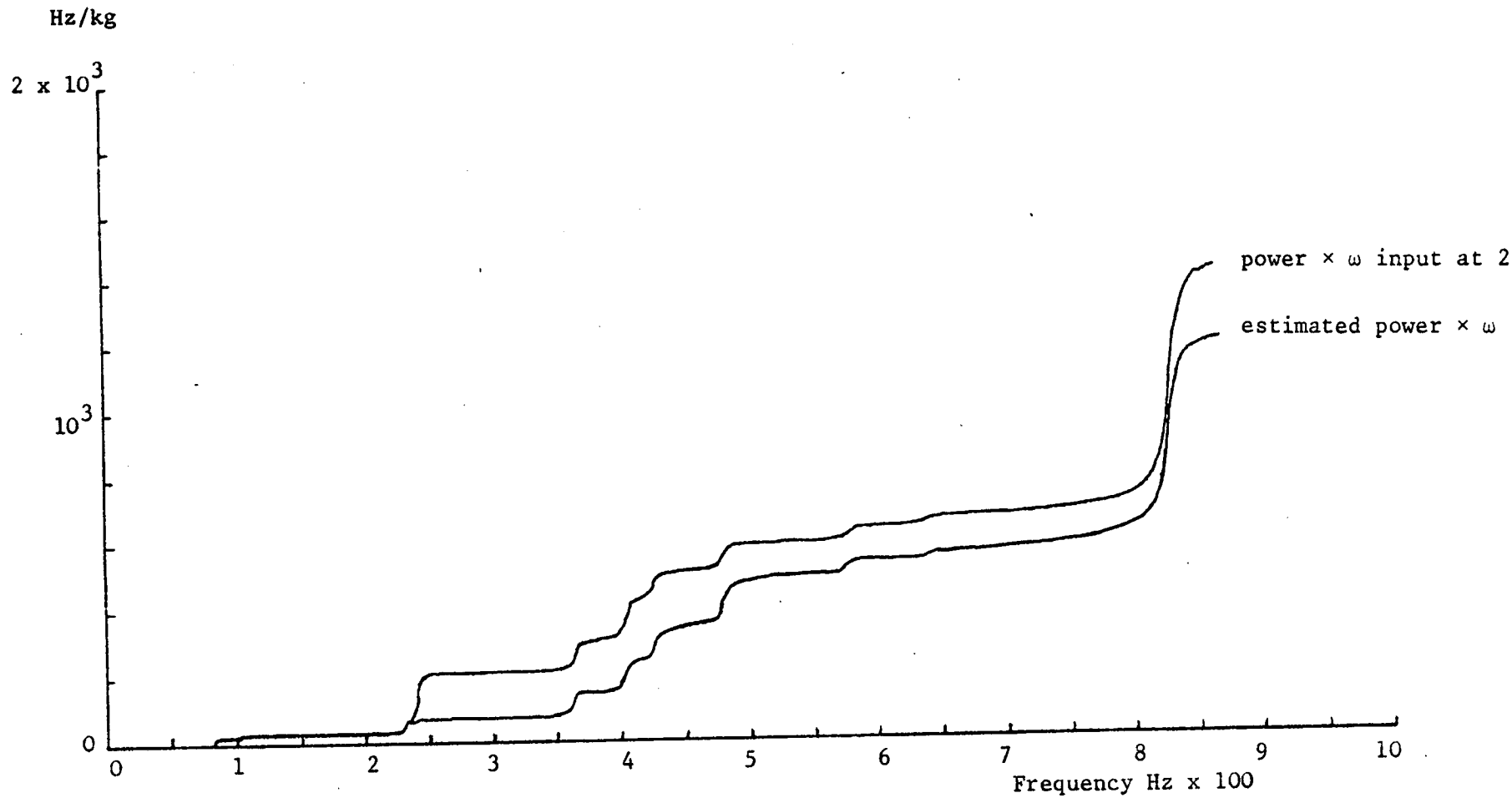

Figure 7.9 Integral under curves in figure 7.8, comparison of $\omega \times$ power input at position 2 with estimate of power input using $|\hat{I}_{13}|$

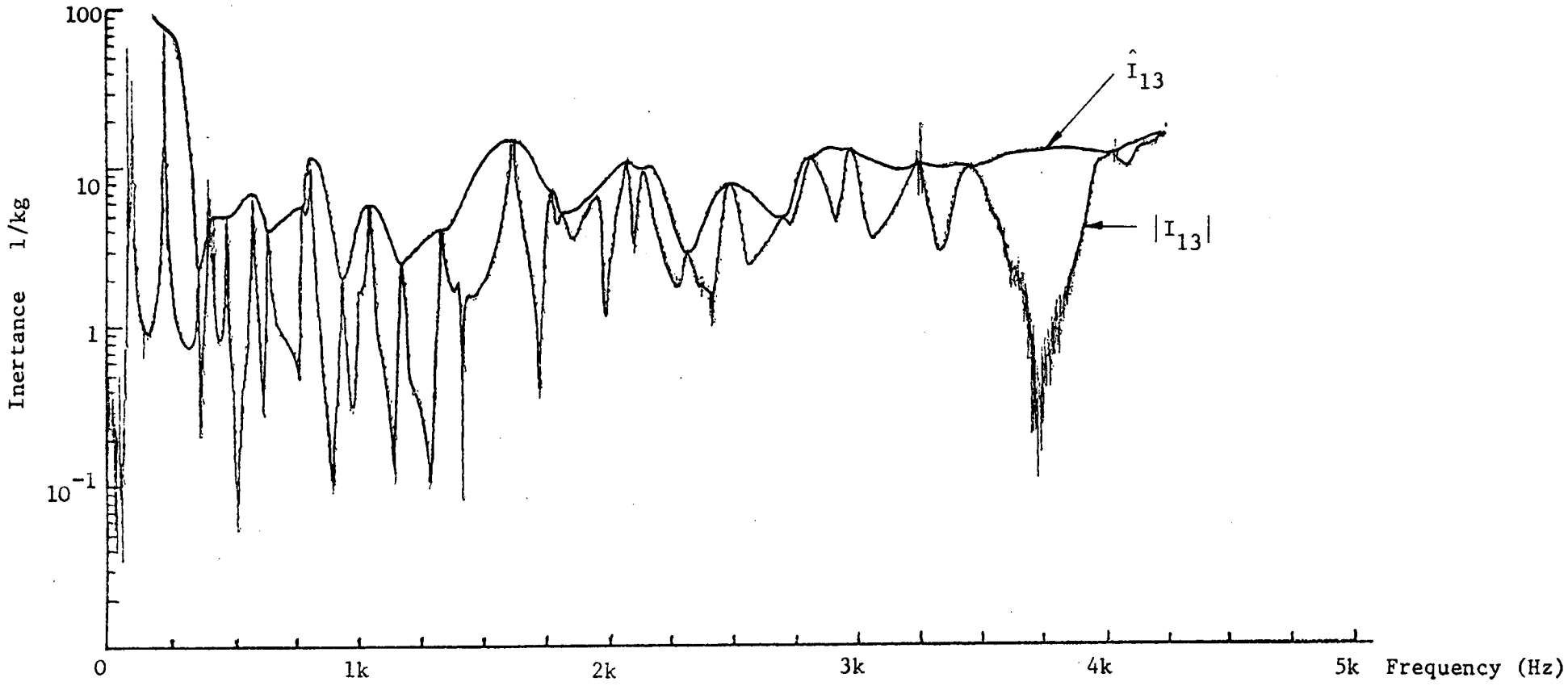

Figure 7.10. Modulus of transfer inertance between points 1 and 3 $|I_{13}|$ and envelope of peaks $\hat{I}_{13}$.

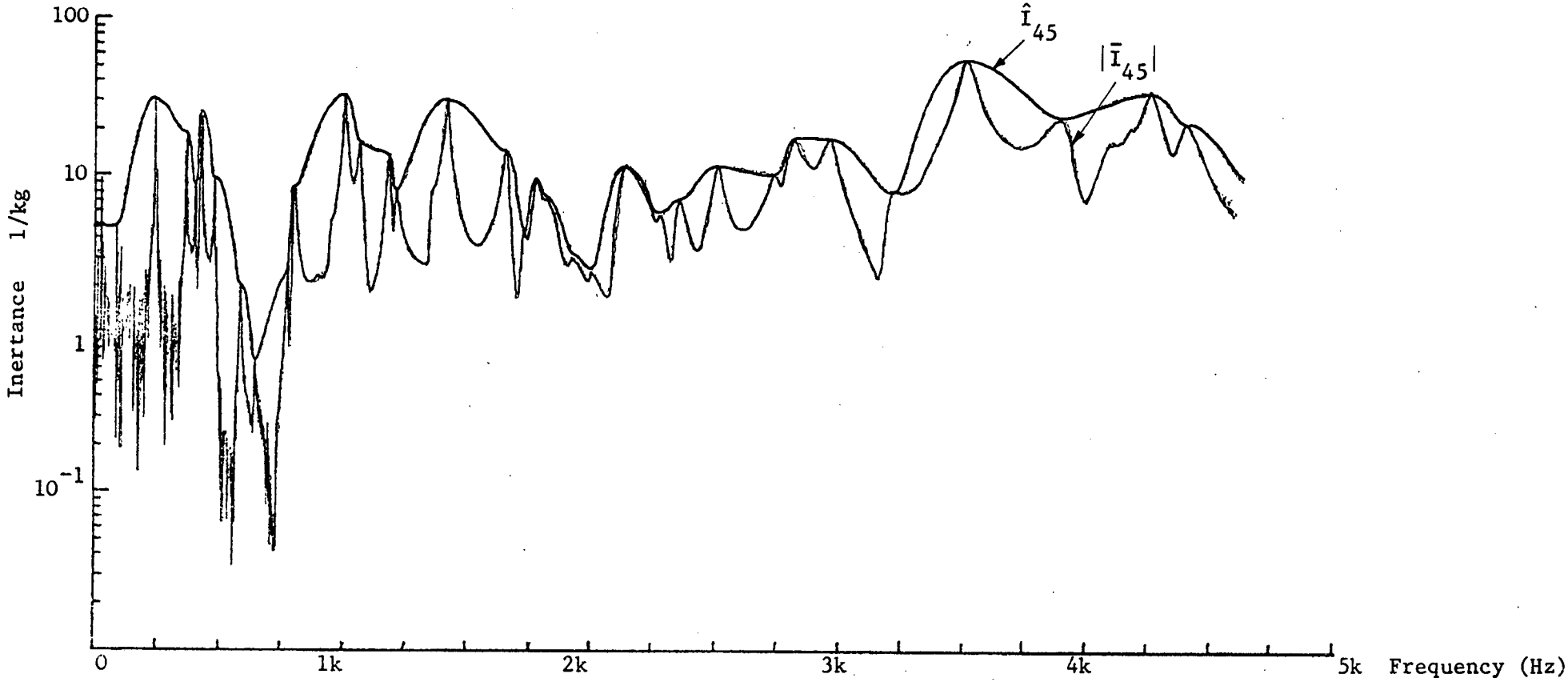

Figure 7.11. Modulus of transfer inertance between points 4 and 5 $|\bar{I}_{45}|$ and envelope at peaks $\hat{I}_{45}$

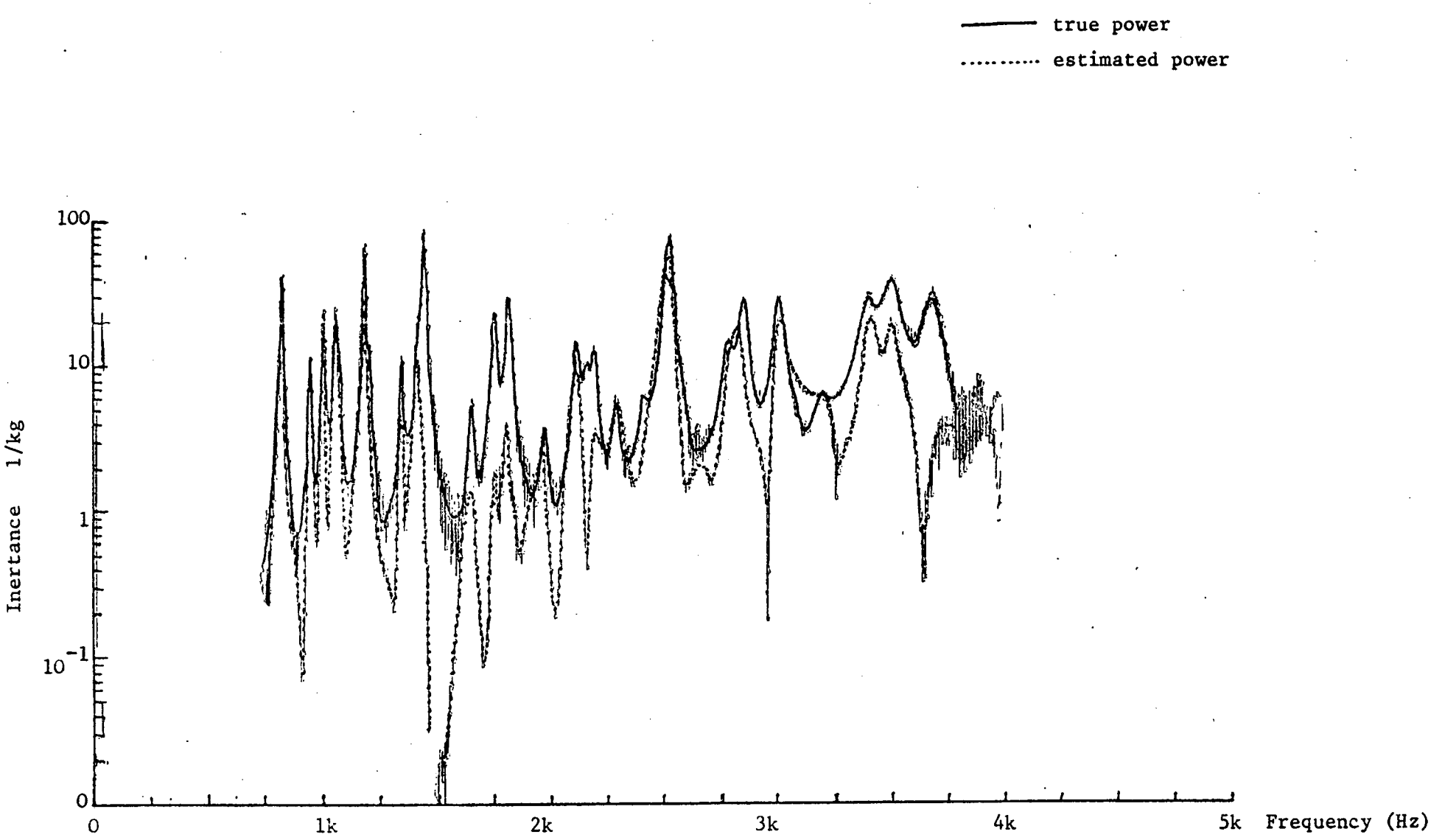

Figure 7.12 $\frac{\omega \times \text{Power/Hz}}{\langle \text{Force} \rangle^2}$ input at position 2 compared with that estimated from $\hat{I}_{13}$.

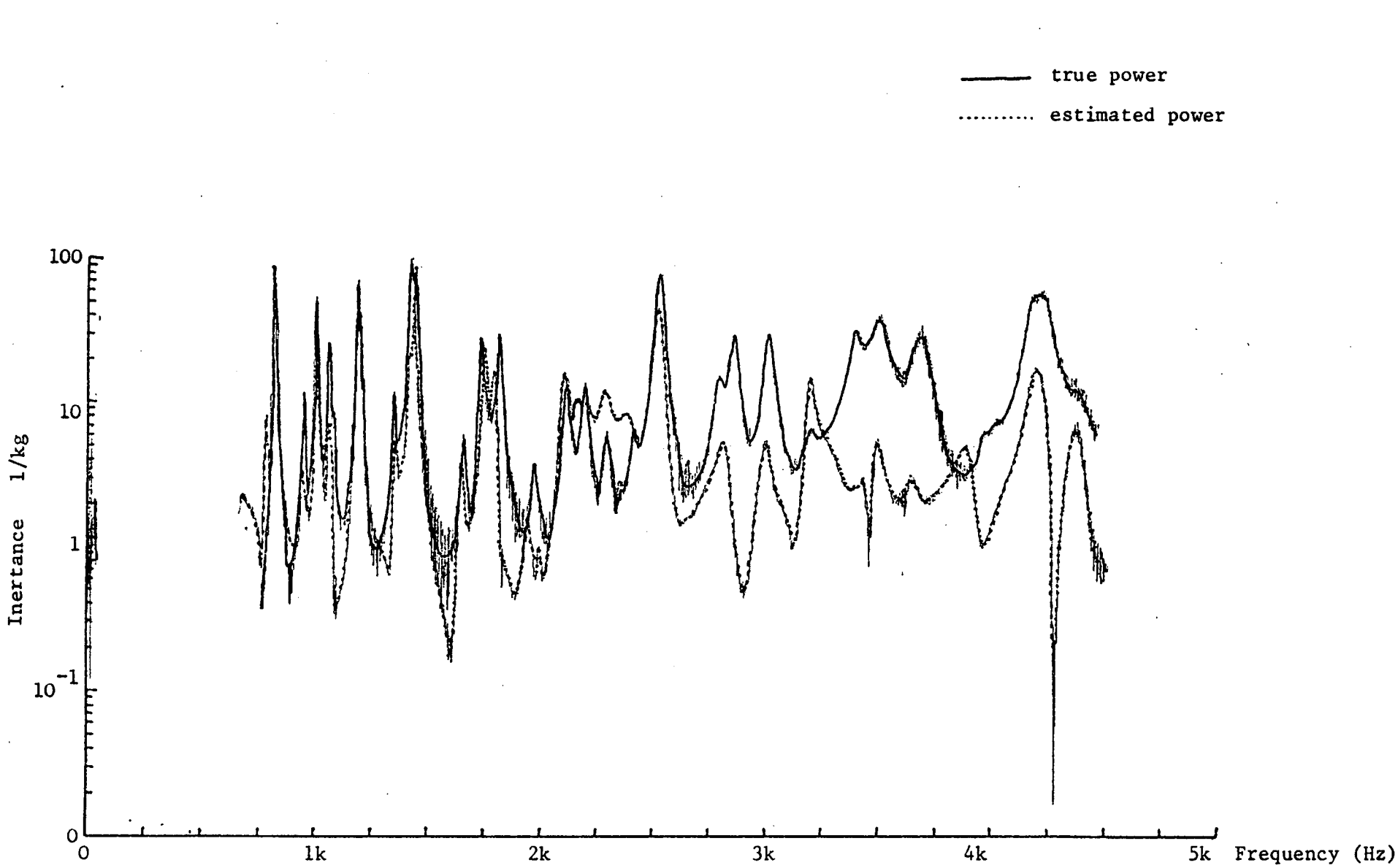

Figure 7.13. $\frac{\omega \times \text{Power/Hz}}{\langle \text{Force} \rangle^2}$ input at position 2 compared with that estimated using $\hat{I}_{45}$.

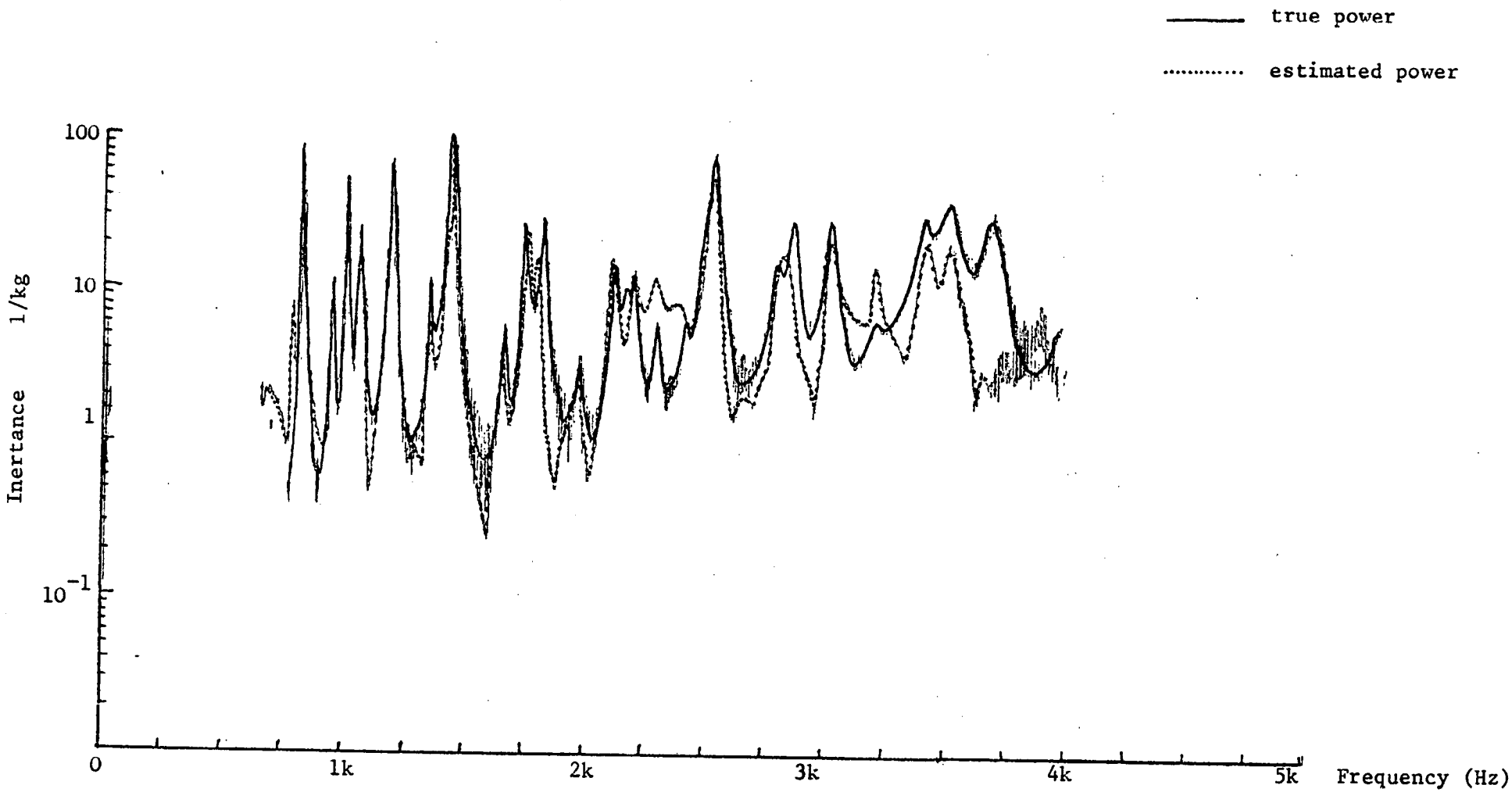

Figure 7.14 $\frac{\omega \times \text{Power/Hz}}{\langle \text{Force} \rangle^2}$ input at position 2 compared with that estimated from $\hat{I}_{13}$ and $\hat{I}_{45}$.

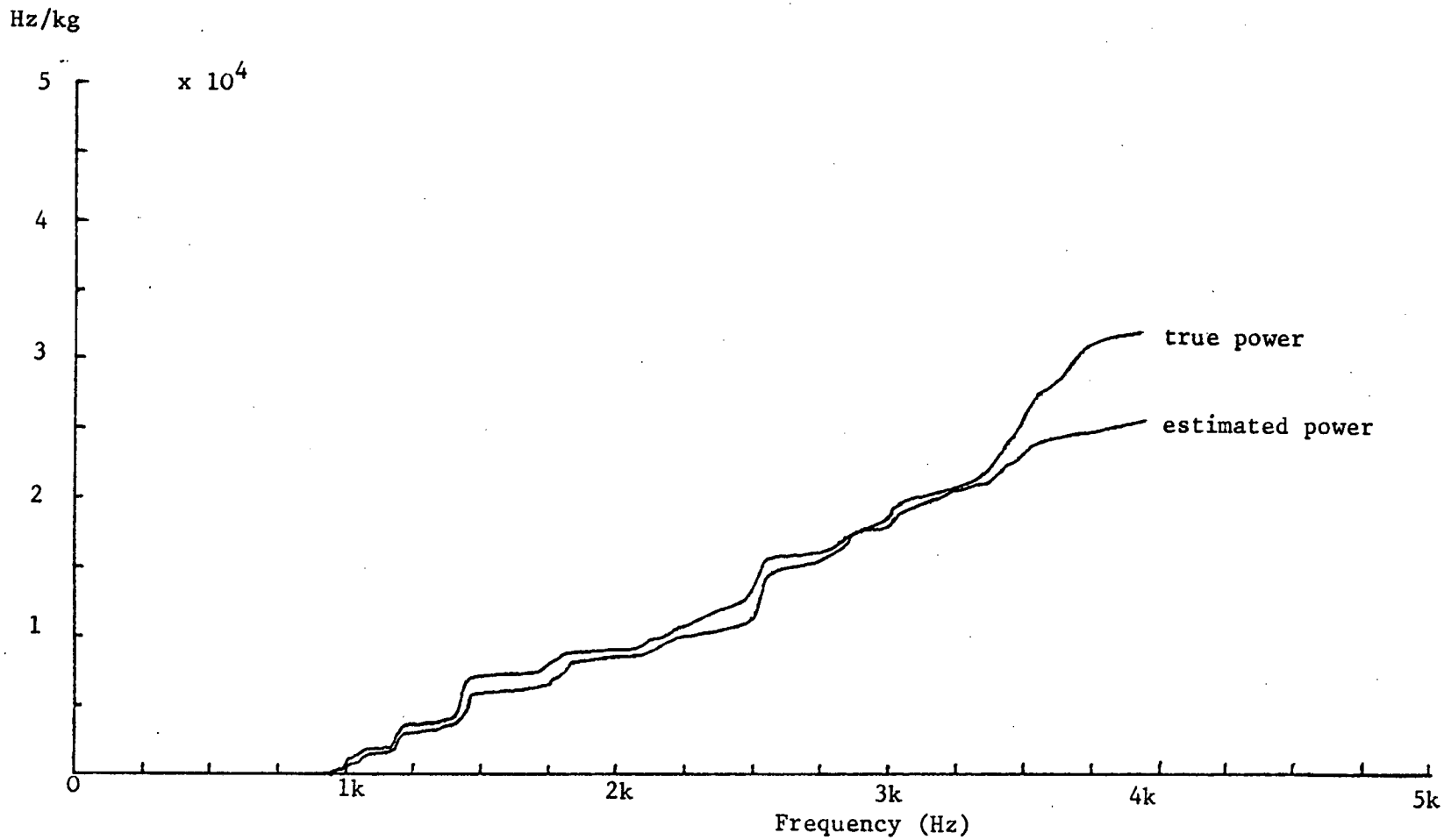

Figure 7.15 Comparison of the running integrals of the curves in figure 7.14, in $\omega \times \frac{\text{Power}}{\langle \text{Force} \rangle^2}$

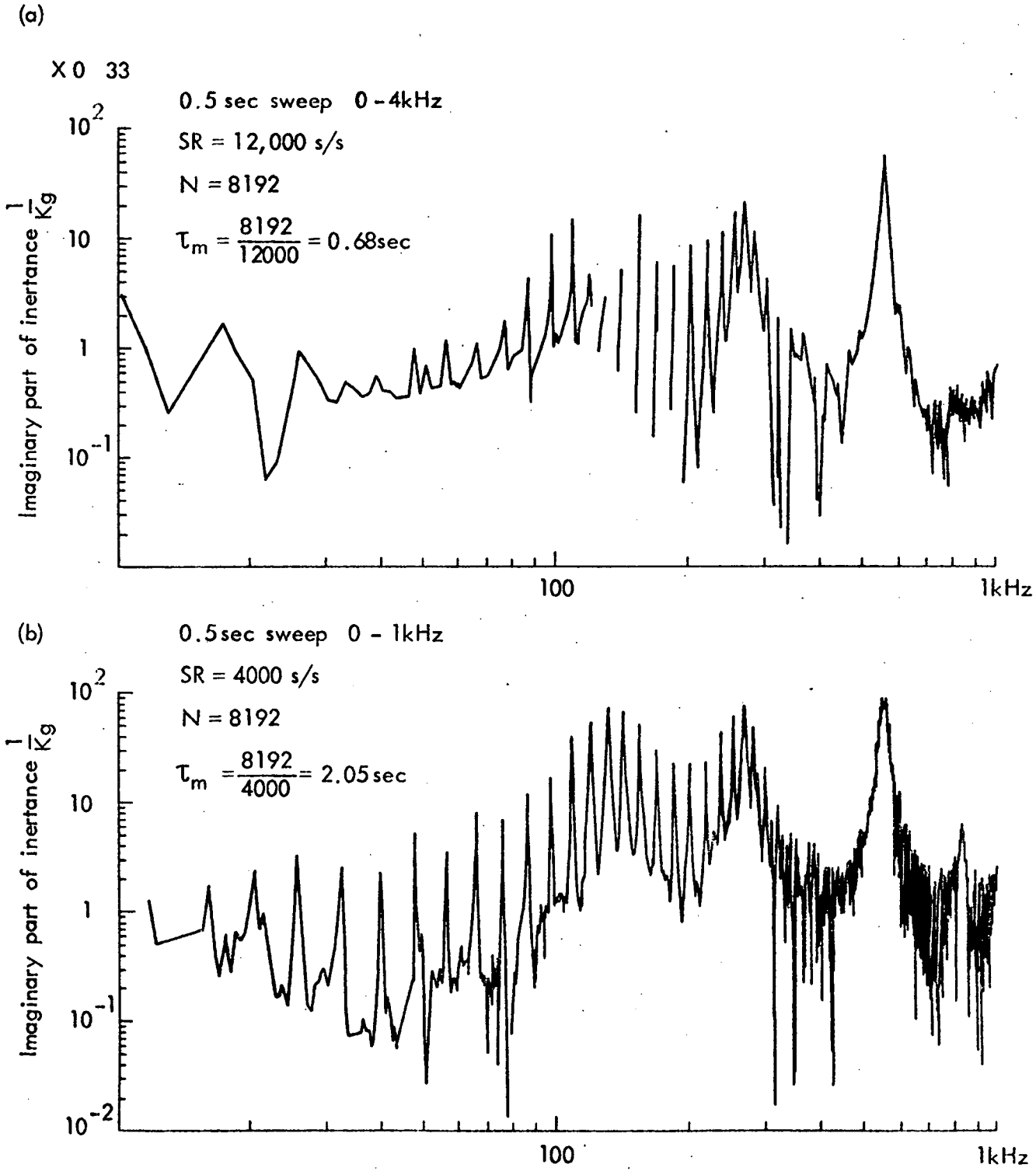

Fi g. 8.1(a) and (b) Examination of the effects of digitisation parameters on derived frequency response data.

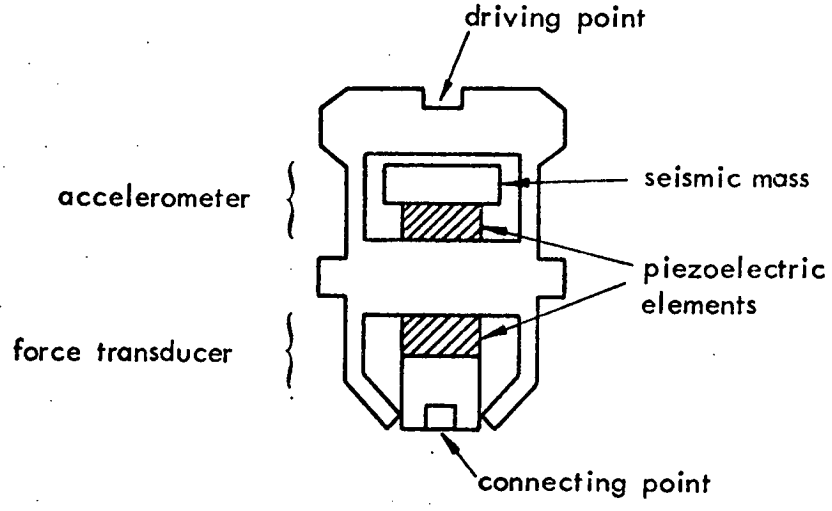

Fig. 8.2 Schematic section through an "impedance head".

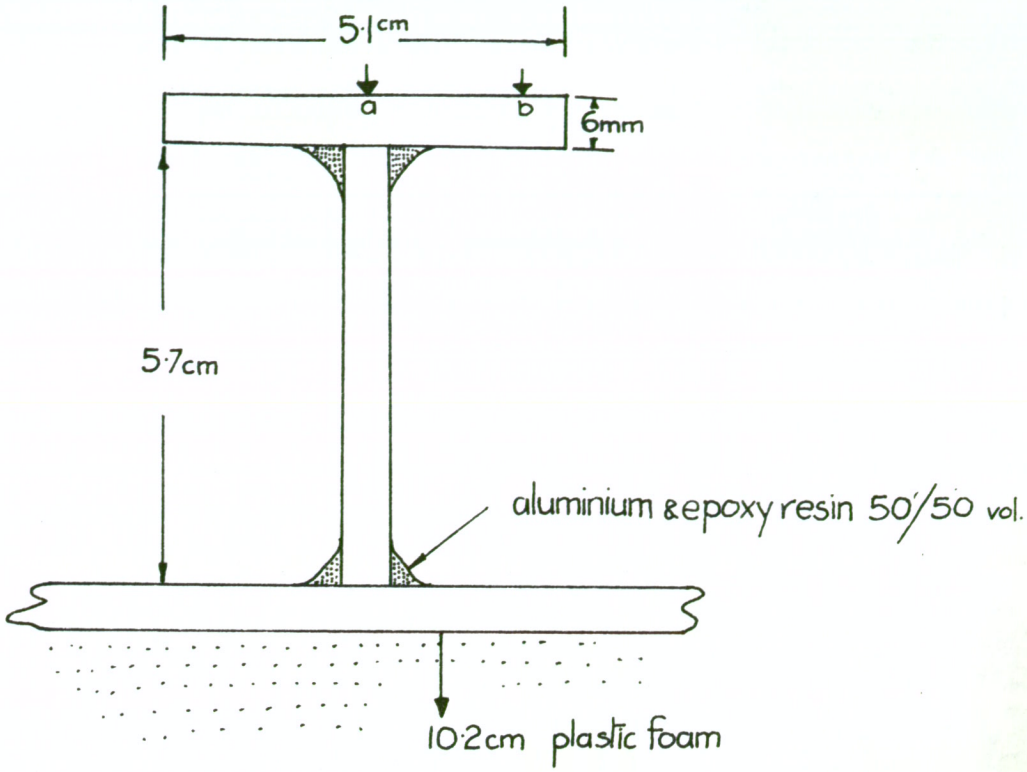

Fig. 10.1 Cross section of a beam.

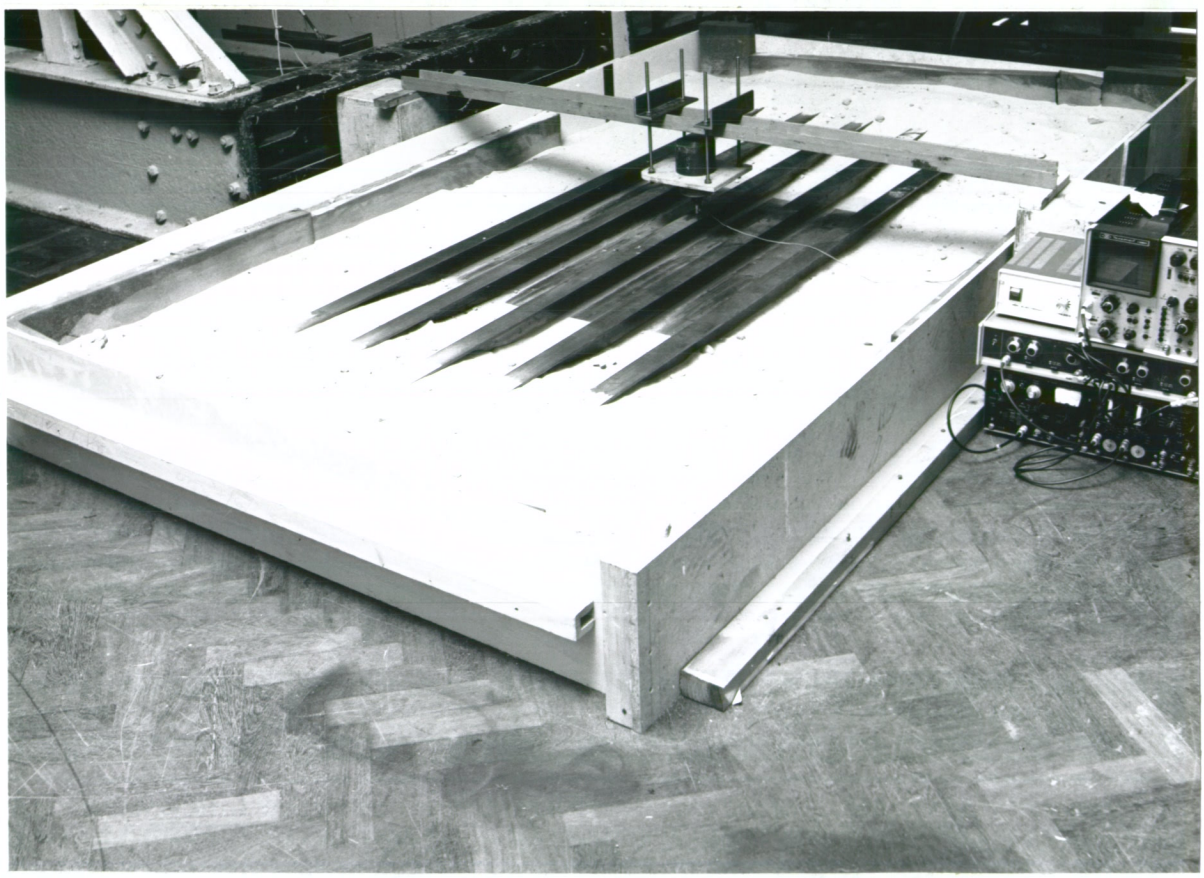

Fig. 10.2 Layout showing measurement of the point inertance of the central beam.

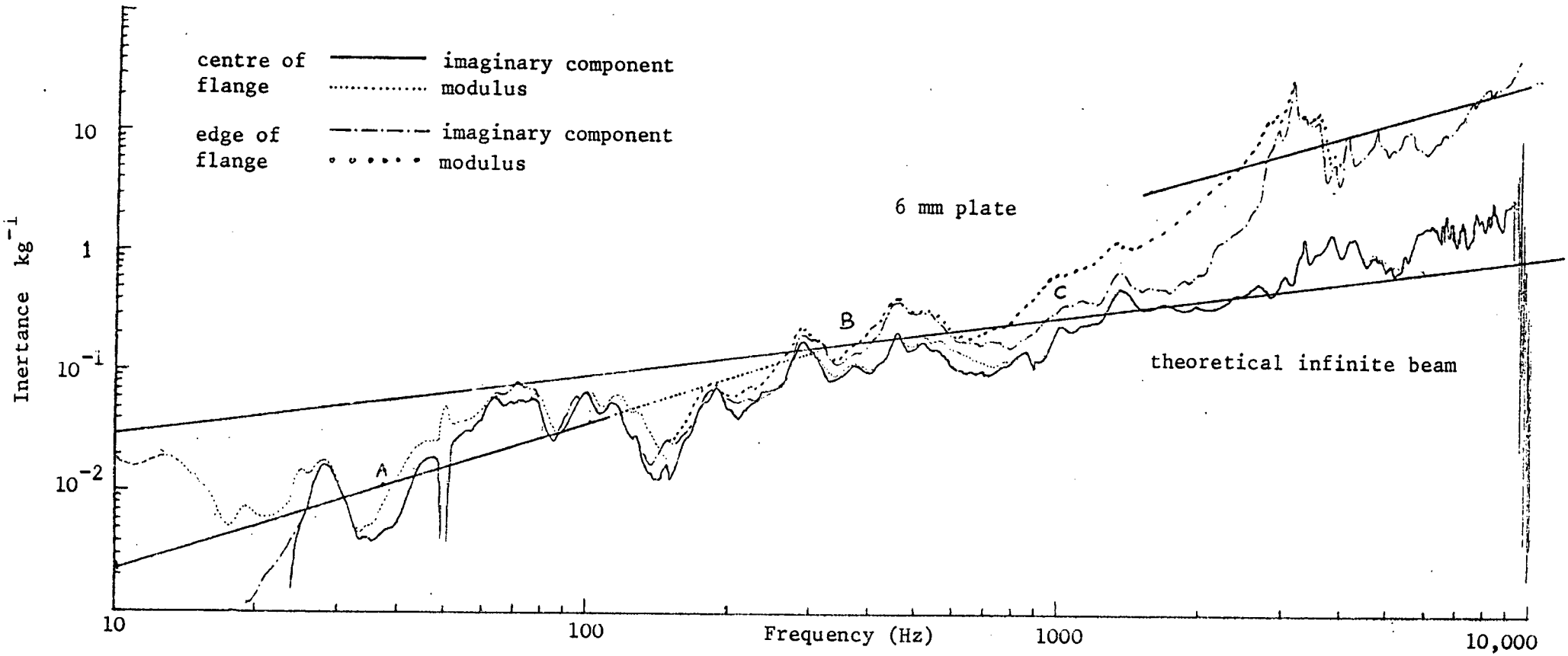

Fig. 10.3 Measured inertance at the centre and edge of the beam top flange

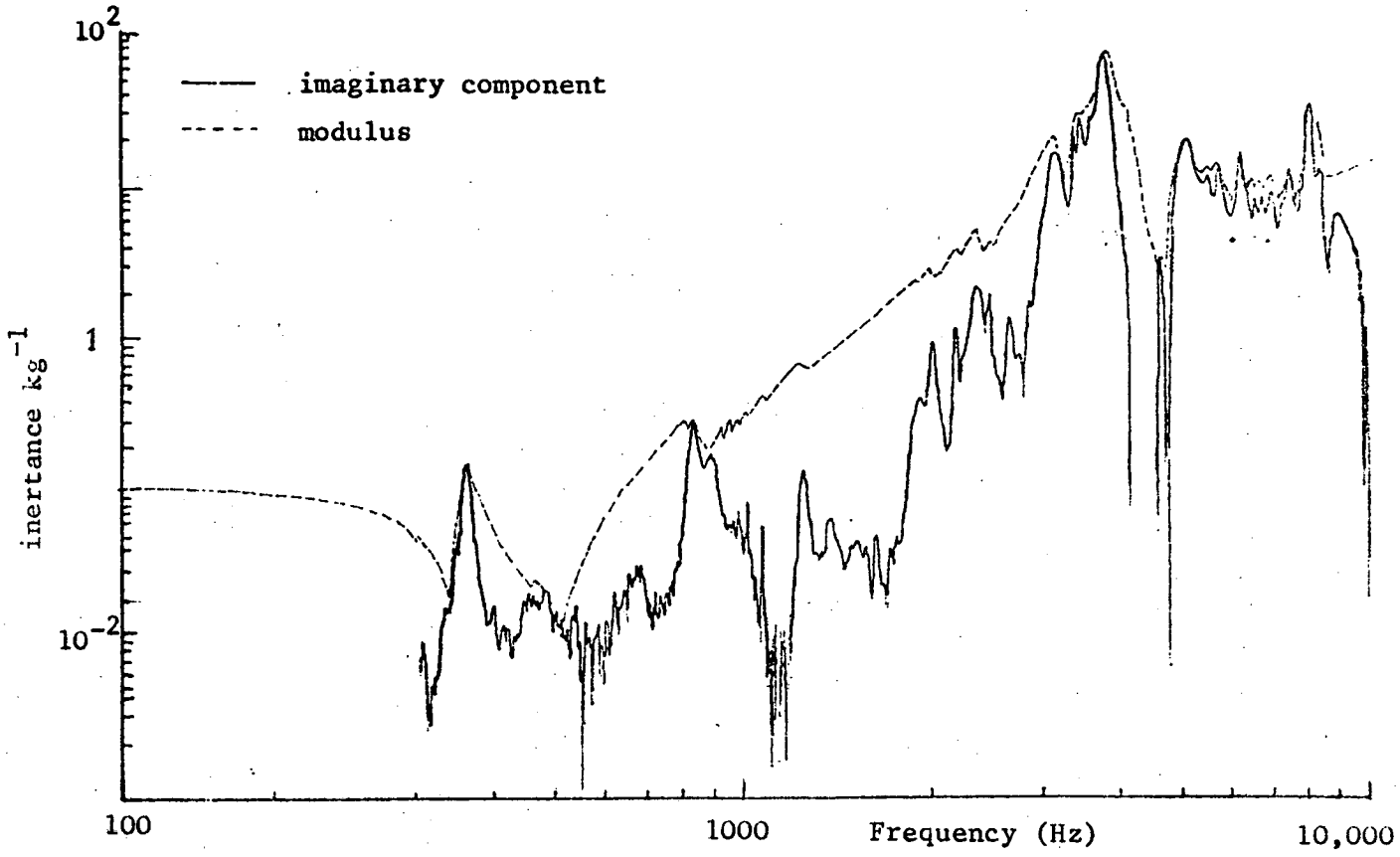

Fig. 10.4 Imaginary component of inertance and modulus of inertance of the motor foot (point 1)

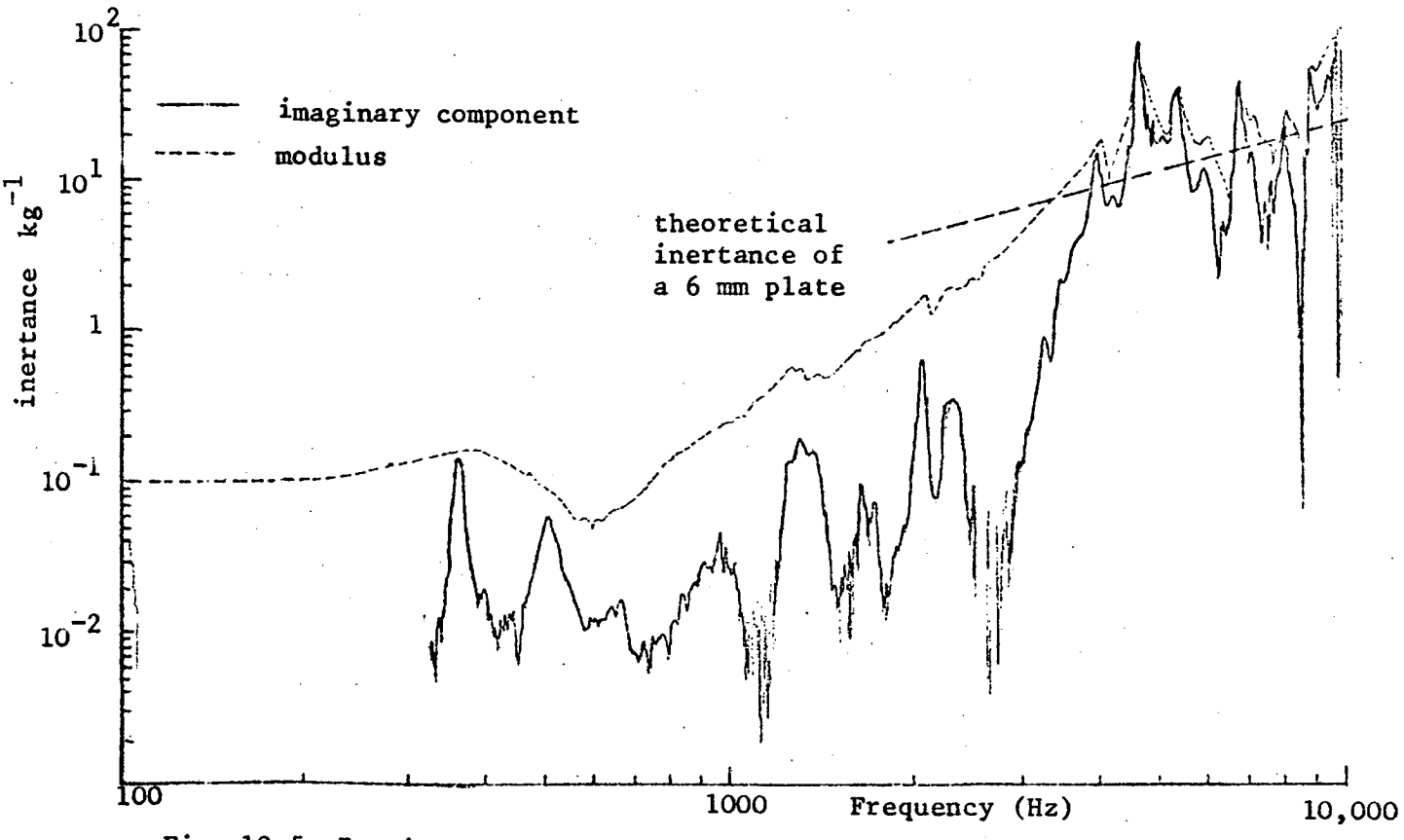

Fig. 10.5 Imaginary component of inertance and modulus of inertance at excitation point of the motor (point 5)

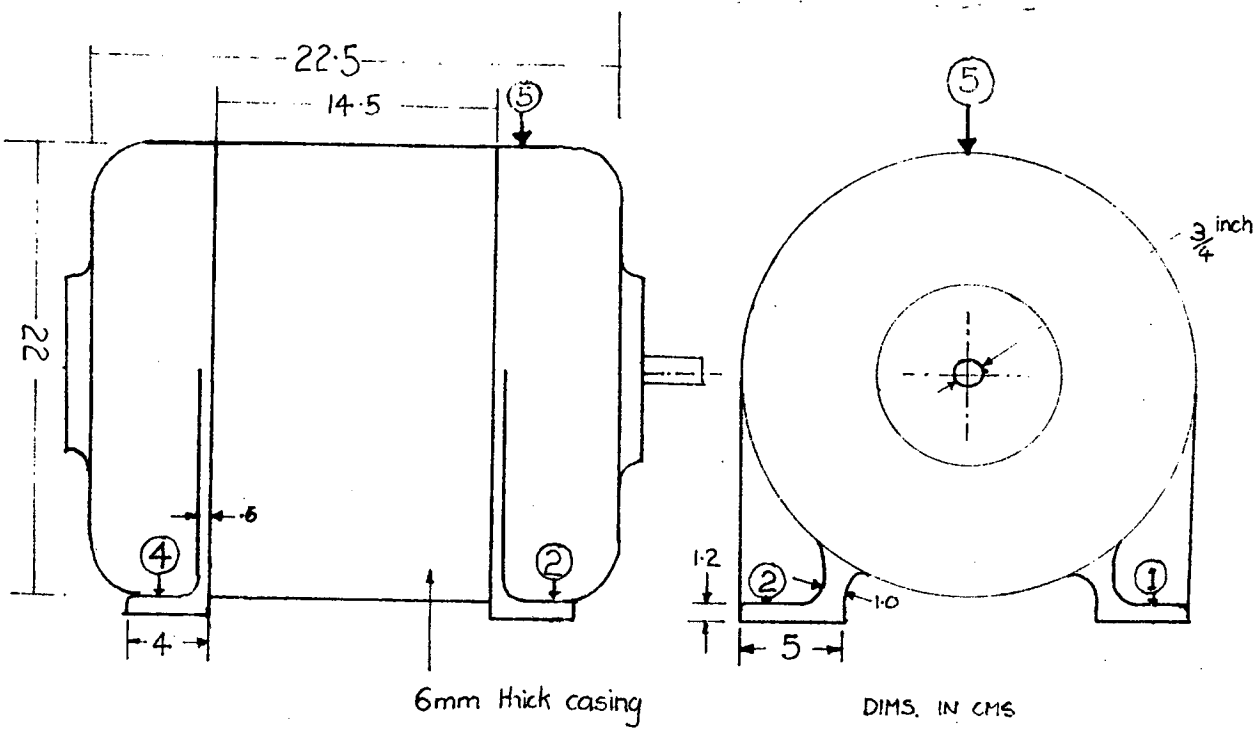

Fig. 10.6 Front and side elevation of the NECO D.C. motor frame 7A, 1.5 hp

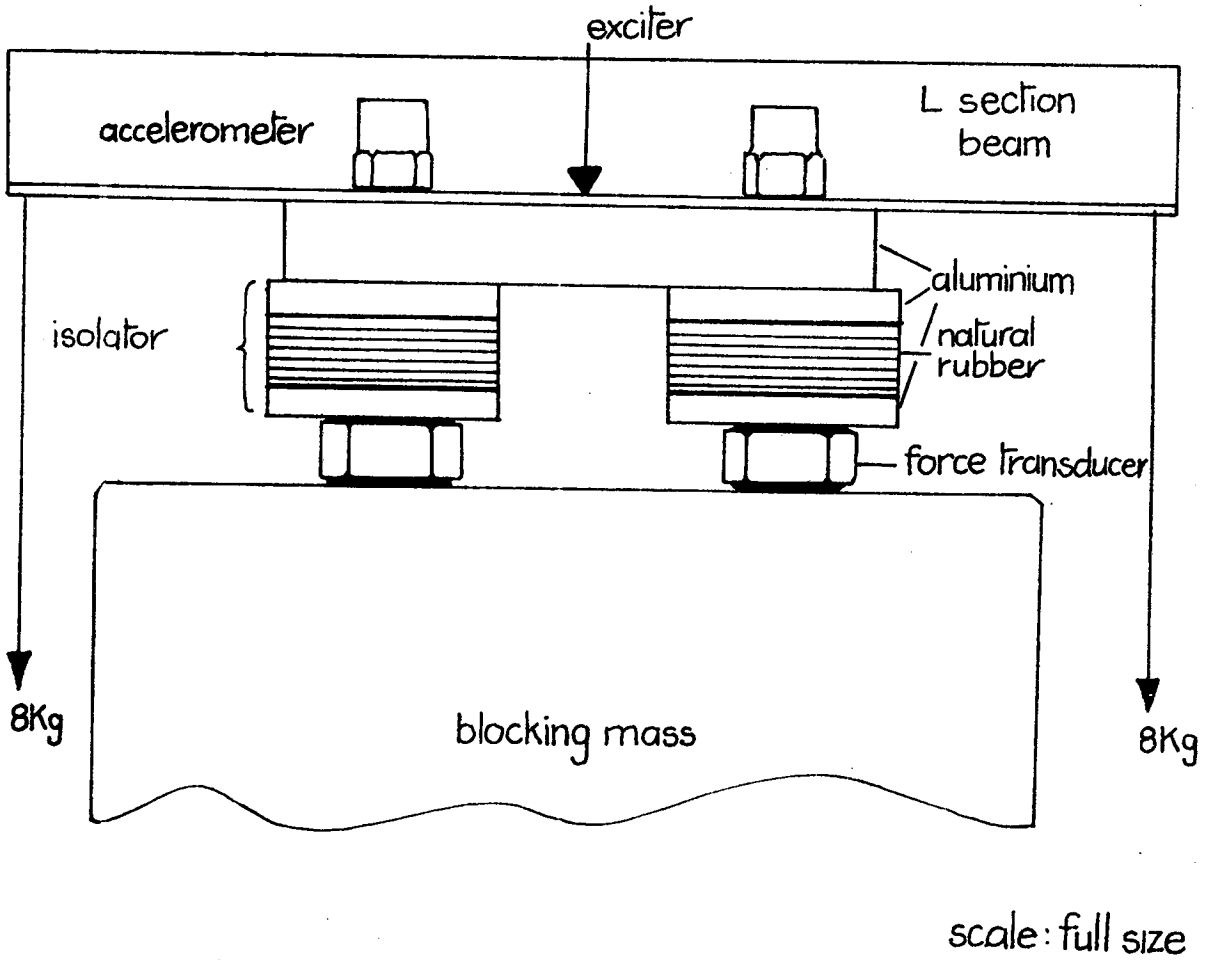

Fig. 10.7 Configuration to measure isolator transfer apparent mass.

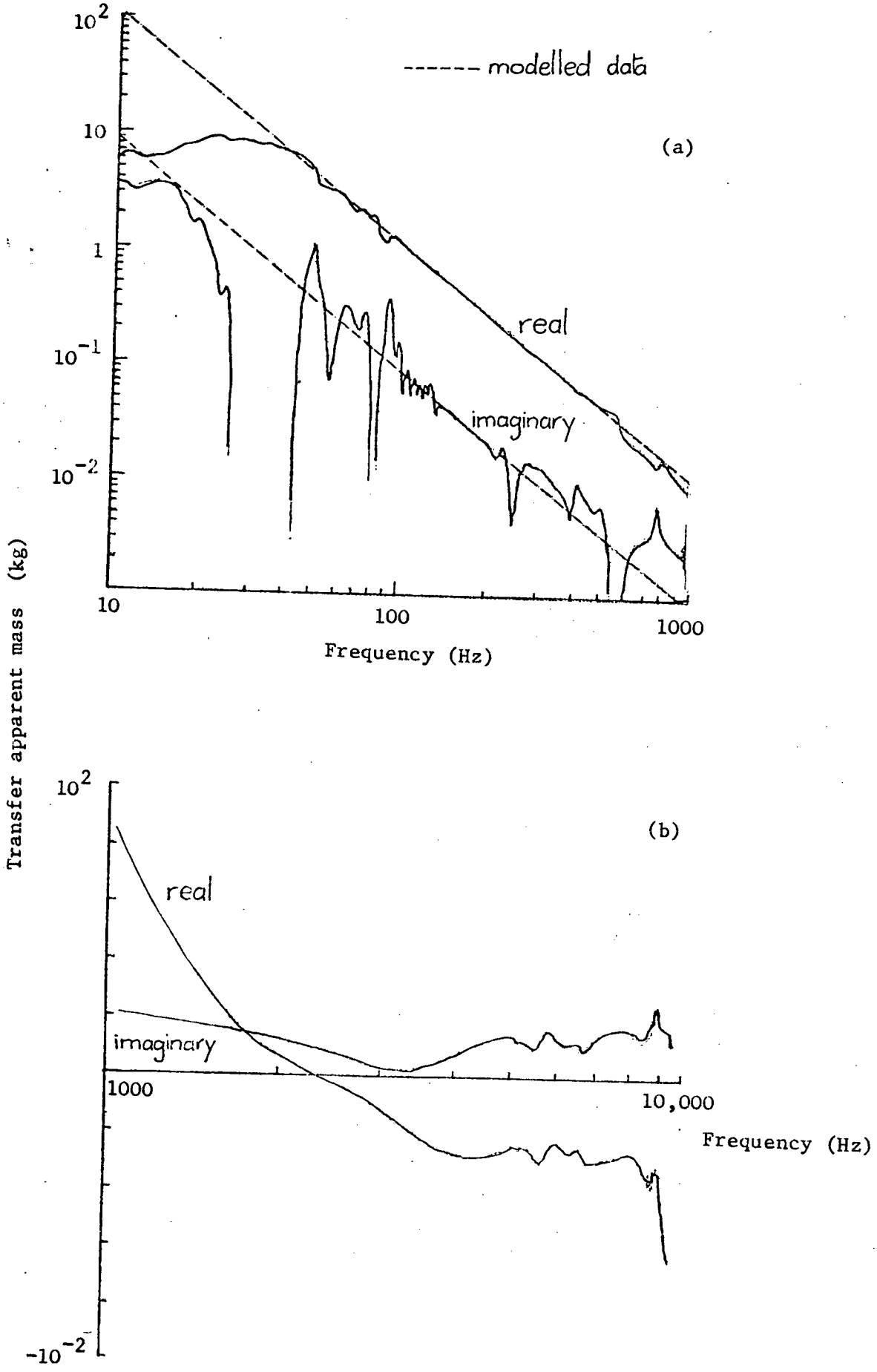

Fig. 10.8 Real and imaginary components of transfer apparent mass of isolator 1, 10 Hz - 1 kHz, 1 kHz - 10 kHz.

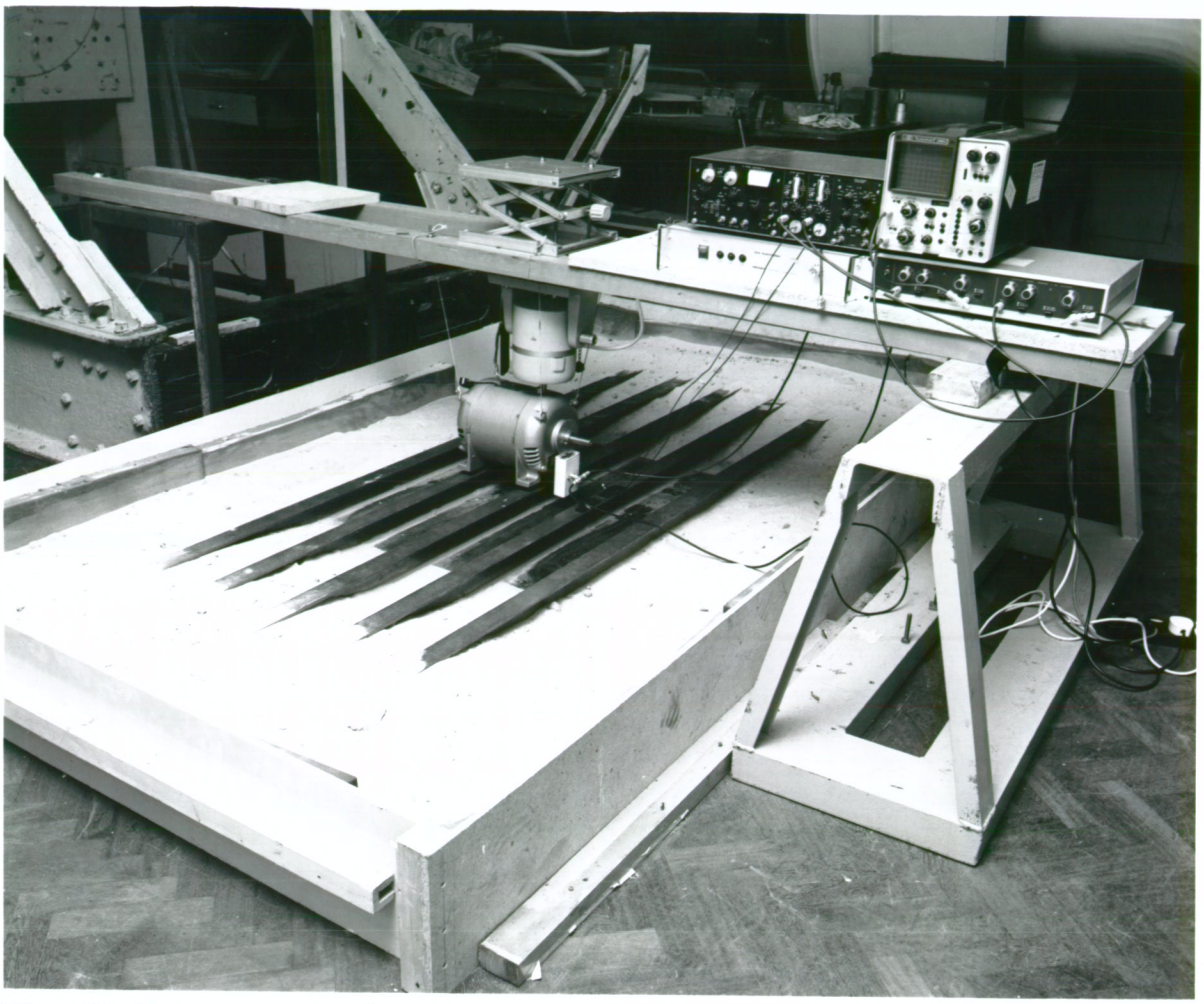

Fig. 10.9 Layout showing D.C. motor in position on plate, supported by one isolator and nylon cord suspension.

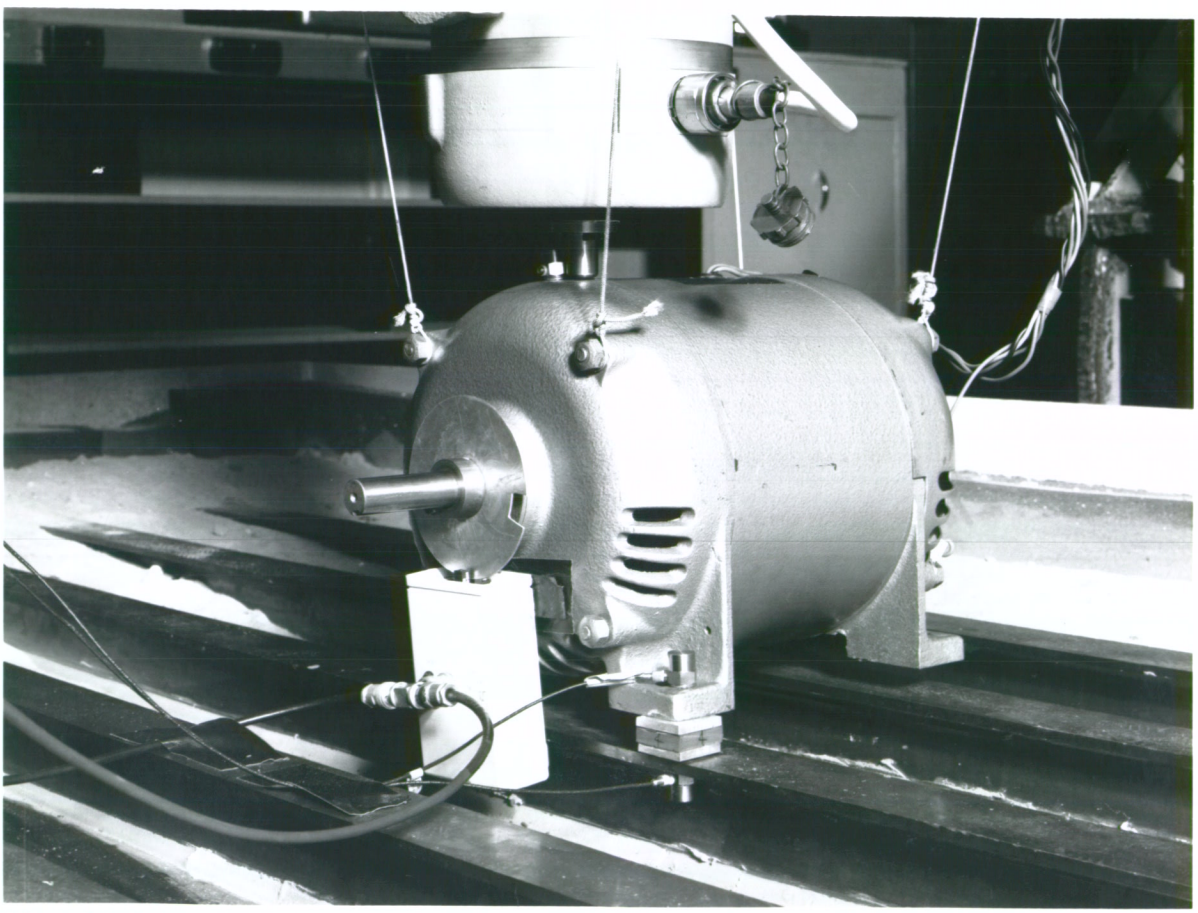

Fig. 10.10 Close up of the motor, showing the accelerometer arrangement on the isolator, and the hammer exciter above the casing.

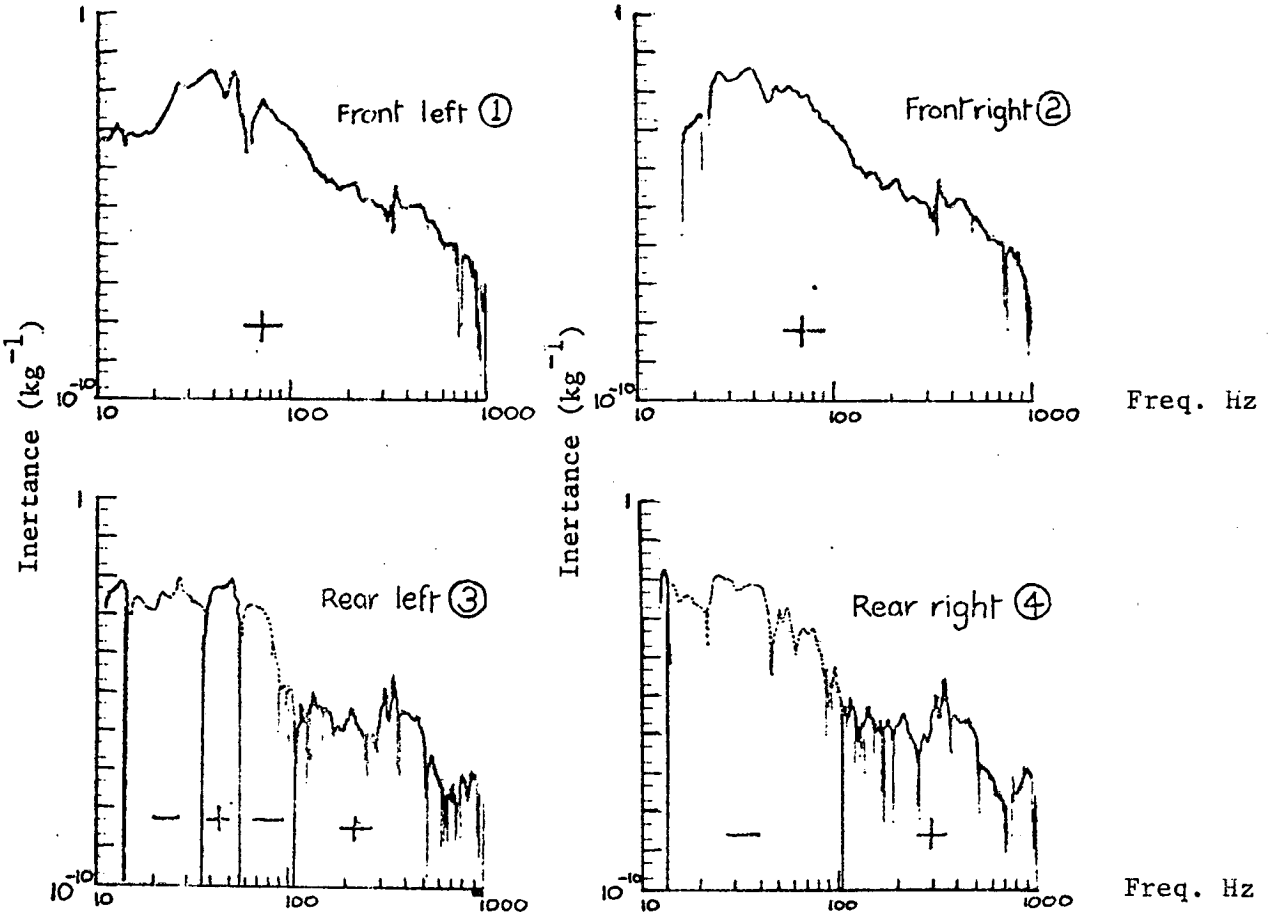

Fig. 10.11 Normalised ω × power transmitted by each isolator.

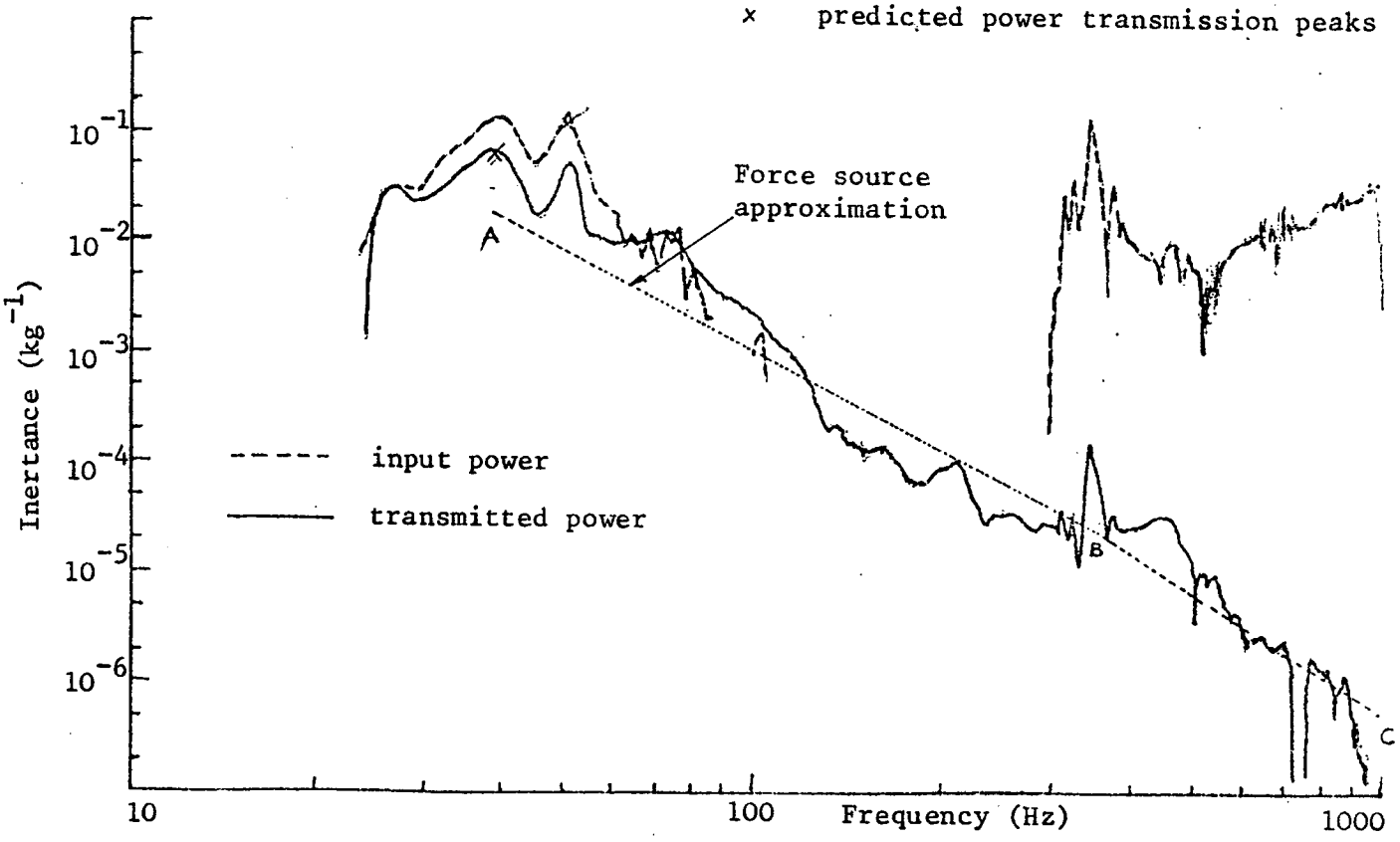

Fig. 10.12 ω × power input to the motor and total ω × power transmitted by the four isolators

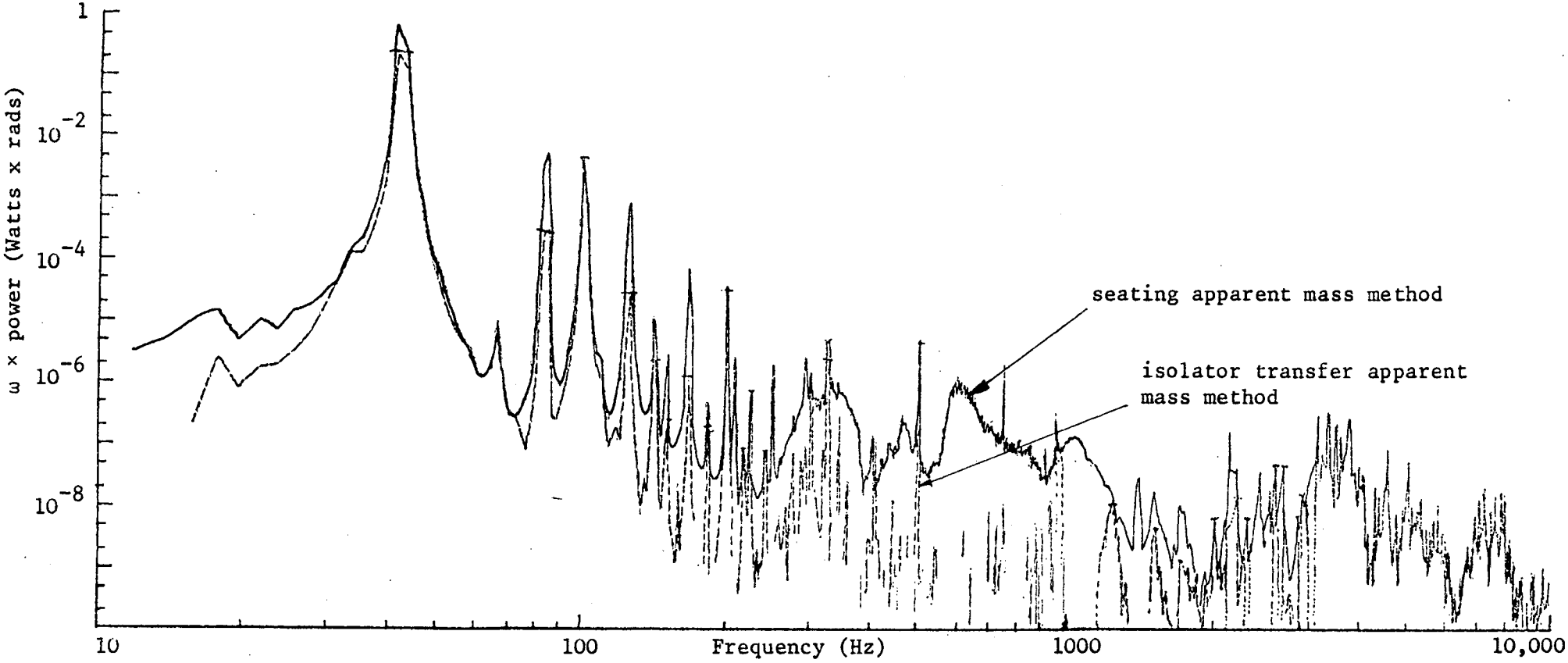

Fig. 10.13 ω × power transmitted by the single isolator, free running motor, measured using the isolator transfer apparent mass method and using the seating apparent mass method.

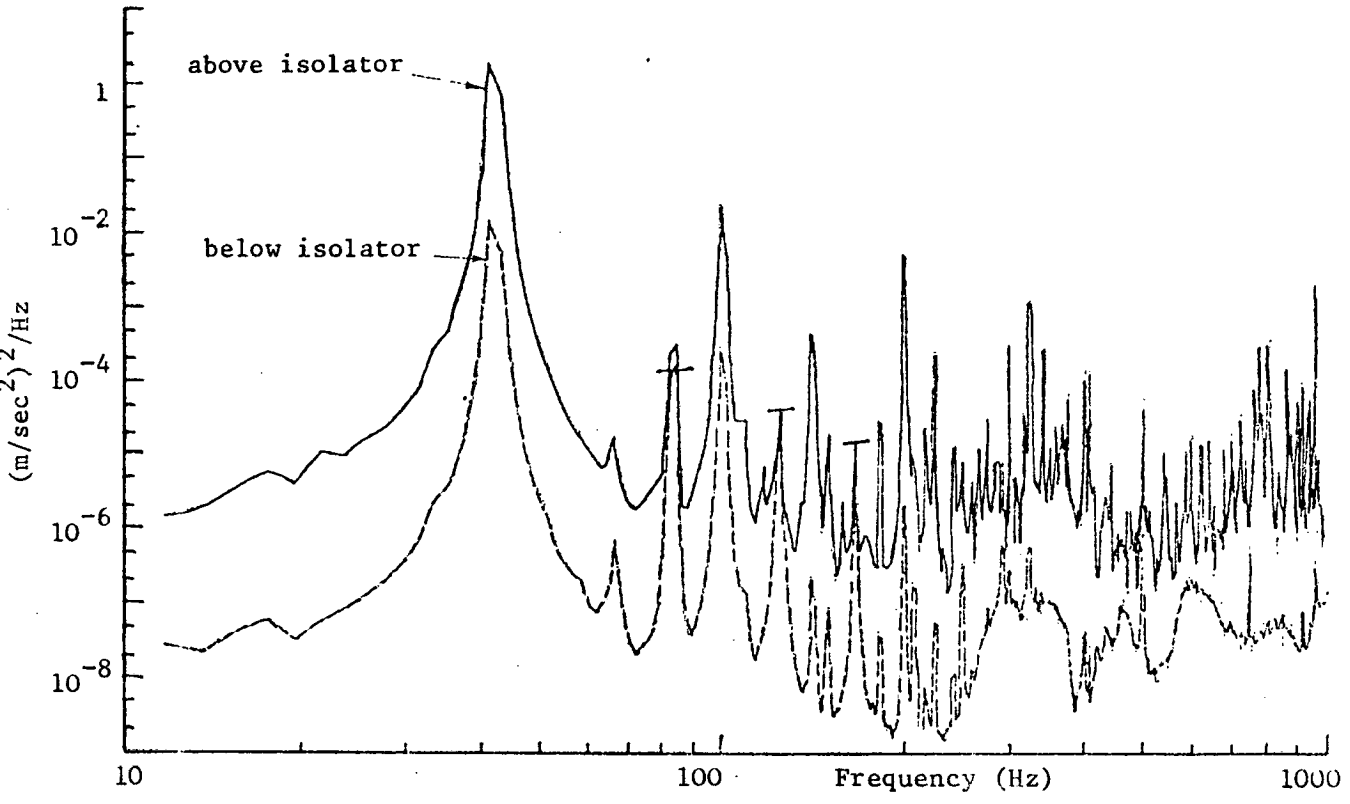

Fig. 10.14 Acceleration spectral densities above and below isolator 1 with free-running motor, 10 Hz - 1 kHz.

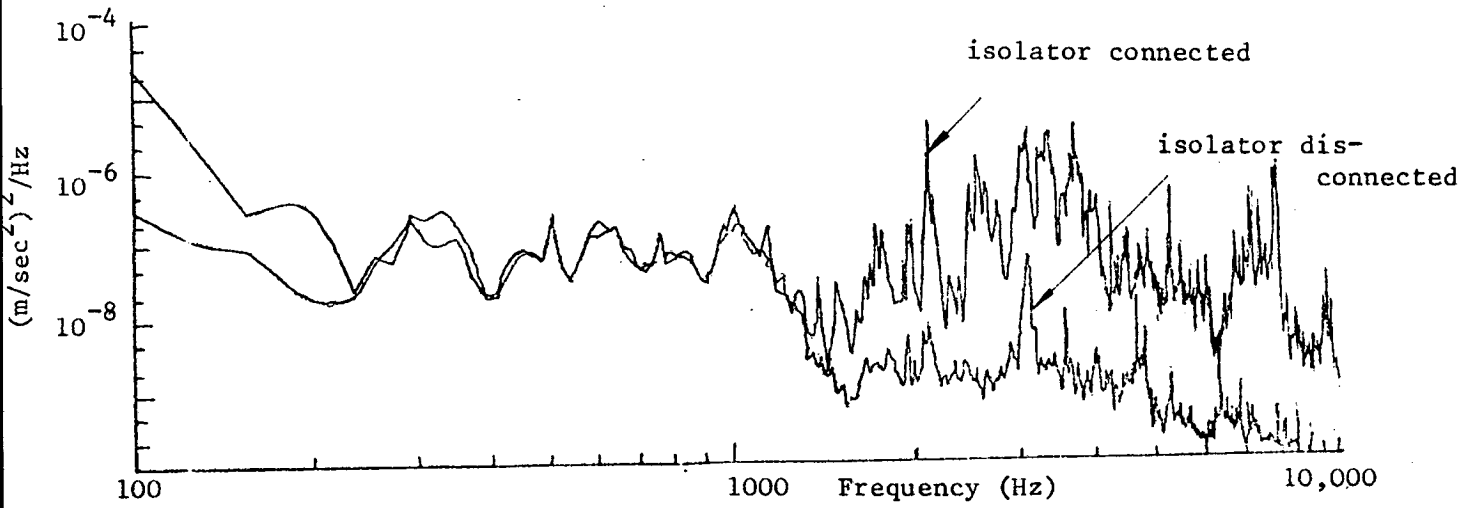

Fig. 10.15 Acceleration spectral densities on seating below isolator 1 with and without the isolator connected, free-running motor, 100 Hz-10 kHz.

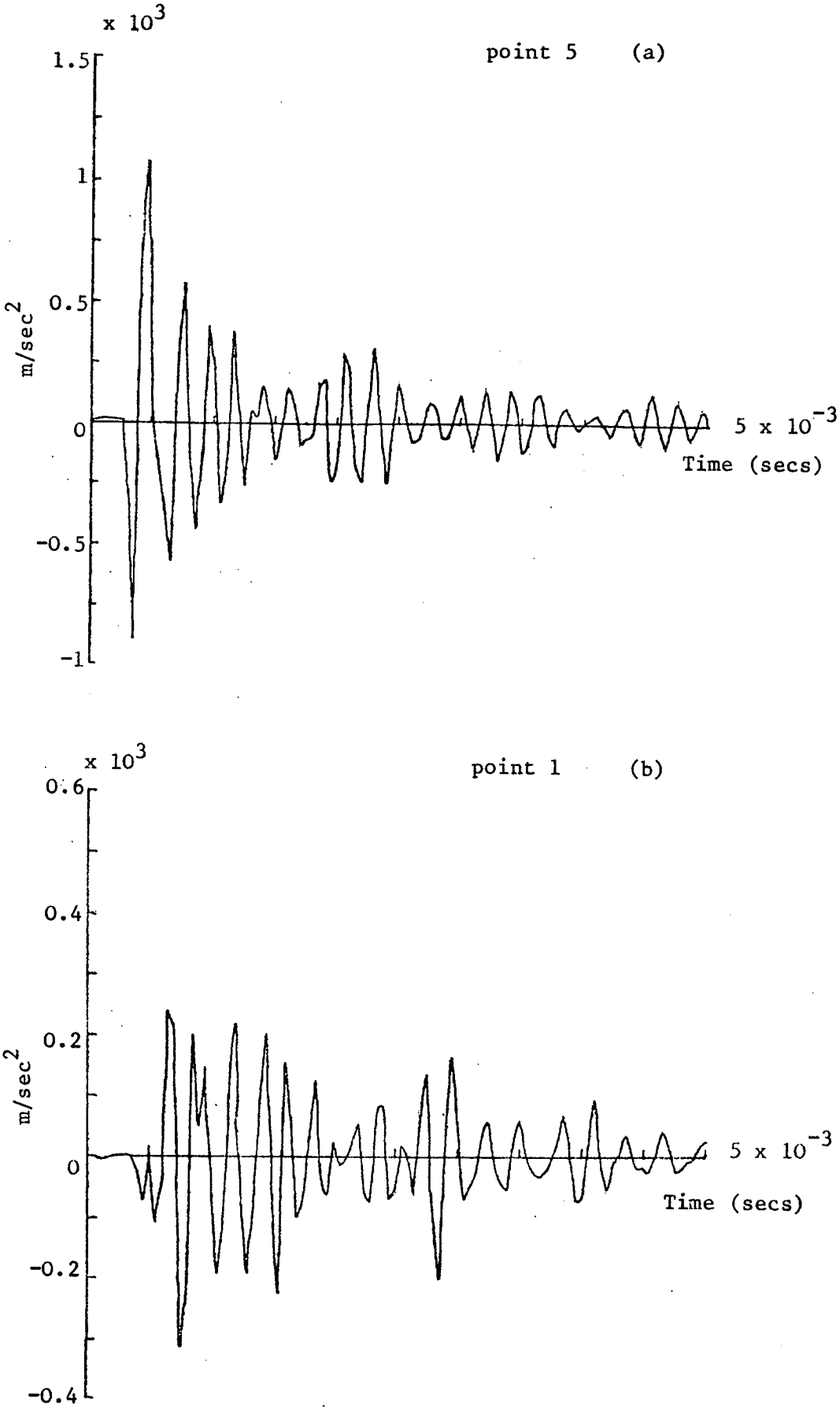

Fig. 10.16(a) and (b). Acceleration time records at the excitation point (5) and the motor foot (point 1), for a single impact at point 5.

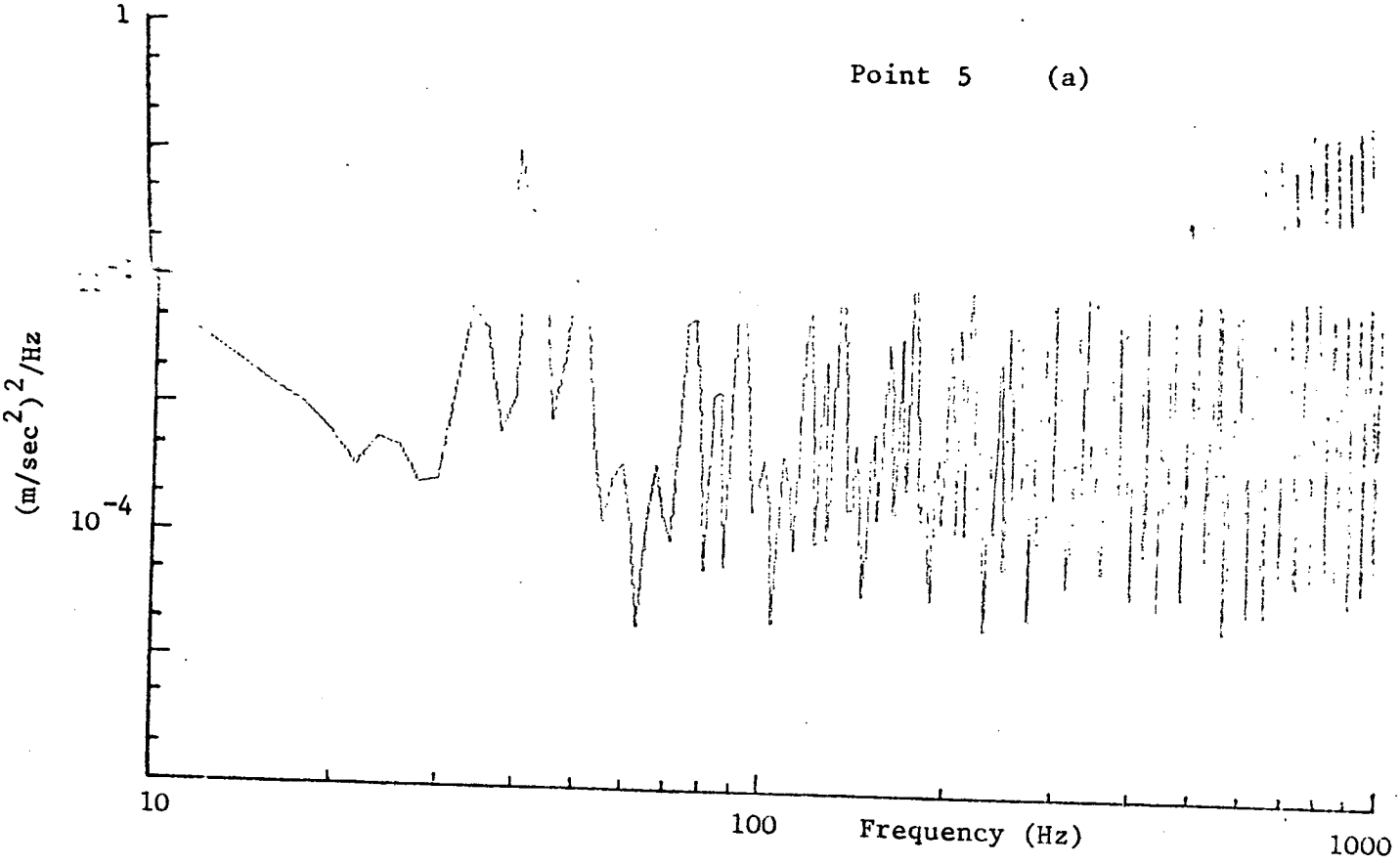

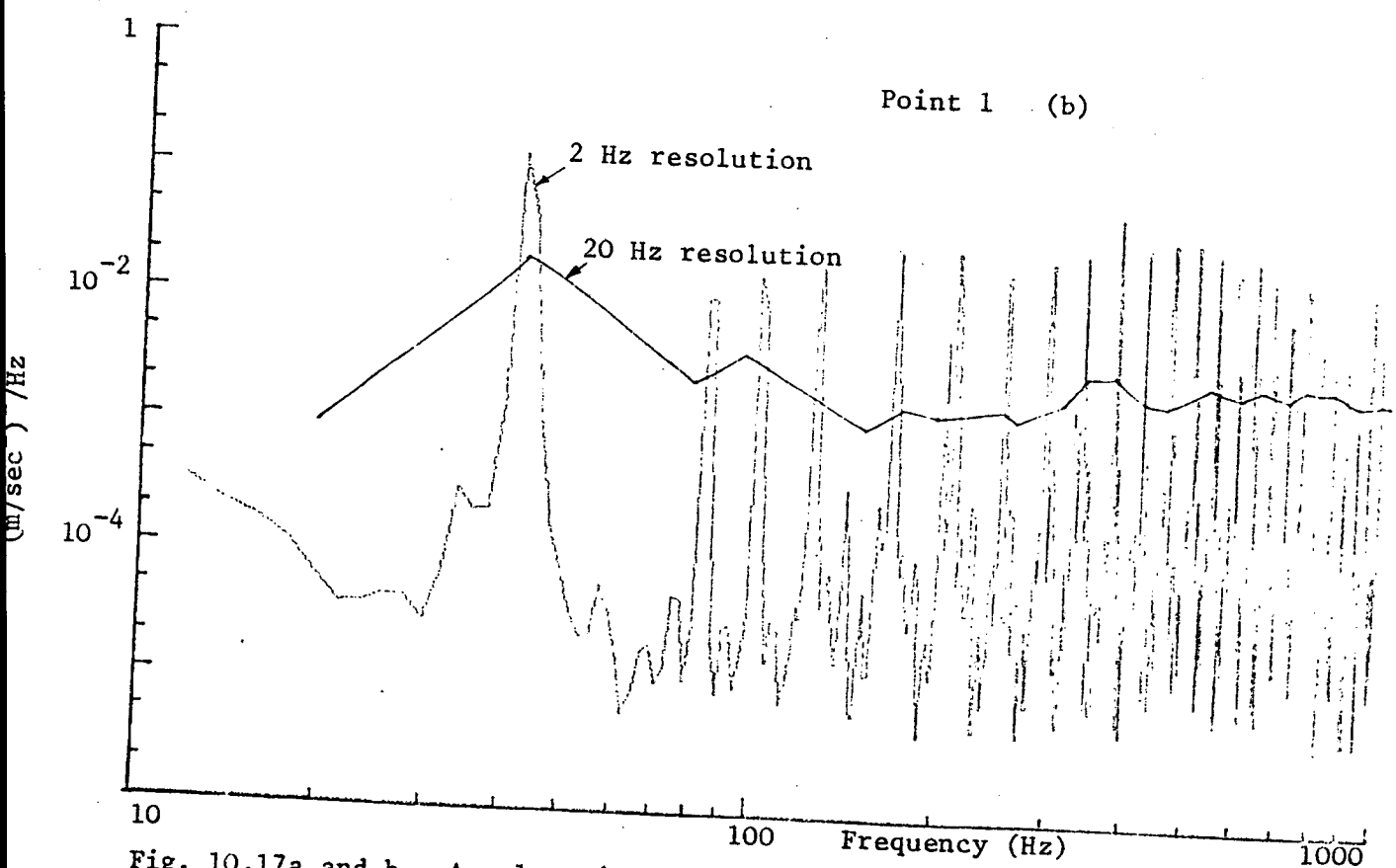

Fig. 10.17a and b. Acceleration spectral density at the excitation point (5) and at the motor foot (point 1), for impact excitation of running motor, 0-1 kHz. Motor suspended on nylon cord.

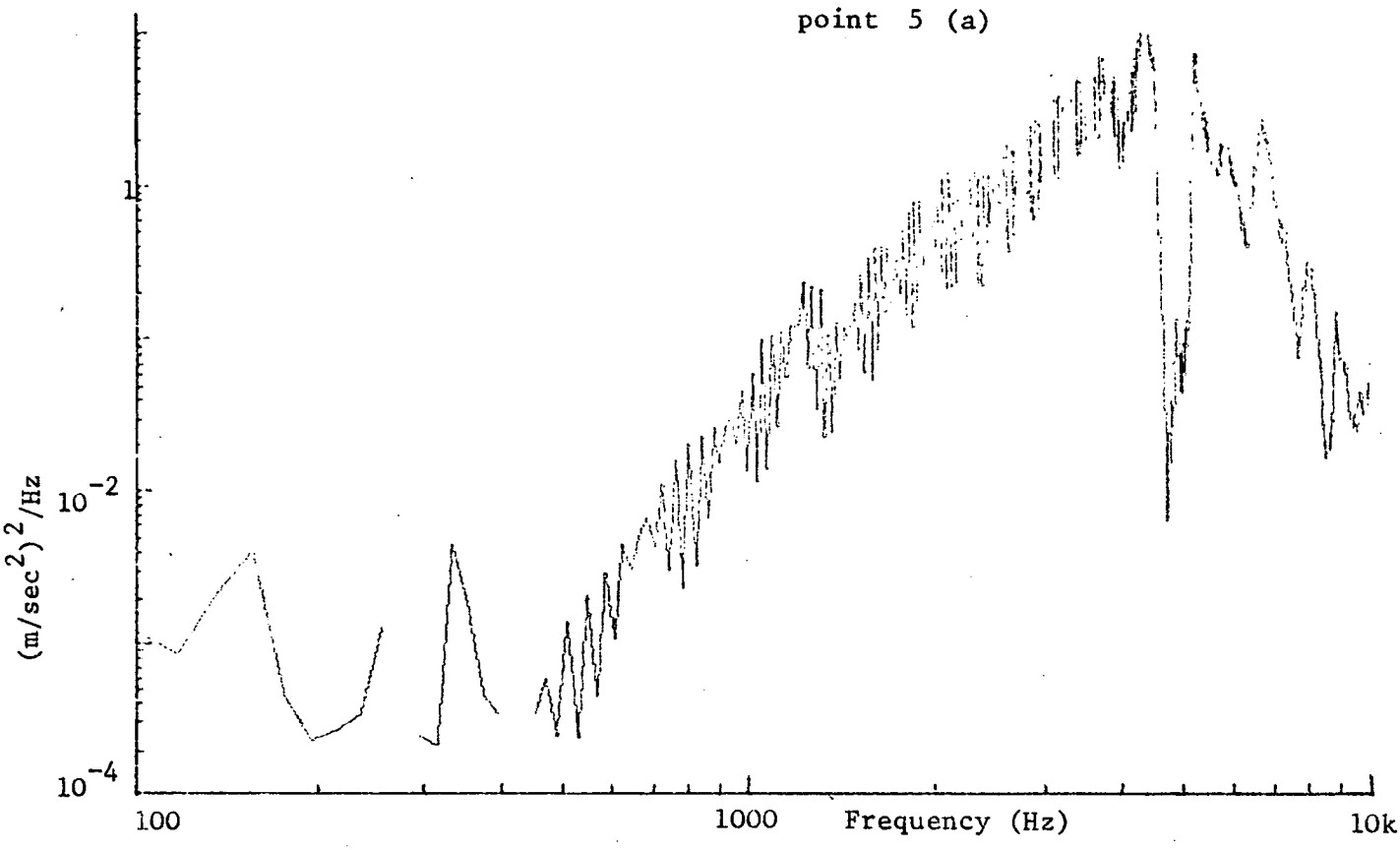

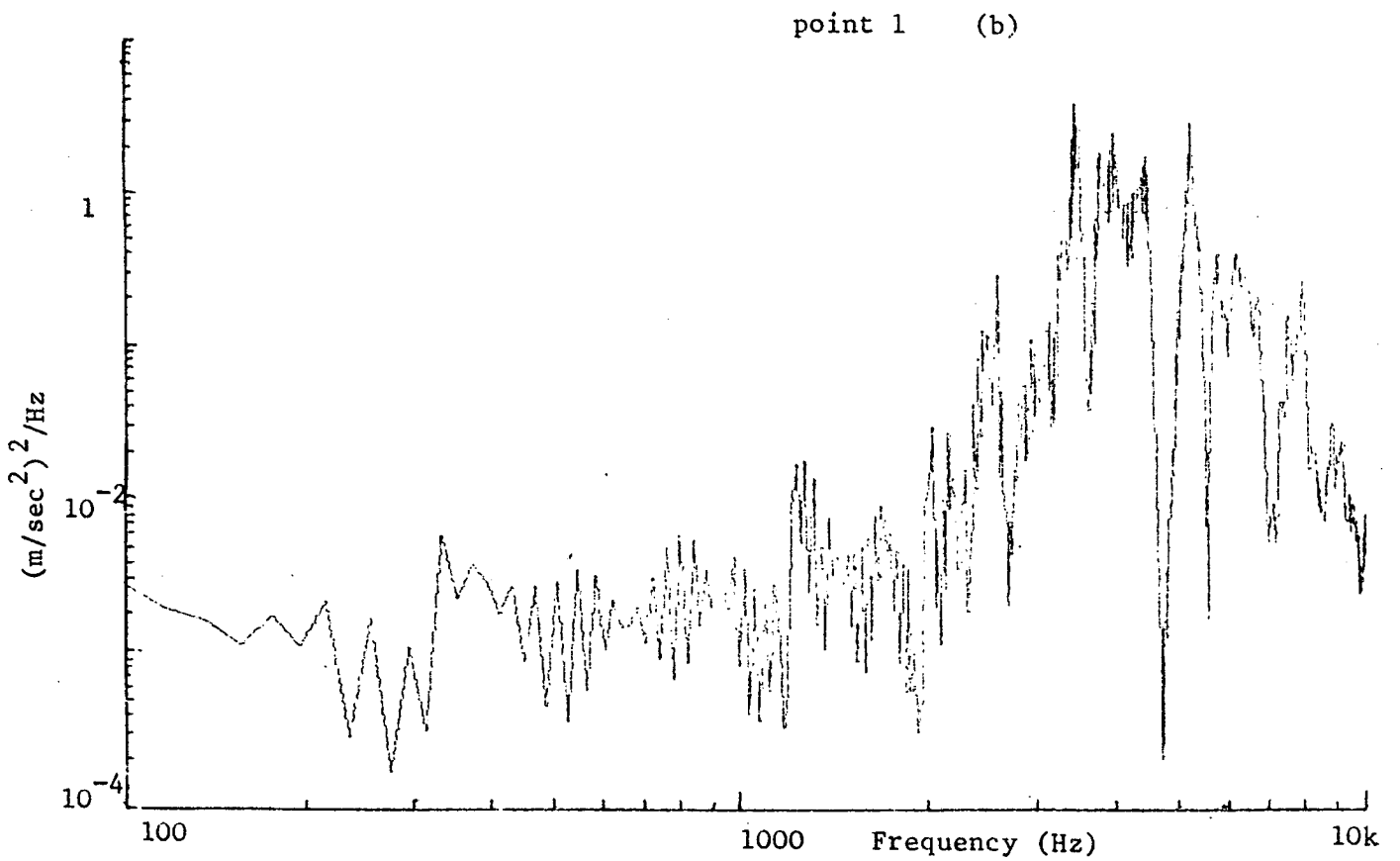

Fig. 10.18a and b. Acceleration spectral density at the excitation point (5) and at the motor foot (point 1), for impact excitation of the running motor, 100 Hz - 10kHz, motor suspended on nylon cords.

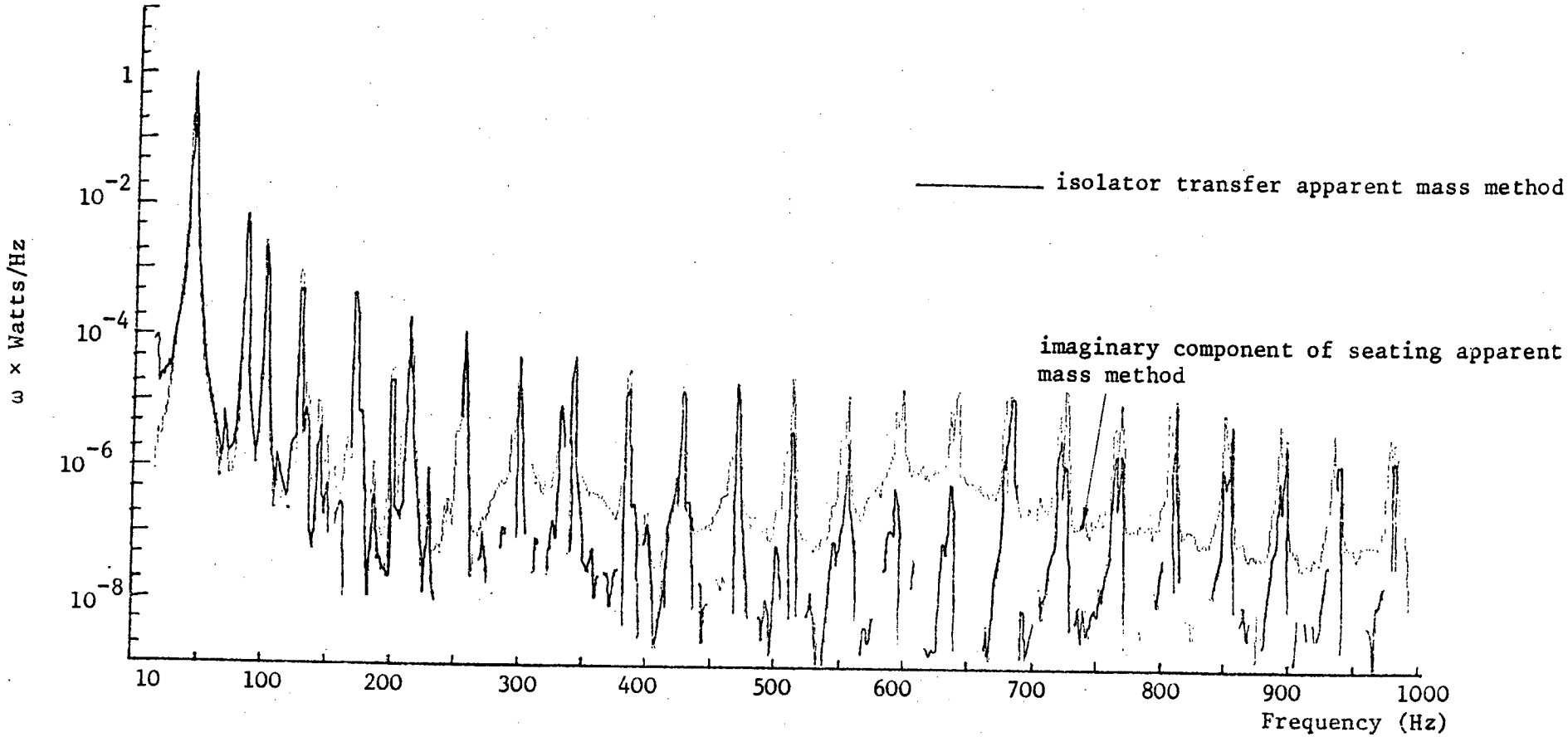

Fig. 10.19 ω × power transmitted by the single isolator to the seating from the impulsively excited running motor, measured using the isolator transfer apparent mass and measured using the seating apparent mass, 0-1kHz.

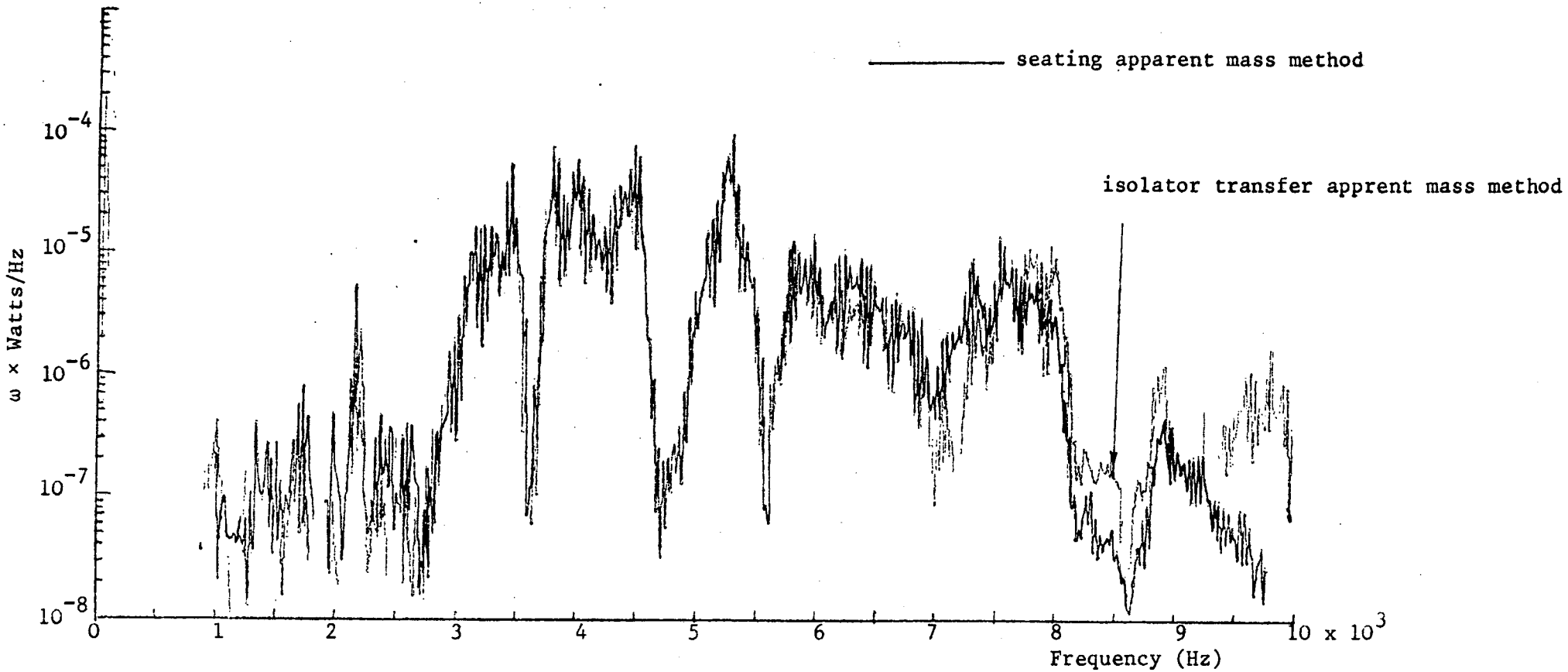

Fig. 10.20 ω × power/Hz transmitted by the single isolator to the seating from the impulsively excited running motor, measured using the isolator transfer apparent mass method and measured using the seating apparent mass method, 0-10 kHz.

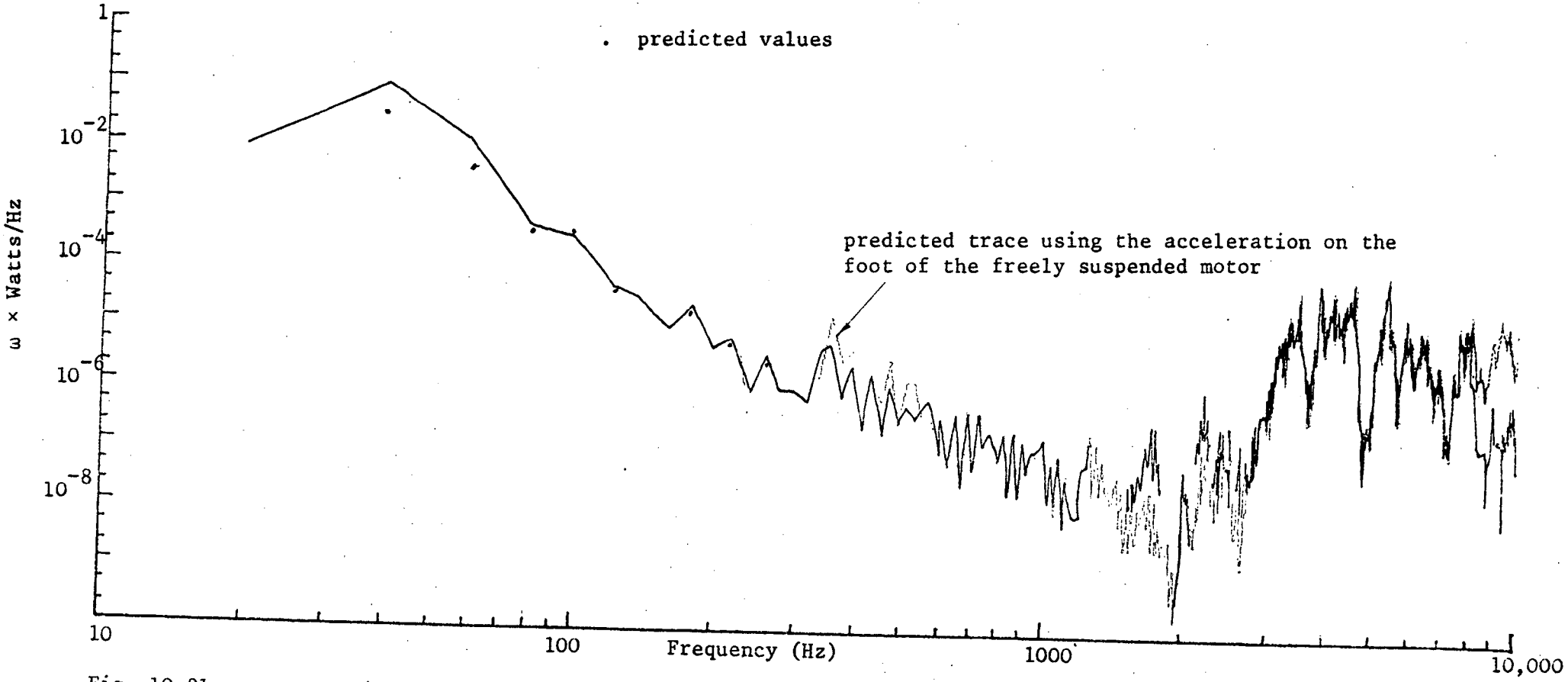

Fig. 10.21 ω × power/Hz transmitted by the single isolator to the seating by the impulsively excited running motor measured using the isolator transfer apparent mass method, and predicted using the acceleration on the foot of the freely suspended motor, resolution 20 Hz, 10 Hz - 10 kHz.

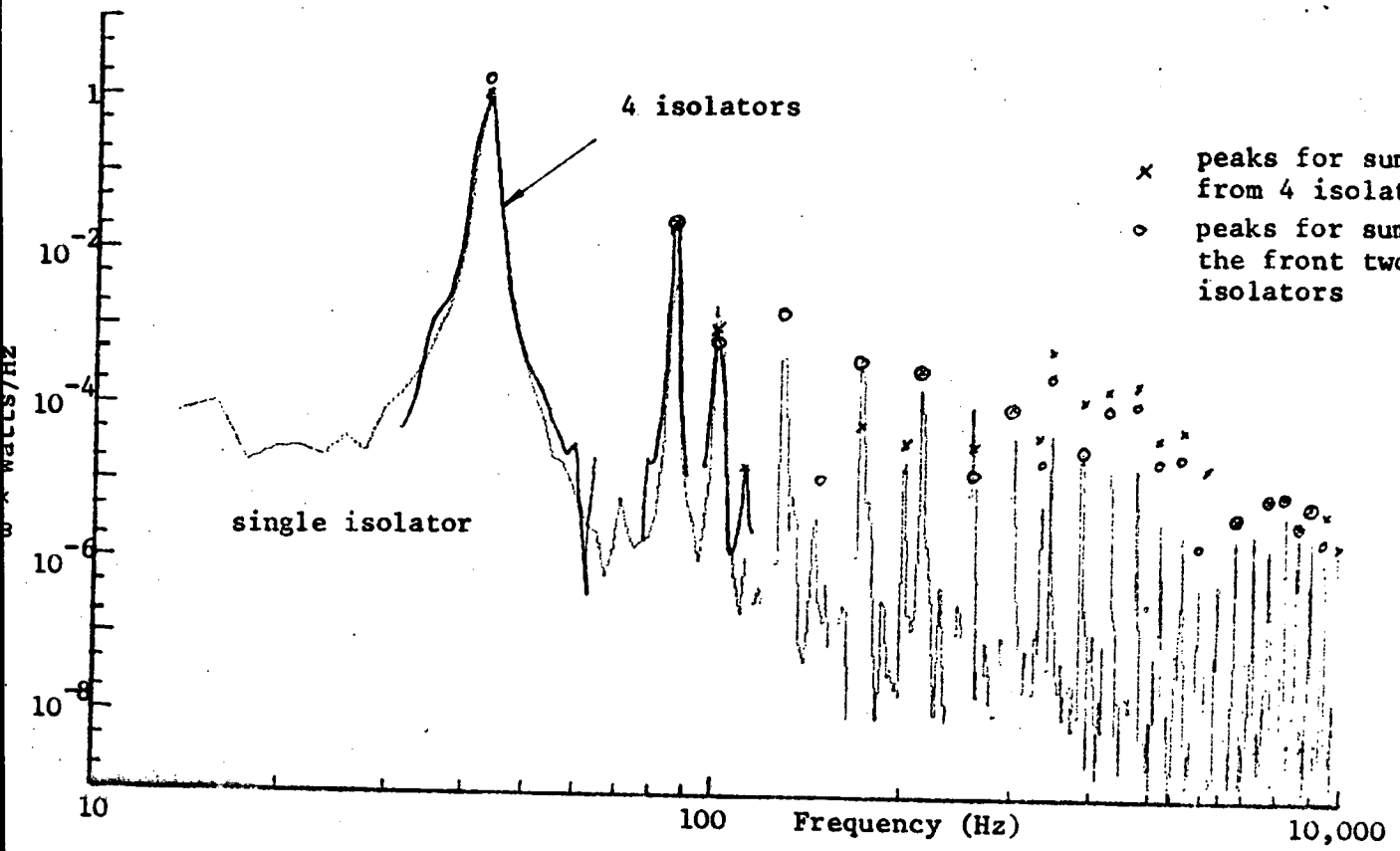

Fig. 10.22 ω × power/Hz, transmitted by 4 isolators, compared with that transmitted by the single isolator, impulsively excited running motor, 10 Hz - 1 kHz

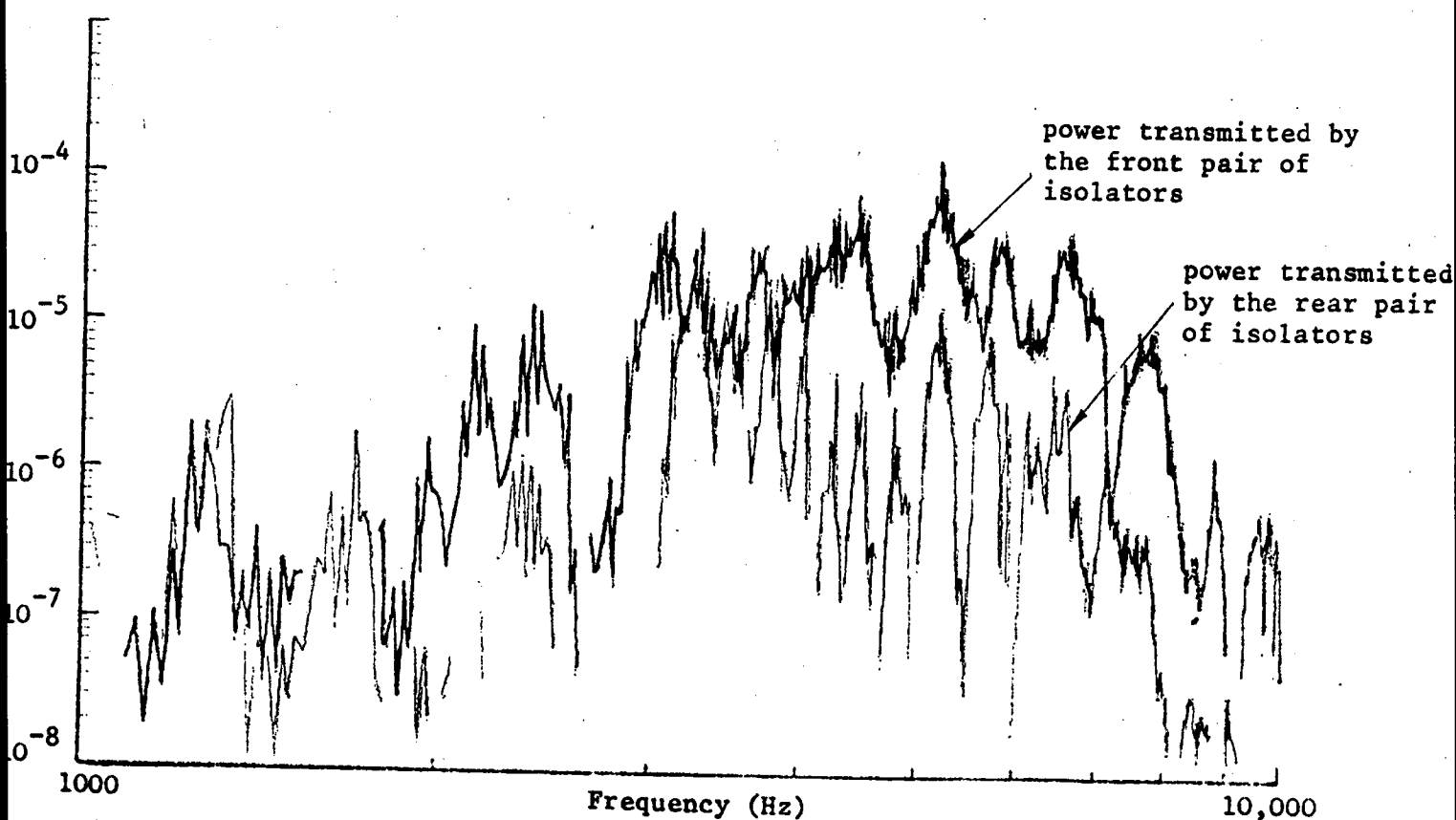

Fig. 10.23 ω × power/Hz transmitted by the front pair of isolators compared with that transmitted by the rear pair of isolators, impulsively excited running motor, 1 kHz - 10 kHz.

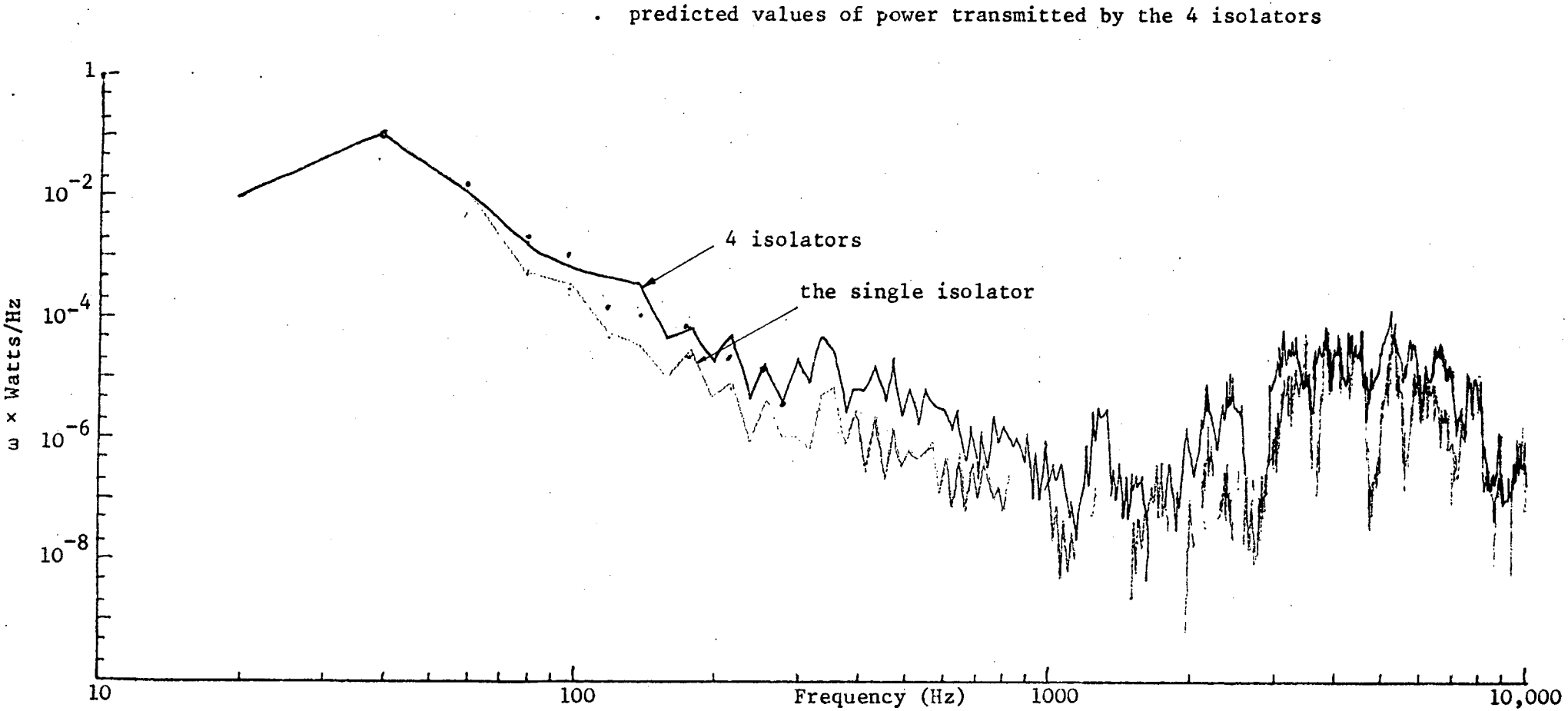

Fig. 10.24 Comparison of ω × power/Hz transmitted by the four isolators with that transmitted by the single isolator, impulsive excitation of the running motor, 10 Hz - 10 kHz, 20 Hz resolution.

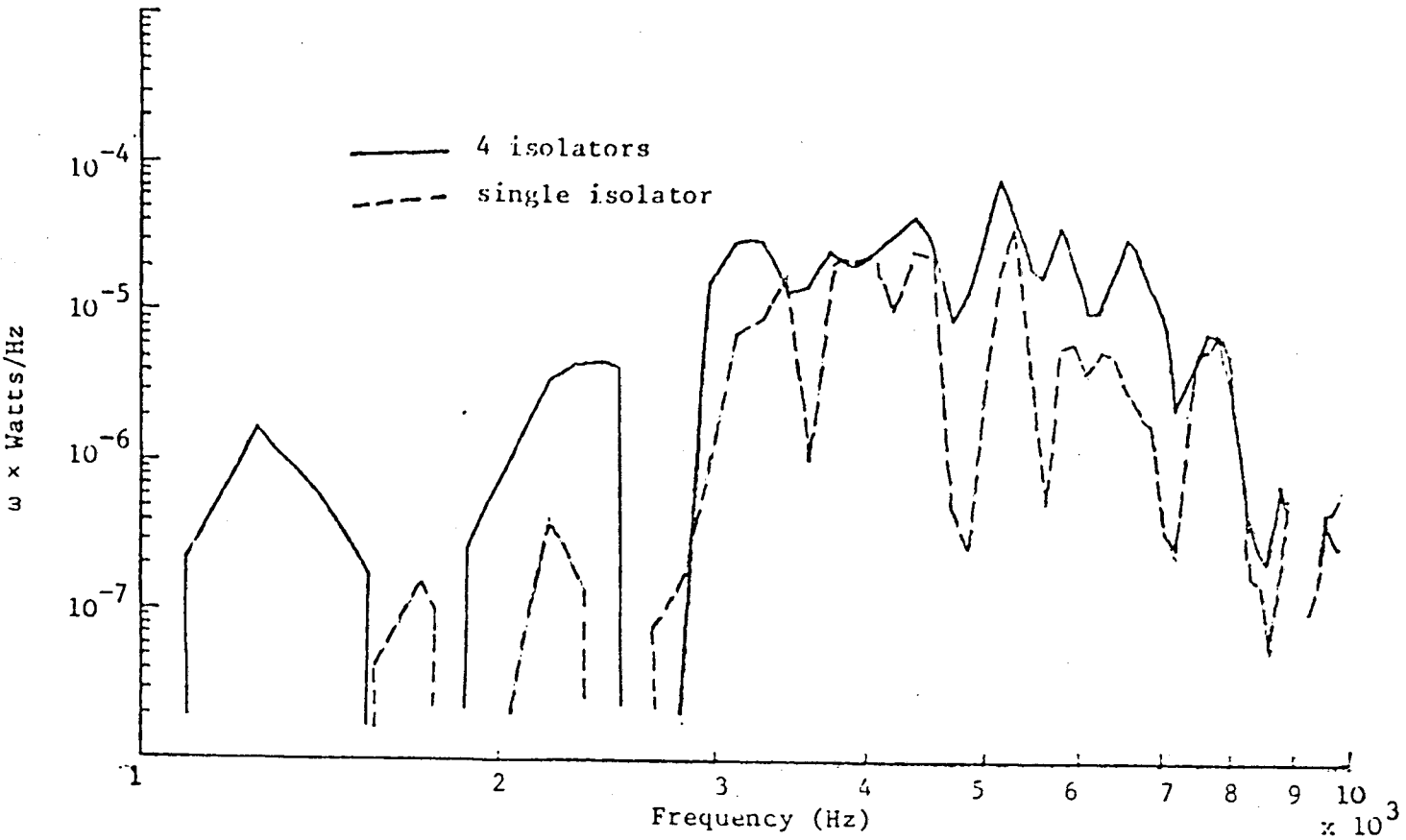

Fig. 10.25 ω × power/Hz transmitted by four isolators compared with that transmitted by a single isolator, measured using isolator transfer apparent mass, resolution 160 Hz, impulsive excitation of running motor.

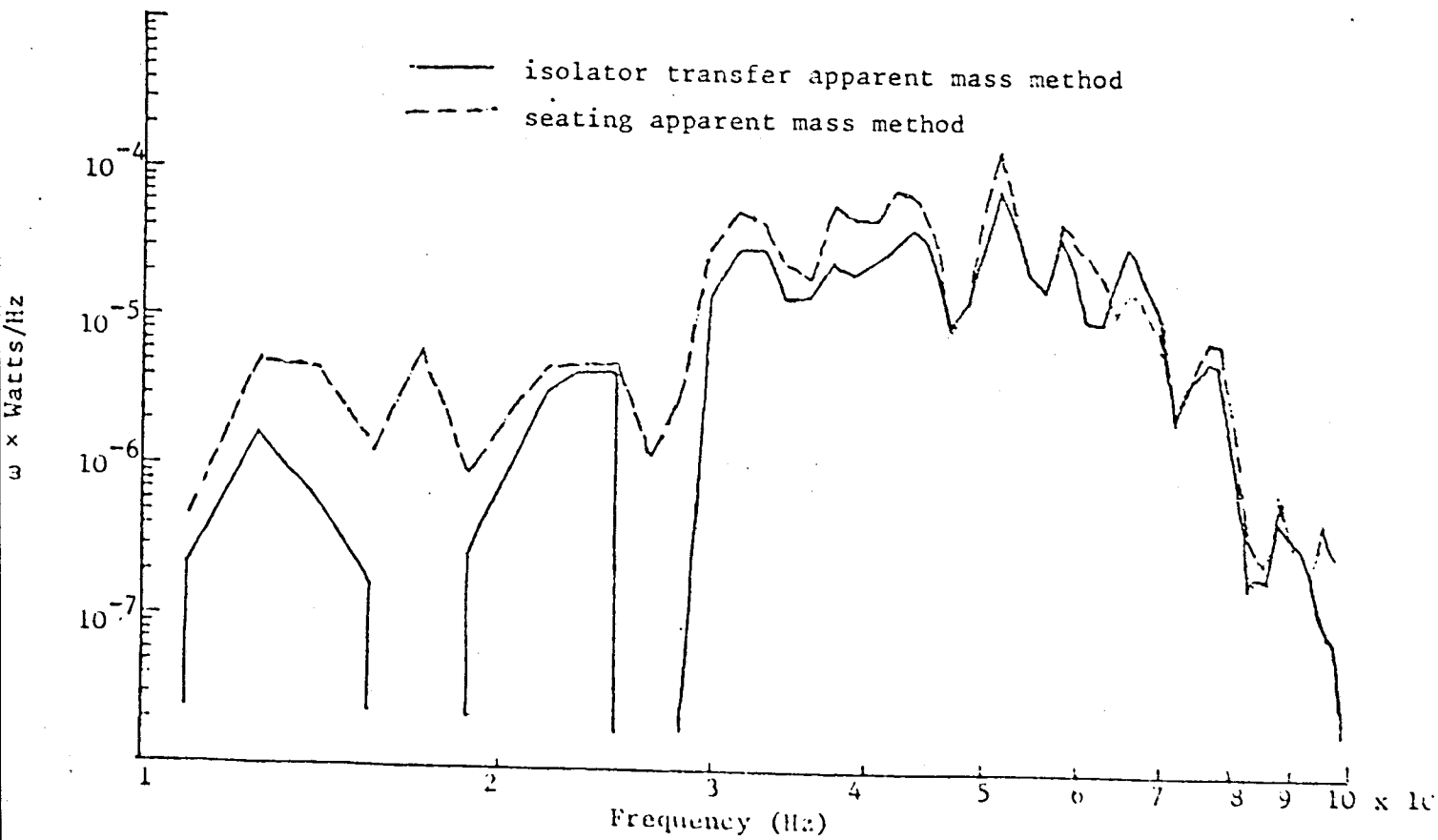

Fig. 10.26 ω × power/Hz transmitted by 4 isolators, measured using the isolator transfer apparent mass and measured using the seating apparent mass, resolution 160 Hz, impulsive excitation of running motor.

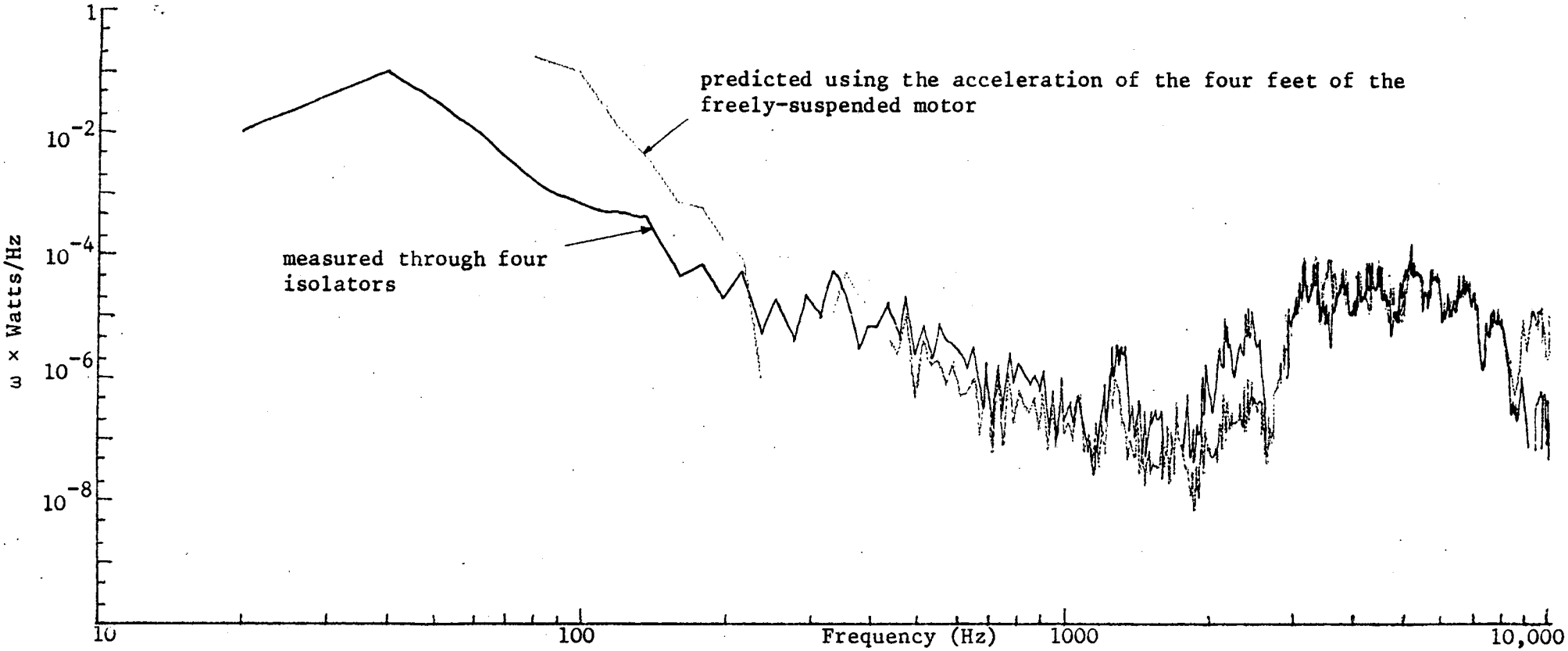

Fig. 10.27 Comparison of ω × power/Hz measured with that predicted using the acceleration at the four feet of the freely suspended motor, 20 Hz resolution, 10 Hz - 10 kHz.

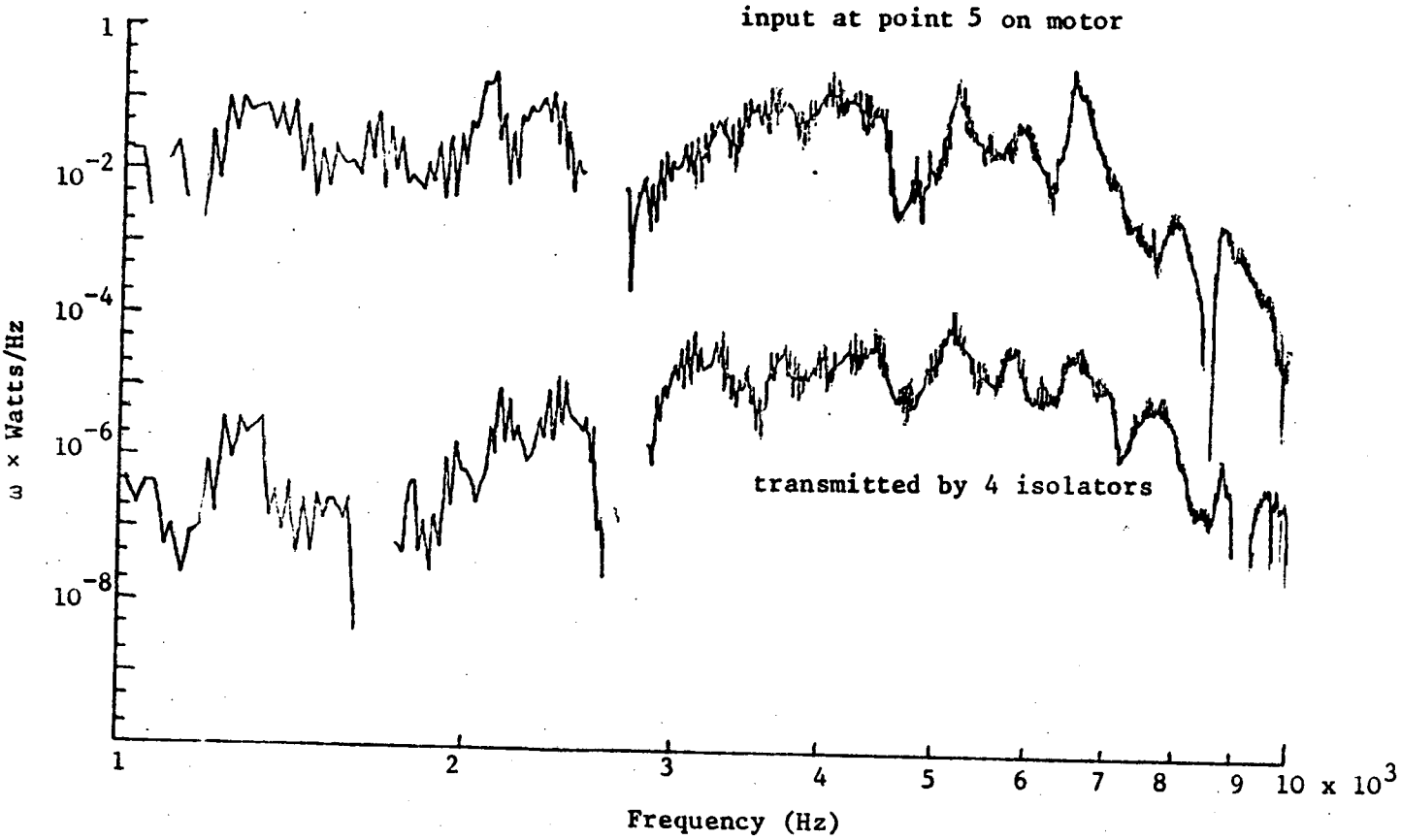

Fig. 10.28 ω × power/Hz input at point 5 on motor and ω × power/Hz transmitted by the four isolators, impulsive excitation of the running motor, 20 Hz resolution, 1 kHz - 10 kHz.